IOWA STATE UNIVERSITY
Digital Repository

Retrospective Theses and Dissertations

Iowa State University Capstones, Theses and Dissertations

2005

Predicting temperature and strength development of the field concrete

Zhi Ge
Iowa State University

Follow this and additional works at: https://lib.dr.iastate.edu/rtd

 Part of the Civil Engineering Commons

Recommended Citation
Ge, Zhi, "Predicting temperature and strength development of the field concrete " (2005). *Retrospective Theses and Dissertations*. 1730.
https://lib.dr.iastate.edu/rtd/1730

This Dissertation is brought to you for free and open access by the Iowa State University Capstones, Theses and Dissertations at Iowa State University Digital Repository. It has been accepted for inclusion in Retrospective Theses and Dissertations by an authorized administrator of Iowa State University Digital Repository. For more information, please contact digirep@iastate.edu.

www.manaraa.com

Predicting temperature and strength development of the field concrete

by

Zhi Ge

A dissertation submitted to the graduate faculty

in partial fulfillment of the requirements for the degree of

DOCTOR OF PHILOSOPHY

Major: Civil Engineering (Civil Engineering Materials)

Program of Study Committee:
Kejin Wang, Major Professor
James K. Cable
Halil Ceylan
William Duckworth
David J. White

Iowa State University

Ames, Iowa

2005

Copyright © Zhi Ge, 2005. All rights reserved.

UMI Number: 3200417

INFORMATION TO USERS

The quality of this reproduction is dependent upon the quality of the copy submitted. Broken or indistinct print, colored or poor quality illustrations and photographs, print bleed-through, substandard margins, and improper alignment can adversely affect reproduction.

In the unlikely event that the author did not send a complete manuscript and there are missing pages, these will be noted. Also, if unauthorized copyright material had to be removed, a note will indicate the deletion.

UMI®

UMI Microform 3200417

Copyright 2006 by ProQuest Information and Learning Company.

All rights reserved. This microform edition is protected against unauthorized copying under Title 17, United States Code.

ProQuest Information and Learning Company
300 North Zeeb Road
P.O. Box 1346
Ann Arbor, MI 48106-1346

Graduate College
Iowa State University

This is to certify that the doctoral dissertation of

Zhi Ge

has met the dissertation requirements of Iowa State University

Signature was redacted for privacy.

Committee Member

Signature was redacted for privacy.

Committee Member

Signature was redacted for privacy.

Committee Member

Signature was redacted for privacy.

Committee Member

Signature was redacted for privacy.

Major Professor

Signature was redacted for privacy.

For the Major Program

TABLE OF CONTENTS

LIST OF FIGURES vii

LIST OF TABLES xii

ABSTRACT xiv

ACKNOWLEDGMENTS xvi

CHAPTER 1 INTRODUCTION 1

1.1. GENERAL 1
1.2. RESEARCH APPROACH 3
1.3. SCOPE OF THE DISSERTATION 5

CHAPTER 2 LITERATURE REVIEW 7

2.1 CEMENTITIOUS MATERIALS AND PROPERTIES 7
2.1.1 Ordinary Portland Cement (OPC) 7
2.1.2 Supplemental Cementitious Materials (SCMs) 12
2.1.2.1 Fly Ash 12
2.1.2.2 Ground Granulated Blast Furnace Slag (GGBFS) 14
2.2 HYDRATION OF PORTLAND CEMENT 16
2.2.1 Portland Cement Hydration 17
2.2.2 Factors that Influence Cement Hydration 20
2.2.2.1 Cement Type 20
2.2.2.2 Sulfate Content 23
2.2.2.3 Fineness 23
2.2.2.4 Water/Cement (w/c) Ratio 24
2.2.2.5 Curing and Initial Temperature 26
2.2.2.6 SCMS 27
2.2.2.7 Chemical Admixture 30
2.3 MEASUREMENTS FOR CEMENT HYDRATION 32
2.3.1 Calorimetry 32
2.3.2 Maximum Heat of Hydration 35
2.3.3 Degree of Hydration 35
2.3.3.1 Degree of Cement Hydration at Time t 35
2.3.3.2 Ultimate Degree of Hydration 36
2.4 CONCRETE MATURITY 37
2.4.1 Nurse-Saul Maturity 37
2.4.2 Equivalent Age Maturity 38

2.4.3 Activation Energy *41*
2.4.4 Maturity and Strength *44*
2.5 SUMMARY 45

CHAPTER 3 EXPERIMENTAL PROGRAM 47

3.1 CONCRETE MATERIALS AND MIXES 47
3.2 TEST METHODS 50
3.2.1 Quality Control Tests *50*
3.2.2 Heat Signature Test *51*
3.2.3 Maturity Strength Test *54*

CHAPTER 4 MODELING THE HEAT OF HYDRATION OF CEMENTITIOUS MATERIALS 56

4.1 EXISTING HYDRATION MODELS 56
4.1.1 Multi-Component Model *57*
4.1.2 Equal Fractional Rate Model *59*
4.2 HEAT OF CEMENT HYDRATION MODEL 62
4.2.1 General Concept and Approach of Model Development *62*
4.2.2 Model Data Source *66*
4.2.2.1 Data from Semi-Adiabatic Tests 66
4.2.2.2 Data from Literature 70
4.2.3 Model Development *73*
4.2.3.1 Total Heat of Cementitious Materials 73
4.2.3.2 Nonlinear Regression Results 74
4.2.3.3 Models for Hydration Parameters 76
4.2.3.4 Model for Heat of Cementitious Material Hydration 82
4.2.4 Sensitivity Analysis *86*
4.3 SUMMARY 92

CHAPTER 5 MODIFIED MATURITY-STRENGTH MODEL 94

5.1 GENERAL CONCEPT AND APPROACH 94
5.1.1 Maturity-Strength Model *94*
5.1.2 Approach to New Model *96*
5.2 FACTORS CONSIDERED IN STRENGTH DEVELOPMENT 96
5.2.1 Cement Type *97*
5.2.2 W/C Ratio *99*
5.2.3 Admixture *100*
5.2.4 Curing Conditions *101*
5.2.5 Air Content *103*

5.2.6 Cement Content *104*
5.3 DATA SOURCE AND ANALYSIS 104
5.3.1 Data from Laboratory Tests *105*
5.3.2 Data from Literature *108*
5.3.3 Nonlinear Regression Analysis *110*
5.4 MODELING OF CONCRETE STRENGTH PARAMETERS 113
5.5 MODIFIED MATURITY-STRENGTH MODEL 118
5.6 SENSITIVITY ANALYSIS 123
5.7 SUMMARY AND RECOMMENDATIONS 126
5.7.1 Summary *126*
5.7.2 Limitations and Recommendations *126*

CHAPTER 6 PREDICTION OF FIELD CONCRETE TEMPERATURE 128

6.1 GENERAL CONSIDERATIONS 129
6.1.1 Heat Transfer inside Concrete *129*
6.1.2 Rate of Heat Generation *130*
6.1.3 Thermal Properties of Concrete *131*
6.1.3.1 Specific Heat of Concrete 131
6.1.3.2 Thermal Conductivity 132
6.1.4 Boundary Conditions *133*
6.1.4.1 Conduction 134
6.1.4.2 Convection 137
6.1.4.3 Irradiation 138
6.1.4.4 Solar Absorption 141
6.1.5 Initial Pavement Conditions *142*
6.1.5.1 Fresh Concrete Placement Temperature 142
6.1.5.2 Initial Subbase and Subgrade Temperature 143
6.2 FEMLAB MODELING FOR FIELD CONCRETE TEMPERATURE 143
6.3 RESULTS FROM FEMLAB ANALYSIS 147
6.3.1 Effect of Fly Ash and Slag *147*
6.3.2 Effect of Environment Conditions *150*
6.3.3 Effect of Construction and Initial Conditions *152*
6.3.3.1 Effect of Paving Time 152
6.3.3.2 Effect of Concrete Placement Temperature 155
6.3.3.3 Effect of Subbase Temperature 157
6.3.3.4 Effect of Pavement Thickness 159
6.3.4 Temperature Distribution in Transverse Direction *160*
6.3.5 Temperature Distribution at a Certain Time *161*

6.4 SUMMARY 162

CHAPTER 7 APPLICATION OF DEVELOPED MODELS 163

7.1 RESULTS OF EXAMPLE 1--HOT WEATHER CONDITIONS 165
7.2 RESULTS OF EXAMPLE 2--COLD WEATHER CONDITIONS 168
7.3 APPLICATION OF THE MODELING RESULTS 171
7.4 SUMMARY 172

CHAPTER 8 SUMMARY AND RECOMMENDATIONS 174

8.1 SUMMARY 174
8.2 MAJOR RESEARCH FINDINGS 175
8.3 LIMITATIONS AND RECOMMENDATIONS 177

REFERENCES 179

APPENDIX A. HEAT OF HYDRATION MODEL 189

APPENDIX B. MATURITY-STRENGTH MODEL 195

APPENDIX C. TEMPERATURE PREDICTION 207

LIST OF FIGURES

Figure 1.1: Flow Chart of the Research Approach 4
Figure 2.1: Typical Oxide Composition of an OPC (Mindess and Young 1981) 8
Figure 2.2: Fly Ash Particles at 3,000x Magnification 13
Figure 2.3: Effects of Different Fly Ash on Strength Development (Data from Douglas and Pouskouleli 1991) 14
Figure 2.4: Effect of Al_2O_3 and CaO on the 28-day Compressive Strength (Adapted from Wang et al. 2004) 15
Figure 2.5: Effect of Al_2O_3 and CaO on Heat of Hydration (Adapted from Wang et al. 2004) ... 16
Figure 2.6: OPC Hydration Process 19
Figure 2.7: Temperature Increase of Mass Concrete Under Adiabatic Conditions (Adapted from Mindess and Young 1981) 20
Figure 2.8: Hydration Rate of the Cement Compounds: (a) in pastes of the pure compounds; (b) in a Type I cement paste (Adapted from Mindess and Young 1981) 21
Figure 2.9: Effect of C_3A Content ($C_3S \approx$ constant) on Heat of Hydration (Adapted from Lerch and Bogue 1934) 22
Figure 2.10: Effect of C_3S Content ($C_3A \approx$ constant) on Heat of Hydration (Adapted from Lerch and Bogue 1934) 22
Figure 2.11: Heat of Immediate Hydration with SO_3 Varied (Adapted from Lerch et al 1946) .. 23
Figure 2.12: Heat of Hydration with Specific Surface Varied (Adapted from Lerch et al. 1946) 24
Figure 2.13: Effect of W/C Ratio on the Heat Evolution (RILEM 42-CEA 1981) 25
Figure 2.14: Effect of Curing Temperature on Hydration (Adapted from Escalante-Garcia et al. 2000) 26
Figure 2.15: Effect of Fly Ash on Heat Generation: (a) Class F Fly Ash (Adapted from Kishi and Maekawa 1995); (b) Class C Fly Ash (Adapted from Nocuñ-Wczelik 2001) 28
Figure 2.16: Effect of Slag on Hydration (Adapted from Kishi and Maekawa 1994) 29
Figure 2.17: Heat Evaluation at 20°C, (1) 40% coarse slag (400 m^2/Kg) (2) 40% fine slag (592 m^2/Kg) (3) OPC (Adopted from Uchikawa ,1986) 29

Figure 2.18: Total Heat of Blended Cement with Slag at Different Temperatures (Adapted from Ma et al. 1994) 30
Figure 2.19: Effect of Activation Energy on the Age Conversion Factor 41
Figure 2.20: Activation Energy from Concrete and Mortar Tests (Carino 2004) 44
Figure 2.21: (a) Compressive Strength Gain at Different Curing Temperatures (b) Application of Maturity Function (Adapted from Byfors 1980) 45
Figure 3.1: IQdrum for Heat of Hydration Test 51
Figure 3.2: Output for Types I/II Cement 53
Figure 3.3: Differences in Calculated Adiabatic Results Obtained from Semi-Adiabatic Testing (Adapted from Schindler 2002) 53
Figure 3.4: Maturity Test Setup (Samples Cured in the Curing Room) 54
Figure 3.5: Output for Concrete Temperature and Maturity (Type I/II Cement Concrete) 55
Figure 4.1: Schematic Representation of Independent Hydration Concept and Hydration at Equal Fractional Rates 57
Figure 4.2: Thermal Activity of each Component (Adapted from Maekawa et al. 1999) 58
Figure 4.3: Effect of Hult, β, and τ on the Shape of the Heat Evolution Curve 65
Figure 4.4: Effect of Slag Replacement on Heat of Hydration of Cementitious Materials (Lafarge I/II Cement) 67
Figure 4.6: Effect of Fly Ash Replacement on Heat of Hydration 68
Figure 4.7: Effect of Different Fly Ash on Heat of Hydration 69
Figure 4.8: Effect of Fly Ash and Slag (Lafarge I/II Cement) 69
Figure 4.9: Effect of Fly Ash and Slag (Lafarge I/II Cement) 70
Figure 4.10: Effect of Cement Type on Heat of Hydration 71
Figure 4.11: Predicted and Measured τ 79
Figure 4.12: Predicted and Measured Beta 80
Figure 4.13: Predicted and Measured Hult 80
Figure 4.14: Residue vs Parameters 81
Figure 4.15: Measured vs Predicted Heat of Hydration 83
Figure 4.16: Measured vs Predicted Heat of Hydration for Different Types of Cement (Lerch and Ford 1948) 83

Figure 4.17: Measured vs Predicted Heat of Hydration for Type I/II Cement with Different Levels of Fly Ash 84
Figure 4.18: Measured vs Predicted Heat of Hydration for Type I/II Cement with Different Levels of Slag 85
Figure 4.19: Measured vs Predicted Heat of Hydration for Type I/II Cement with Different Levels of Fly-Slag Mixture (Fly Ash:Slag = 1:3) 85
Figure 4.20: Effect of C_3S 87
Figure 4.21: Effect of C_3A 88
Figure 4.22: Effect of SO_3 88
Figure 4.23: Effect of Blaine 89
Figure 4.24: Effect of w/c 89
Figure 4.25: Effect of Slag Replacement 90
Figure 4.26: HI Effect 91
Figure 4.27: Effect of Fly Ash Replacement 91
Figure 4.28: Effect of CaO of Fly Ash 92
Figure 5.1: Strength of 6×12 in. Concrete Cylinder Made with Different Types of OPC (Adapted from Mindess and Young 1981) 97
Figure 5.2: Concrete Compressive Strength with Cements of Various Fineness w/c = 0.4, S=742 m^2/Kg, R=490 m^2/Kg, O=277 m^2/Kg (Byfors 1980) 98
Figure 5.3: Effect of Cement Type on Strength Gain (Byfors 1980) 98
Figure 5.4: Influence of w/c Ratio on Concrete Strength (Adapted from Byfors 1980) 100
Figure 5.5: Compressive Strength of Various Concrete (Data Adapted from Douglas et al. 1991) 101
Figure 5.6: Compressive Strength Achieved at Different Ages and Temperatures Related to the Corresponding Strength at 20°C (Adapted from Byfors 1980) 102
Figure 5.7: Effect of Temperature on Compressive Strength Development : (a) 1-day and 28-day strength (b) Curing temperature maintained continuously (Adapted from Mindess and Young 1981) 102
Figure 5.8: Effect of Moist Curing on Strength Gain (Adapted from Byfors 1980) 103
Figure 5.9: Influence of Air Content on Compressive Strength (Mindess and Young 1981) 104

Figure 5.10: Effect of Slag Replacement on Strength Development 105
Figure 5.11: Effect of Different Slags on Strength Development 106
Figure 5.12: Effect of Fly Ash Replacement on Strength Development 107
Figure 5.13: Effect of Different Fly Ash on Strength Development 107
Figure 5.14: Effect of Fly Ash- Slag on Strength Development 108
Figure 5.15: Strength Development for Different Types of Cement 109
Figure 5.16: Predicted and Measured S_u 115
Figure 5.17: Predicted and Measured τ 116
Figure 5.18: Predicted and Measured β 116
Figure 5.19: Residual vs Strength Parameters 117
Figure 5.20: Measured vs Predicted Strength 119
Figure 5.21: Measured vs Predicted Strength, Types III and V Cement 120
Figure 5.22: Measured vs Predicted Strength for Lafarge Types I/II Cement with Different Levels of Slag Replacement (w/b = 0.42) 121
Figure 5.23: Measured vs Predicted Strength for Lafarge Types I/II Cement with Different Levels of Fly Ash Replacement (w/b = 0.42) 122
Figure 5.24: Measured vs Predicted Strength for Lafarge Types I/II Cement with Different Levels of Slag and Fly Ash Replacement (w/b = 0.42; slag : FA = 3:1) 122
Figure 6.1: Heat Transfer Mechanism 134
Figure 6.2: Flowchart of FEMLAB Modeling Process 144
Figure 6.3: Cross Section of the Pavement 145
Figure 6.4: Mesh Model of the Pavement System 146
Figure 6.5: Effect of SCMs on Field Concrete Temperature (Constructed at 10:00 AM, Summer Conditions) 149
Figure 6.6: Heat Generation for Different Cementitious Materials (Constructed at 10:00 AM, Summer, Middle layer) 150
Figure 6.7: Effect of Environmental Conditions on Pavement Temperature (10:00 AM, OPC) 151
Figure 6.8: Effect of Paving Time on Pavement Temperature (Summer Conditions) 154

Figure 6.9: Effect of Concrete Placement Temperature on Pavement Temperature (Summer Conditions, Paved at 10:00 AM, Subbase Temperature 25°C) 156
Figure 6.10: Effect of Initial Subbase Temperature on Pavement Temperature (Summer Conditions, Paved at 10:00 AM) 158
Figure 6.11: Effect of Pavement Thickness on Pavement Temperature (Summer Conditions) ..159
Figure 6.12: Temperature Distribution with Different Distances from the Edge (Summer Conditions, Middle Layer) 160
Figure 6.13: Temperature Distribution inside Concrete Slab at One Day 161
Figure 7.1: Procedures for Concrete Temperature and Strength Prediction 163
Figure 7.2: Heat of Hydration of Field Concrete under Hot Weather Conditions 166
Figure 7.3: Field Concrete Temperature and Strength under Hot Weather Conditions 167
Figure 7.4: Heat of Hydration of Field Concrete under Cold Weather Conditions 169
Figure 7.5: Field Concrete Temperature and Strength under Cold Weather Conditions 170
Figure 7.6: Flowchart of Use of Developed Models for Concrete Mix Design and Performance Control 171

LIST OF TABLES

Table 2.1: Typical Composition of OPC (Mindess and Young 1981) 8
Table 2.2: Typical Oxide Composition of OPC (Mindess and Young 1981) 9
Table 2.3: Chemical Requirements for Different Cement Types (*ASTM C 150* 2002) 11
Table 2.4: Physical Requirements for Different Cement Types (*ASTM C 150* 2002) 11
Table 2.5: Typical Range of Chemical Composition of Fly Ash (Roy et al. 1985) 14
Table 2.6: Hydration Characteristics of Cement Compounds 21
Table 2.7: Variability of Adiabatic and Semi-Adiabatic Test Results (Adapted from Morabito 1998) 34
Table 2.8: Specific Heat of Hydration of Individual Compounds 35
Table 3.1: Chemical Compositions of Cement and SCMs 48
Table 3.2: C-3 Concrete Mix Proportion 49
Table 3.3: SCM Replacement Level by Weight 50
Table 4.1: Cement Chemical Composition (Adapted from Lerch et al. 1948) 72
Table 4.2: Criteria and Stop Limits for Nonlinear Regression 74
Table 4.3: Summary of Nonlinear Regression Results from the Laboratory Test Data 75
Table 4.4: Summary of Nonlinear Regression Results for Literature Data (Lerch et al. 1948) 76
Table 5.1: Estimated Parameters for Laboratory Test 111
Table 5.2: Estimated Strength Parameters for Literature Data (Wood 1992) 112
Table 5.3: Chemical Composition and Properties of OPC 123
Table 5.4: Summary of the Sensitivity Analysis 125
Table 6.1: Typical Specific Heat Values for Concrete Components 132
Table 6.2: Typical Thermal Conductivity Values of Concrete with Different Types of Aggregate (Mehta et al. 1993) 133
Table 6.3: Properties of Various Base Materials (Andersen et al. 1992) 135
Table 6.4: Thermal Properties of Various Materials 136
Table 6.5: Solar Radiation Values (McCullough and Rasmussen 1999) 141
Table 6.6: Variables for Temperature Analysis (°C) 147
Table 6.7: Ranges of Initial Condition Variables under Summer Conditions 147

Table 7.1: Material Properties.....164
Table 7.2: Pavement Conditions.....164
Table 7.3: Maximum Temperature Drop for Hot Weather Conditions.....168

ABSTRACT

Concrete temperature and strength development is essential to in-service concrete performance. Undesirable temperature development may cause concrete to crack under some environmental conditions, and it may result in insufficient strength development. Concrete strength is important for construction operations, such as joint cutting and pavement opening time.

In this study, heat signature and maturity-strength tests were conducted on 23 different concrete mixes. A semi-adiabatic calorimeter was used for the heat signature test. Based on the test data, as well as the data from citied literature, a combined model for predicting temperature and strength development of concrete pavement under various construction and environmental conditions is presented. Using commercial finite-element software, FEMLAB (Finite Element Modeling Laboratory), the model can well predict the temperature and strength distributions inside a concrete pavement with time.

In the proposed temperature model, concrete temperature development was determined based on the heat of hydration of cementitious materials and the field environmental conditions of pavement. The general heat of hydration model was developed to predict heat of hydration of cementitious materials. The heat exchange between the pavement and environment was computed based on the transient heat transfer mode of FEMLAB. Material variables, pavement structure variables, and environmental variables were considered.

The modified maturity-strength model was developed based on the laboratory and literature data. The model considers the effects of the cement chemical and physical properties, amount and chemical composition of fly ash and slag, water/cement ratio, air content and curing conditions.

The integrated model was applied to study field concrete temperature and strength development under two different field conditions. The included analyses indicate that the modeling results well correlated with the experimental results. The new model can be used to

optimize concrete mix design, to assess field concrete strength development, and to select optimal concrete placement temperature and construction conditions for minimal thermal stress.

Keywords: Pavement Temperature, Concrete Compressive Strength, Cement Hydration, Boundary Condition, Maturity.

ACKNOWLEDGMENTS

I would like express my sincere thanks to my advisor Dr. Kejin Wang for her gentle leadership and unerring guidance. I also extend my thanks to Dr. James K. Cable, Dr. Brian Coree, Dr. Halil Ceylan, Dr. William Duckworth, and Dr. David J. White for serving as my dissertation committee and providing critical review on my dissertation. I would also like to extend my thanks to Dr. James Cable for his support of the FEMLAB software.

Part of this study required laboratory work. Special thanks are given to many individuals who worked together with me in the laboratory. Without the help supplied by Jiong Hu, Shihai Zhang, Gang Lu, Tyson Rupnow and Benjamin Hermanson, much of this work would not have been possible.

Valuable advice and assistance in the XRF test provided by Scott Schlorholtz at Iowa State University's Materials Analysis and Research Laboratory is also greatly appreciated.

CHAPTER 1
INTRODUCTION

1.1. General

Concrete has been extensively used for paving highways and airports as well as business and residential streets since the first concrete pavement was completed in 1893. It is estimated that approximately 60% of the interstate highway system at the United States is built with Portland cement concrete (PCC). However, quality control during construction is always a challenge in concrete practice.

Concrete temperature management is one aspect of pavement quality control. The importance of field concrete temperature control has been realized for many years. Andersen et al. (1992) states that the temperature and moisture of concrete in the early age strongly influence early strength development and long-term durability of concrete. If not addressed, concrete thermal conditions can cause significant problems, including thermal cracking and strength loss. Researchers have demonstrated that early age concrete temperature during the first 24 to 72 hours has a major influence on long-term pavement performance (Hankins et al. 1991, McCullough et al. 1998).

Pavement temperature is primarily determined by the cement hydration process and by heat exchange with the surrounding environment. Cement hydration generates heat, and it is a key factor for the prediction of concrete temperature. The hydration process reflects the characteristics of concrete materials and mix proportions as well as the change in construction practices and environmental conditions. Cement hydration also consequently influences concrete workability, setting behavior, strength gain rates, and pore structures. The rate of cement hydration is closely related to the cement's chemical composition and water/cement ratio (w/c). The use of supplementary cementitious materials (SCMs) in concrete can significantly influence the cement hydration process. Supplementary cementitious materials generally reduce the heat of hydration and result in a lower concrete

temperature, which in turn reduces the thermal cracking risk. Currently, there is limited guidance to quantify the influence of SCMs on cement hydration.

Concrete's compressive strength is generally used as a measure of overall concrete quality, because it is related to many other properties of concrete, such as elastic modulus and durability, and it is easy to test. Concrete strength at early age is also essential for construction operations, such as joint cutting times, formwork removal times, and pavement opening time. Guo (1989) states, "Knowledge of the early-stage strength of concrete is of special importance when concreting has to be carried out during cold weather."

Like the hydration process, concrete compressive strength is also influenced by many factors, such as concrete materials, mix proportion, environmental conditions, and the age of the concrete. The influence of time and environmental temperature on the development of concrete strength has been studied for several decades. In 1951, Saul introduced the term "maturity" that approximates the complex effect of time and temperature on concrete strength development. Today, the maturity method is widely used because of its simplicity and low cost. This method, which predicts the strength development of field concrete, is generally based on the concrete temperature measured in the field and on the maturity-strength relationship developed in the laboratory or field.

A great deal of work has also been done in developing models that predict concrete temperature and the relationship between concrete temperature and strength. Most existing models are able to predict concrete strength development under both hot and cold weather conditions, but they often do not consider concrete containing SCMs or their chemical compositions although SCMs have become an essential component of concrete. Various individual models have been developed to predict cement hydration and concrete temperature prediction respectively. Very few researchers have intergrated them, and therefore, these individual models cannot be directly used for concrete mix design and performance prediction.

The goal of the present study is to develop a series of models that allows researchers and engineers to predict pavement concrete temperature and strength development before

concrete mixture is designed and placed. The following factors are considered in the new models:

- Types of cement
- Usage of different type and amount of fly ash and slag
- Mix design
- Weather conditions
- Construction conditions
- Pavement design

The finite-element software, FEMLAB, is used in the model to calculate the heat transfer between pavement concrete and the environment. The developed models from this study can also be used to assess field concrete performance or to select the most appropriate materials and construction practices for better concrete performance.

1.2. Research Approach

To predict concrete temperature and strength development of a pavement system based on concrete materials, mix proportion, and environmental conditions, the following three models are developed and then effectively integrated in the present study:

1. Heat of hydration
2. Concrete temperature
3. Maturity –strength

Figure 1.1 shows the overall approach for the model development. First, various materials and mix design variables are selected for testing and modeling. Then, four groups of tests are performed: (1) quality control, including air content, slump, and unit weight; (2) heat of hydration; (3) concrete compressive strength; and (4) maturity. Results from the heat of hydration tests combined with the literature data set are used to develop the heat of hydration model. The developed heat of hydration model together with construction and weather conditions are input into the temperature model to produce field concrete

temperature development with time. The maturity-strength model is developed from the results of the maturity and strength tests. Field concrete maturity is calculated from the predicted temperature history. Finally, the field concrete compressive strength is predicted by the calculated maturity.

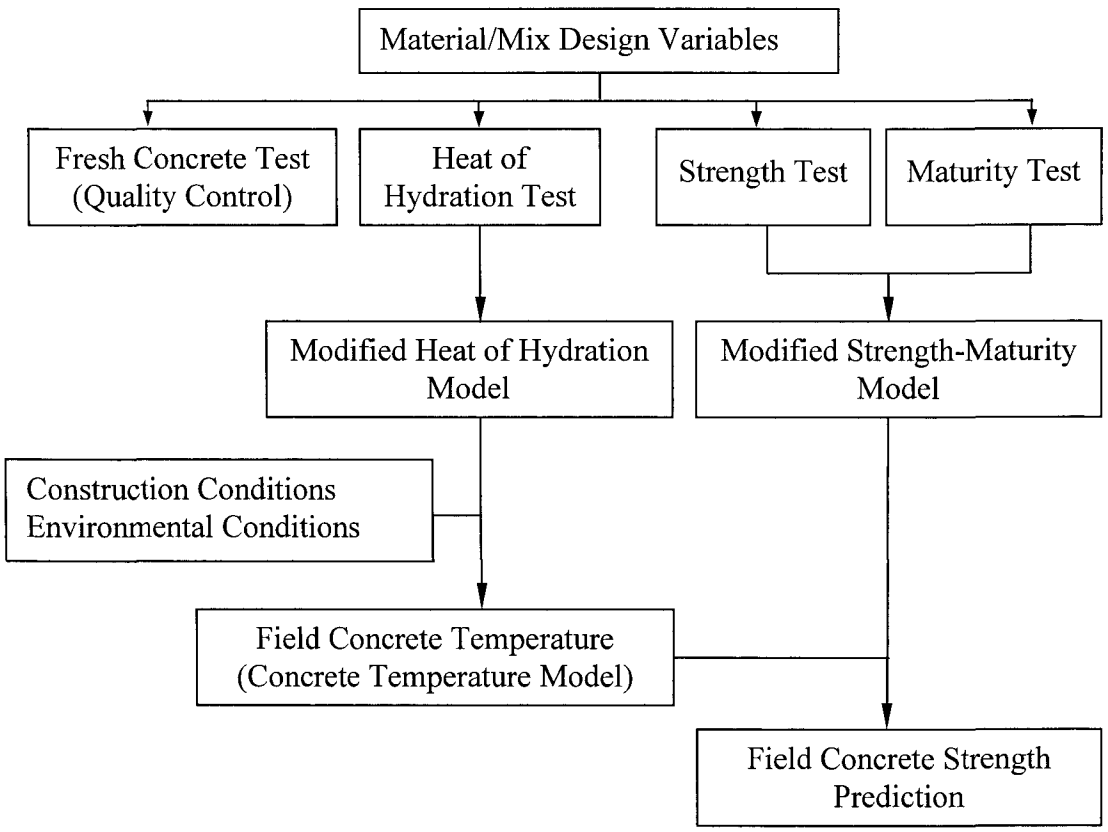

Figure 1.1: Flow Chart of the Research Approach

Both the modified heat of hydration and strength-maturity models are developed in three steps: (1) Collection of test and literature data; (2) Selection of the proper existing model; and (3) Statistical analysis of the relationship among the parameters of the selected model and the material and concrete properties.

To evaluate the effect of SCMs on heat of hydration and concrete strength, a standard cement source was chosen, and then different levels of mineral admixtures, fly ash, and ground-granulated blast furnace slag were used with the cement. The influence of cement

type was studied using the heat of hydration and strength data from literature, which included 20 different cements and covered all five types of cement.

1.3. Scope of the Dissertation

This dissertation contains eight chapters, including the experimental work and model development and application.

Chapter 1 presents the general background, research objective and approach, and scope of the dissertation.

Chapter 2 presents a literature review. It provides the necessary background and terminology for concrete technology as well as reviews the cement hydration factors influencing cement hydration and concrete maturity.

Chapter 3 provides the details of the laboratory tests. Material properties, concrete mix information, and the design of the experimental program are documented in this chapter. All of the test procedures are listed.

Chapter 4 details the development of the heat of hydration model. The model was based on laboratory and literature data. Parameters--including cement type, amount and chemical composition of the SCM, and w/c --have been considered and incorporated into this model. The nonlinear regression method was applied to perform the statistical analysis.

Chapter 5 covers the development of the maturity-strength model. Like the heat of hydration model, it is based on laboratory and literature data. The w/c, air content, and chemical composition of cement and SCMs are included in the model.

In Chapter 6, the finite model for concrete temperature is developed, and the environmental conditions affecting concrete temperature are considered. The model developed in Chapter 4 is used to provide the heat generation of concrete. The FEMLAB software is used to calculate the temperature.

In Chapter 7, the three developed models as described in Chapters 4-6 are effectively integrated and used to predict the concrete temperature and strength of a pavement under two different field conditions, hot weather and cold weather. The effect of SCMs replacement is also studied for both weather conditions.

The summary of the conducted work, overall conclusions of this study and recommendations for future research are presented in Chapter 8. Several appendixes are included at the end of the dissertation; they contain statistical analysis results obtained during model development, graphs of the temperature prediction, and other data.

CHAPTER 2
LITERATURE REVIEW

2.1 Cementitious Materials and Properties

Concrete is one of the most important and widely used construction materials in the world. It is a composite material, consisting of cementitious material, aggregate, and water. The cementitious materials in concrete react with water, forming binders inside concrete. According to *ASTM C 219, Standard Terminology Relating to Hydraulic Cement*, cementitious material is "an inorganic material or a mixture of inorganic materials which sets and develops strength by chemical reaction with water by formation of hydrates, and which is capable of doing so underwater." The concrete properties are affected by the type and chemical composition of cementitious materials. The composition and hydration of cement and supplemental cementitious materials (SCM) will be reviewed in this section.

2.1.1 Ordinary Portland Cement (OPC)

Ordinary OPC is the most important cement. It is primarily composed of alite (C_3S), belite (C_2S), aluminate (C_3A), and aluminoferrite (C_4AF). These compounds account for over 90% of OPC, and to a large extent, are responsible for cement's hydraulic properties. Table 2.1 and Figure 2.1 show the typical composition of OPC. The total percentage does not equal 100 because of the impurities in the cement.

Table 2.1: Typical Composition of OPC (Mindess and Young 1981)

Chemical Name	Chemical Formula	Shorthand Notation	Weight Percent
Tricalcium silicate	$3CaO{\cdot}SiO_2$	C_3S	50
Dicalcium silicate	$2CaO{\cdot}SiO_2$	C_2S	25
Tricalcium aluminate	$3CaO{\cdot}Al_2O_3$	C_3A	12
Tetracalcium aluminoferrite	$4CaO{\cdot}Al_2O_3{\cdot}Fe_2O_3$	C_4AF	8
Calcium sulfate didydrate (gypsum)	$CaSO_4{\cdot}2H_2O$	$C\bar{S}H_2$	3.5

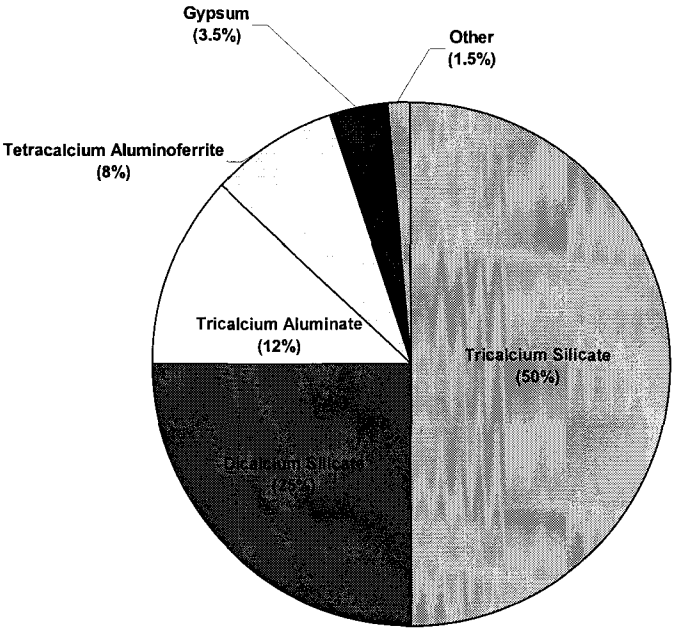

Figure 2.1: Typical Oxide Composition of an OPC
(Mindess and Young 1981)

The chemical compound can be determined by direct analysis. However, this method is complicated and requires expensive equipment and special skill. Therefore, the chemical composition of cement is traditionally written in oxides, which gives rise to the unique but universally used notation listed in Table 2.2. Chemical analysis of OPC is routinely performed using standard methods, such as X-ray Fluorescence Spectroscopy and chemical analysis, and is reported as its oxide. The oxide composition can be converted to the chemical composition as shown in Table 2.1 by the Bogue calculation (Bogue 1947). A

simple Bogue calculation is given in *ASTM C 150, Standard Specification for Portland Cement, (*Equations 2.1-2.7).

Table 2.2: Typical Oxide Composition of OPC (Mindess and Young 1981)

Oxide	Shorthand Notation	Common Name	Weight Percent
CaO	C	Lime	63
SiO_2	S	Silica	22
Al_2O_3	A	Alumina	6
Fe_2O_3	F	Ferric oxide	2.5
MgO	M	Magnesia	2.6
K_2O	K	Alkalis	0.6
Na_2O	N	Alkalis	0.3
SO_3	$\bar{S}$	Sulfur trioxide	2.0
CO_2	$\bar{C}$	Carbon dioxide	-
H_2O	H	Water	-

When A/F ≥ 0.64

$$C_3S = 4.071C - 7.600S - 6.781A - 1.430F - 2.852\bar{S} \quad 2.1$$

$$C_2S = 2.867S - 0.7544C_3S \quad 2.2$$

$$C_3A = 2.650A - 1.692F \quad 2.3$$

$$C_4AF = 3.043F \quad 2.4$$

When A/F < 0.64

$$C_3S = 4.071C - 7.600S - 4.479A - 2.859F - 2.852\bar{S} \quad 2.5$$

$$C_3A = 0 \quad 2.6$$

$$C_4AF + C_2F = 2.1000A + 1.702F \quad 2.7$$

Today, various types of cement have been developed to satisfy the requirement of different construction conditions. According to *ASTM C 150* OPC is classified into five primary classes (Types I-V). Type I cement is general-purpose cement suitable for all uses

that do not require the properties of other types of cement. "It is used where cement or concrete is not subject to specific exposures or to an objectionable temperature rise due to heat generated by hydration." Type II cement is used where moderate sulfate resistance or moderate heat of hydration is desired. To achieve a higher sulfate-resistant ability, the C_3A content is lowered. If high early age strength is desirable or concreting at a low-temperature environment, Type III cement should be used. Type III can be manufactured by increasing the C_3S content; however, it is more common to grind the cement more finely. The finer cement has a higher surface area, which allows for a higher rate of hydration and a more rapid development of strength after reacting with water. Type III cement produces more heat at early age and is more economical than Type I cement due to its chemical and physical features. In large-volume concrete, thermal cracking is a frequent problem during construction. Therefore, Type IV cement, a low heat of hydration cement, can be selected. Since heat of cement hydration can also be reduced by using various cementitious materials, Type IV cement is rarely available in the United States. Concrete is often used for foundation and marine structures, where sulfate content in soil and ground water is high. In this case, Type V cement has a limit on the maximum amount of C_3A.

The standard chemical and physical requirements of the five types of OPC according to *ASTM C150* can be found in Tables 2.3 and 2.4. Table 2.4 shows that the maximum heat of hydration and strength requirements are different for different cement. The 7-day maximum heat of hydration is 70 cal/g for Type II cement and only 60 cal/g for Type IV cement. The maximum 28-day heat for Type IV cement is 70 cal/g.

Table 2.3: Chemical Requirements for Different Cement Types (*ASTM C 150* 2002)

Chemical Compound	Cement Type				
	I	II	III	IV	V
SiO_2, min, %	-	20.0	-	-	-
Al_2O_3, max, %	-	6.0	-	-	-
Fe_2O_3, max, %	-	6.0	-	6.5	-
MgO, max, %	6.0	6.0	6.0	6.0	6.0
SO_3, max, %					
- When C_3A is 8% or less	3.0	3.0	3.5	2.3	2.3
- When C_3A is more than 8%	3.5	-	4.5	-	-
Loss on ignition, max, %	3.0	3.0	3.0	2.5	3.0
C_3S, max, %	-	-	-	35	-
C_2S, min, %	-	-	-	40	-
C_3A, max, %	-	8	15	7	5
C_4AF+2C_3A, max, %	-	-	-	-	25

Table 2.4: Physical Requirements for Different Cement Types (*ASTM C 150* 2002)

Physical Requirement	Cement Type				
	I	II	III	IV	V
Fineness, specific surface, m^2/kg					
- Turbidimeter test, min	160	160	-	160	160
- Air Permeability test, min	280	280	-	280	280
Time of setting					
- Gillmore test					
- Initial set, min., not less than	60	60	60	60	60
- Final set, min, not more than	600	600	600	600	600
- Vicat test					
- Initial set, min., not less than	45	45	45	45	45
- Final set, min, not more than	375	375	375	375	375
Heat of hydration a					
- 7 days, max., cal/g	-	70	-	60	-
- 28 days, max., cal/g	-	-	-	70	-

[a]This applies only when specifically requested.

2.1.2 Supplemental Cementitious Materials (SCMs)

Today SCMs, such as fly ash and slag, are widely used to replace part of OPC. The use of SCMs generally improves the concrete's properties, such as heat generation, workability, ultimate strength, impermeability, and durability. These improvements are due to the physical properties of the SCMs and also the Pozzolanic reaction, which will be described in detail later. Supplemental cementitious materials also reduce economic and environmental concerns by reducing carbon dioxide emissions and lowering energy requirements for OPC clinker production. Currently in Iowa, two types of SCMs are being used in pavement construction: fly ash and ground granulated blast furnace slag (GGBFS).

2.1.2.1 Fly Ash

Fly ash is a byproduct of modern power plants. During the burning of powdered coal, volatile matter and carbon burn off after the coal passes through the high-temperature zone in the furnace. Most of the mineral impurities, such as clays, quartz, and feldspar, will melt at the high temperature. The fused matter is solidified as spherical particles of glass as it is quickly transported to a low-temperature zone. Some of the mineral matter agglomerates form bottom ash; however, most of it flies out with the flue gas stream and is subsequently removed from the gas by electrostatic precipitators (Mehta et al. 1993).

Fly ash is typically finer than OPC and lime. The spherical particles, which typically range between 10 and 100 microns in size, improve the fluidity and workability of fresh concrete (Figure 2.2).

Minerals associated with the coal and the burning conditions affect the chemical compositions. Generally, anthracitic or bituminous coals give ashes high in glass, SiO_2, Al_2O_3, and Fe_2O_3 but low in CaO. However, ashes from sub-bituminous coals or lignites are higher in CaO and often higher in crystalline phases (Taylor 1997).

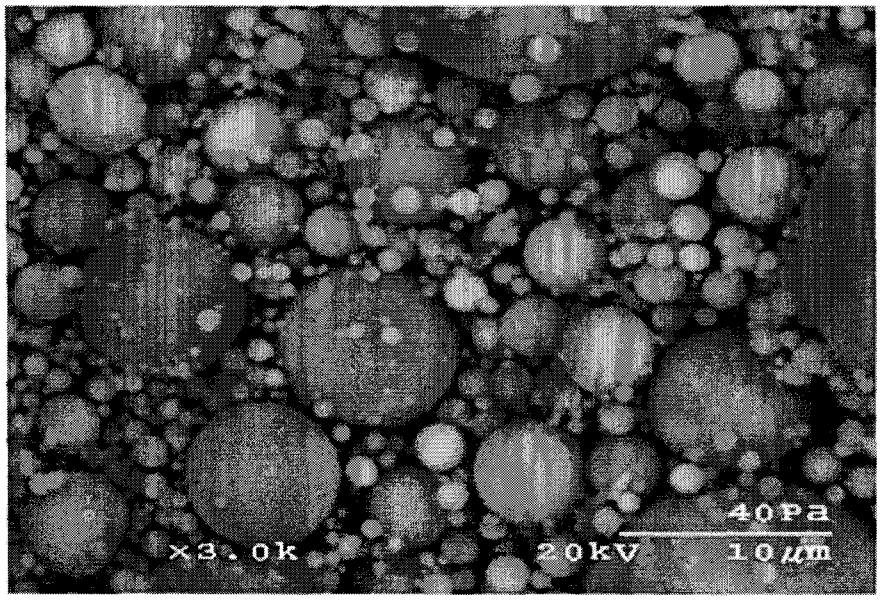

Figure 2.2: Fly Ash Particles at 3,000x Magnification

According to *ASTM C 618*, fly ash can be classified as Class F or Class C. Class F fly ash is normally produced from burning anthracite or bituminous coals. It typically contains less than 10% CaO. Table 2.5 presents some typical ranges of fly ash chemical composition. Class F fly ash possesses little or no cementitious value at low temperatures. However, in the presence of moisture, it can react with lime at ordinary temperatures to form cementitious compounds. Class C fly ash is normally produced from lignite or sub-bituminous coal. It typically contains more than 20% CaO. Class C fly ash has more cementitious properties in addition to pozzolanic properties. Different types of fly ashes have different effects on concrete strength development due to their different chemical compositions. As Figure 2.3 shows, Class C fly ash is more reactive. The long-term strength of concrete with fly ash could be higher than that of concrete without fly ash. The improvement in strength is caused by the pozzolanic reaction.

Table 2.5: Typical Range of Chemical Composition of Fly Ash (Roy et al. 1985)

Chemical Composition	Range of Chemical Composition (% by Weight)	
	Class F Fly Ash	Class C Fly Ash
SiO_2	38-65	33-61
Al_2O_3	11-63	8.0-26
Fe_2O_3	3.0-31	4.0-10
CaO	0.6-13	14-37
MgO	0.0-5.0	1.0-7.0
Na_2O	0.0-3.1	0.4-6.4
K_2O	0.7-5.6	0.3-2.0
SO_3	0.0-4.0	0.5-7.3

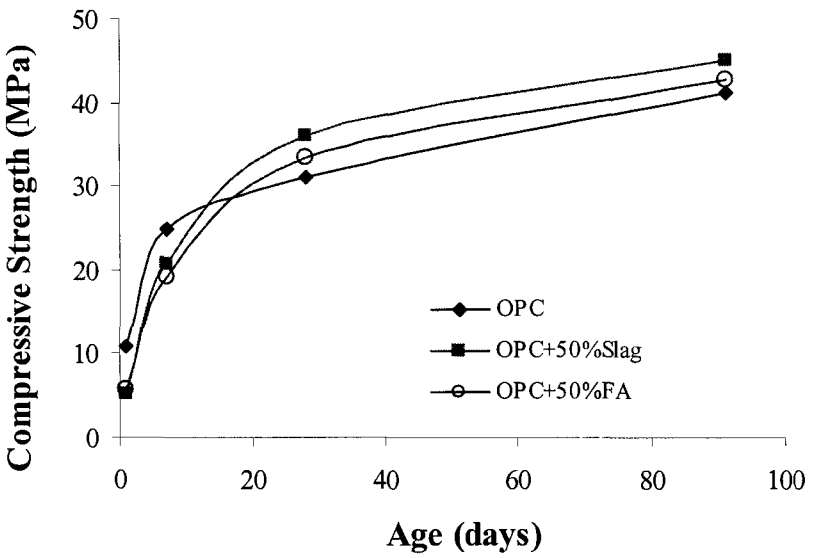

Figure 2.3: Effects of Different Fly Ash on Strength Development
(Data from Douglas and Pouskouleli 1991)

2.1.2.2 Ground Granulated Blast Furnace Slag (GGBFS)

Blast -furnace slag is defined in *ASTM C 989* as "the non-metallic product consisting essentially of silicates and alumina silicates of calcium and other bases that is developed in a molten condition simultaneously with iron in a blast furnace." In iron production, the blast-furnace is charged with iron ore, flux stone (limestone and dolomite), and coke for fuel.

Molten iron and slag are obtained from the furnace at 2700°F. The slag can be cooled in several ways to form different chemical compositions. If the slag is slowly cooled in air, the chemical components of slag are usually in the form of crystalline melilites. Crystal melilites do not react with water at ordinary temperatures. However, if the slag is rapidly quenched by water or the combination of air and water, the chemical compositions form noncrystalline or glassy states. The water-quenched product is called granulated slag due to the sand-sized particle. The slag quenched by air and a limited amount of water is called pelletized slag. Normally, granulated slag contains more glass. However, both products have satisfactory cementitious properties when ground to 400 to 500 m^2/kg (Mehta et al. 1993). Ground granulated blast furnace slag is classified as Grades 80, 100, or 120 depending on its mortar strength when blended with an equal mass of OPC. The hydraulic reactivity of slag is important for properties of the blended cement with slag. The reactivity is related to its physical and chemical compositions. Wang et al. (2004) found that the Al_2O_3 has a positive effect on the reactivity. However, the effect depends on CaO content (Figure 2.4). They suggested that the Al_2O_3 should be higher than 10.5% and the CaO content higher than 40% by mass. Figure 2.5 shows the effect of slag composition on the heat of hydration. The heat of hydration increases with rising Al_2O_3 and CaO content.

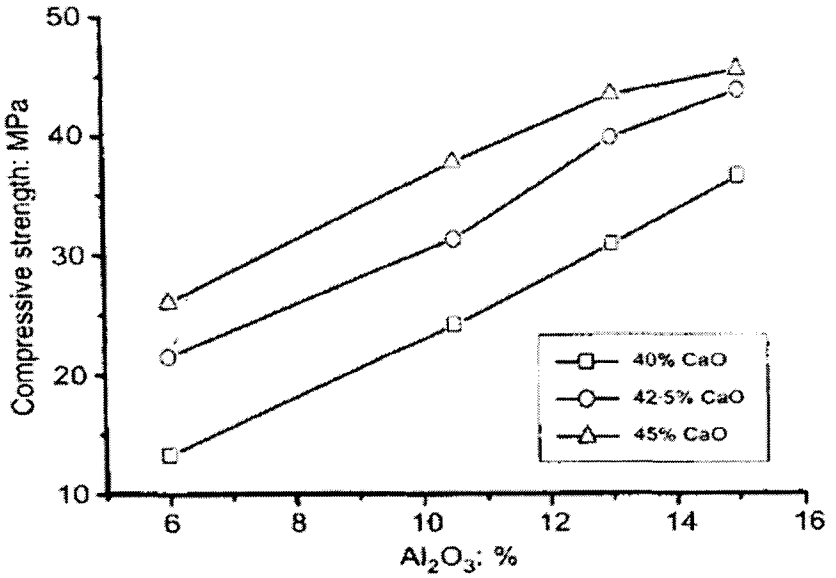

Figure 2.4: Effect of Al_2O_3 and CaO on the 28-day Compressive Strength (Adapted from Wang et al. 2004)

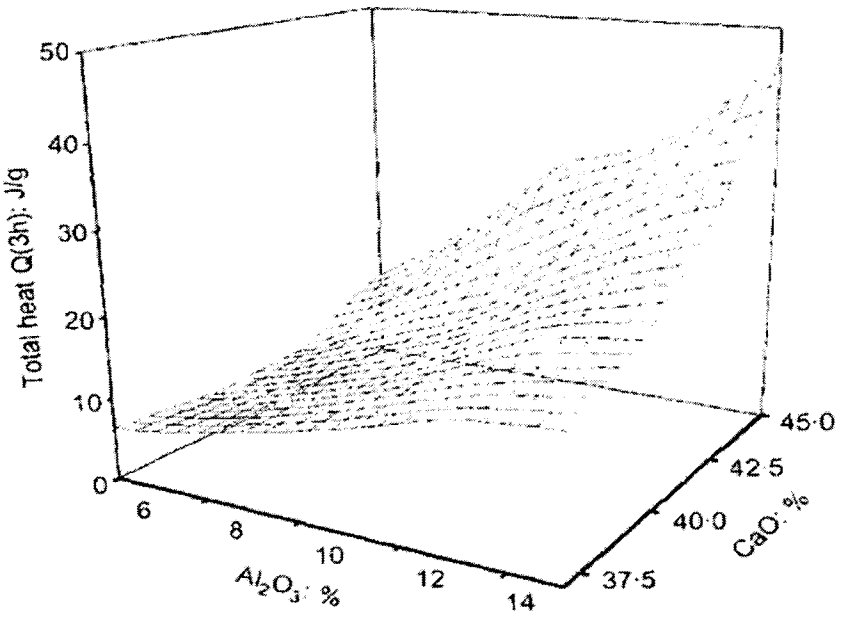

Figure 2.5: Effect of Al_2O_3 and CaO on Heat of Hydration
(Adapted from Wang et al. 2004)

Fly ash and GGBF slag share similarities in mineralogical character and reactivity and are essentially noncrystalline. The reactivity of the high-calcium glassy phase of fly ash and slag appears to be of a similar order. The particle size, characteristic, and composition of glass and glass content are the primary factors that determine the fly ash and slag's reactivity. The reactivity of the glass phase of fly ash and slag varies with the material's thermal history. When cooled at a higher temperature and a faster rate, glass has a more disordered structure and is more reactive.

2.2 Hydration of Portland Cement

The setting and hardening of concrete is caused by the chemical reaction between cement clinkers and water, and by the precipitation of hydration products, which form a hardened structure with porosity. Cement hydration is the key to concrete performance in terms of durability and strength. It is affected by several factors, such as cement type, fineness, w/c ratio, and SCM. These factors will be discussed below.

2.2.1 Portland Cement Hydration

The hydration process involves two types of reaction: through-solution hydration and solid-state hydration. Through-solution hydration involves dissolution of anhydrous compounds to their ionic constituents, formation of hydrates in the solution, and eventual precipitation of hydrates. Through-solution hydration dominates the early stage of hydration. Solid-state hydration occurs directly at the surface of the anhydrous cement compounds (Mehta et al. 1993).

To understand the chemistry of OPC hydration, it is necessary to first consider the hydration process of the cement clinker components. As mentioned earlier, the clinker is mainly composed of calcium silicates, aluminates, and aluminoferrites.

Calcium silicates include tricalcium silicate and dicalcium silicate. The hydration reactions of these two calcium delicates are stoichiometrically very similar (Equations 2.8 and 2.9). Their reaction products are calcium silicate hydrates (C-S-H) gel and calcium hydroxide. C-S-H gel, a poorly crystalline material, is the main binder of hardened OPC paste and is the principal contributor to early compressive strength development. The formula $C_3S_2H_3$ is only a rough approximation; different calcium silicate hydrates with different structures are formed during the process of hydration reaction.

$$2C_3S + 6H \rightarrow C_3S_2H_3 + 3CH \qquad 2.8$$

$$2C_2S + 4H \rightarrow C_3S_2H_3 + CH \qquad 2.9$$

Tricalcium aluminate (C_3A) reacts with sulfate ions from the dissolved gypsum. The final hydration products vary with the gypsum content. First, ettringite is formed (Equation 2.10) although it is stable only if there is enough sulfate available. After all of the gypsum is consumed by this reaction, the remaining C_3A will continue to react with the ettringite. In this case, monosulfoaluminate is formed (Equation 2.11). If a new source of sulfate is presented, monosulfoaluminate can convert back to ettringite. Tricalcium aluminate contributes little to the strength of OPC paste.

$$C_3A + 3C\bar{S}H_2 + 26H \rightarrow C_6A\bar{S}_3H_{32} \quad 2.10$$

$$C_3A + C_6A\bar{S}_3H_{32} + 4H \rightarrow C_4A\bar{S}H_{12} \quad 2.11$$

The hydration of tetracalcium aluminoferrite, C4AF, is similar to that of C3A. Two possible hydrates can form, depending on the availability of the gypsum (Equations 2.12 and 2.13).

$$C_4AF + 3C\bar{S}H_2 + 21H \rightarrow C_6(A,F)\bar{S}_3H_{32} + (A,F)H_3 \quad 2.12$$

$$C_4AF + C_6(A,F)\bar{S}_3H_{32} + 7H \rightarrow 3C_4(A,F)\bar{S}H_{12} + (A,F)H_3 \quad 2.13$$

The hydration process of a typical concrete mixture can be studied with a conduction calorimeter that measures the heat liberation rate of cement at a specific constant temperature. Figure 2.6 shows the typical hydration process. Several authors have identified five different stages of the hydration process (Byfors 1980, Mindess et al. 1981, and Nagashima 1992). The duration and detailed characteristics of these stages mainly depends on the clinker composition, the particle size distribution, the w/c ratio, the curing temperature, and the mineral and chemical admixtures (Van Breugel 1997).

Stage 1: This stage occurs immediately after contact with water. The rapid reactions, which show the high rate of heat generation, result from ions dissolving in water and reacting between C_3A and gypsum. The formation of ettringite slows down the reaction by creating a diffusion barrier around the C_3A. Some semistable phase of C-S-H is formed. Most of the time, ettringites are included in this phase, which lasts about 15 to 30 minutes.

Stage 2: Because the rate of hydration is very small and seems to be stagnant, this phase is known as the dormant period. During this phase, the concentration of ions in the solution gradually increases along with the solution of solid phase. The hydrates made of the main compounds, C_3S and C_2S, are not crystallized yet. This period generally lasts less than 5 hours.

Stage 3: Hydration proceeds actively where the rate of heat generation increases. Induced by the increase of the protection layer permeability and the beginning of C-S-H crystallization, this phase ends the dormant period.

Stage 4: The rate of heat generation gradually slows. In this phase, the thickness of the hydrate layer, which covers unhydrated particles, increases and the surface area of the unhydrated parts decreases. The layer of cement hydrates acts as the diffusion area, which governs the permeability of the water and dissolved ions.

Stage 5: The rate of hydration is remarkably reduced by the thicker layer of hydrates around the particles. Cement hydrates almost completely occupy the space originally filled by the water, making it difficult for hydrates to be precipitated. Stages 4 and 5 are known as the diffusion control phase.

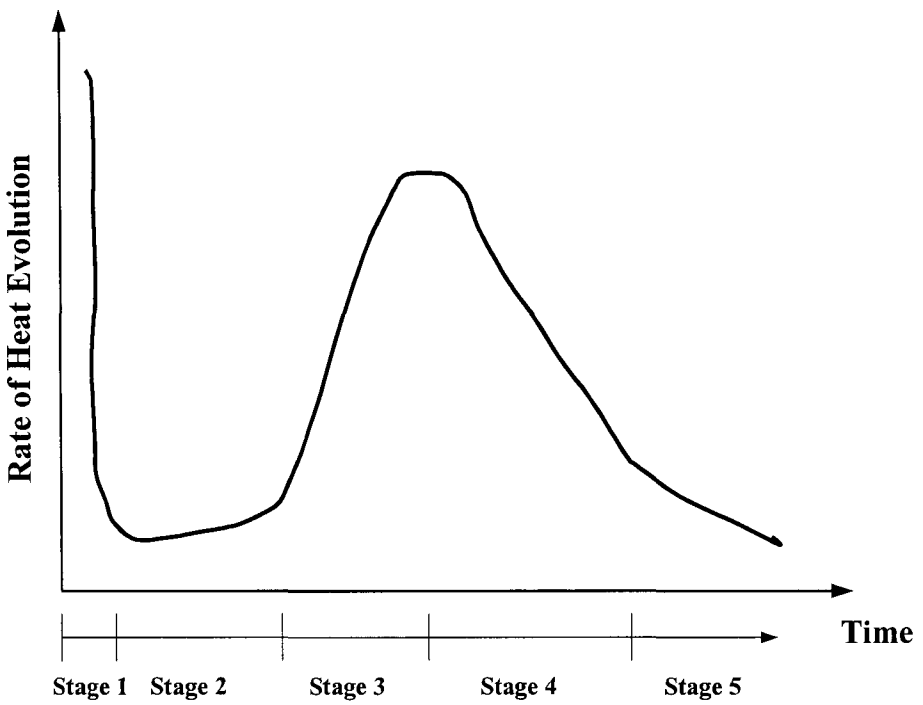

Figure 2.6: OPC Hydration Process

2.2.2 Factors that Influence Cement Hydration

Several factors, such as the cement type, the particle size distribution/fineness, the w/c ratio, the curing temperature, and admixtures affect the process of cement hydration. In this section, the effects of these factors will be discussed.

2.2.2.1 Cement Type

Cement hydration is an exothermic process. The temperature increase of concrete mainly depends on the cement hydration. The heat generation rates for different types of cement under the same condition, which can be measured as a rise in temperature, vary significantly. In Figure 2.7, the temperature rise for Type III cement is about 45°C. However, the increase for Type IV cement is only 25°C. The difference in heat generation rates for various cement is mainly due to the chemical composition and the cement fineness.

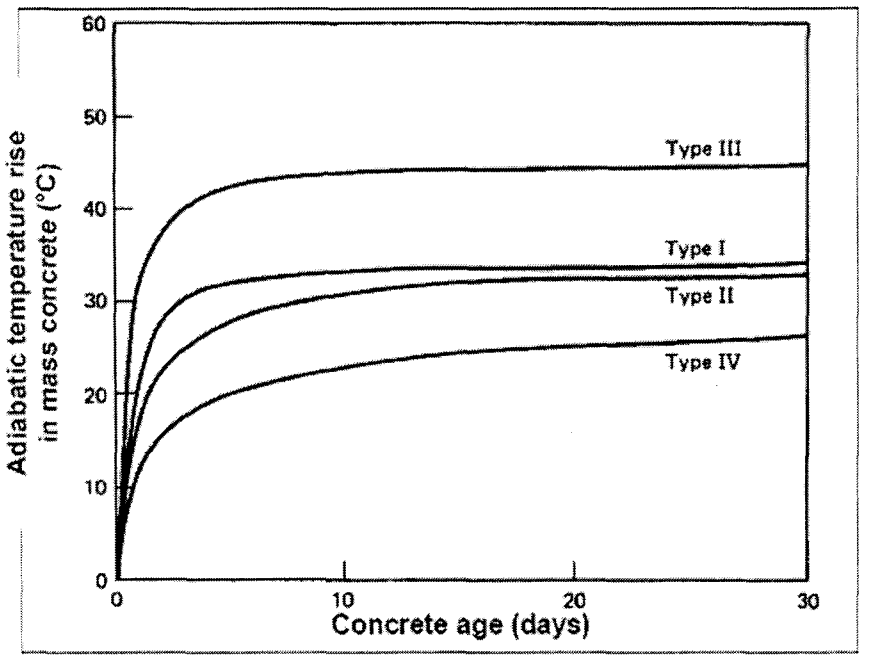

Figure 2.7: Temperature Increase of Mass Concrete Under Adiabatic Conditions (Adapted from Mindess and Young 1981)

The effect of chemical composition can be identified by evaluating the rate of hydration of the individual compound and its percentage in the cement. Each chemical

compound shows a different hydration rate and total liberated heat. The hydration characteristics of cement compounds are listed in Table 2.6. The rates of the pure cement compounds are given in Figure 2.8(a). It can be seen that C_3A reacts the fastest, followed by C_3S and C_2S. The presence of gypsum slows the early age reaction of C_3A. The hydration rate of the compounds in typical cement is plotted in Figure 2.8(b). The figures show that C_3S and C_2S react more rapidly than they do in their pure pastes. C_4AF falls between C_3S and C_2S. Both figures indicate that C_3A and C_3S are the most reactive compounds; their total liberated heat is also high.

Table 2.6: Hydration Characteristics of Cement Compounds

Compounds	Reaction Rate	Amount of Heat Liberated	Contribution to Cement Heat Liberation
C_3S	Moderate	Moderate	High
C_2S	Slow	Low	Low
$C_3A + C\bar{S}H_2$	Fast	Very High	Very High
$C_4AF + C\bar{S}H_2$	Moderate	Moderate	Moderate

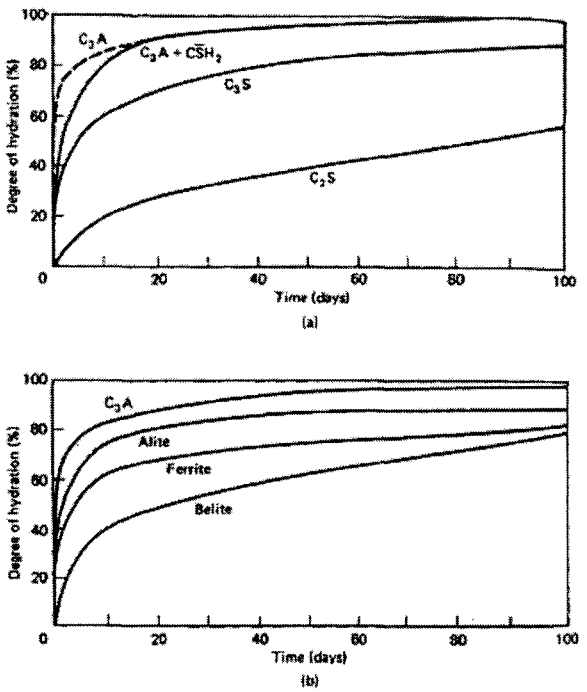

Figure2.8: Hydration Rate of the Cement Compounds: (a) in pastes of the pure compounds; (b) in a Type I cement paste (Adapted from Mindess and Young 1981)

Lerch and Bough (1934) studied the effect of C_3A and C_3S on the heat of hydration of pastes. Figure 2.9 indicates that C_3A content significantly increased the rate and amount of generated heat. The total heat is almost doubled when the C_3A increases from 0 to 20%. Regardless of the C_3A content, the reaction is stable after 16 hours. Figure 2.10 shows the effect of C_3S, which is similar to C_3A.

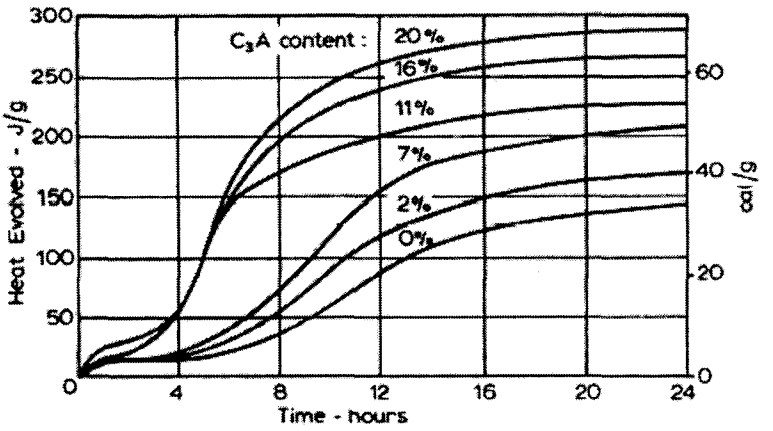

Figure 2.9: Effect of C_3A Content ($C_3S \approx$ constant) on Heat of Hydration (Adapted from Lerch and Bogue 1934)

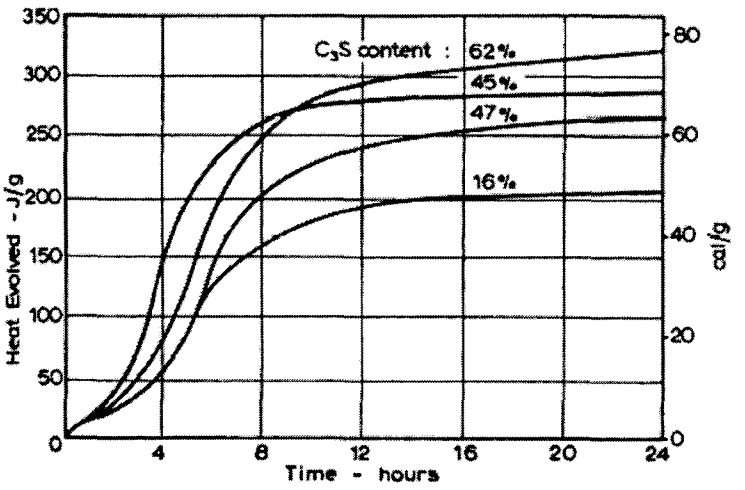

Figure 2.10: Effect of C_3S Content ($C_3A \approx$ constant) on Heat of Hydration (Adapted from Lerch and Bogue 1934)

2.2.2.2 Sulfate Content

During the final process of cement production, a small amount of gypsum is added and interground with the clinker to control the early reaction of tricalcium aluminate. Equations 2.10 and 2.11 describe these reactions. With a low or over dosage of sulfate, the cement will have false or flash set. The proper amount of sulfate required for cement varies with cement composition and fineness.

Lerch (1946) conducted a series of tests to study the effect of gypsum on hydration in terms of the heat liberation. He found that heat liberated in 30 minutes, was reduced by increasing SO_3 content regardless of the content of C_3A (Figure 2.11). This finding could be explained by the theory that alumina is less soluble in a lime-gypsum solution than in limewater (Lerch et al. 1929). Adding gypsum saturates the solution more quickly and the reaction of C_3A is retarded. Therefore, the heat of hydration is reduced.

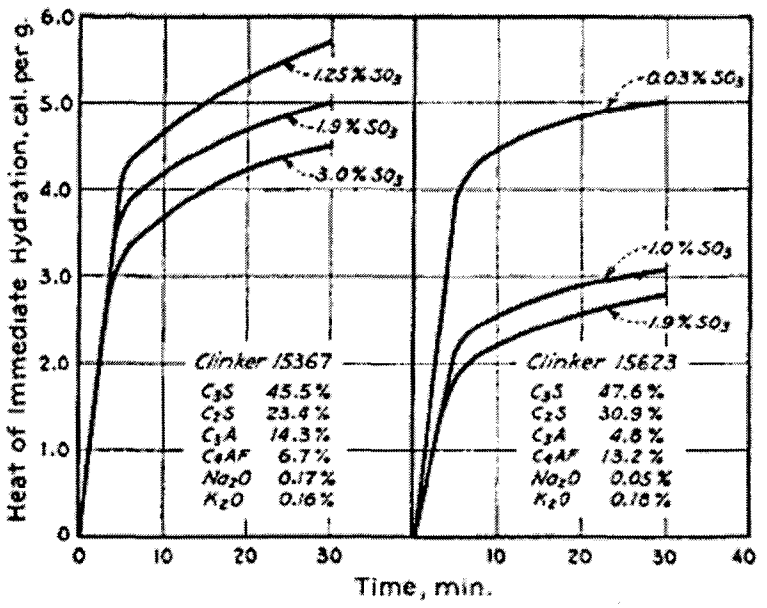

Figure 2.11: Heat of Immediate Hydration with SO_3 Varied
(Adapted from Lerch et al 1946)

2.2.2.3 Fineness

Fineness is another factor that can affect the hydration of cement. Fineness of cement affects the placeability, workability, and water content of a concrete mixture. It is normally

measured in terms of specific surface area. The average Blaine fineness of modern cement ranges from 3,000 cm^2/g to 5,000 cm^2/g. Although cement with different particle distribution might have the same specific surface area, the specific surface area is still considered to be the most useful measure of cement fineness.

Since hydration occurs at the surface of cement particles, finely ground cement will have a higher rate of hydration. It has a higher specific surface area, which means there is more area in contact with water. The finer particles will also be more fully hydrated then coarser particles. However, the total heat of hydration at very late ages is not significantly affected. Figure 2.12 shows how the fineness increases the early age heat of hydration for two different types of clinkers.

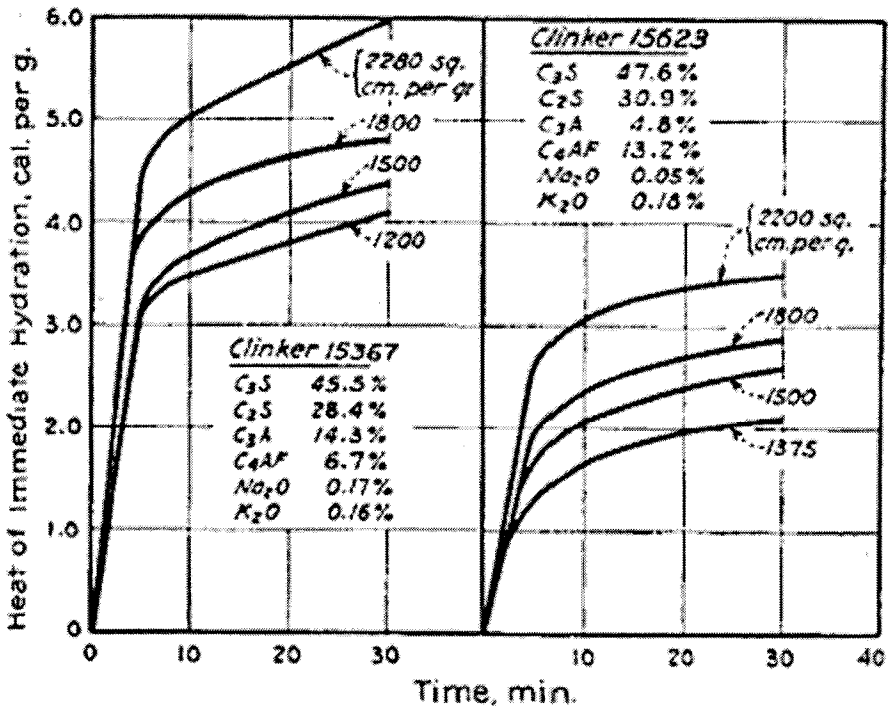

Figure 2.12: Heat of Hydration with Specific Surface Varied
(Adapted from Lerch et al. 1946)

2.2.2.4 Water/Cement (w/c) Ratio

An important aspect during hydration is the decrease in porosity. The precipitated hydration products, which have lower specific gravities and larger specific volumes, cause

cement grains to expand continuously as the hydration of cement proceeds. However, the volume of the hydration product is less than the total volume of the cement and water that reacted to form it. The hydration product will not fill the volume made available for it. If external water is available, the cement will hydrate continuously until either the cement is completely hydrated or until the available space within the paste is completely filled. Complete hydration of cement is generally assumed to require a w/c ratio of about 0.4 (Van Breugel 1997). According to Young et al., hydration will stop when the amount of water is not enough to form a saturated C-S-H gel. A minimum w/c ratio of 0.42 is required for complete hydration. If external water is not available, the cement will dry as hydration proceeds. Additionally, when the internal relative humidity drops below about 80%, hydration will stop.

Cement with a high w/c ratio has more water and microstructural space available for hydration of cement, which in turn results in a higher ultimate degree of hydration. Since the heat of hydration is directly related to the degree of hydration, the heat generation is affected by the w/c ratio (Figure 2.13). The rate of heat evolution at early ages is not significantly affected by the w/c ratio. However, consistent with the findings of Byfors (1980), the heat evolution rate starts to decrease as the w/c ratio decreases.

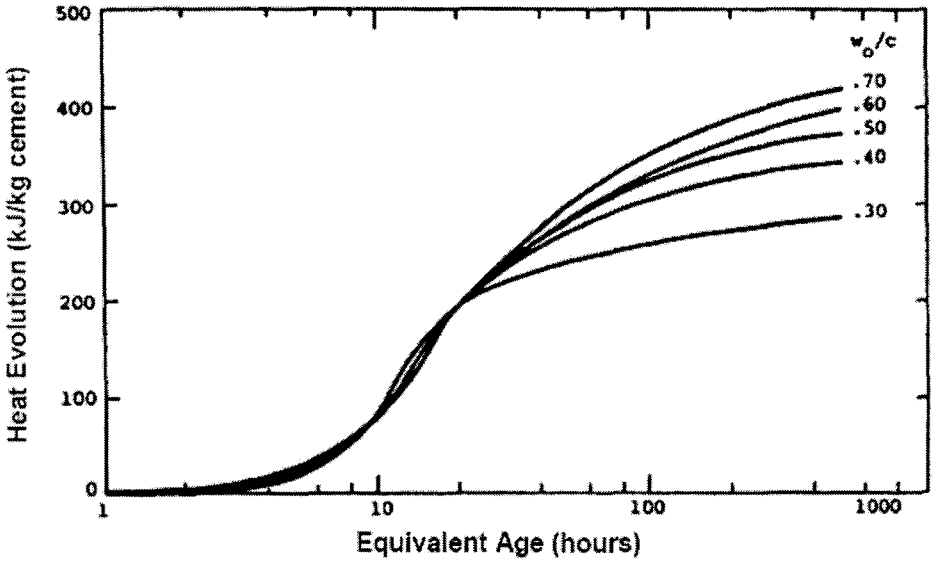

Figure 2.13: Effect of W/C Ratio on the Heat Evolution (RILEM 42-CEA 1981)

2.2.2.5 Curing and Initial Temperature

Normally, concrete pavement is cast from spring to fall. During this period, the environmental temperature is completely different. Therefore, the environmental temperature needs to be considered. A number of investigators have studied the effect of curing temperature on cement hydration (Figure 2.14). Cement hydration is accelerated at early ages under high environmental temperature but decelerated later on. The initial hydration under high temperatures forms "shell," a coat layer of hydration products on the surface of the cement particles, which delays the continuation hydration. The shell is denser with increasing temperature. Cement hydration under lower temperatures is generally higher than cement hydration under higher temperatures. Blended cement with fly ash is similar to OPC. The initial reaction temperature has a similar effect on the rate of cement hydration. The higher the initial reaction temperature, the higher the hydration rate at early age. However, at later age, the hydration under lower initial reaction temperatures could be higher.

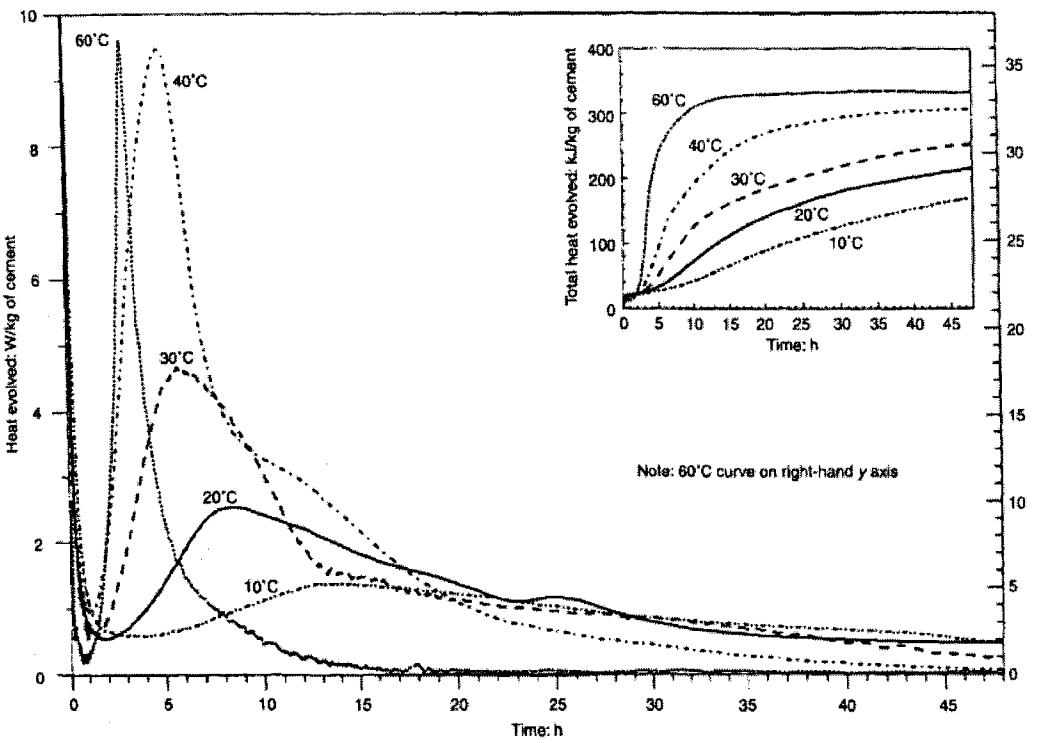

Figure 2.14: Effect of Curing Temperature on Hydration
(Adapted from Escalante-Garcia et al. 2000)

2.2.2.6 SCMS

Supplemental cementitious material concrete normally displays slow hydration, accompanied by low temperature, slow setting, and low early age strength. This effect is more pronounced as the proportion of SCMs in the blended cement increases and when the concrete is cured at a low temperature. The properties of the SCM concrete are caused by the reduction of the cement content and also by the Pozzolanic reaction. It is generally accepted that the silicate and aluminate phase of SCMs react with $Ca(OH)_2$ during cement hydration to form calcium silicate and aluminate hydrates (Lea 1970). This reaction is known as the Pozzolanic reaction (Equation 2.14).

$$S + CH + H \rightarrow CSH \qquad 2.14$$

The Pozzolanic reaction is slower than C_3S hydration; however, the reaction rate is similar to C_2S. As a result, the Pozzolanic reaction produces less heat than the cement hydration. The effect of Pozzolanic reaction on concrete strength will be discussed in Chapter 5.

Fly ash

Various researchers have studied the effect of fly ash on cement hydration. Crow et al. (1981) determined that adding a low-calcium fly ash reduces the heat of hydration of cement. Some high-calcium Class C fly ash with self-cementitious properties may react very quickly with water, releasing excessive heat just like normal OPC hydration (Joshi et al. 1997). The total heat of hydration of fly ash normally depends on the content of CaO. Schindler (2003) recommended the total heat be equal to 1,800 times the percent of CaO. Figure 2.15(a) shows that the addition of fly ash not only decreases the maximum heat generation rate but also postpones the peak of hydration. As the fly ash ratio increases, the peak becomes wider. Figure 2.15(b) shows that the retardation of cement hydration mainly occurs during the dormant and acceleration periods. When cement-fly ash cement mixes with water, the Ca^{2+} ion in pure solution is removed by the fly ash, which reacts like a Ca sink. The depressed $Ca2^{+}$ concentration delays the nucleation and crystallization of CH and C-S-H, retarding hydration (Langan et al. 2002).

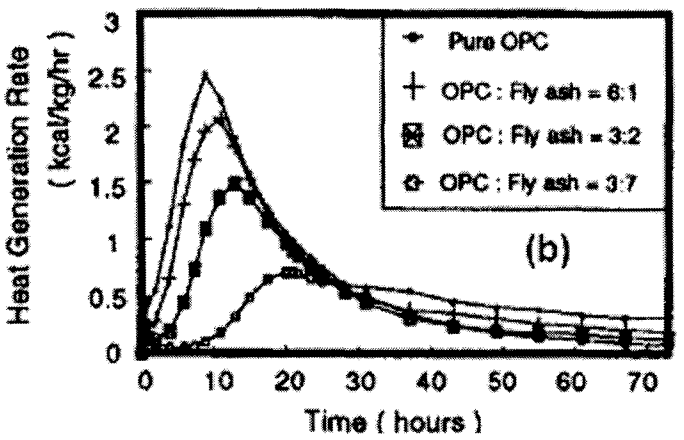

(a)

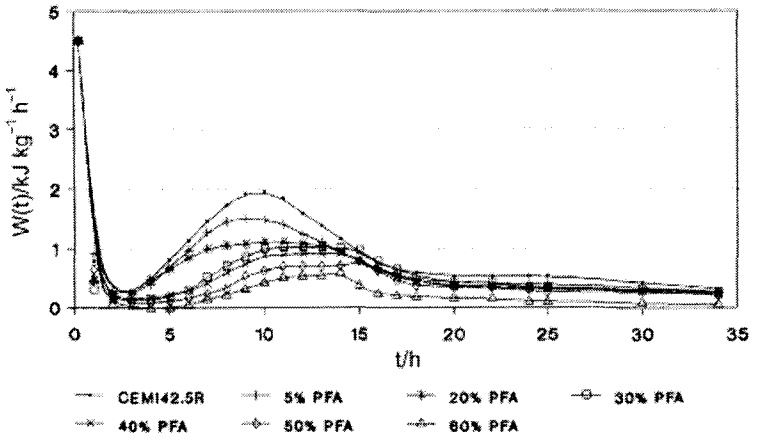

(b)

Figure 2.15: Effect of Fly Ash on Heat Generation: (a) Class F Fly Ash (Adapted from Kishi and Maekawa 1995); (b) Class C Fly Ash (Adapted from Nocuñ-Wczelik 2001)

GGBF slag

Figure 2.16 shows the effect of different levels of slag on the heat generation ratio. There are two peaks for slag-blended cement; the first is caused by cement hydration and the second is due to slag reaction. The slag-blended cement reaches the first peak at the same time as the pure OPC, indicating that adding GGBF slag into concrete will not delay the reaction of cement. The second peak is unaffected by the amount of replacement slag. Kishi et al.(1994) explained that the slag can react independently as long as sufficient Ca(OH) is released from the cement hydration.

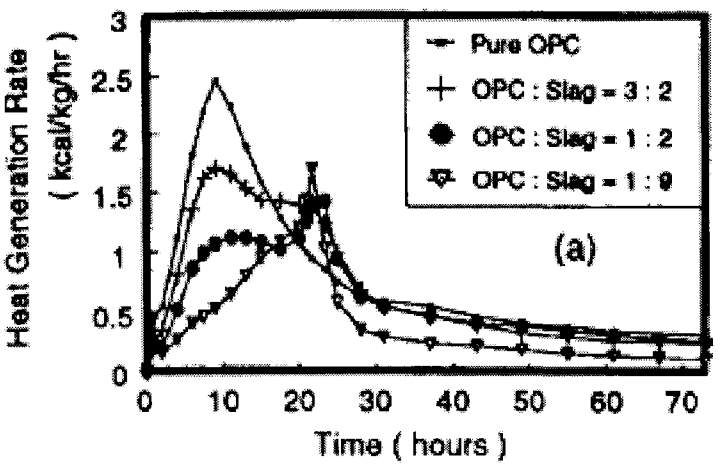

Figure 2.16: Effect of Slag on Hydration (Adapted from Kishi and Maekawa 1994)

However, Hogan and Meusel (1981) found that the setting time of slag-blended cement is delayed; there is a 10- to 20-minute delay for each 10% addition of slag. On the other hand, Uchikawa (1986) found that the peak of cement hydration was accelerated, due to the finely ground slag's consumption of Ca^{2+} in the liquid phase, when the fineness of the slag was increased (Figure 2.17).

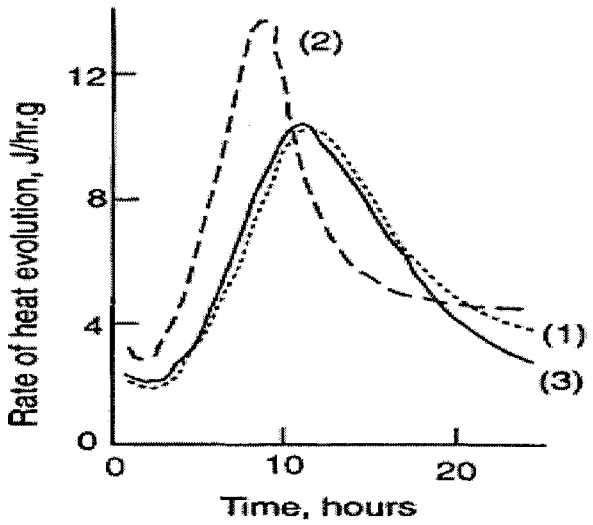

Figure 2.17: Heat Evaluation at 20°C,
(1) 40% coarse slag (400 m^2/Kg) (2) 40% fine slag (592 m^2/Kg) (3) OPC
(Adopted from Uchikawa ,1986)

Ma et al. (1994) studied the hydration of blended cement containing 65% slag at different temperatures ranging from 10°C to 55°C. In this study, the total heat of blended cement during the first 20 hours was significantly reduced. The test results also showed that temperatures less than 40°C have little effect on the total heat. However, the total heat increases rapidly with temperatures above 40°C (Figure 2.18). Consistent with the findings of Klierger et al. (1994)., these results indicate that the slag-blended cement has low reactivity at room temperature and is strongly heat activated.

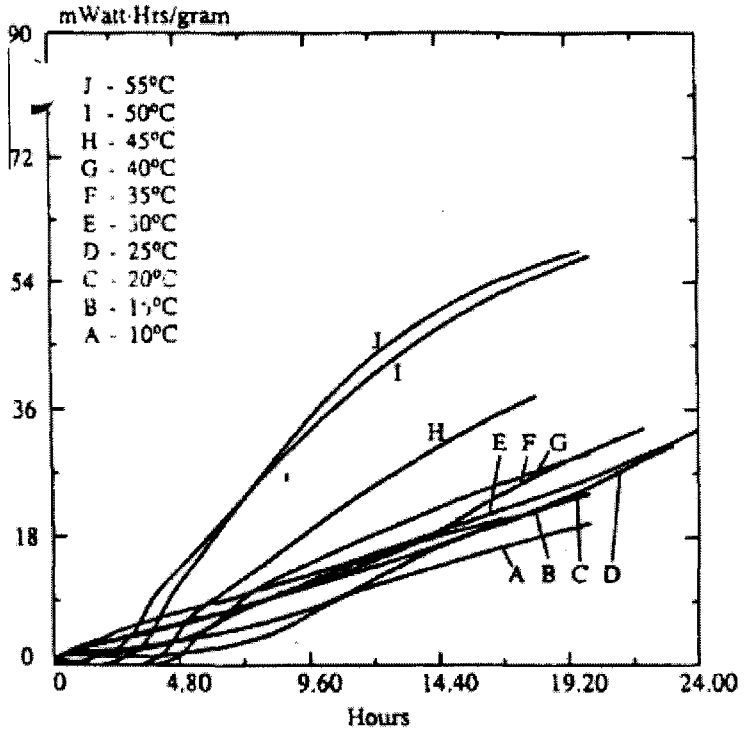

Figure 2.18: Total Heat of Blended Cement with Slag at Different Temperatures (Adapted from Ma et al. 1994)

2.2.2.7 Chemical Admixture

Chemical admixture is added to modify the setting time and reduce the water requirement of the concrete mix. Chemical admixtures may significantly change the cement hydration rate, and therefore, the heat generation. *ASTM C 494* classified the chemical admixtures into the following seven types:

Type A—Water-reducing

Type B—Retarding

Type C—Accelerating

Type D—Water-reducing and retarding

Type E—Water-reducing and accelerating

Type F—Water-reducing high range

Type G—Water-reducing, high range, and retarding

Water reducers are defined as admixtures that decrease the requirement of water to achieve a given workability. They sometimes accelerate or retard the concrete setting. When a water reducer is used without changing the mix proportion, the heat of hydration and temperature rise of concrete at early age may increase. Using a water reducer can decrease the cement content at a given strength and slump, which in turn results in the reduction of heat generation and temperature rise (Massazza et al. 1980).

Retarder is an admixture that delays the setting and initial hardening of concrete. The ingredients of the retarder are similar to that of the water reducers. Ben-Bassat (1995) states that "the heat of hydration and temperature rise of concrete containing retarder are less at early age, and they are equal at about 3-7 days."

Accelerator is used to speed up the strength gain at early ages and reduce the setting time. Accelerating admixtures are normally used in a cold environment or where the early gain of strength and short setting time are required. An accelerator can increase the rate of heat evolution at the setting stage. Depending on the chemical composition of the accelerators, the rate of heat liberation in the hardening stage may also increase (Nagataki 1995).

High-range, water-reducing agents (superplasticizers) are a new class of water-reducing agents. The workability of high-range, water-reducing agents increase more often than normal water-reducing agents. The use of superplasticizers mildly retards the setting of concrete, which in turn can reduce the heat generation in the setting period. However, superplasticizers do not affect the total heat of concrete.

2.3 Measurements for Cement Hydration

2.3.1 Calorimetry

The heat of hydration is commonly determined by the dissolution method or calorimeters. The three types of commonly used calorimeters are adiabatic, semi-adiabatic, and isothermal. The heat of hydration can also be determined according to *ASTM C 186, Standard Test Method for Heat of Hydration of Hydraulic Cement*. The advantage of this method is that it can be used for samples at any age. However, it can only be used for paste samples.

It is impossible to achieve an adiabatic environment. However, the calorimeter is considered to be adiabatic as long as the temperature loss of the sample is not greater than 0.02 K/h. The heat loss is prevented by controlling the temperature of the surrounding environment with insulating materials such as water, air, and heated containers. Water is the most popular insulating material.

Adiabatic heat measurements are most convenient for producing a continuous heat of hydration curve under curing conditions close to mass curing. Also, adiabatic hydration curves are the most suitable starting points for temperature calculation in hardening structures. One major drawback of an adiabatic calorimeter is that the effect of the curing temperature on the rate of hydration is measured implicitly. The activation energy is required to convert the results to the thermal reference temperature. The results can also be affected by the assumption of the thermal properties of the materials. The advantage is that the heat evolution of an actual concrete mixture can be determined.

Ballim (2004) conducted the adiabatic calorimeter test to obtain the rate of heat evolution and used this as an input to calculate the mass concrete temperature. De Schutter et al. (1995) and Tanaka et al. (1995) performed adiabatic tests to estimate the heat of hydration of blast furnace slag blended cement.

The semi-adiabatic calorimeter is similar to the adiabatic calorimeter, but it allows a certain amount of heat loss to the environment. The maximum heat loss should be less than

100 J/(h·K). The calculated adiabatic curve from the semi-adiabatic test is lower than the curve from the true adiabatic test because the temperature development in semi-adiabatic tests is lower due to heat loss. The semi-adiabatic method is suitable for pastes, mortars, and concrete samples. It is widely used for determining the heat signature of concrete.

Isothermal calorimeters are usually used for paste samples. These tests are conducted at a constant temperature. The heat of cement hydration is directly measured by monitoring the heat flow from the specimen. The total heat evolution can be determined by summing the measured heat over time. The disadvantage is that the duration of this test is normally limited to 7 days due to the signal sensitivity limitations. Beyond this point, it is hard to distinguish the signal from its background. Also, isothermal tests do not consider the cement reactivity change due to the temperature change. It is hard to predict the temperature increase of concrete from these results, since the conditions in the real structure where the temperature continually changes are not reflected.

Isothermal calorimeters are more widely used for studying the kinetic reaction of pure cement pastes. Many researchers have applied this method to study the cement heat signature. Ma et al. (1994) conducted isothermal calorimeter tests to study the hydration behavior of blended cements containing fly ash, silica fume, and GGBFS over the temperature range of 10°C to 55°C. The relationship between the blended cement reactivates and the curing temperature were established. Xiong and Van Breugel (2001) used the 3114/3236 TAM Air isothermal calorimeter to determine the kinetics of cement hydration processes at different temperatures and applied the results to the numerical simulation model. Some other researchers also used this method to determine cement's activation energy.

RILEM conducted the "Round Robin" test program to compare the performance of different types of calorimeters. Fourteen different organizations participated in the program to compare the adiabatic curves and the predicted adiabatic temperature curves from semi-adiabatic calorimeters and to find the main factors that affect the results from different calorimeters. The same materials and mixing proportions were used in all tests. For the adiabatic test, the organizations found that 50% of the adiabatic temperature rise variations

are in a narrow range of only 2K and that the specimen size and the temperature do not significantly affect the temperature rise. For the semi-adiabatic test, the mean temperature rises are 2% to 3% below the results from the adiabatic tests, indicating that the semi-adiabatic calorimeter could be used to predict the adiabatic temperature rise. Table 2.7 shows the summary of the test data.

Table 2.7: Variability of Adiabatic and Semi-Adiabatic Test Results (Adapted from Morabito 1998)

	Rise After 24 Hours		Rise After 48 Hours		Rise After 72 Hours	
	Adiabatic	Semi-adiabatic	Adiabatic	Semi-adiabatic	Adiabatic	Semi-adiabatic
Mean values (K)	36.7	35.9	43	41.6	44.7	44.6
Highest variability	+8.9%	+4.8%	+6.9%	+5.8%	+6.3	+4.4%*
Lowest variability	-13.2%	-12.5%	-10.3%	-12%	-9.6%	-4.8%*

*Calculated on four tests

Except for the three calorimeters discussed above, other simple tests are used to test the sample temperature. These tests include the coffee cup, Dewar, and bucket.

Coffee cup is an easy test to conduct with past samples. Together with the thermalcouple, it gives the temperature of the test samples and reference sand. The temperature difference and shape of the curves are analyzed. It is a good method to check the compatibility of materials and it works well for the SCM or admixtures with cement.

The Dewar test can test the temperature development over time for different sized samples. The size of the sample depends on the size of the dewar. The quality of the insulation could vary for different dewars. The Dewar test is easy and cheap, but it can only provide the temperature. Lafarge uses the bucket to test the temperature history of a concrete sample. A 4x8 sample, surrounded by insulation, is used in the test. The temperature is recorded over time using the thermocouple.

2.3.2 Maximum Heat of Hydration

One of the important characteristics of the cement hydration process is the maximum heat of hydration. The total amount of heat measured at a macro level is the sum of the chemical reaction and the heat of adsorption. The latter is about 2.5% of the total heat. The heat of completed cement hydration can be determined from the cement clinker composition, based on the assumptions that the heats of hydration of the individual constituents are known and the superposition of the individual heats of hydration are justified. Table 2.8 lists the values of the specific heat liberated from each individual compound. Since the equation from Lerch and Bogue (1934) considers the heat generated from free CaO and also MgO, these values are used in this study.

Table 2.8: Specific Heat of Hydration of Individual Compounds

Reference	C_3S	C_2S	C_3A	C_4AF	Free C	MgO
Woods(1932)	570	260	840	125	-	-
Bogue(1929)	500	260	866	125	-	-
Lerch and Bogue (1934)	500	260	866	420	1166	850
Thorwaldson(1930)	-	-	-	1166	-	-
Adam(1976)	-	-	500/	170/	840	-
	-	-	630	290	1256	-
Newkirk(1952)	560	1360	300	-	-	-

2.3.3 Degree of Hydration

2.3.3.1 Degree of Cement Hydration at Time t

The term "degree of hydration" is used to describe the extent of the hydration process and defined as the ratio between the amount of cement that has reacted at time t and the original cement amount. The degree of hydration can be indicated or approximated by several parameters: liberated heat of hydration, amount of chemically bound water, chemical shrinkage, amount of Ca(OH), specific surface of the cement paste, strength, and dielectric properties of the cement. Among these parameters, liberated heat and amount of chemically

bound water are used most often to indicate the degree of hydration. These parameters define the degree of hydration as follows:

$$\alpha(t) = \frac{H(t)}{H_{total}} \qquad 2.15$$

$$\alpha(t) = \frac{W_n(t)}{W_{n\,total}} \qquad 2.16$$

Where, H (t) is the heat generated at time t, H_{total} is the total amount of heat that can be liberated, $W_n(t)$ is the chemically bounded water at t, and $W_{n\ total}$ is the total amount of chemically bounded water.

In this study, the degree of hydration is defined as Equation 2.15. This concept has been used since the early 1930s (Lerch et al. 1948). Parrott et al. (1990) found that there is an excellent linear relationship between the degrees of hydration and heat liberation. On the other hand, Brown et al. (1985) reported discrepancies between these two.

2.3.3.2 Ultimate Degree of Hydration

The total cement hydration requires a w/c ratio of 0.42. However, cement with normal fineness cannot reach 100% hydration at a normal w/c ratio even in a 100-year period (Young 1981). Under site condition curing, the 28-day degree of hydration of ordinary concrete falls between 0.6 and 0.8. Roy et al. (1982) found a degree of hydration of 0.7 in a 10-year cement paste.

Two factors govern the extent of the ultimate cement hydration:

- Space available for deposition of hydration products
- Amount of water available for the reaction with the cement

Cement hydration ends once there is no space for depositing hydration products. The available space decreases as the w/c ratio decreases. Under this condition, the ultimate degree of hydration can be expressed as follows:

$$\alpha_u = \frac{w/c}{0.36} \leq 1.0 \qquad 2.17$$

The complete hydration of cement is generally assumed to require a w/c of 0.42. In the case of sufficient free water, Hansen (1986) estimated the ultimate degree of hydration using the following equation:

$$\alpha_u = \frac{w/c}{0.42} \leq 1.0 \qquad 2.18$$

By considering these factors, Mills (1966) was able to perform numerous tests to determine the ultimate degree of hydration. He measured the chemically bound water after hydration was complete. From these tests, he suggested the following equation for the ultimate degree of hydration:

$$\alpha_u = \frac{1.031 \cdot w/c}{0.194 + w/c} \qquad 2.19$$

This equation better estimates the ultimate degree of hydration actually reached in practice. However, this equation does not consider the type of cement and the fineness. The finer the cement, the higher the ultimate degree of hydration will be.

2.4 Concrete Maturity

As discussed above, the cement hydration process depends on the curing temperature and on time. Concrete hydration is the key for other properties. For a given mixture, concrete strength is a function of the time and thermal history. The concept of maturity is introduced to account for the effect of temperature and time on cement hydration and also the development of concrete mechanical properties.

2.4.1 Nurse-Saul Maturity

The concept of concrete maturity was developed in the late 1940s and early 1950s. Saul (1951) pointed out that "Concrete of the same mix at the same maturity has approximately the same strength whatever combination of temperature and time to make up

that maturity." This is known as the "maturity rule." The maturity function can be expressed as follows:

$$M = \sum_{0}^{t} (T - T_0)\Delta t \qquad 2.20$$

Where

M = Maturity at time t (It is also called the temperature-time factor.)

T = Average temperature of the concrete during time interval Δt

T_0 = Datum temperature

This equation has become known as the Nurse-Saul function. A value of –10°C (14°F) has been recommended for the datum temperature in this equation. When a concrete sample was cured under the datum temperature, the cement hydration and strength gain stopped. The datum temperature could be different for different cement and also could be affected by the adding of SCMs.

2.4.2 Equivalent Age Maturity

Later Rastrup (1954) and McIntosh (1956) introduced the concept of equivalent age. Equivalent age represents the time at a specified temperature that is required to produce maturity equal to the maturity achieved by a curing period at temperatures different from the specified temperature, which is normally 20°C. They modified the Nurse-Saul maturity function as follows:

$$M = \int_0^t K(T)dt = \int_0^{teq} K(T_{ref})dt = K(T_{ref})t_{eq} \qquad 2.21$$

$$t_{eq} = \int_0^t \frac{K(T)}{K(T_{ref})}dt = \int_0^t f(T)dt \qquad 2.22$$

Where

K(T) = Rate constant at temperature T

$K(T_{ref})$ = Rate constant at the isothermal reference temperature T_{ref}

T_{ref} = Reference temperature, normally 20°C

t_{eq} = Equivalent age

f(T) = Age conversion factor at temperature T

Several expressions have been proposed for the rate constant K(T). Copeland et al. (1962) suggested the Arrhenius law (Equation 2.23) for quantifying the effect of temperature on the early rate of cement hydration.

$$K(T) = A\exp(-\frac{E}{RT}) \qquad 2.23$$

Where

A = Constant of proportionality

E = Activation energy (J/mol)

R = Universal gas constant, 8.314 J/(mol K)

T = Absolute reaction temperature (°K)

Based on the Arrhenius law, the equivalent age t_{eq} could be expressed as follows:

$$t_{eq} = \int_0^t \frac{K(T)}{K(T_{ref})}dt = \int_0^t \frac{A\exp(-\frac{E}{R(273+T)})}{A\exp(-\frac{E}{R(273+T_{ref})})}dt \qquad 2.24$$

$$= \int_0^t \exp(-\frac{E}{R}(\frac{1}{273+T} - \frac{1}{273+T_{ref}}))dt$$

Equation 2.24 indicates that the age conversion factor f(T) in Equation 2.22 is a nonlinear function. The exact value of the age conversion factor at different temperatures depends on the value of E. Freiesleben Hansen, and Pedersen (1985) proposed the activation

energy for OPC based on strength tests. These values represent a number of Danish cements as well.

For $T \geq 20°C$

$$E = 33{,}500 \text{ J/mol} \tag{2.25}$$

For $T < 20°C$

$$E = 33{,}500 + 1{,}470\ (20\text{-}T) \text{ J/mol} \tag{2.26}$$

Figure 2.19 shows the calculated age conversion factors at different temperatures, using the different activation energy levels of 30, 45, and 60 KJ/mol and the activation energy proposed by Freiesleben Hansen, and Pedersen. The reference temperature is 20°C. At the reference temperature, all of the values are equal to one regardless of the activation energy. At the highest temperature, the age conversion factor becomes more nonlinear with high activation energy. At the lowest temperature, all of the values are smaller than one. The higher the activation energy, the higher the age conversion factor is. Therefore, it is important to select the right activation energy to predict the equivalent age of the specific concrete mixture.

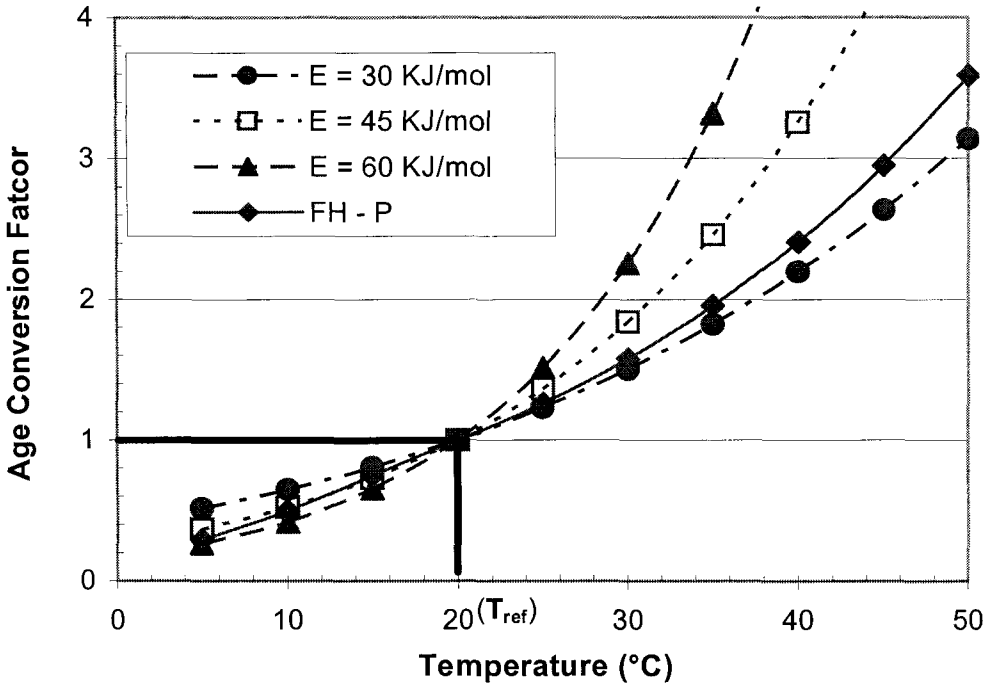

Figure 2.19: Effect of Activation Energy on the Age Conversion Factor

2.4.3 Activation Energy

The activation energy is regarded as the energy barrier to the chemical reaction. When the collision happens between the cement and water molecules, only molecules with kinetic energy higher than the activation energy can react. In the case of concrete, the activation energy is referred to as "apparent" because cement hydration involves several simultaneous and coupled chemical reactions. The characteristics of the individual mix, including cement composition, fineness, and mineral admixtures, influences the apparent activation energy (Ea). The w/c ratio may also have an effect on Ea. Carino (1984) initially found that the w/c ratio has little effect on Ea, except possibly for very low ratios. However, his later study with Tank (1992) showed that the Ea was dependent on the w/c ratio for several mix combinations. Kjellsen et al. (1993) and D'Aloia et al. (2002) also pointed out that Ea is dependent on the degree of hydration and it decreases at later age.

The apparent activation energy E_a could be determined in several ways. One of them is the strength test. This method is described in *ASTM C 1074 Standard Practice for*

Estimating Concrete Strength by the Maturity Method. Concrete specimens are made and cured at several different temperatures. The strength age data is analyzed to obtain the activation energy. Recently calorimetric approaches have been proposed to determine E_a. It has been confirmed that E_a obtained based on heat of hydration is similar to E_a based on *ASTM C 1074*. Wirquin et al. (2002) shows that "calorimetric and mechanical means give very similar E_a values as the observed differences are close to 3 KJ/mol. The E_a determined by the method of "superposition" on the basis of the calorimetric results may legitimately be used to predict the strength of young concrete." Table 2.9 shows the activation energy values from different researchers. The values from the chemical shrinkage method are higher than other values. The values of Type I cement are close to the *ASTM 1074* recommended value, which is 40 to 45 KJ/mol. Table 2.9 also indicates that the replacement of cement with GGBFS increases the activation energy. On the other hand, fly ash reduces the activation energy.

Some literature also suggests that the activation energy should change with curing temperature. Below, RILEM (1998) recommends the activation energy for OPC and slag cement. The same value for slag cement is recommended regardless of the percentage of slag replacement.

For OPC

$$\frac{E_A}{R} = \begin{cases} 4000 \quad J/mol & for \quad T \geq 20^0 C \\ 4000 + 175(20 - T) \quad J/mol & for \quad T \geq 20^0 C \end{cases} \qquad 2.27$$

For slag cement

$$\frac{E_A}{R} = 6000 \text{ J/mol} \qquad 2.28$$

Table 2.9: Activation Energy from Literature

CEMENT	SPECIMEN	TYPE OF TEST	EA (KJ/MOL)	REFERENCE
TYPE I	MORTAR	STRENGTH	42	CARINO 1981
TYPE I	MORTAR	STRENGTH	44	CARINO 1984
	CONCRETE		41	
OPC	PASTE	HEAT OF HYDRATION	42-47	GAUTHIER ET AL. 1982
OPC+70% BFS[A]			56	REGOURD ET AL. 1980
OPC	PASTE	CHEMICAL SHRINKAGE	61	GEIKER 1983
RHC[B]			57	
OPC	PASTE	CHEMICAL SHRINKAGE	67	GEIKER AND KNDSEN 1982
TYPE I/II	PASTE	HEAT OF HYDRATION	44	ROY ET AL. 1982
TYPE I/II+50%BFS			49	
TYPE I	PASTE	HEAT OF HYDRATION	39	MA ET AL. 1994
TYPE I+17% F FA[C]			26.7	
TYPE I+65%BFS			49.3	
OPC	CONCRETE	HEAT OF HYDRATION	38.4	WIRQUIN ET AL. 2002
		STRENGTH	35.6	
OPC + SUPERPLASTICIZER	CONCRETE	HEAT OF HYDRATION	39.3	
		STRENGTH	37.5	
TYPE I +15%FA[C]	MORTAR	STRENGTH	26.58	WANG ET AL. 2003
TYPE I +15%FA[C]+20%BFS[A]			32.9	

[a]GGBFS, [b]Rapid-hardening cement, [c]Fly ash

Xiong and Van Breugel (2001) proposed an expression (Equation 2.29) based on the isothermal calorimetry study and stated that "numerical simulation using HYMOSTRUC with this form of activation energy agrees quite well with experimental adiabatic data, especially at early age. The significant change in the value of Ea may suggest a change in the mechanisms of the hydration processes."

$$E_a[\alpha(t),T] = (44.92 - 0.043 \times T) \times \exp(-0.00017 \times T) e^{-\alpha(t)} \text{ KJ/mol} \qquad 2.29$$

Most E_a tests are performed using the mortar of past samples. Carino and Tank (1992) conducted an extensive study on activation energy using both mortar and concrete containing different materials and also two different w/c ratios. According to his study, the activation of a concrete mixture could be obtained form the mortar samples. Figure 2.20 shows the relationship of activation energy between the concrete and mortar samples.

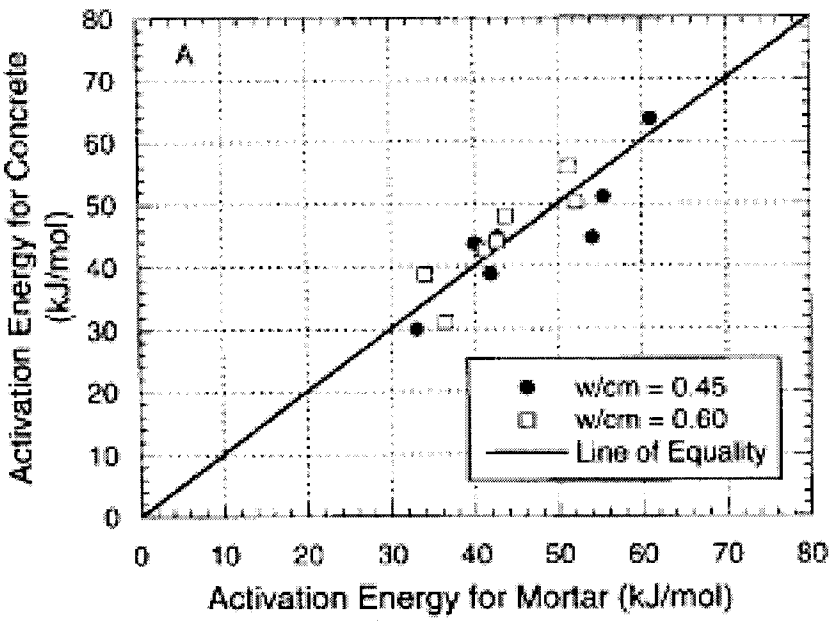

Figure 2.20: Activation Energy from Concrete and Mortar Tests (Carino 2004)

2.4.4 Maturity and Strength

Figure 2.21 shows the test results of previous work. The development of compressive strength has been determined under different curing temperatures (Figure 2.21(a)). The

maturity function, equivalent age, was applied to account for the effect of temperature. Figure 2.21(b) shows that the equivalent age is able to account for the sample's thermal history. Despite the different curing conditions, the compressive strength is almost the same at the same equivalent age. This figure also demonstrates that maturity can be used as a nondestructive method to predict in situ concrete strength, which will be discussed in Chapter 6.

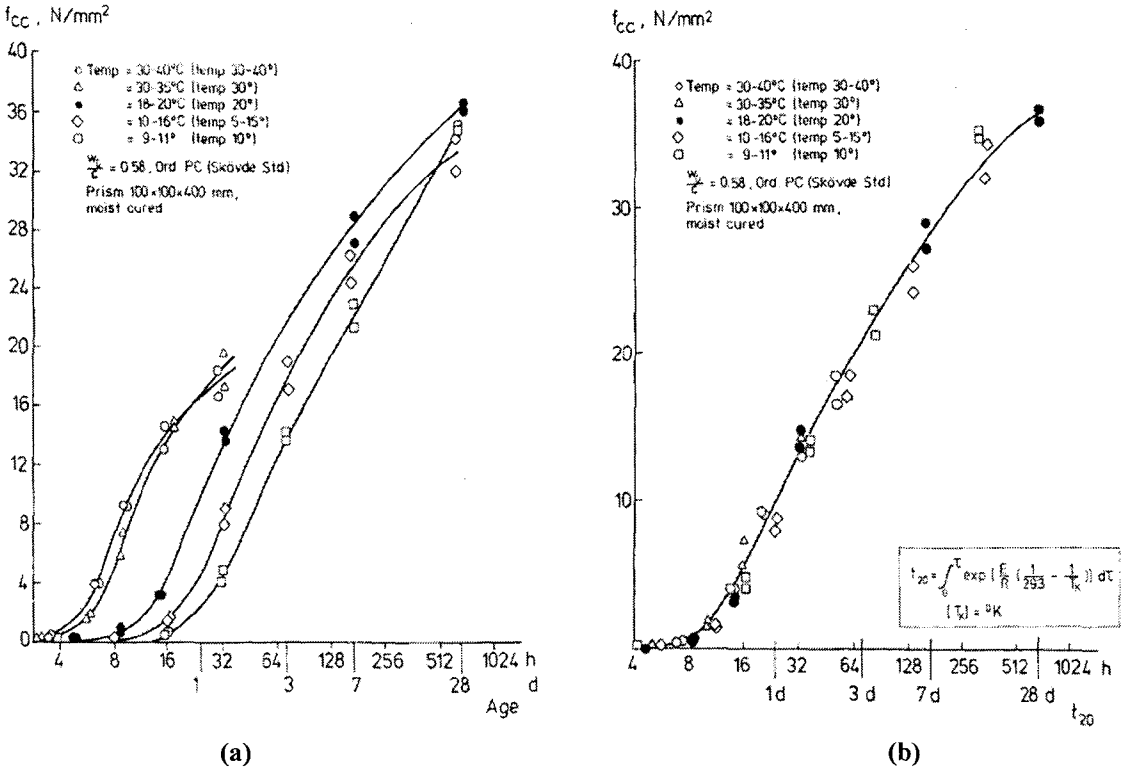

Figure 2.21: (a) Compressive Strength Gain at Different Curing Temperatures (b) Application of Maturity Function (Adapted from Byfors 1980)

2.5 Summary

Portland cement hydration is a complicated process that can be separated into five stages. Several reactions occur at the same time. Along with the reactions, heat is generated. The total heat can be determined according to the heat generation of each composition.

Several factors affect the process of heat generation. The most important factors are the chemical composition, fineness, mineral admixture, w/c ratio, and curing temperature.

Degree of hydration can be determined by the generated heat and non-evaporable water. There is good consistency between these two methods. The ultimate degree of hydration depends on the availability of water and space.

Concrete maturity is introduced and used to predict concrete strength. Maturity is often expressed by either the time-temperature factor or the equivalent age. The Arrhenius law for concrete maturity prediction has proven to be the best predictor of the rate of cement reaction at an early age. In the equivalent age function, proposed by Freiesleben Hansen, and Pedersen according to the Arrhenius law, a new parameter, activation energy, is introduced. The ASTM suggests using the strength method to determine the activation energy. Later, some researchers found that activation energy could also be determined by calorimeter tests. Both test methods provide similar results.

CHAPTER 3 EXPERIMENTAL PROGRAM

The objective of the experiment is to characterize the hydration and strength development of concrete containing different types and different replacement levels of supplemental cementitious materials (SCMs). The test results will be used to calibrate the selected hydration and strength model. During the laboratory test phase, the quality control tests (slump, air content, and unit weight), heat signature tests (semi-adiabatic test), and strength-maturity tests were performed.

3.1 Concrete Materials and Mixes

Type I/II cement was selected for all of the laboratory tests conducted. The effects of different types of cement on cement hydration and concrete strength development were studied using test data from published literature (listed in Chapter 4). The Type I/II cement was from the Lafarge Cement Plant at Davenport, Iowa. It contains 53.19% C_3S, 19.37% C_2S, 6.6% C_3A, and 10.50% C_4AF and has a specific surface area of 373 m^2/Kg. The specific density of cement is 3.20. Four different types of fly ash, including Class C and Class F, and three types of slag from different sources were used to make various blended cementitious materials together with the Type I/II cement. The chemical compositions of all cementitious materials are listed in Table 3.1. These four fly ash were selected because their CaO content covers a large range from 1.51% to 28.89%. The Class F fly ash from Petersburg has the lowest CaO but high SiO_2. The fly ash from Coal Creak contains high SiO_2 and alkali. Fly ashes from Salix and Muscatine contain high CaO and low SiO_2. Due to limited sources, only three types of slag were selected. The chemical compositions for different types of slag are similar. Leigh slag contains more Al_2O_3, which affects the strength and heat development. The Al_2O_3 contents for S.T. and Holcim slag are similar.

Table 3.1: Chemical Compositions of Cement and SCMs

Chemical Compound	Type I/II Cement	Fly Ash				GGBF Slag		
		Class F-Petersburg	Class C-Coal Creak	Class C-Muscatine	Class C-Salix	Leigh	S.T.	Holcim
CaO	62.32	1.51	16.77	27.11	28.89	36.61	36.74	37.13
SiO_2	20.75	45.33	46.92	31.83	32.62	35.68	37.32	37.18
Al_2O_3	4.49	23.02	15.11	19.02	19.32	11.24	9.00	9.17
Fe_2O_3	3.45	23.52	7.06	5.99	6.46	0.70	0.70	0.91
MgO	2.88	0.64	4.94	4.47	4.56	10.11	10.34	10.17
K_2O	0.67	1.76	2.17	0.27	0.35	0.41	0.37	0.43
Na_2O	0.09	0.36	3.30	2.12	1.86	0.34	0.31	0.32
SO_3	2.74	0.31	1.31	3.51	2.48	-	-	-
TiO_2	0.34	1.07	0.58	1.67	1.59	1.14	0.36	0.45
P_2O_5	0.10	0.17	0.20	1.03	1.11	0.02	0.02	0.02
SrO	0.05	0.05	0.44	0.52	0.48	0.08	0.04	0.04
Mn_2O_3	0.53	0.03	0.04	0.14	0.10	0.60	0.90	0.95
BaO	-	0.05	0.74	0.82	0.80	-	-	-
S	-	-	-	-	-	1.71	0.97	1.06
LOI	0.1	1.6	0.1	0.2	0.1	-	-	-

The limestone used as concrete coarse aggregate was from Fort Dodge, Iowa. The specific gravity was 2.67. The aggregate was sieved and recombined to obtain a desired gradation. The coarse aggregate was also saturated for 24 hours and dried to the surface saturated dry (SSD) condition before mixing. The fine aggregate, river sand, was from Cordova, Illinois, with a specific gravity of 2.67.

Twenty-three concrete mixes were prepared. All of the mixes have the same mix proportion (Table 3.2), but different SCM replacement levels. The replacement level of SCMs ranges from 0 to 60% (Table 3.3). The water/cement (w/c) ratio ranges from 0.40 to 0.42. Due to high slump, water reducer was not used for the mixes containing more than 30% of fly ash.

Table 3.2: C-3 Concrete Mix Proportion

Materials	**Source**	**Weight/Amount**
Coarse aggregate	Fort Dodge	63.20 lb/ft^3
Fine aggregate	Cordova	50.6 lb/ft^3
Cementitious materials	Lafarge Type I/II+SCMs	20.83 lb/ft^3
Water	Tap water	8.33 lb/ft^3
Water reducer	WRDA-82	21.60 ml
Air entraining	Daravair 1400	2.80 ml

Table 3.3: SCM Replacement Level by Weight

Mix No.	Cement (%)	FA (%)	Slag (%)
1	100	0	0
2	100	0	0
3	85	15	0
4	70	30	0
5	55	45	0
6	40	60	0
7	85	0	15
8	70	0	30
9	55	0	45
10	40	0	60
11	85	3.75	11.25
12	70	7.50	22.50
13	55	11.25	33.75
14	40	15	45
15	85	11.25	3.75
16	70	22.50	7.50
17	55	33.75	11.25
18	40	45	15
19	70	30 (Coal Creek)	0
20	70	30 (Class F)	0
21	70	30 (Salix)	0
22	70	0	30 (Lehigh)
23	70	0	30 (S.T.)

3.2 Test Methods

3.2.1 Quality Control Tests

To check concrete quality, several standard tests, including slump, unit weight, and air content test, were performed on fresh concrete. Concrete slump was tested according to *ASTM C 143, Standard Test Method for Slump of Hydraulic Cement Concrete* and ranges from 1.75 to 5.25 inches. Unit weight of concrete was measured according to *ASTM C 138, Standard Test Method for Density (Unit Weight), Yield and Air Content (Gravimetric) of Concrete.* The unit weight for all concrete mixes was consistent; it was in the range of 140 and 150 pounds per cubic feet. The air content of fresh concrete was measured by the pressure method following *ASTM C 231, Standard Test Method for Air Content of Freshly Mixed Concrete by the Pressure Methods.* Most of the concrete mixes have air content values

between 5% and 8%. Only the mix with 30% Class F fly ash had a low value of 3.8%. The air content was consistent with the designed value of 6%.

3.2.2 Heat Signature Test

The cement heat signature test was conducted using the semi-adiabatic calorimeter (IQ drum, as shown in Figure 3.1) manufactured by Digital Site Systems, Inc., Pittsburgh, Pennsylvania. The IQ drum consists of (1) a 6 inchx12 inch cylinder chamber for concrete specimens in the center, (2) a 6-inch layer of insulation materials outside the chamber, (3) a thermal sensor, and (4) a data logger mounted on the outside wall. During the test, the thermal sensor is inserted into the concrete specimen to record the test data. The semi-adiabatic calorimeter allows a certain amount of heat loss during the test period. The thermal loss can be calculated from the test data and from the calibration factor, which is determined from a calibration test.

Figure 3.1: IQdrum for Heat of Hydration Test

To initiate the calibration test, water was first heated to about 40° C. The plastic cylinder with a certain amount of heated water was placed in the chamber. The water temperature and heat loss was recorded for at least 72 hours. Based on the test data, the calibration factor was determined. Once the calibration factor was obtained, the concrete heat signature test could be conducted.

The concrete specimen was prepared according to *ASTM C 192, Standard Practice for Making and Curing Concrete Test Specimens in the Laboratory*. Immediately following the mixing, the concrete was placed into the 6 inch×12 inch cylinder in three layers and rodded 25 times for each layer. Then, the sample was weighed and put into the drum together with an inserted sensor. The IQdrum was sealed promptly after the sample was added. The test data were recorded every 15 minutes with the aid of a computer program. The entire test took about 7 days under room conditions.

Before mixing, the mixing proportion and physical properties of the raw materials were input into the software, which provided the desired test results: the thermal history and the heat evolution process of the concrete. Figure 3.2 shows the output from the software. The left graph shows the temperature and maturity (equivalent age) development with time. The right graph shows the heat development and rate of heat evolution with maturity. In this graph, maturity is used instead of real time because temperature sensitivity must be considered. Due to the heat loss, the temperature increase is lower under semi-adiabatic conditions than under adiabatic conditions. As a result, the cement hydrates faster under adiabatic conditions. Therefore, only considering heat loss with time is not sufficient. The influence of the hydration temperature should also be considered. Figure 3.3 shows the effect of considering the temperature sensitivity. The difference between the true and "false" calculation is about 2° C, but the difference will be larger for blended concrete because more cement still has to hydrate at later age. The software is able to provide the maturity. However, the software uses the same activation energy, 40,000 J/mol, which ASTM recommends for Type I cement without admixtures. As stated in Section 2.4.1.3, the activation energy is different for different mixtures. In this case, maturity was recalculated according to Equation 2.24, using a different activation energy for different concrete.

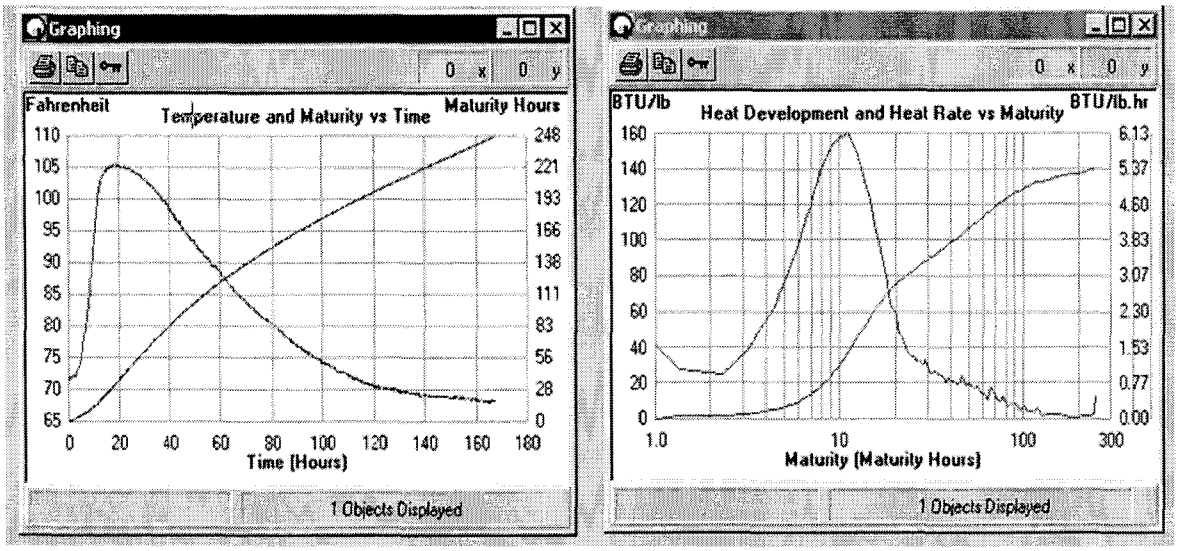

Figure 3.2: Output for Types I/II Cement

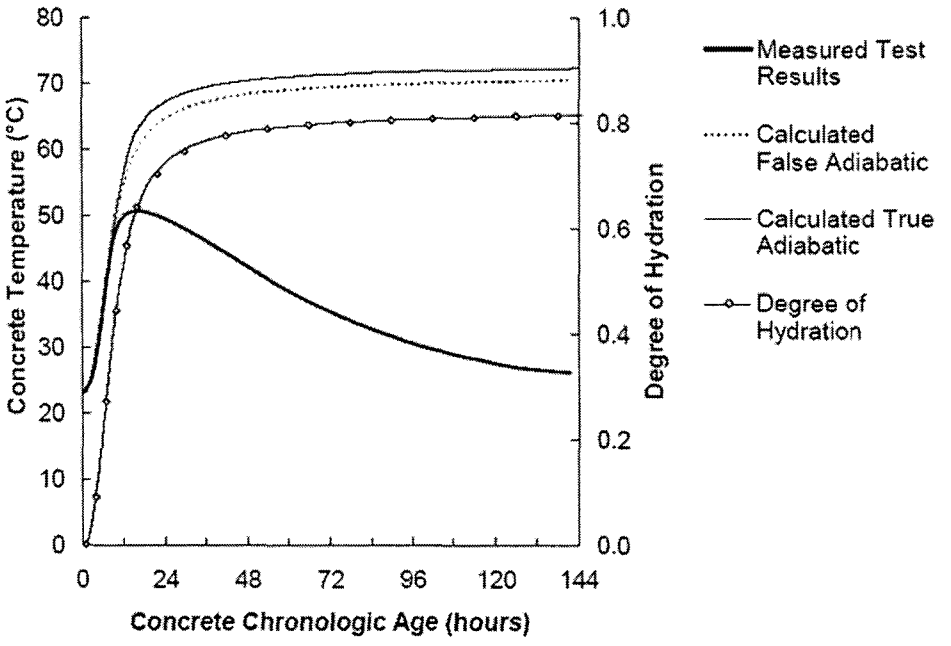

Figure 3.3: Differences in Calculated Adiabatic Results Obtained from Semi-Adiabatic Testing (Adapted from Schindler 2002)

3.2.3 Maturity Strength Test

The setup for the maturity test is shown in Figure 3.4. The 4 inchx8 inch cylinder samples for the maturity and strength tests were prepared according to *ASTM C 192*. A total of 17 samples were prepared for each mix. To monitor the sample's thermal history, the thermocouples were inserted into the centers of two randomly selected samples right after the casting. The temperature was recorded every 15 minutes by the Digital Site Systems, Inc data logger. The samples were stored in the curing room with a constant temperature around 75°F and 100% humidity. After 1 day of curing, the samples were demolded and stored in the curing room again until the test date. The strength tests were performed at 1, 3, 7, 14, and 28 days according to *ASTM C39, Standard Test Method for Compressive Strength of Cylindrical Concrete Specimens*. The average value of three samples was used in the maturity strength modeling. Maturity data was retrieved at the end of the test period. The software provided the temperature and calculated maturity (equivalent age) with time (Figure 3.5). The temperature of the concrete specimens increased about 4 degrees after about 10 hours and then dropped to room temperature after about 1 day. For the same reason as the IQ drum, the maturity provided by the software was not used in the strength modeling, that is, the software uses the same activation energy, 40,000 J/mol, for every concrete mixture. The maturity was recalculated using Equation 2.24 with different activation energy.

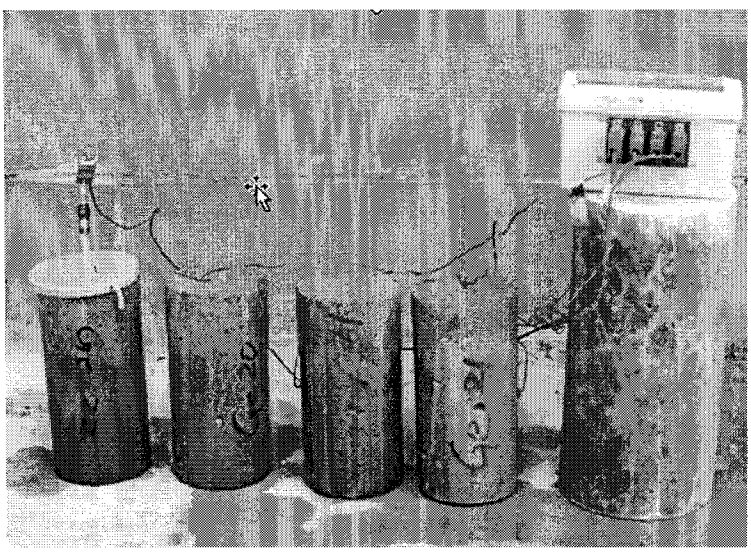

Figure 3.4: Maturity Test Setup (Samples Cured in the Curing Room)

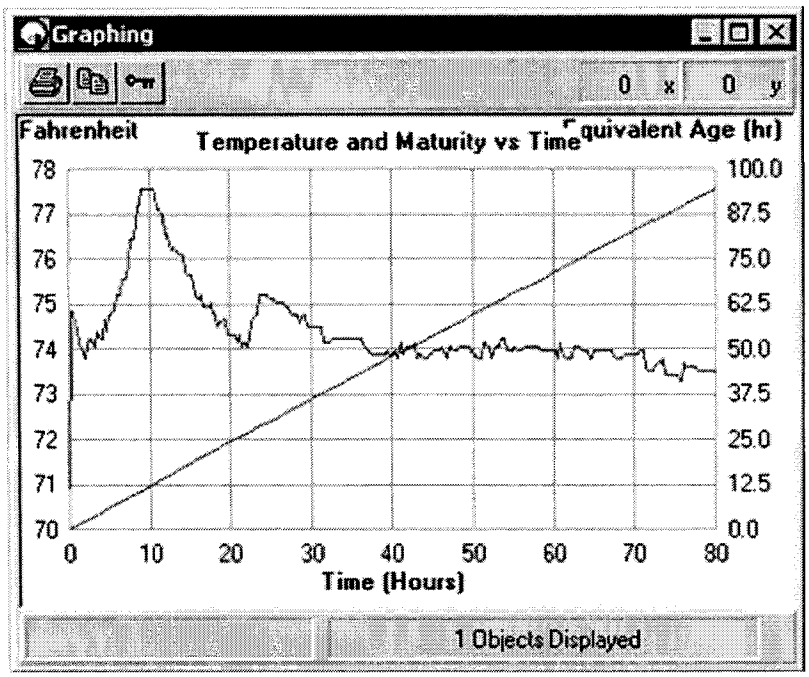

Figure 3.5: Output for Concrete Temperature and Maturity (Type I/II Cement Concrete)

CHAPTER 4
MODELING THE HEAT OF HYDRATION OF CEMENTITIOUS MATERIALS

The heat of concrete hydration is critical for concrete structures. If too much heat is rapidly generated inside a concrete structure, it may cause the concrete to crack due to the thermal differentiation. It is not uncommon for large-volume concrete structures like dams and bridge piers to crack; less heat is necessary for this type of structure. On the other hand, when construction occurs under cold conditions, providing proper curing leads to greater heat retention in concrete, which benefit concrete strength development. In both situations, being able to predict the process of heat evolution would be beneficial, enabling precautionary measures to be taken to prevent concrete from cracking and distress.

This chapter describes the development of a model for the heat of hydration generated by various cementitious materials under different curing conditions. In this model, the chemical compositions and physical characteristics of the cementitious materials are emphasized.

4.1 Existing Hydration Models

As discussed in Section 1.2, the cement hydration process is complicated and results from the individual hydration process of the four major components in OPC: C_3A, C_3S, C_2S, and C_4AF (Figure 2.8). At each stage of cement hydration, there is more than one chemical composition hydrate. An interdependency exists among these reactions. Due to the Pozzolanic reaction, the hydration process becomes more complicated when the supplemental cementitious materials (SCMs) are added to the cement.

There are two major types of modeling. One is multiple-component hydration modeling, which is based on the independent hydration concept that assumes no interaction occurs between hydrating constituents. The other type is the equal fractional rates concept,

which assumes that all constituents react uniformly. Figure 4.1 illustrates the concepts of independent hydration and fractional rates.

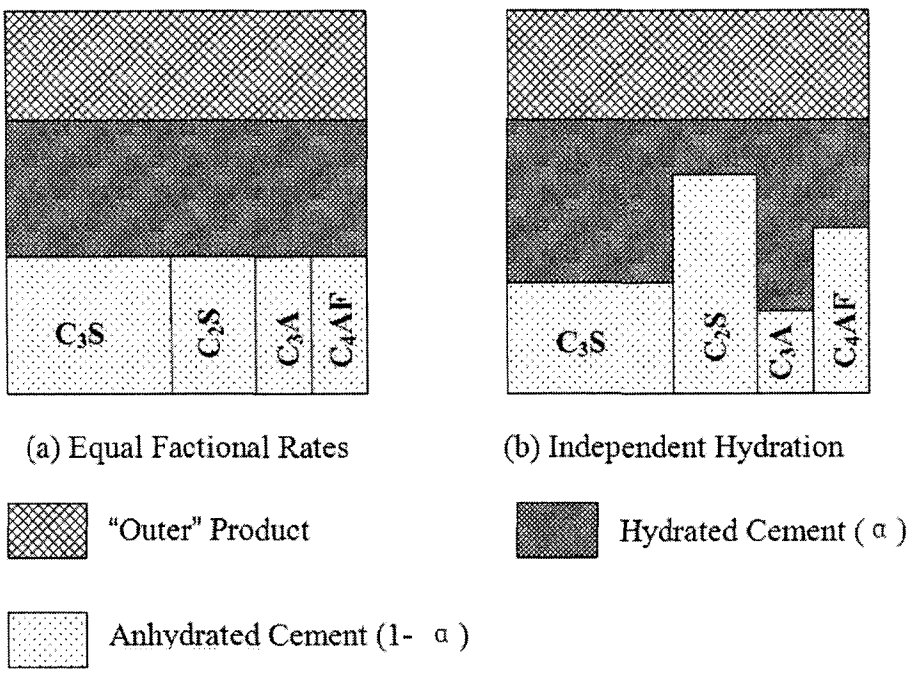

Figure 4.1: Schematic Representation of Independent Hydration Concept and Hydration at Equal Fractional Rates

4.1.1 Multi-Component Model

Parrott (1984) suggested that cement hydration is a simple sum of hydration of all individual components. He assumed that there is no interdependence among the individual reactions. However, the interdependency exists in the process of cement hydration. Kishi and Maekawa (1994) and Maekawa et al. (1999) proposed a multi-component model for cement hydration containing fly ash and slag and considered the interdependency. The model is expressed as Equation 4.1.

$$Q_i = \gamma\beta_i\lambda\mu s_i Q_{i,T_0}(H_i)\exp\left\{-\frac{E_i}{R}\left(\frac{1}{T}-\frac{1}{T_0}\right)\right\} \qquad 4.1$$

Where,

γ = Delaying effect of chemical admixture and fly ash in the initial hydration exothermic process

β_i = Availability of free water, used to take the interdependence among component reactions into account.

λ = Amount of $Ca(OH)_2$, which governs the mutual interaction between Pozzolanic materials and cement

μ = Parameter expressing the effects of mineral compositions

s_i = Parameter expressing the fineness of OPC

$Q_{i,T0}$ = Reference heat generation rate of component I at constant temperature T_0

H_i = Accumulated heat

E = Activation Energy

R = Gas constatn

The reaction process of each mineral compound is expressed by the reference heat rate and the thermal activity. The reference heat rate gives the heat rate characteristic of the mineral at a specific constant temperature. The thermal activity describes the temperature dependency of each reaction. In this model the thermal activities, E/R, are different for each mineral compound (Figure 4.2). However, the thermal activities of fly ash and slag are constant with no consideration of the different types of fly ash and slag.

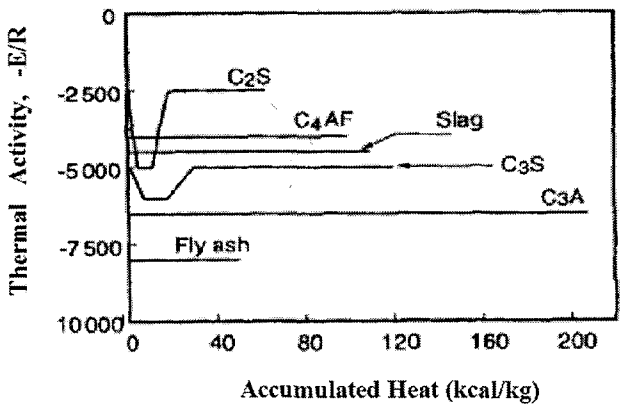

Figure 4.2: Thermal Activity of each Component (Adapted from Maekawa et al. 1999)

4.1.2 Equal Fractional Rate Model

Although cement hydration is a complex process, it is possible to treat the cement as a single material. Thus modeling the heat development characteristics of various types of cement is simplified. To achieve this, a thermal activity (E/R) value is used that represents the whole cement rather than each mineral compound as described in the multi-component model.

Suzuki et al. (1989) proposed the expression of the hydration process using the adiabatic temperature rise (Equation 4.2).

$$T_a(t) = T_\infty\left(1 - \exp\left(-r(t - t_0)^s\right)\right) \qquad 4.2$$

Where,

$T_a(t)$ = Adiabatic temperature rise at t days after casting

T_∞ = Ultimate temperature rise

r, s t_0 = Experimental constants

This model represents heat evolution characteristics under thermally isolated conditions and can only be applied to the adiabatic situation.

In real situations, however, most concrete is not fully thermal isolated. To adequately capture the general properties of cement hydration, the temperature rise due to cement hydration should be taken into account. Several models considering thermal activity have been developed and are listed below.

(1)Byfors 1980; Oh et al. 2003; Janasson 1984

$$\alpha = \exp\left(-a_c\left(\ln\left(1+\frac{t_{eq}}{b_c}\right)\right)^{-c_c}\right) \qquad 4.3$$

$$t_{eq} = \int \beta_T \beta_{W/C} \beta_W dt \qquad 4.4$$

Where,

α = Degree of hydration

a_c, b_c, c_c = Hydration parameters

t_{eq} = Equivalent age

β_T, $\beta_{W/C}$, β_W = Effect of temperature, water/cement (w/c) ratio, water distributions on rate of reaction

(2)De Schutter, Taerwe, 1995

$$q(\alpha,T) = q_{\max,20} \cdot f(\alpha) \cdot g(T)$$
$$g(\alpha) = \exp\left[\frac{E}{R}\left(\frac{1}{293} - \frac{1}{273+T}\right)\right] \qquad 4.5$$
$$f(\alpha) = c \cdot [\sin(\alpha\pi)]^a \cdot \exp(-b\alpha)$$

Where,

q = Rate of heat generation

α = Degree of hydration

a,b,c = Hydration parameters

T = Temperature

(3)Freiesleben Hansen, and Pedersen 1985, Pane et al. 2002

$$\alpha(t_{eq}) = \alpha_u \cdot \exp\left(-\left[\frac{\tau}{t_{eq}}\right]^{\beta}\right) \qquad 4.6$$

Where,

$\alpha(t_{eq})$ = Degree of hydration at equivalent age of t_{eq}

α_u = Ultimate degree of reaction

τ = Hydration time parameter

β = Hydration slope parameters

Dabic et al. (2000) described a model that divides the hydration process into three separate processes, which are governed by nucleation and growth, boundary reactions, and diffusion respectively. The governing equations are listed in Equations 4.7 through 4.9. The parameters of KNG, n, K1, and KD were determined from the test data. This model predicts the pure cement hydration well, but for cement containing SCMs, deviations are shown in boundary reactions and diffusion-controlled periods.

- Nucleation and growth govern the hydration process.

$$\begin{cases} \alpha = 1 - \exp\left(-(K_{NG}t)^n\right) \\ \dfrac{d\alpha}{dt} = nK_{NG}^n t^{n-1} \exp\left(-(K_{NG}t)^n\right) \end{cases} \quad 4.7$$

- Boundary reactions govern the hydration process.

$$\begin{cases} 1-(1-\alpha)^{1/3} = k_1 t \\ \dfrac{d\alpha}{dt} = 3k_1(1-k_1 t)^2 \end{cases} \quad 4.8$$

- Diffusion governs the hydration process.

$$\begin{cases} \left(1-(1-\alpha)^{1/3}\right)^{1/2} = k_D t \\ \dfrac{d\alpha}{dt} = \dfrac{3}{2}k_D \dfrac{\left(1-(k_D t)^{1/2}\right)^2}{(k_D t)^{1/2}} \end{cases} \quad 4.9$$

Where,

α = Degree of hydration

K_{NG}, n, K_1, and K_D = Hydration parameters

t = Time

Van Breugel (1995) developed a computer-based numerical model called HYMOSTRUC, based on microstructure development. This model can predict cement hydration in paste as a function of the particle size distribution, chemical composition, water/cement (w/c) ratio, and reaction temperature. Bentz et al. (1998) developed a three-dimensional (3D) model for cement hydration and microstructure development. This model

is able to predict hydration for cement containing silica fume. However, this model requires a two-dimensional image from SEM/X-ray analysis and the particle size distribution of the cement to establish a 3D representation of the cement.

4.2 Heat of Cement Hydration Model

Due to its complexity, no pure mechanistic models are available to account for every reaction in blended cement hydration. The heat of hydration model presented in this chapter is an empirical-mechanistic model. The model was developed based on the test and literature data. Numerous parameters affect the heat of hydration process; it is impossible to consider all of these factors. The present model only considers the following major variables:

- Cement chemical composition and fineness
- SCM replacement level and chemical composition
- W/c ratio
- Curing temperature

Unlike other models, the new model will consider the chemical compositions of different fly ash and slag.

4.2.1 General Concept and Approach of Model Development

As stated in Chapter 2, the degree of hydration can be expressed by the liberated heat and the total heat of the cementitious materials (Equation 2.15), which can be also expressed as Equation 4.10. The total heat, the heat generated at 100% hydration, of the cementitious materials in the equation can be determined by the amount of cement and SCMs.

$$H(t) = \alpha(t) \cdot H_{total} \tag{4.10}$$

$$H_{total} = H_{cement} \cdot p_{cement} + H_{FA} \cdot p_{FA} + H_{Slag} \cdot p_{Slag} \tag{4.11}$$

Where,

$H(t)$ = Heat generated at time t (KJ/Kg)

H_{total} = Total hydration heat of the cementitious materials (KJ/Kg)

H_{cement}, H_{FA}, H_{slag} = Total hydration heat of cement, fly ash, and slag (KJ/Kg)

P_{cement}, P_{FA}, Pslag = Weight of cement, fly ash, and slag

Cement will not be 100% hydrated. The hydration process will stop at the ultimate degree of hydration, α_u. The heat generated at that time is called the ultimate heat of hydration. By combining Equations 4.6 and 4.10, the heat of hydration liberated by a cementitious material, at a given time, can be expressed by Equation 4.12.

$$H(t) = H_{total} \cdot \alpha_u \cdot \exp\left(-\left[\frac{\tau}{t_{eq}}\right]^{\beta}\right) \text{ or} \qquad 4.12(a)$$

$$H(t) = H_{ult} \cdot \exp\left(-\left[\frac{\tau}{t_{eq}}\right]^{\beta}\right) \qquad 4.12(b)$$

Where,

H_{total} = Total hydration heat of the cementitious materials (KJ/Kg)

α_u = Ultimate degree of hydration

H_{ult} = Ultimate heat of hydration of the cementitious materials (KJ/Kg)

τ,β = Hydration parameters

t_{eq} = Equivalent age (hour)

Equation 4.12 is used in this study to describe concrete heat development with time. Three parameters--H_{ult}, β, and τ--control the process of hydration. The qualitative influence of these three parameters is shown in Figure 4.3. In each figure, only one parameter is changed; the other two parameters are fixed to show the effect of this parameter. The change of H_{ult} can only affect the ultimate heat of hydration without changing the shape of the curve.

Changing of parameters β and τ will change the shape of the heat evolution curve with the same ultimate heat.

Hydration model development can be divided into the following three steps:

Step 1. Calculating the equivalent age from the raw semi-adiabatic heat signature tests and literature data

To calculate the equivalent age, the reference temperature and activation energy have to be selected. The literature data applied in this modeling were conducted under 70°F. Therefore, 70°F (21.1°C) was selected as the reference temperature. The activation energy was calculated by Equations 4.13 and 4.14, which Schindler and Folliard (2003) developed.

$$E = 22100 \cdot f_E \cdot p_{C_3A}{}^{0.3} \cdot p_{C_4AF}{}^{0.25} \cdot Blaine^{0.35} \quad 4.13$$

$$f_E = 1 - 1.05 \cdot p_{FA} \cdot (1 - \frac{p_{FACaO}}{0.4}) + 0.4 \cdot p_{SLAG} \quad 4.14$$

Where,

f_E = Modification factor for SCMs

p_{C3A}: = Weight ratio of C_3A in terms of the total cement content

p_{C4AF}: = Weight ratio of C_4AF in terms of the total cement content

Blaine: = Blaine value, specific surface area of cement (m^2/kg)

p_{FACaO}: = Weight ratio of the CaO content of the fly ash

Step 2. Performing the nonlinear regression analysis to obtain H_{ult}, β, and τ values for each set of data.

Step 3. Establishing the relationship among the hydration parameters, H_{ult}, β, and τ, and the properties of the cementitious materials through the statistic analysis. This is the model for heat of hydration.

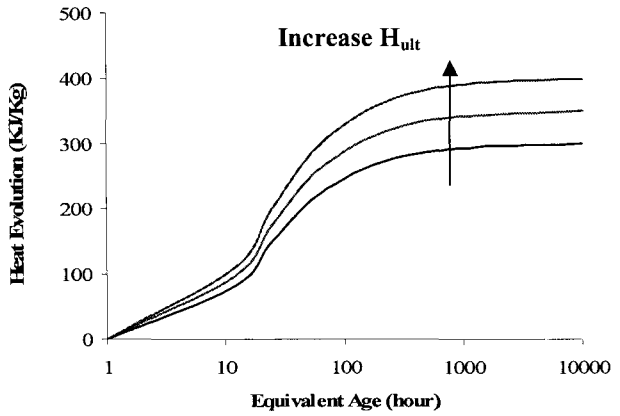

(a) Effect of H_{ult}

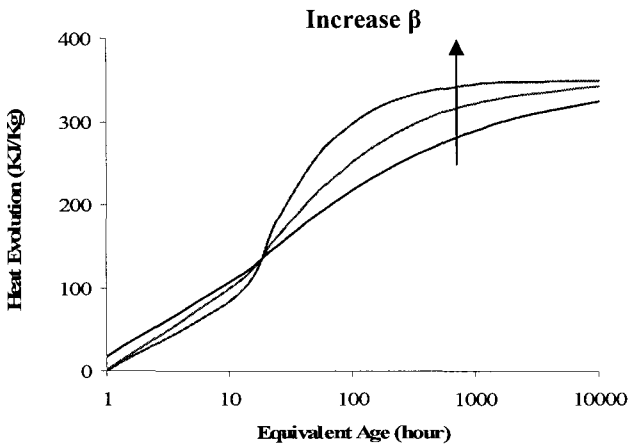

(b) Effect of β

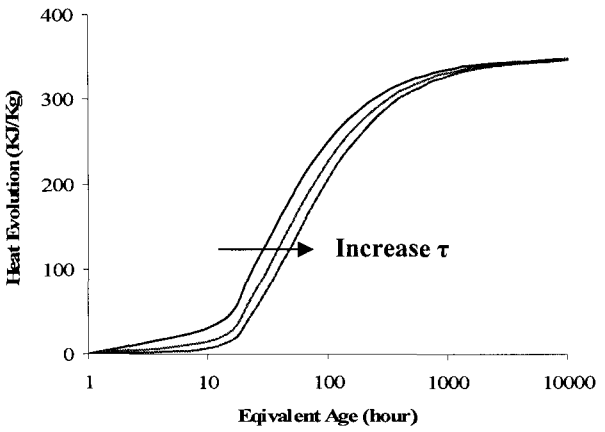

(c) Effect of τ

Figure 4.3: Effect of Hult, β, and τ on the Shape of the Heat Evolution Curve

4.2.2 Model Data Source

It is important to obtain sufficient, representative data during the development of the heat of hydration model. The more detailed and comprehensive the data set, the better the model becomes. Two sets of data, laboratory and literature data, were employed for model development.

4.2.2.1 Data from Semi-Adiabatic Tests

The properties of the concrete materials and the mixing proportions are described in Section 3.1. Semi-adiabatic tests have been performed for concrete made with these materials and mix proportions and are used to characterize the hydration of the cementitious materials. These semi-adiabatic test results are divided into three groups: (1) slag replacement, (2) fly ash replacement, and (3) replacement containing slag -fly ash.

Slag replacement

Figure 4.4 shows the characteristics of heat generation for cement with different levels of slag replacement. Although the total heat of slag hydration is similar to that of Type I/II cement, the replacement with slag can significantly reduce the heat generation at an early age. The reduction increases as the slag replacement increases. Note that the reduction is not proportional to the slag replacement. As the equivalent age increases, the difference is reduced due to the Pozzolanic reaction, which is discussed in Section 2.2.2.6. The ultimate degree of hydration of cementitious material is also increased when the slag is added.

Figure 4.5 indicates that blended cement with different slag has different heat of hydration characteristics. At an early age, the generated heat is similar for all three cements containing different slag. After about 20 hours, the cement with Leigh slag increases much faster than the other two cements with Holcim and S.T. slag. At about 6 days, the generated heat of cement with Leigh slag exceeds the Type I/II cement. However, cement containing Holcim and S.T. slag still generates lower heat than Type I/II cement.

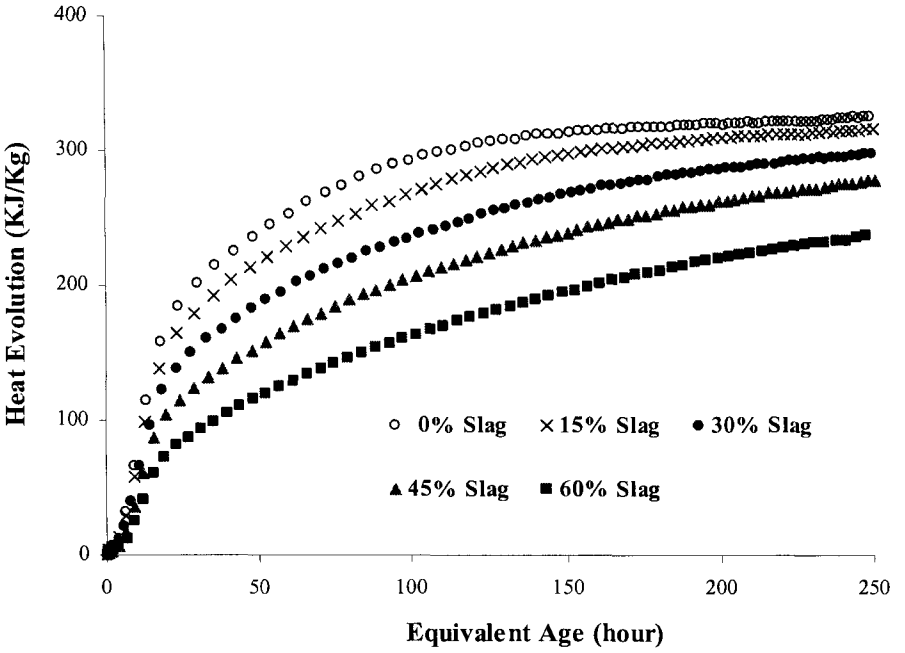

Figure 4.4: Effect of Slag Replacement on Heat of Hydration of Cementitious Materials (Lafarge I/II Cement)

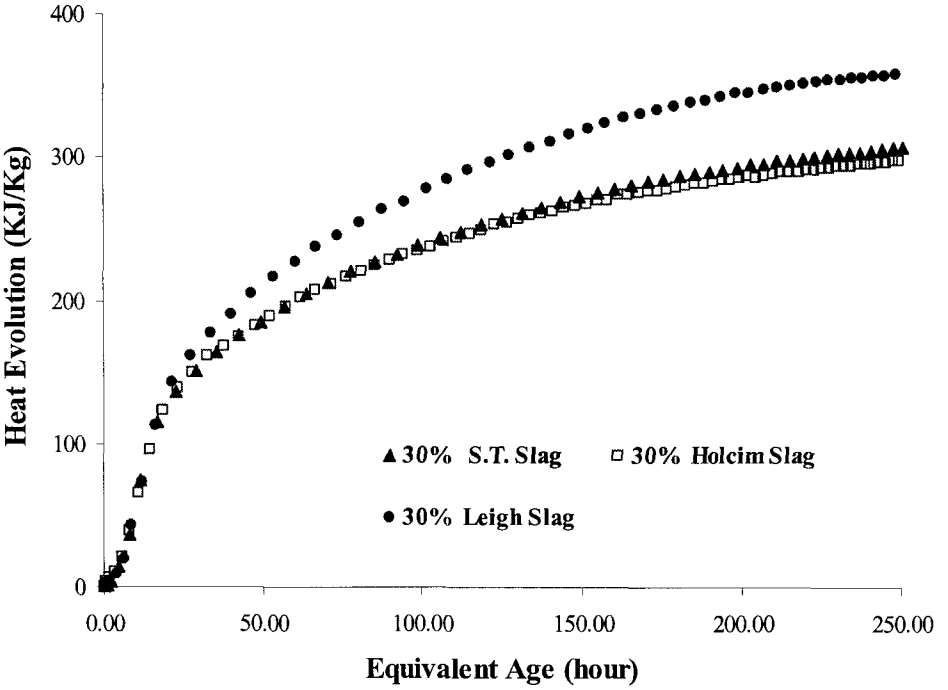

Figure 4.5: Effect of Different Slag on Heat of Hydration (Lafarge I/II Cement)

Fly ash replacement

Figures 4.6 and 4.7 show the influence of fly ash on the process of cement hydration. Fly ash has the similar effect as the slag. However, at the same replacement level, the heat reduction caused by fly ash replacement is smaller than the heat reduction caused by slag. Cement containing 15% fly ash generated more heat than Type I/II cement at an later age. Cements containing 30% and 45% of fly ash have very similar hydration heat around 7 days. They are close to Type I/II cement. Figure 4.7 indicates that the different types of fly ash have different heat curves. The Class F fly ash has the lowest hydration heat, provided that the Class F fly ash is less reactive than the Class C fly ash. Even for Class C fly ash, the fly ash with the higher CaO content will generate more heat than those with lower CaO.

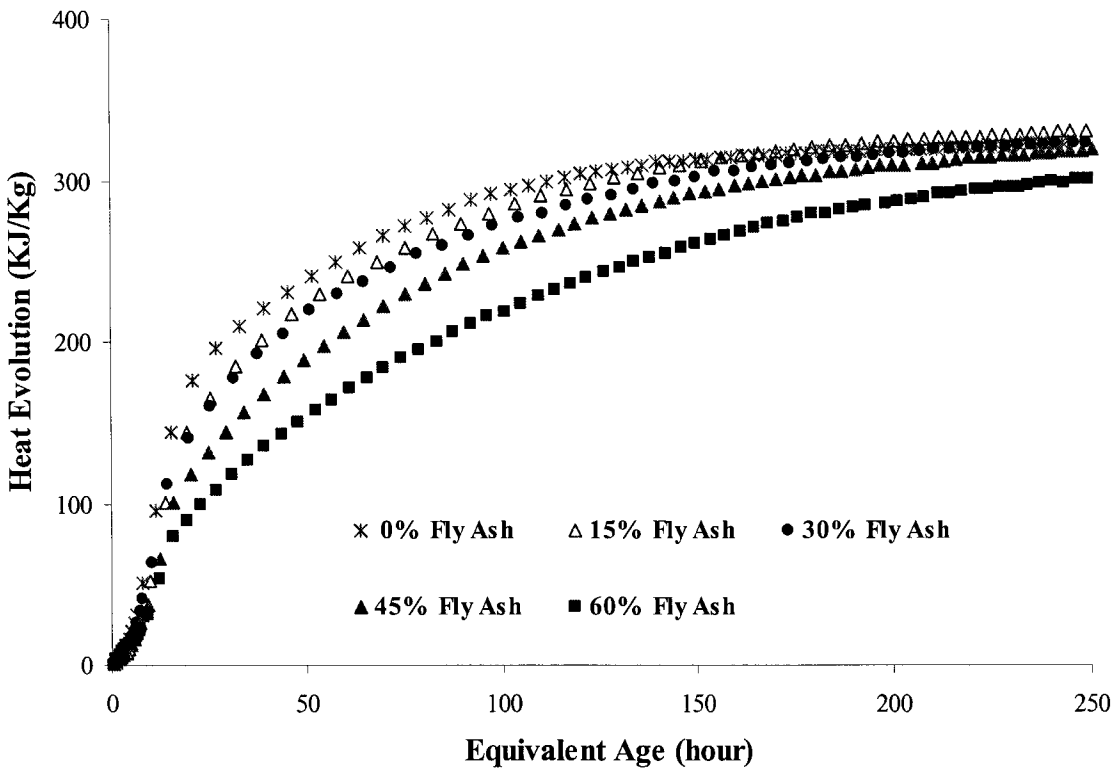

Figure 4.6: Effect of Fly Ash Replacement on Heat of Hydration

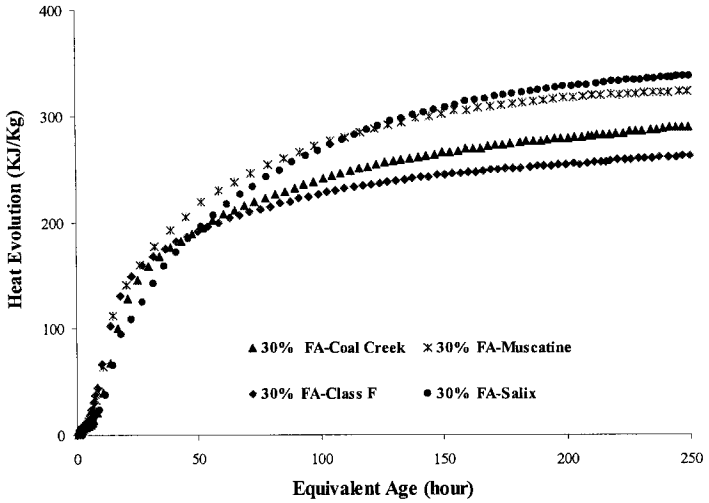

Figure 4.7: Effect of Different Fly Ash on Heat of Hydration

Slag-fly ash replacement

The ternary mix is used to check the interaction between the fly ash and slag. The effect of the slag and fly ash mixture has a similar effect as the fly ash and slag (figures 4.8 and 4.9). When the fly ash dominates, it reacts like the fly ash and vice versa. The generated heat is reduced at an early age regardless of fly ash-to-slag ratio. At an later age, the heat of evolution is different for different fly ash-to-slag ratios.

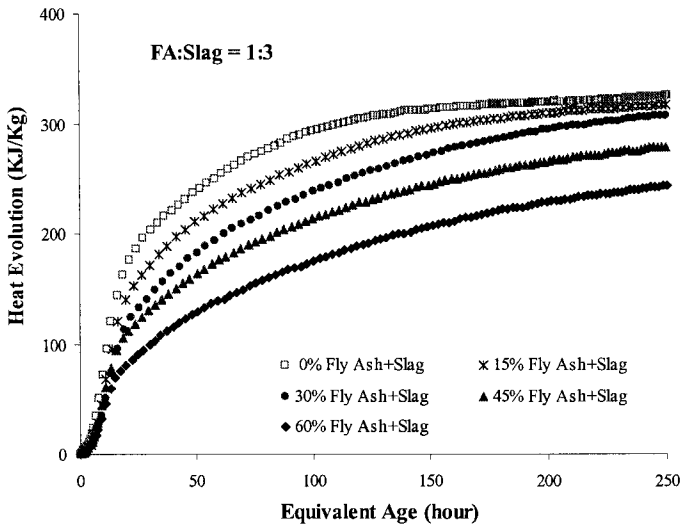

Figure 4.8: Effect of Fly Ash and Slag (Lafarge I/II Cement)

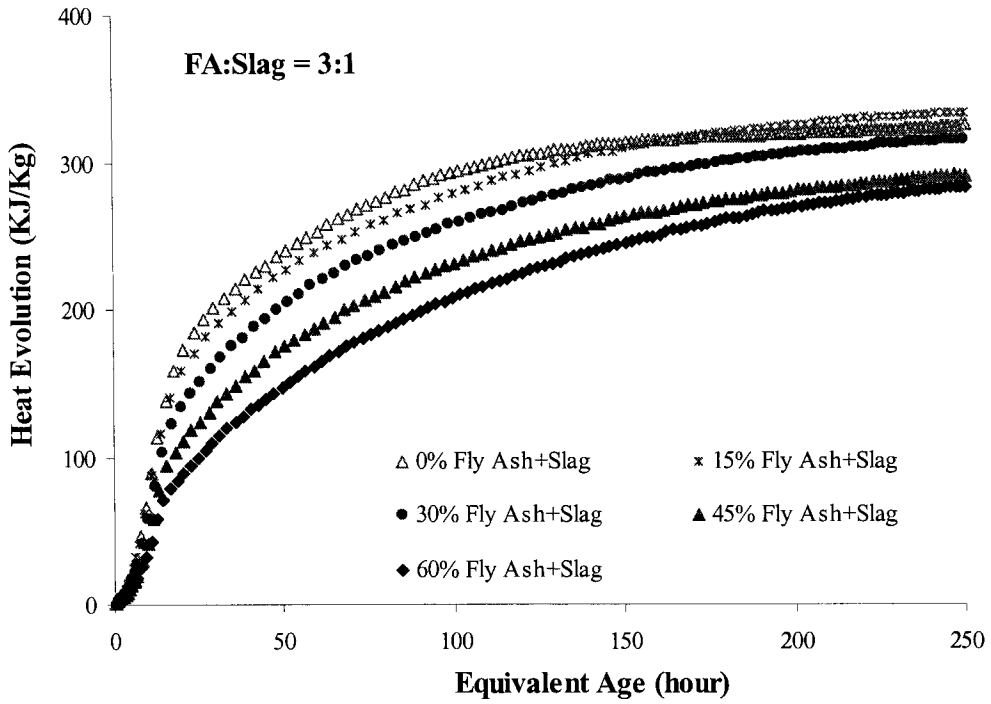

Figure 4.9: Effect of Fly Ash and Slag (Lafarge I/II Cement)

4.2.2.2 Data from Literature

As discussed in Section 2.22, cement type affects the hydration process. To study the quantitative effect of cement type on heat of hydration, the literature data were adopted in this study. Lerch and Ford (1948) conducted a heat evolution test on a series of cement from Type I to Type V. The conduction calorimeter was used in the study. The neat cement pastes with a w/c ratio of 0.4 were tested under 70°F for up to 1 year. Verbeck et al. (1950) provided the value of heat of hydration at 6 and half years. Figure 4.10 shows the heat evolution curves for different types of cement. These curves represent the average values for each type of cement.

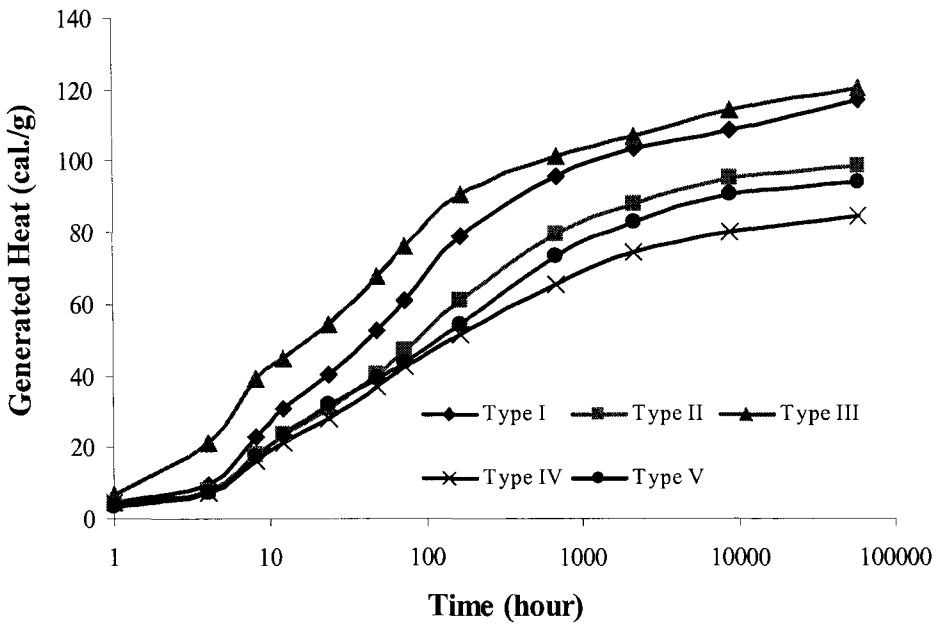

Figure 4.10: Effect of Cement Type on Heat of Hydration

On average, Type III cement has the highest hydration heat at any given time. Type IV cement has the lowest value. The difference among these cements is mainly caused by the variation in chemical compositions and physical properties, which are listed in Table 4.1. On average, Type I cement contains 50.2% C_3S, 23.7% C_2S, and 10.7% C_3A and has a specific surface area of 341.3 m2/Kg. Type II cement only contains 41.5% C_3S and 5.4% C_3A but contains a higher amount of C_2S: 33.3%. The specific surface area is 321.0 m2/Kg. Type III cement, on the other hand, contains high amounts of C_3S (60%), and the specific surface area is 534.5 m2/Kg. The C_2S is only 13.5%. The C_3A, 9%, is similar to Type I cement. The high C3S content and specific surface area of Type III cement contribute to the high heat of hydration. Type IV cement has a very high C_2S content of 51.5% and low C_3S and C_3A, 25.3% and 4.9% respectively. The specific surface area is 366.5 m^2/Kg. The C_3S, C_2S, and C_3A content and the specific surface area for Type V cement are 41%, 39%, and 3.7% and 348.3 respectively.

Table 4.1: Cement Chemical Composition (Adapted from Lerch et al. 1948)

Cement No.	Calculated Compounds Percent by Weight					From Chemical Analyses Percent by Weight					Blaine m2/kg
	C_3S	C_2S	C_3A	C_4AF	$CaSO_4$	Free Cao	MgO	Na_2O	k_2O	SO_3	
Type I Cement											
11	50	22	12.1	7.2	2.7	0.4	3.7	0.21	0.51	1.6	343.6
12	45	28	12.6	7.3	2.7	0.1	3.1	0.28	0.4	1.6	327.6
13	50	26	10.1	6.5	2.8	1.6	1.1	0.04	0.19	1.6	342.8
14	42.5	32	8.2	9.2	2.9	0.2	2.5	0.06	1.3	1.7	342.4
15	64.5	10	12.1	7.5	3.2	0.4	0.8	0.08	0.23	1.9	322.9
16	53.5	21	7.5	10.7	2.9	0.7	2.1	0.23	0.46	1.7	326.1
17	52	23	10.4	9.3	2.9	0.4	1.1	0.08	0.43	1.7	398.5
18	44.5	28	13.2	6.8	3.1	0.3	2.6	0.12	0.13	1.8	326.8
Average	50.2	23.7	10.7	8.1	2.9	0.5	2.1	0.14	0.45	1.7	341.3
Type II Cement											
21	40	41	6.4	9.7	2.1	0.7	1.3	0.22	0.4	1.2	289.1
22	41.5	33.5	6.6	11.7	2.4	0.1	3.2	0.24	0.37	1.4	306.5
23	51	24	3.7	16.6	2.6	0.4	0.9	0.59	0.14	1.5	310.9
24	41	29	5.4	14.8	3	0.9	3.1	0.06	1.3	1.8	369.7
25	34	39	4.7	14.9	3.2	0.2	2.2	0.21	0.54	1.9	328.7
Average	41.5	33.3	5.4	13.5	2.7	0.5	2.1	0.26	0.55	1.6	321.0
Type III Cement											
31	56	17	10.8	6.4	3.8	1.5	3.3	0.23	0.22	2.2	579.5
33	60	13	10.4	7.7	3.9	1.8	1.4	0.21	0.44	2.3	527.2
34	64	10.5	5.7	10.1	2.9	2.3	2.5	0.28	0.28	1.7	496.9
Average	60	13.5	9.0	8.1	3.5	1.9	2.4	0.24	0.31	2.1	534.5
Type IV Cement											
41	20	51	4.5	15.2	3.4	0.4	3	0.06	1.19	2	367.9
42	27	55	3.5	8.2	2.6	0.2	1.8	0.16	0.26	1.5	350.1
43	25	48	6.2	13.8	3.6	0.1	1.6	1	0.08	2.1	384.6
Average	25.3	51.5	4.9	11.6	3.2	0.3	1.9	0.39	0.39	1.9	366.5
Type V Cement											
51	41	39	3.7	10	2.4	0.5	1.7	0.08	0.22	1.4	348.3

4.2.3 Model Development

4.2.3.1 Total Heat of Cementitious Materials

To determine the total hydration heat of cementitious materials (Equation 4.11), it is necessary to know the total hydration heat of OPC, fly ash, and slag. The total heat of OPC is the sum of the specific heat of its chemical compounds. The specific heat of the individual compounds is shown in Table 2.8. The values proposed by Lerch and Bogue (1934) are used. Kishi et al. (1995) recommended a total heat generation value of 461 KJ/Kg for slag. This value is adopted in this study. Limited data is available for the total hydration heat of fly ash. Kishi et al. (1995) suggested a value of 209 KJ/Kg for fly ash with 8.8% CaO. In this study, it is assumed that the ultimate degree of hydration is the same for different types of fly ash. Based on this assumption and the semi-adiabatic test data, the following equation is proposed for determining the total heat of hydration for different types of fly ash based on the CaO content.

$$H_{total,FA} = 15.9 \cdot (p_{CaO} \times 100) + 74.3 \qquad 4.15$$

In this equation only, the CaO content is considered because CaO is the most reactive compound in fly ash. The total heat of hydration of fly ash in Equation 4.15 should be evaluated, based on the long-term heat signature test. The test results from the semi-adiabatic heat signature tests alone cannot be used to verify the accuracy of Equation 4.15, since the ultimate hydration heat is related to both the total hydration heat and the ultimate degree of hydration.

Based on the assumed total heat of fly ash and slag hydration and Table 2.8, the total heat of cementitious materials is now calculated as Equation 4.16.

$$\begin{aligned} H_{total} = {} & 500C_3S + 260C_2S + 866C_3A + 420C_4AF + 1186\,free\,CaO + 850MgO \\ & + 624SO_3 + 461Slag + FA(15.9 \cdot (p_{CaO} \times 100) + 74.3) \end{aligned} \qquad 4.16$$

4.2.3.2 Nonlinear Regression Results

Nonlinear regression is applied to fit the hydration parameters H_{ult}, τ, and β for each set of data using Equation 4.12(b). The software JMP was used to perform statistical analysis. The nonlinear regression command in JMP fits the nonlinear models using least-squares function. Iterative methods are used to search for the least-squares estimates. The following criteria and stop limits were used to control the regression (Table 4.2). Iterations stop when one of the three criteria--objective change, parameter change, and gradient--is met.

Table 4.2: Criteria and Stop Limits for Nonlinear Regression

Criterion	Stop Limit
Iteration	60
Shortening	15
Objective Change	0.0000001
Parameter Change	0.0000001
Gradient	0.000001

Table 4.3 summarizes the nonlinear regression results of all laboratory test data. It shows that the ultimate degree of hydration increases as the SCM replacement level increases. Almost 95% of the cementitious materials has been hydrated as 60% SCM is added to the cement. The time parameter τ also increases when SCM was added. In Equation 4.6, as the equivalent age equals τ, 36.7% of the ultimate degree of hydration has occurred. The larger the τ, the slower the early age hydration. On the other hand, the slope parameter β decreases as the SCM replacement level increases. The increasing β means a lower hydration rate before equivalent age reaches τ and a higher hydration rate after that. The difference in parameters β and τ, caused by adding the SCMs, is mainly due to the Pozzolanic reaction, which is slow and initiated late with low hydration heat when compared to the C_2S reaction.

Table 4.3: Summary of Nonlinear Regression Results from the Laboratory Test Data

FA	Slag	Htotal	Hult	α_u	τ	β
0	0	466.3	346.9	0.74	14.784	0.897
0	0	466.3	352.6	0.76	16.269	0.890
15	0	472.3	377.3	0.80	21.648	0.826
30	0	478.2	390.0	0.82	27.000	0.721
45	0	484.2	420.2	0.87	33.639	0.647
60	0	490.1	440.0	0.90	50.328	0.575
0	15	465.5	364.9	0.78	19.379	0.753
0	30	464.7	400.0	0.86	30.093	0.579
0	45	463.9	429.9	0.93	49.334	0.499
0	60	463.1	440.0	0.95	89.29	0.445
3.75	11.25	467.2	381.0	0.82	23.251	0.728
7.50	22.50	468.1	397.2	0.85	32.728	0.647
11.25	33.75	469.0	417.4	0.89	42.166	0.501
15	45	469.9	444.4	0.95	80.048	0.429
11.25	3.75	470.6	374.5	0.80	18.790	0.790
22.50	7.50	474.8	388.0	0.82	24.972	0.673
33.75	11.25	479.1	400.0	0.83	35.487	0.588
45	15	483.4	459.0	0.95	61.246	0.497
30	0	425.8	346.0	0.81	24.677	0.773
30	0	358.3	295.8	0.83	16.120	0.788
30	0	486.6	410.0	0.84	35.469	0.800
0	30	464.7	441.0	0.95	29.752	0.701
0	30	464.7	405.8	0.87	30.047	0.588

Table 4.4 summarizes the regression results of the test set from Lerch et al (1948). Type III cement has the highest total heat of hydration, 120 cal/g due to its high C_3S content. Type IV cement has the lowest total heat of hydration, 90 cal/g, due to its low C_3S and C_3A content. Type III cement hydrates the fastest. On average, it has the lowest average τ value, only 12.575. The fast reaction is due to the high percent of C_3S and to the high specific surface area. Types II, IV, and V cement have similar τ values of 35 to 36 hours. On average,

Type IV cement has the lowest β value, 0.387. Type I cement has the highest β value, 0.498. The difference in β value among these five types of cements is only 0.111.

Table 4.4: Summary of Nonlinear Regression Results for Literature Data (Lerch et al. 1948)

Cement No.	Htotal	τ	β	Cement No.	Htotal	τ	β
Type I				**Type II**			
11	117	26.214	0.479	21	103	39.129	0.440
12	113	30.323	0.602	22	105	42.276	0.500
13	112	33.043	0.410	23	105	38.438	0.436
14	105	18.524	0.482	24	105	28.412	0.368
15	121	18.245	0.547	25	97	30.266	0.409
16	112	22.826	0.465	Average	103	35.704	0.431
17	113	22.874	0.464	**Type IV**			
18	114	24.611	0.536	41	90	30.059	0.373
Average	113	24.583	0.498	42	88	47.880	0.372
Type III				43	93	30.501	0.415
31	121	10.989	0.491	Average	90	36.147	0.387
33	120	11.513	0.453	**Type V**			
34	119	15.224	0.397	51	98	35.052	0.404
Average	120	12.575	0.447				

4.2.3.3 Models for Hydration Parameters

This section describes the development of models for the hydration parameters, H_{ult}, τ, and β. These parameters are expressed as functions of the chemical compositions of cement, fly ash, and slag and also the replacement level of fly ash and slag.

Since not all of the chemical properties of cement are independent of each other, multivariate analysis was performed to check the correlations among the chemical composition and Blaine Index of the cement samples. The results show that there are strong linear relationships for C_3S and C_2S as well as C_3A and C_4AF. The r values are -0.97 and -

0.75 respectively. Therefore, the C_2S and C_4AF are not used in the following analysis. After the initial analysis, the parameters of cement selected for the model development of hydration parameters τ and β are C_3A, C_3S, SO_3, and Blaine. The test results, shown in Table 4.3, also indicate that the replacement level and type of SCMs affect the hydration parameters τ and β. Since CaO is the most important parameter for fly ash, it will be included in the model to account for the difference in fly ash. The hydraulic index (HI), proposed by Mantel (1994) (Equation 4.17), is used to account for the different types of slag.

$$HI = \frac{CaO + MgO + Al_2O_3}{SiO_2} \qquad 4.17$$

Thus, parameters τ and β can be expressed as follows:

Hydration Time Parameter τ

τ = f(C_3A, C_3S, SO_3, Blaine, FA, FA-CaO, Slag)

Hydration Slope Parameter β

β= f(C_3A, C_3S, SO_3, Blaine, FA, Slag , HI)

Where,

C_3A, C_3S, SO_3 = Cement compounds

Blaine = Blaine fineness of cement (m^2/Kg)

Slag = Weight ratio of slag to cementitious material

FA = Weight ratio of fly ash to cementitious material

FA-CaO = Weight ratio of fly ash CaO to fly ash

HI = Hydraulic Index, defined in Equation 4.17

According to Equation 4.12, the ultimate heat of hydration is a function of the total heat and the ultimate degree of hydration. The total hydration heat, H_{total}, is shown in Equation 4.16. Therefore, the ultimate degree of hydration, α_u, will be modeled to predict the ultimate heat of hydration. Mills (1966) developed the ultimate hydration model for different

cement, based on solid theory and test results (Equation 2.19). This model takes into account the effect of the w/c ratio. However, the test results also show that SCMs can influence the ultimate degree of hydration. Therefore, the Mills' model is only used as the base model, and the influence of the SCMs is added to this base model. The ultimate degree of hydration is thus expressed as follows:

$$\alpha_u = \frac{1.031 \cdot w/c}{0.194 + w/c} + \Delta\alpha \qquad 4.18$$

Where,

w/c = W/c ratio

$\Delta\alpha$ = Additional hydration caused by SCMs

Nonlinear analysis was performed for the combined data set containing laboratory tests and the Lerch test. The criteria and stop limits are the same as listed in Table 4.2. The results are listed in Equations 4.19 to 4.21.

$$\tau = 2.649 \cdot C_3S^{-0.541} \cdot C_3A^{-0.122} \cdot SO_3^{-1.191} \cdot Blaine^{-0.567} \cdot \exp(3.018 \cdot slag + 8.365 \cdot FA \cdot FA - CaO) \qquad 4.19$$

$$\beta = C_3S^{0.280} \cdot C_3A^{0.143} \cdot SO_3^{1.378} \cdot Blaine^{-0.994} \cdot \exp(-9.210 \cdot slag \cdot (1 - 0.568 \cdot HI) + 11.272) \cdot (1 - 0.519 \cdot FA) \qquad 4.20$$

$$\alpha_u = \frac{1.031 \cdot w/cm}{0.194 + w/cm} + 0.361 \cdot FA + 4.285 \cdot slag \cdot (0.730 \cdot HI - 1) \le 1 \qquad 4.21$$

Where,

C_3S = Weight ratio of C_3S to cement

C_3A = Weight ratio of C_3A to cement

SO_3 = Weight ratio of SO_3 to cement

Blaine = Blaine value, specific surface area of cement (m^2/Kg)

Slag = Weight ratio of slag to cementitious material

FA = Weight ratio of fly ash to cementitious material

FA-CaO = Weight ratio of fly ash CaO to fly ash

HI = Hydraulic Index, defined in Equation 4.17

The predicted values and experimentally determined values for each parameter are plotted in Figures 4.11 to 4.13. These figures indicate that the proposed Equations 4.19 to 4.21 accurately predict the parameters by considering the effect of cement chemical composition, cement fineness, SCMs, chemical composition of SCMs, thermal activity, and w/c ratio.

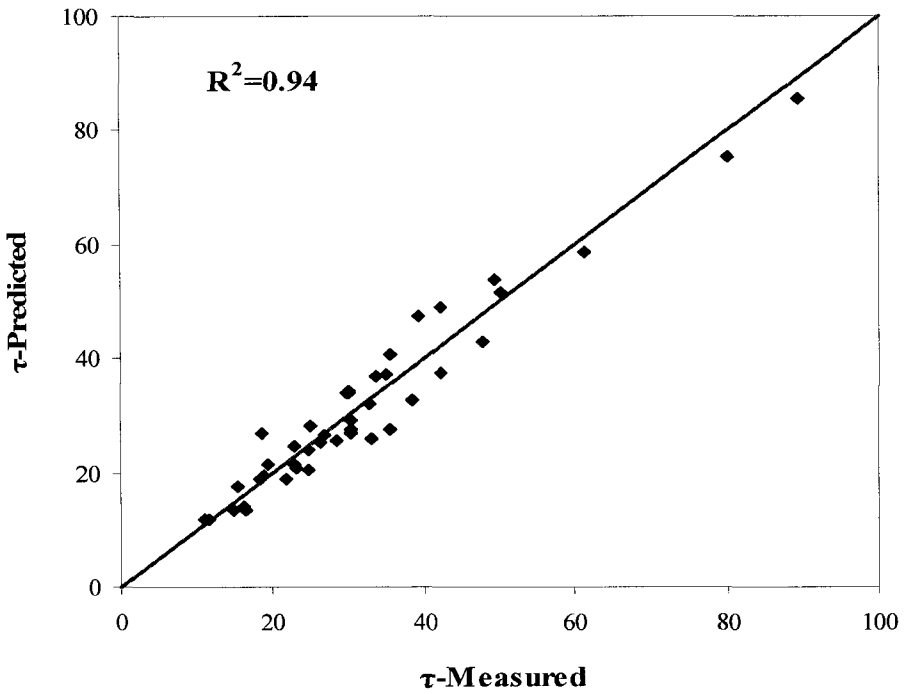

Figure 4.11: Predicted and Measured τ

The goodness-of-fit models are evaluated by the R square value and the plot of the residue. The R square for τ is 0.94, which means 94% of the variation of the experimentally determined values can be explained by the model, which account for the cement chemical composition, fineness, SCMs, chemical compositions of SCMs, and w/c ratio. The R square for β, only 0.88, is lower than the R square for τ. The R square for the ultimate hydration model is 0.93.

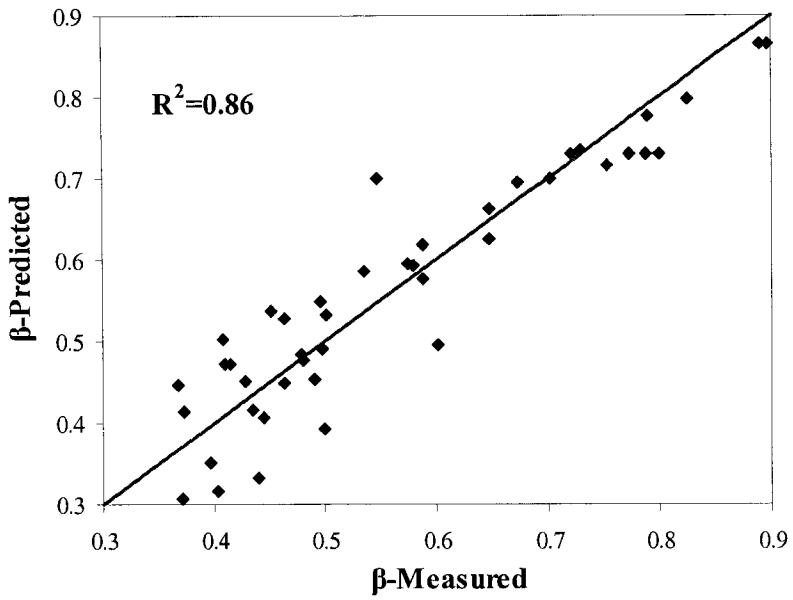

Figure 4.12: Predicted and Measured Beta

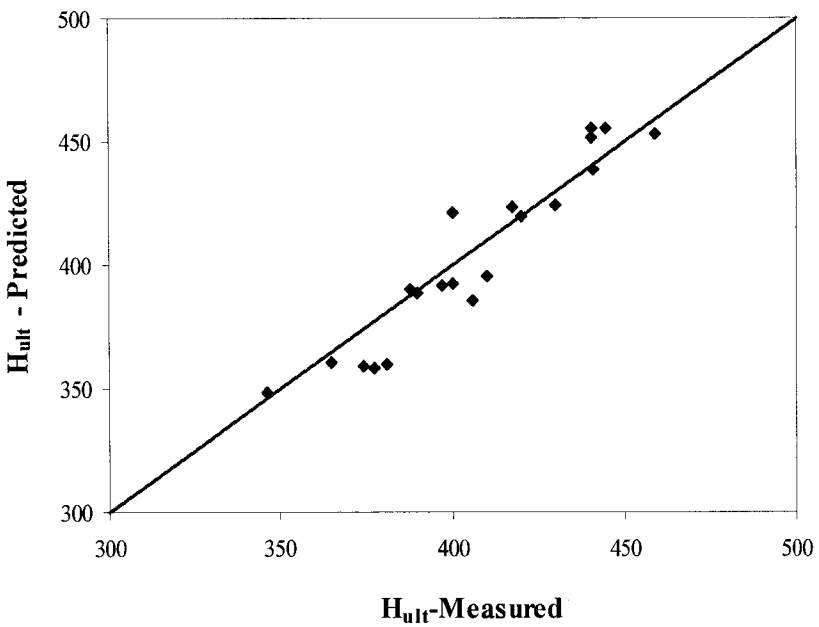

Figure 4.13: Predicted and Measured Hult

Figure 4.14 shows the scatter plots of each measured parameter versus the residuals, which are the difference between the measured values and the predicted values. The residues are randomly distributed; no apparent patterns are observed in any plot.

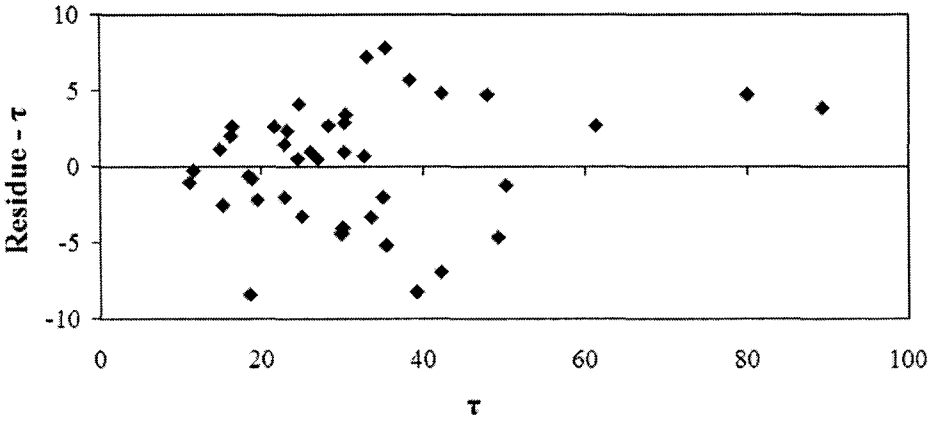

(a)

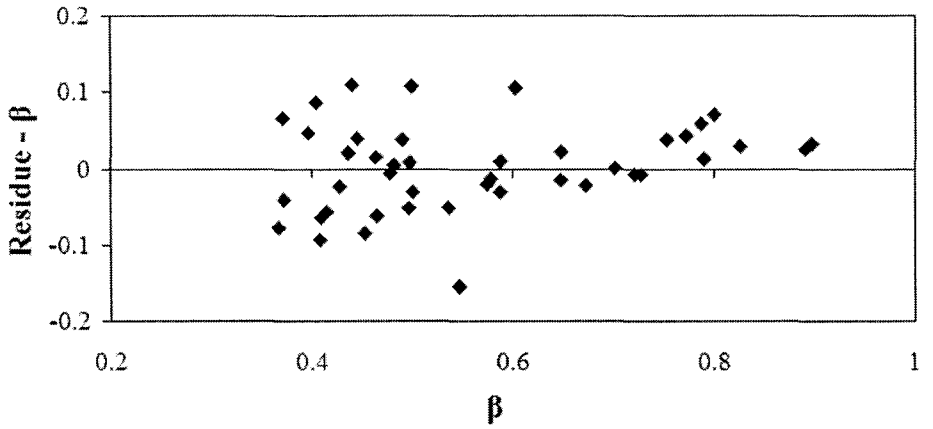

(b)

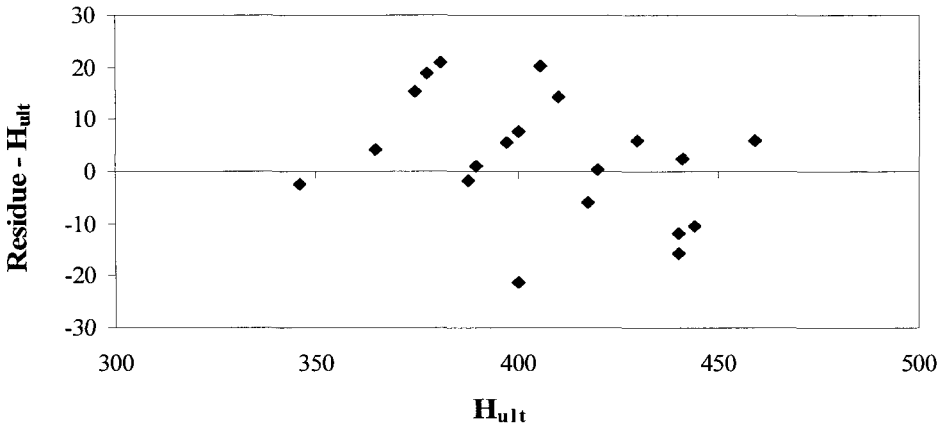

(c)

Figure 4.14: Residue vs Parameters

4.2.3.4 Model for Heat of Cementitious Material Hydration

Combining Equations 4.19 to 4.21 with the overall model, Equation 4.12, the heat development of different cementitious materials can be predicted. The model of the heat of cementitious material hydration can be expressed as follows:

$$H(t) = H_{ult} \cdot \exp\left(-\left[\frac{\tau}{t_{eq}}\right]^{\beta}\right) \qquad 4.22$$

$$H_{total} = 500C_3S + 260C_2S + 866C_3A + 420C_4AF + 1186 free\ CaO + 850MgO + 624SO_3 + 461 slag + FA(15.9 \cdot (p_{CaO} \times 100) + 74.3) \qquad 4.22\ (a)$$

$$\tau = 2.649 \cdot C_3S^{-0.541} \cdot C_3A^{-0.122} \cdot SO_3^{-1.191} \cdot Blaine^{-0.567} \cdot \exp(3.018 \cdot slag + 8.365 \cdot FA \cdot FA - CaO) \qquad 4.22\ (b)$$

$$\beta = C_3S^{0.280} \cdot C_3A^{0.143} \cdot SO_3^{1.378} \cdot Blaine^{-0.994} \cdot \exp(-9.210 \cdot slag \cdot (1 - 0.568 \cdot HI) + 11.272) \cdot (1 - 0.519 \cdot FA) \qquad 4.22\ (c)$$

$$\alpha_u = \frac{1.031 \cdot w/cm}{0.194 + w/cm} + 0.361 \cdot FA + 4.285 \cdot slag \cdot (0.730 \cdot HI - 1) \leq 1 \qquad 4.22\ (d)$$

The overall prediction of all test values using this model is presented in Figure 4.15. A high R^2 value, 0.99, is achieved for the overall prediction, indicating that the overall prediction of the heat of hydration is fairly accurate. The goodness of the prediction model for every admixture is presented in the Appendix. The following section will show the typical results for five different types of cement and cement with different levels of SCMs. The major chemical compositions and Blaine value for each mixture are listed in the figures.

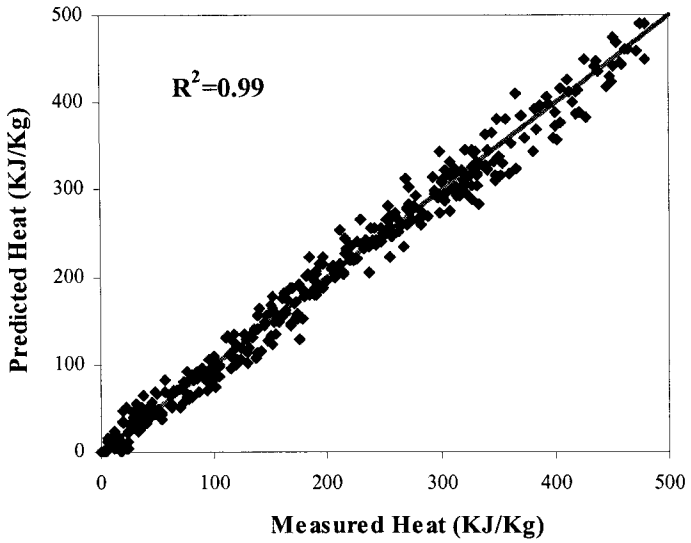

Figure 4.15: Measured vs Predicted Heat of Hydration

Figure 4.16 shows the predicted and measured heat of cement hydration for different types of cement tested by Lerch and Ford (1984). The figure shows that most test data are falling on or very close to the predicted curve, indicating that the proposed model is able to accurately predict the heat of hydration for different types of cement.

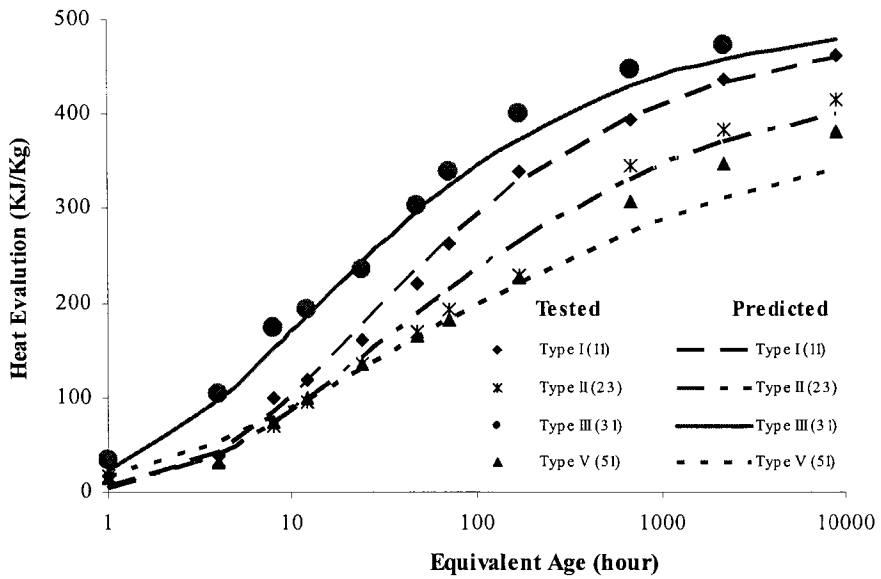

Figure 4.16: Measured vs Predicted Heat of Hydration for Different Types of Cement (Lerch and Ford 1948)

The prediction results for cementitious materials containing different amounts of fly ash and slag are presented in Figures 4.17 to 4.19. These figures demonstrate that the proposed model can accurately predict the heat of hydration behaviors for cementitious materials containing different levels of fly ash and slag, and also fly ash and slag mixtures. As the figures show, most of the measured data points fall on the prediction curve. The difference is fairly small.

These figures also show that adding cementitious materials reduces the heat generation of cement, especially at an early age. However, the later age heat of hydration of cementitious materials exceeds that of the cement. As the SCM content increases, the time during which both cement and cementitious materials have the same heat of hydration becomes longer.

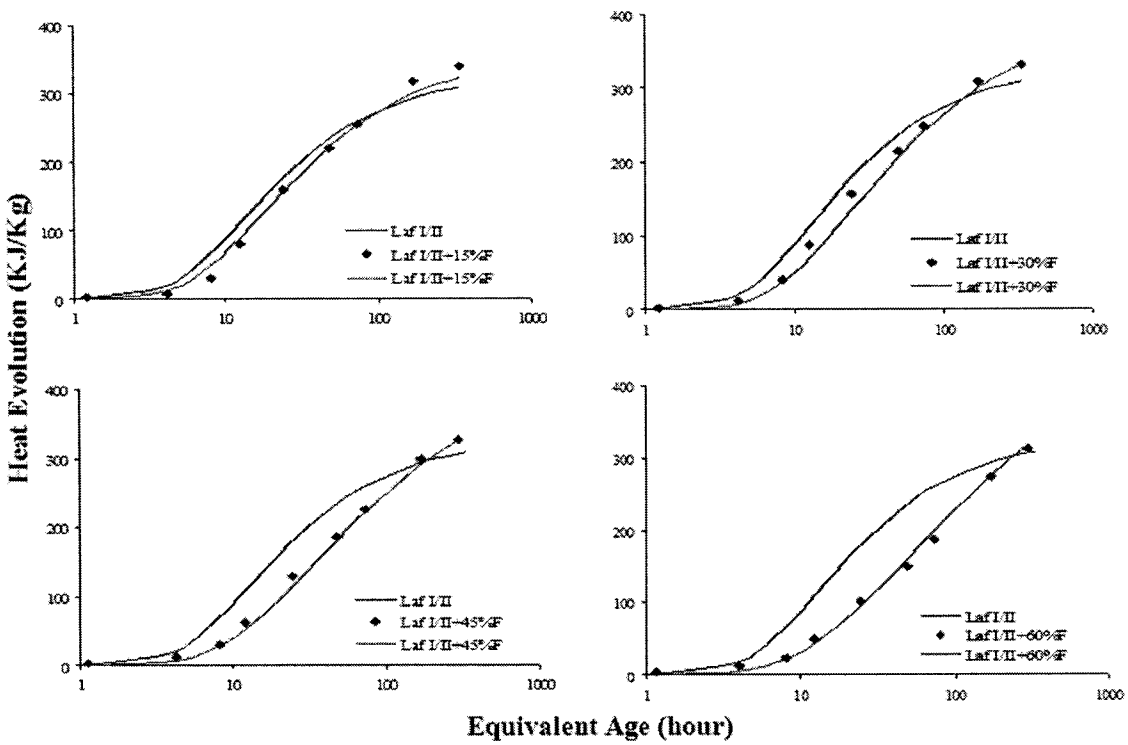

Figure 4.17: Measured vs Predicted Heat of Hydration for Type I/II Cement with Different Levels of Fly Ash

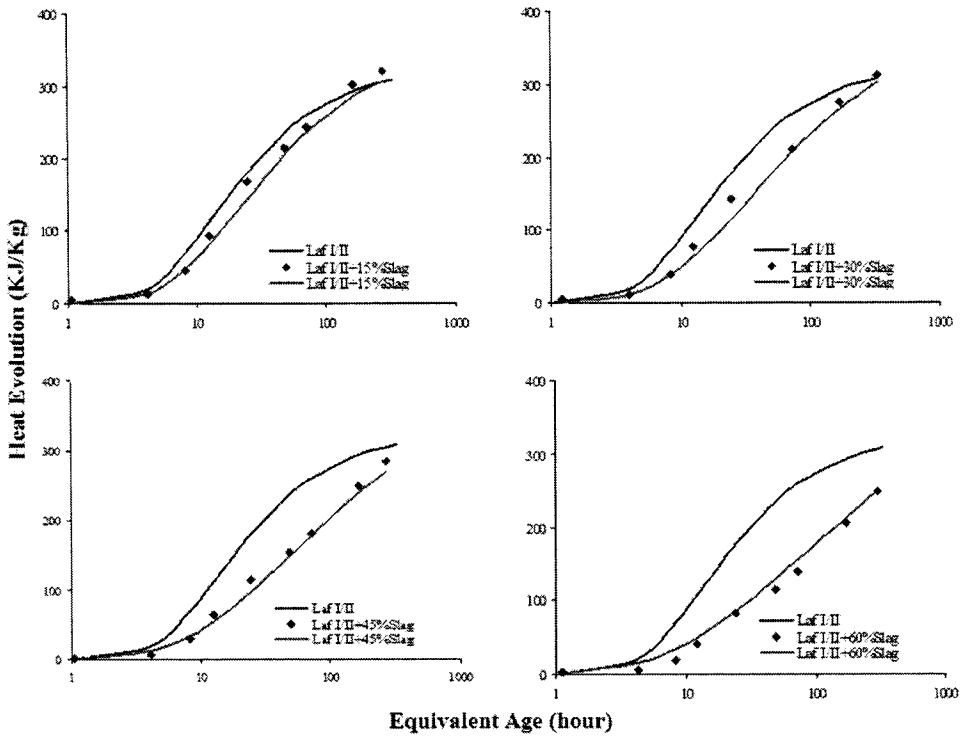

Figure 4.18: Measured vs Predicted Heat of Hydration for Type I/II Cement with Different Levels of Slag

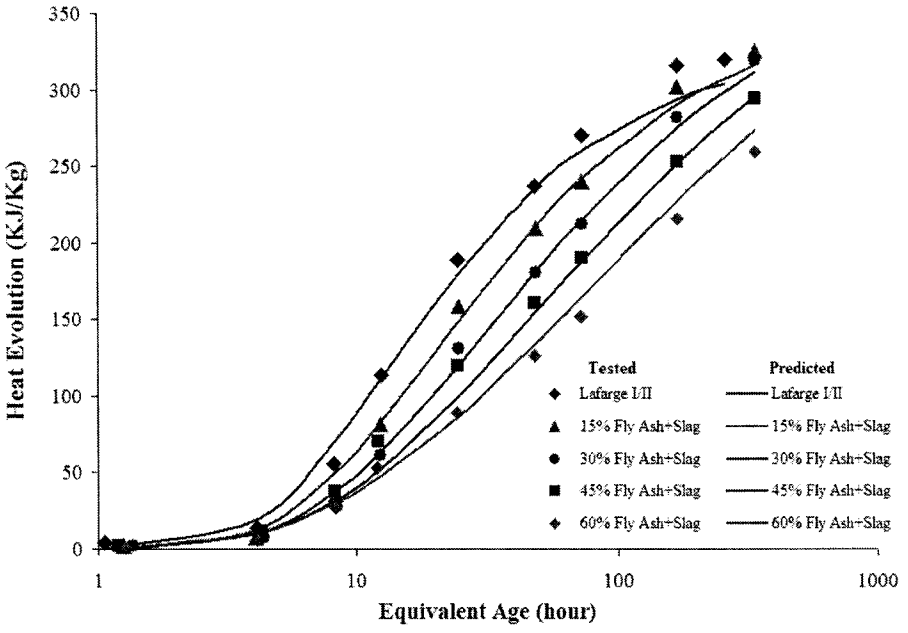

Figure 4.19: Measured vs Predicted Heat of Hydration for Type I/II Cement with Different Levels of Fly-Slag Mixture (Fly Ash:Slag = 1:3)

4.2.4 Sensitivity Analysis

In this section, the sensitivity analysis of the newly developed heat of hydration model is provided. The results of sensitivity analysis provide insight into the contribution of each parameter of the overall hydration process. The average values of the cement chemical compositions are chosen as the baseline with a w/c ratio of 0.42. Only one parameter is changed at a time. In real cement, it is impossible to change the content of only one chemical composition while keeping others the same since the percentage of all chemical compositions should add up to 100. However, the sensitivity analysis performed by this strategy is able to provide the influence of each parameter on the heat of hydration. Therefore, it is assumed that it is appropriate to change only one parameter at a time while keeping others constant.

Figures 4.20 to 4.23 show the effect of changing OPC chemical compositions. Figure 4.20 shows the effect of C_3S. The contents of the remaining chemical compositions are listed in the figure. C_3S is an important component of cement, making up about 50%. Type IV cement has the lowest C_3S content and Type III cement has the highest C_3S content. The figure indicates that increasing C_3S increases the rate of cement hydration. The cement with the highest C_3S content has a much higher degree of hydration than the cement with the lowest C_3S content. The difference is reduced at every late age because the ultimate degree of hydration is the same for all cement with the same w/c ratio. However, for the first few hours, the effect is not apparent. The effect of the changing C_3S content is one of the reasons why Type III cement generates more heat than other cements.

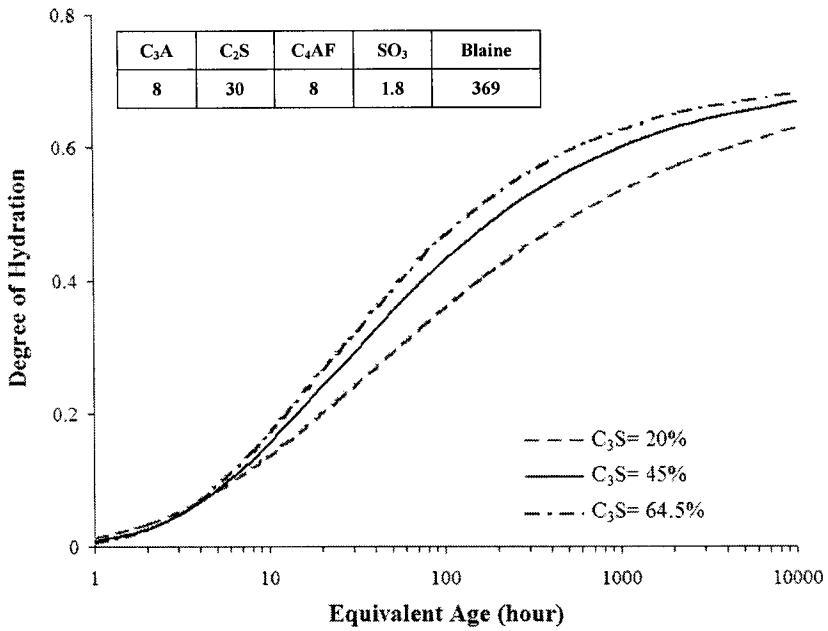

Figure 4.20: Effect of C_3S

Figure 4.21 shows that the increase of the C_3A content has a similar effect as the C_3S. After about 10 hours, the higher the C_3A content, the higher the degree of the hydration. However, the effect is not as significant as the effect of the C_3S, because the variation of the C_3A content is less than the variation of the C_3S. As Figure 4.16 shows, the lower C_3A content can cause the lower hydrate rates for Type V cement.

Figure 4.22 shows the effect of SO_3. It indicates that the SO_3 has a significant effect on the shape of cement hydration. Low SO_3 content causes fast hydration at every early age and slow hydration at later age and vice versa. Therefore, it is important to add gypsum, hemihydrate, or anhydrate to the clinker during the grind process to achieve the final cement with the desired sulfate content.

In Figure 2.23, the fine cement with a high Blaine value hydrates much faster at an early age. Since the fine cement has a larger contact area with water, more cement can hydrate. The later age hydration starts to slow down.

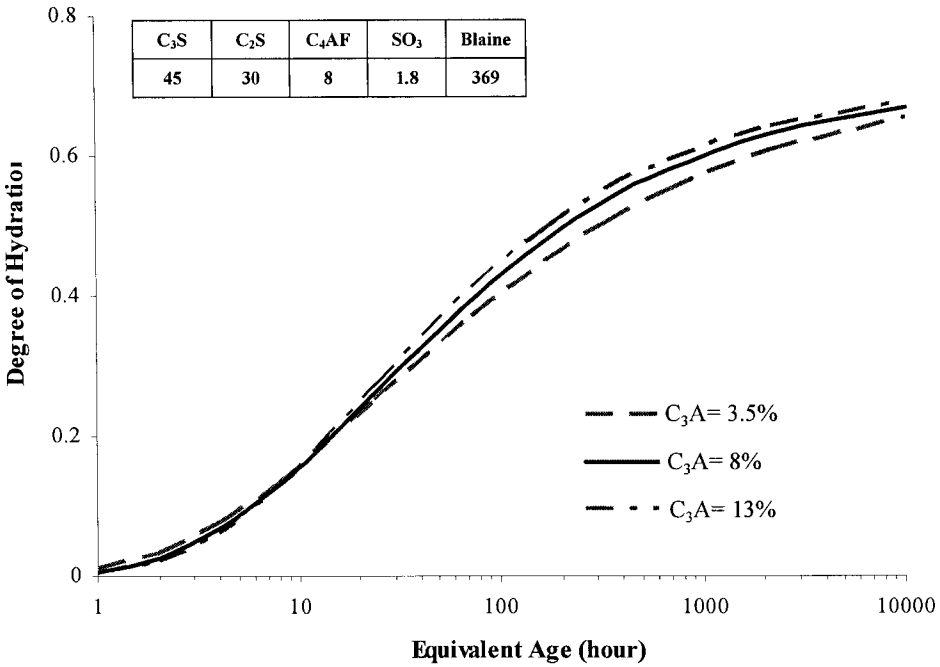

Figure 4.21: Effect of C_3A

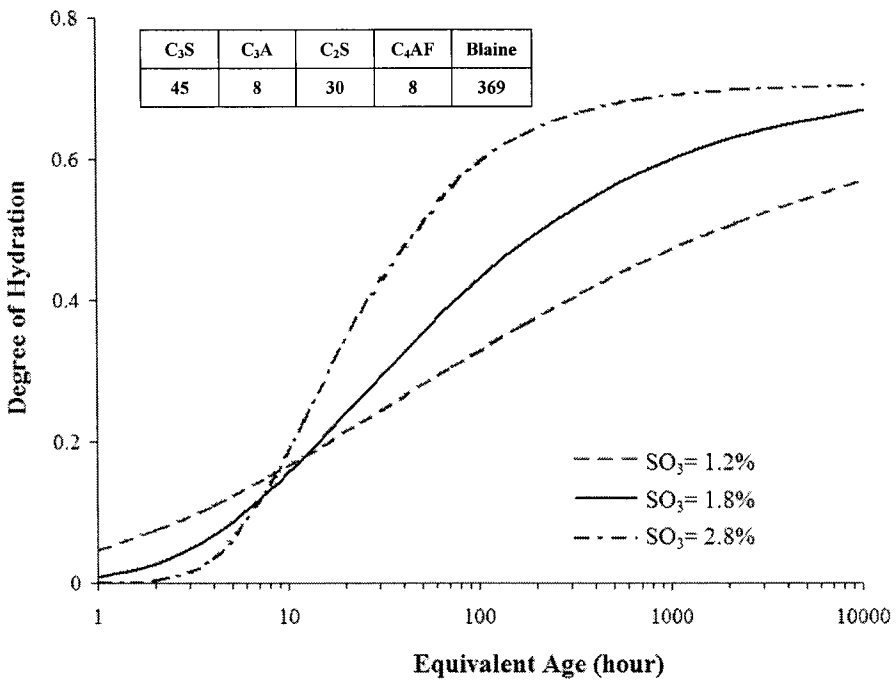

Figure 4.22: Effect of SO_3

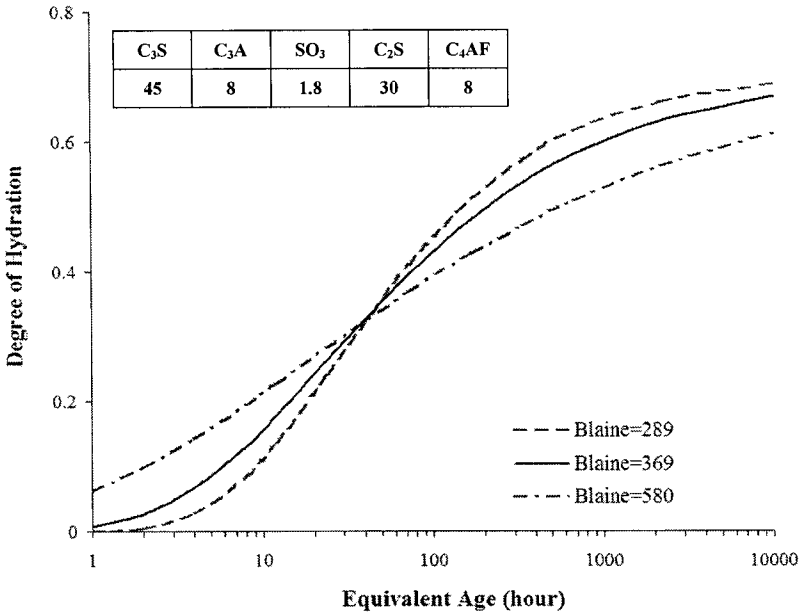

Figure 4.23: Effect of Blaine

As shown in Equation 4.21, the w/c ratio has an effect on the ultimate degree of hydration. The effect is clearly shown in Figure 4.24. The w/c ratio has a more significant effect on later age hydration. The higher the w/c ratio, the higher the later age degree of hydration.

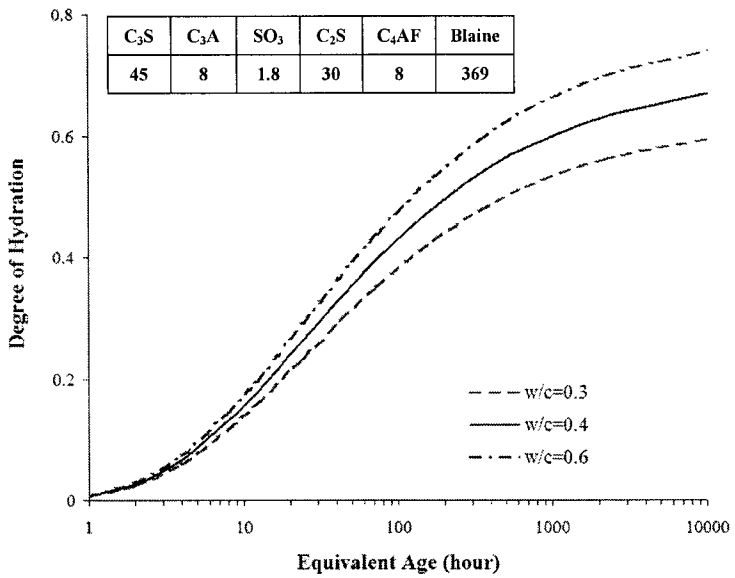

Figure 4.24: Effect of w/c

The test results in Section 4.22 demonstrate that replacing cement with different levels and types of SCMs can change the cement hydration process. These effects are illustrated in Figures 4.25 to 4.28. Figure 4.25 shows that increasing the replacement level of slag decreases the degree of hydration. However, at a later age, the cementitious material with a high percentage of slag will have a higher later age degree of hydration. Figure 4.26 shows the influence of the slag HI variation. In cementitious materials containing high HI slag, the cement hydration proceeds faster after a certain time.

Replacing fly ash with cement has the same influence as the slag replacement (Figure 4.27). The CaO content of fly ash can also affect the hydration (Figure 4.28).

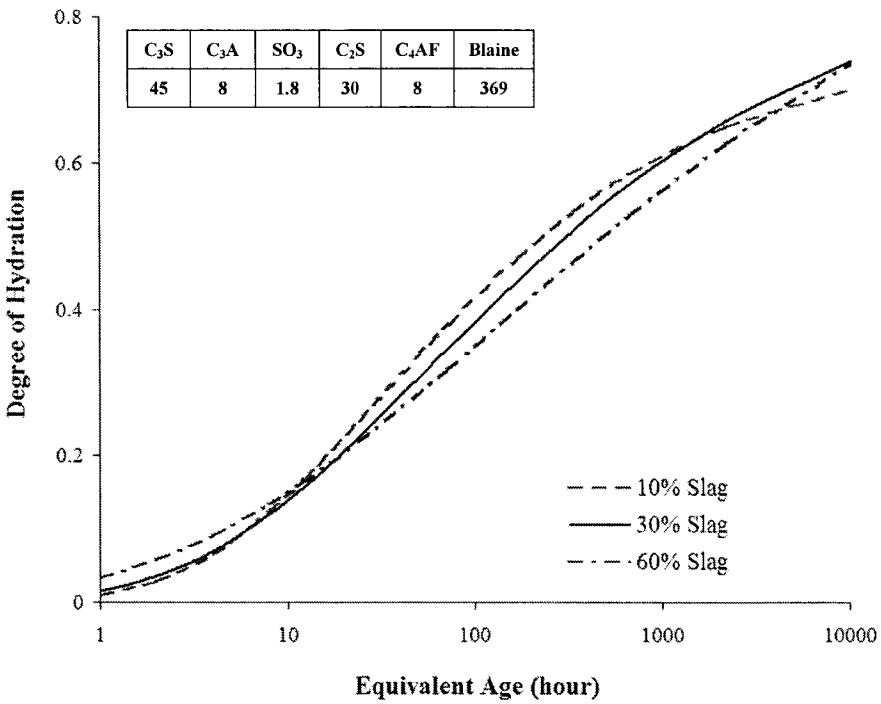

Figure 4.25: Effect of Slag Replacement

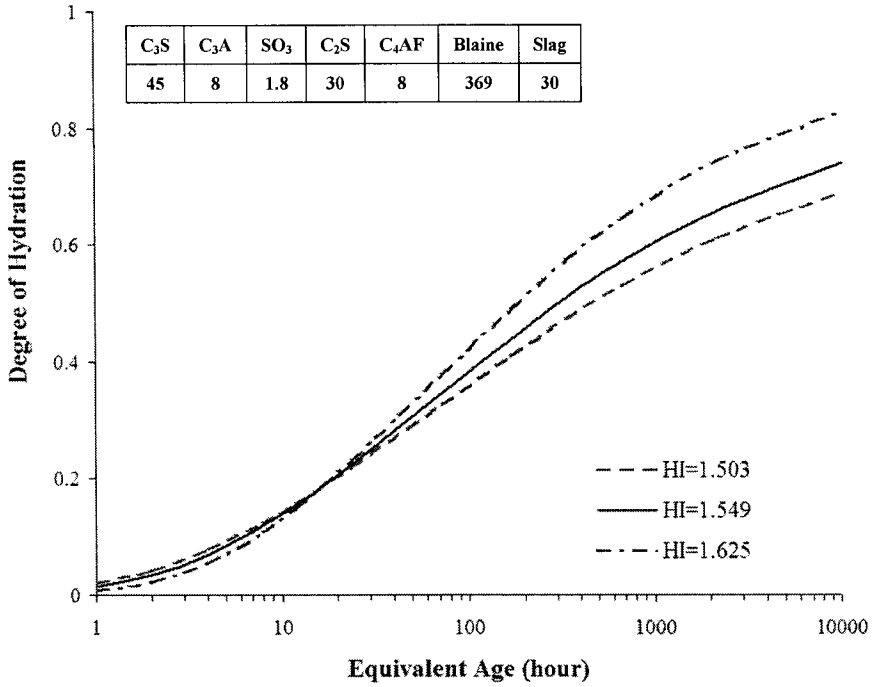

Figure 4.26: HI Effect

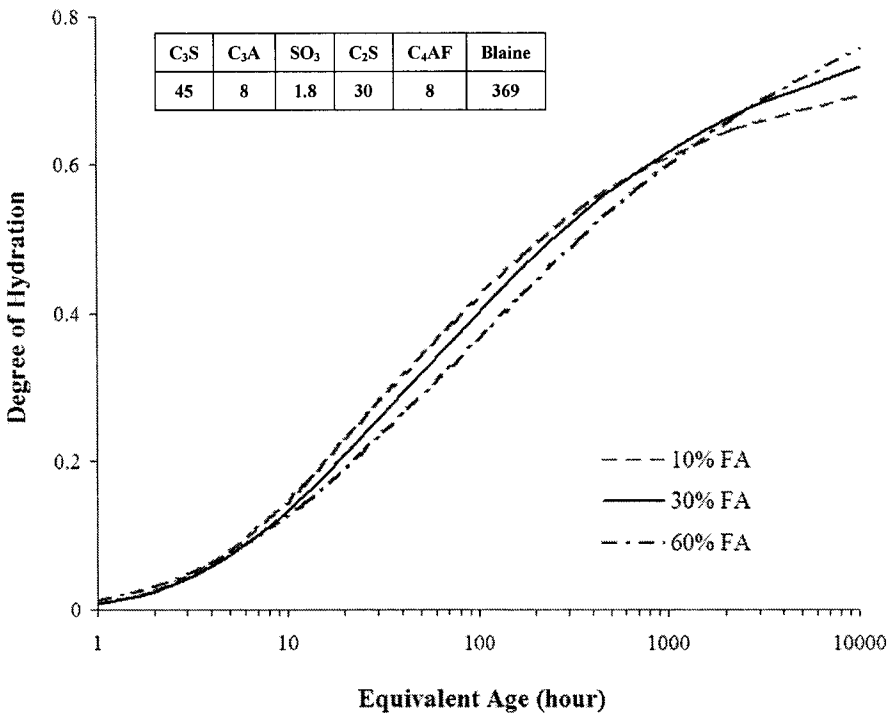

Figure 4.27: Effect of Fly Ash Replacement

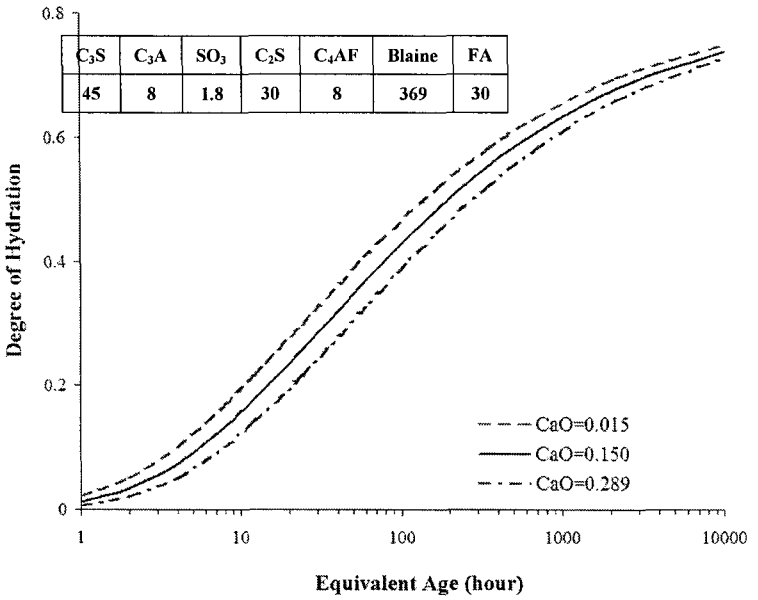

Figure 4.28: Effect of CaO of Fly Ash

4.3 Summary

This chapter presented the development of the heat of hydration model for different cementitious materials. To characterize the heat of hydration for cementitious materials, 23 concrete mixtures were tested by semi-adiabatic calorimeter testing. In addition to these 23 tests, Lerch and Ford's (1948) test results were used of another 20 tests on different types of cement, expanding the database. With these two sets of data, statistical analysis was performed to develop the heat of hydration model. In addition, sensitivity analysis was performed to determine the effect of each variable in the newly-developed heat of hydration model. The final model uses a reference temperature of 21.1°C and considers the following factors:

- Cement chemical composition: C_3S, C_3A, SO_3
- Cement fineness: Blaine value
- Mineral admixture, slag and fly ash
- Chemical composition of the slag and fly ash
- W/c ratio
- Curing temperature, thermal activity

The modeling results show that the proposed heat of hydration model is able to accurately predict the heat generation for cementitious materials. However, during the development of the heat of hydration model, several assumptions were made.

- The total heat of hydration for slag is constant.
- The total heat of the fly ash is only related to the CaO content.
- The ultimate degree of hydration is the same for cementitious materials containing different types of fly ash.
- The ultimate degree of hydration for cement is only a function of the w/c ratio.
- Chemical admixtures have no effect on cement hydration.

Because of these assumptions, there are limitations for this model. To improve the heat of hydration model, the following recommendations are proposed:

- If high accuracy is required, semi-adiabatic testing is recommended to obtain the real parameters in the model.
- More semi-adiabatic tests are recommended to expand the database. The model should be modified based on the larger database.
- The chemical admixture should be incorporated into the model.
- Cement particle distribution also affects cement hydration, even for cements with the same Blaine value. It is necessary to include a new parameter in the model to account for the particle distribution.

CHAPTER 5
MODIFIED MATURITY-STRENGTH MODEL

The strength of hardened concrete is often used for concrete design and quality control. This chapter describes the development of the maturity-strength model for concrete made with various cementitious materials under different curing conditions. In the present study, the maturity of concrete is represented by the equivalent age, t_{eq}.

5.1 General Concept and Approach

5.1.1 Maturity-Strength Model

Many mathematical models of maturity-strength have been proposed in past publications. Plowman (1956) found that there is a linear relationship between maturity and strength. Therefore, he suggested the following equation.

$$S = a + b\log(t_{eq}) \qquad 5.1$$

Where,

S = Compressive strength

a, b = Constants

t_{eq} = Equivalent age

The constants a and b are related to the water/cement (w/c) ratio and the type of cement. However, this function predicts ever-increasing strength with increasing maturity. Also, only intermediate strength increases linearly with maturity (Carino 2004).

Bernhardt (1956) proposed a hyperbolic maturity-strength function, Equation 5.2. This function was adopted by ACI Committee 229 to estimate concrete strength development (Carino 2004).

$$S = \frac{t_{eq}}{\frac{1}{A} + \frac{t_{eq}}{S_u}} \qquad 5.2$$

Where,

t_{eq} = Equivalent age

A = Initial slope of strength-maturity curve

S_u= Ultimate or limiting strength

This equation assumes that concrete starts to gain strength from zero equivalent age. However, concrete starts to develop strength after setting. *ASTM C 1074* recommends a similar formula that takes into account the setting time.

$$S = S_u \cdot K \cdot \frac{t_{eq} - t_{eq0}}{1 + K \cdot (t_{eq} - t_{eq0})} \qquad 5.3$$

Where,

K = Curve fit constant for strength prediction

t_{eq} = equivalent age

t_{eq0} = Equivalent age, at which concrete starts to gain strength

Freiesleben Hansen, and Pedersen (1985) suggested an exponential form of the maturity-strength maturity, which is similar to the maturity-heat of hydration formula.

$$S = S_u \cdot \exp(-\left(\frac{\tau}{t_{eq}}\right)^{\beta}) \qquad 5.4$$

Where,

τ = Time parameter

β = Slope parameter

According to the test data, Carino (2004) pointed out that, for strength beyond 50% of the limiting strength, Equation 5.1 proposed by Plowman does not model the strength gain as accurately as Equations 5.3 and 5.4. Therefore, Equation 5.1 is not considered for the present model development.

5.1.2 Approach to New Model

The process of maturity-strength model development is similar to the modeling of the heat of hydration. It contains three steps:

Step 1: Calculating the equivalent age from the maturity test data (To be consistent with the heat of hydration model, the 70°F (21.1°C) was selected as the reference temperature.)

Step 2: Performing nonlinear regression analysis to fit each set of the data obtained from Step 1 with Equations 5.3 and 5.4. The two purposes for this step are as follows: selecting one maturity-strength relationship from Equations 5.3 and 5.4 and obtaining the strength parameters of the selected maturity-strength model for each set of data.

Step 3: Establishing the relationship between the parameters in the selected maturity-strength relationship and the factors that affect concrete strength development through statistical analysis, which is the model for strength development.

5.2 Factors Considered in Strength Development

Concrete compressive strength increases exponentially at early age. After a few days, the rate of the strength gain becomes slower but the strength gain continues as long as water can reach the unhydrated cement particles. Numerous factors can affect the way that concrete strength develops. The factors considered in the developed model include cement type, w/c ratio, air content, mineral admixture, and curing conditions.

5.2.1 Cement Type

As discussed in Section 2.2.2, cement chemical composition and fineness influence the hydration process, which in turn affects the strength growth. Figure 5.1 shows the influence of the cement types. The sum of the C_3S and C_2S of all five cements are about the same, 75%. The initial rates of strength gain are quite different. Type III cement has a higher early age strength gain rate. Type IV has the lowest rate. However, at 90 days, all types of the strength are the same. Due to C_2S content and fineness, the cement that has a lower rate at early age generally has a higher ultimate strength. Figure 5.2 shows the influence of the fineness on concrete strength gain. It shows that the higher the fineness, the higher the strength, especially at early age. The compressive strength for cement with fineness values of 277 and 490 m^2/Kg becomes very similar after 1 year. Even if the cement types are the same, the influence of the cement make must be considered because the chemical composition and fineness vary for cement from different plants. Figure 5.3 shows the compressive strength curves for three different types of Swedish ordinary Portland cement (OPC). Although they are all ordinary cement, the growth rates are different, especially at early age.

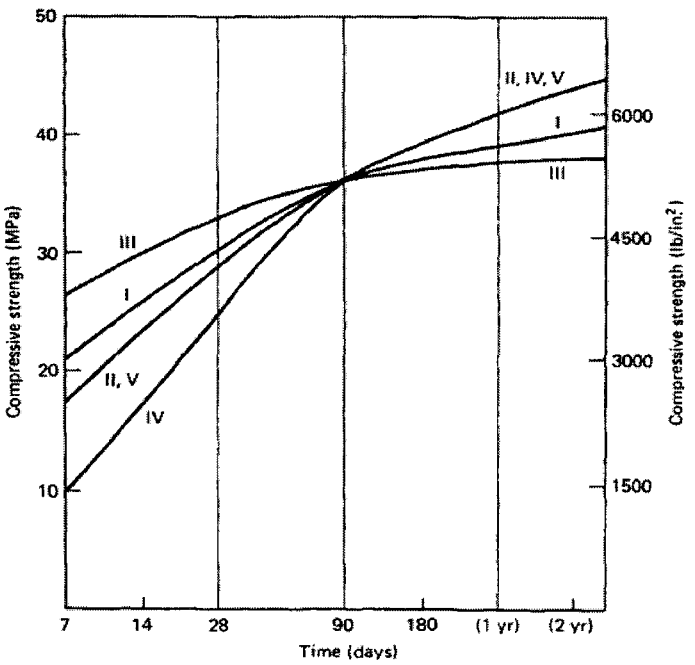

Figure 5.1: Strength of 6×12 in. Concrete Cylinder Made with Different Types of OPC (Adapted from Mindess and Young 1981)

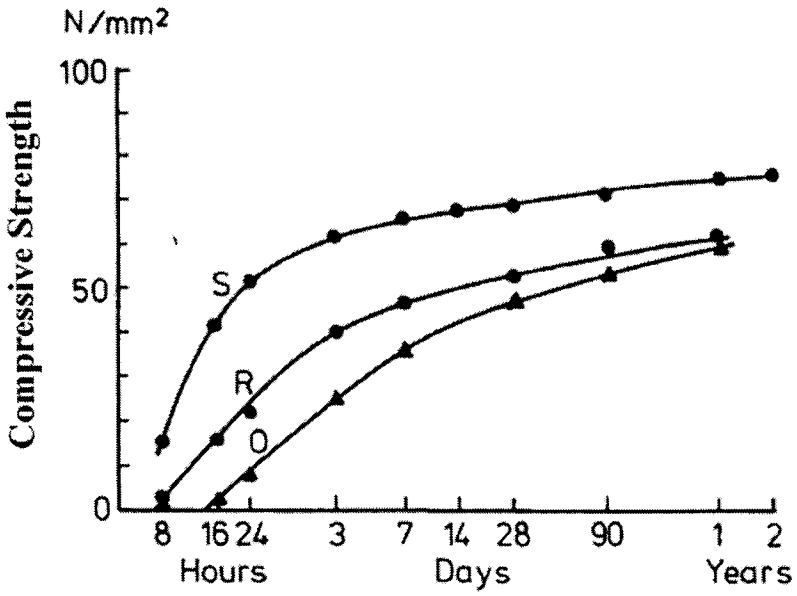

Figure 5.2: Concrete Compressive Strength with Cements of Various Fineness w/c = 0.4, S=742 m^2/Kg, R=490 m^2/Kg, O=277 m^2/Kg (Byfors 1980)

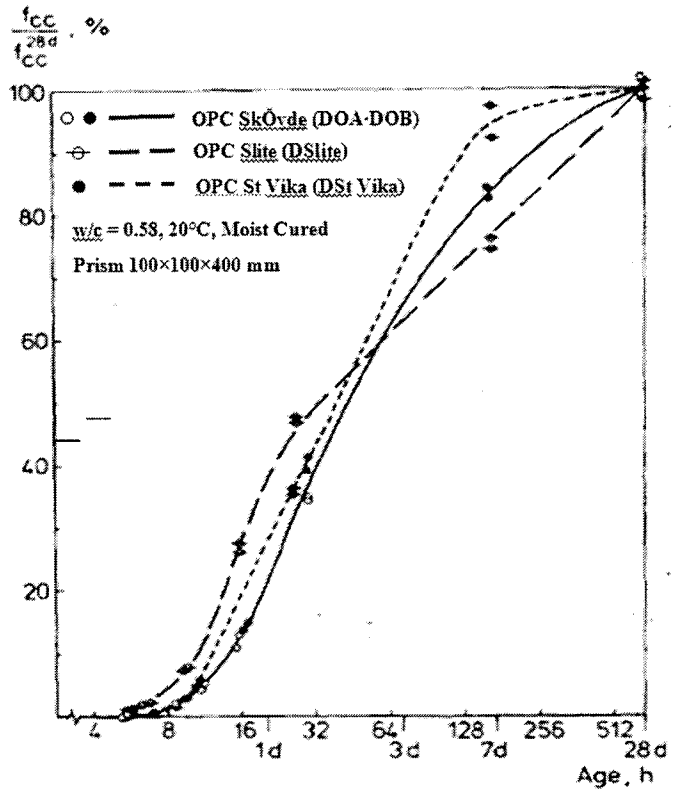

Figure 5.3: Effect of Cement Type on Strength Gain (Byfors 1980)

5.2.2 W/C Ratio

In 1918, Duff Abrams found the relationship between concrete strength and the w/c ratio, which is known as Abram's law. The relationship is expressed as follows (Neville 1972):

$$f_c = \frac{k_1}{k_2^{w/c}} \qquad 5.5$$

Where,

K_1, K_2 = Empirical constants

w/c = Water/cement ratio

Abram's law indicates that there is a linear relationship between the w/c ratio and the compressive strength on a logarithmic scale. For low- and medium-strength concrete made with normal aggregate, the strength improvement is caused by the reduction of the mortar matrix porosity and the improvement of the interface transition (IT) zone, which is the weakest link in concrete. For high-strength concrete, the strength increase is mainly caused by the improvement in the strength of the IT zone. (Mehta and Monteiro 1993)

Figure 5.4 illustrates the influence of w/c ratio on concrete strength gain. Once the strength starts to increase, the low w/c ratio means a higher strength. The final strength is significantly increased from 12 to 48 N/mm^2 by reducing the w/c ratio from 1 to 0.4.

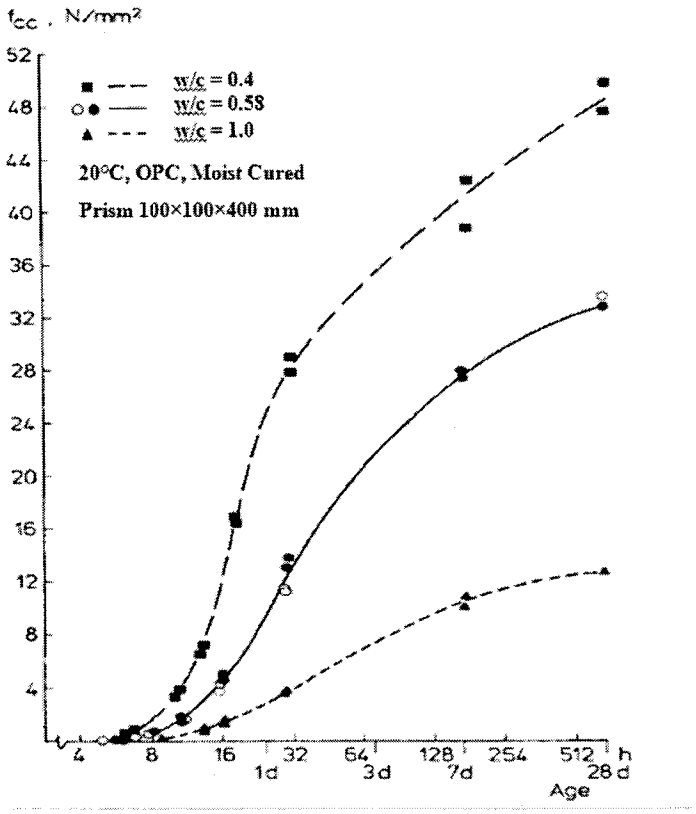

Figure 5.4: Influence of w/c Ratio on Concrete Strength
(Adapted from Byfors 1980)

5.2.3 Admixture

Both mineral and chemical admixtures influence strength development. In this study, the effect of chemical admixtures is not considered. For the mineral admixture or SCMs, only fly ash and slag are considered. Concrete containing SCMs normally has lower early age strength. The reduction of compressive strength depends upon the chemical compositions of the OPC and SCMs, replacement level of SCMs, and concrete curing conditions. After a certain period of curing, the strength of the concrete containing fly ash and slag starts to exceed the normal concrete. This trend, which is mainly caused by the Pozzolanic reaction expressed in Equation 2.14, is shown in Figure 5.5. The reactive silicate of the fly ash and slag reacts with the calcium hydroxide (CH) , which is formed by cement hydration, and forms calcium silicate hydrate (CSH) gel, which is every efficient in filling up large capillary spaces. Both the CH consumption and CSH gel production can increase concrete strength.

The Pozzolanic reaction starts late. The reaction rate is slower than C_3S but comparable to the C_2S reaction.

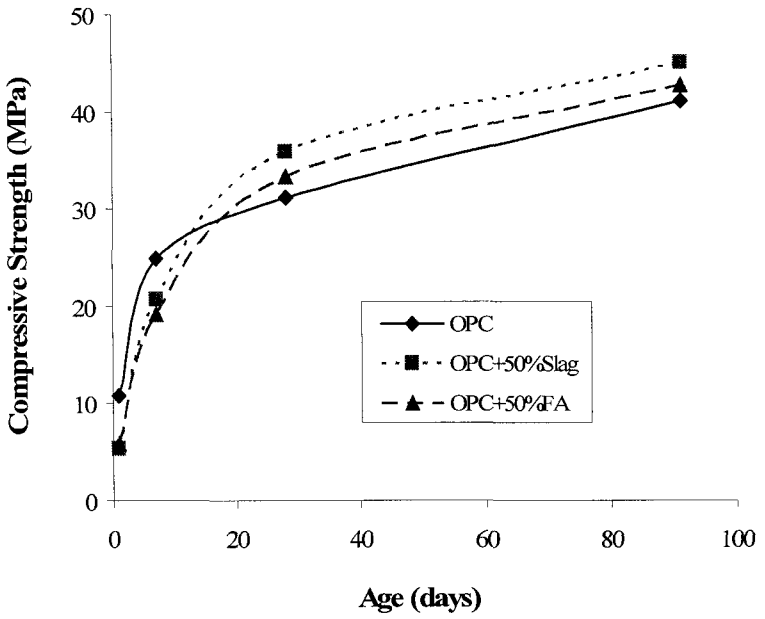

Figure 5.5: Compressive Strength of Various Concrete (Data Adapted from Douglas et al. 1991)

5.2.4 Curing Conditions

According to Guo (1989), temperature influence on strength development is reduced with age (Figure 5.6). The strength of concrete with the same mixing proportion and materials depends on its thermal history. Concrete cured under higher temperatures has higher early strength but lower final strength. The increase of the early age strength is due to the higher rate of cement hydration. The decrease in rate of strength gain at later age is due to diffusion-related hydration (Kjellsen et al. 1991, Verbeck et al. 1968). The rapid hydration caused by high temperatures produces more products, which do not have time to diffuse sufficiently far out from the reaction point. The products prevent further reactions. The nonuniform distribution of the newly formed hydration product causes weak zones in the cement that consequently reduces its strength. The influence of temperature on strength is shown in Figure 5.7.

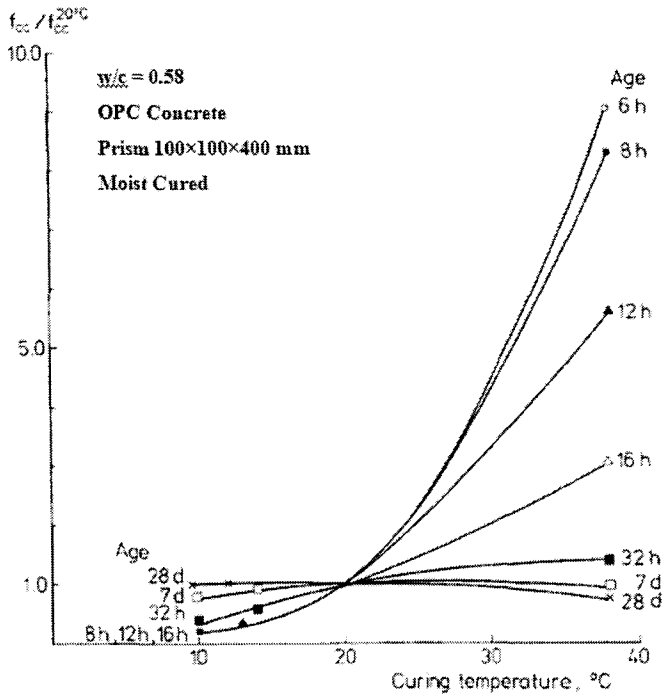

Figure 5.6: Compressive Strength Achieved at Different Ages and Temperatures Related to the Corresponding Strength at 20°C (Adapted from Byfors 1980)

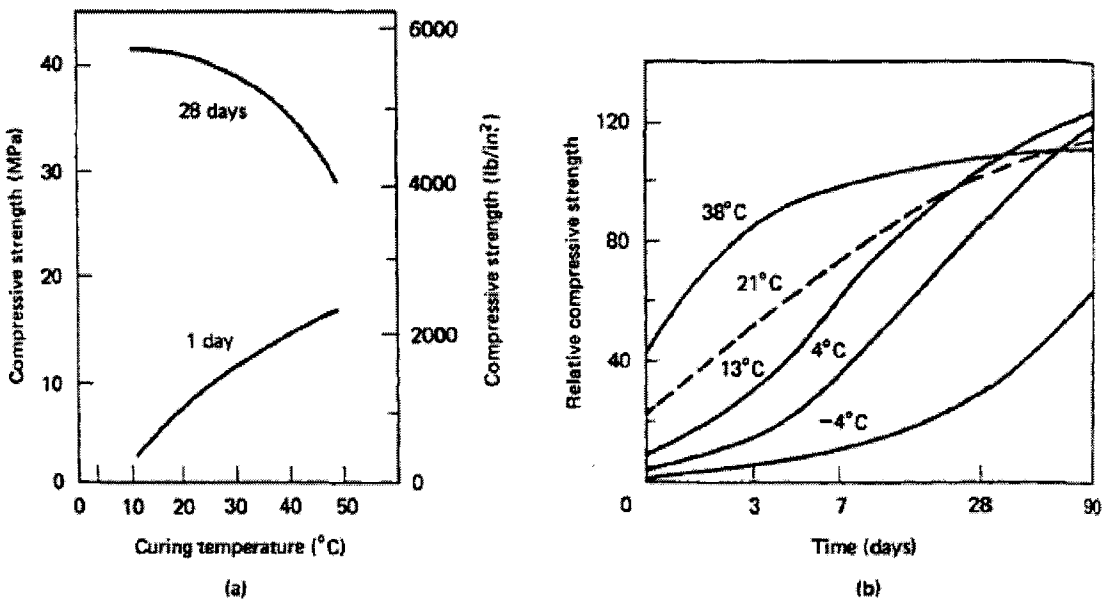

Figure 5.7: Effect of Temperature on Compressive Strength Development : (a) 1-day and 28-day strength (b) Curing temperature maintained continuously (Adapted from Mindess and Young 1981)

Moisture is another factor of curing that affects strength development. Cement hydration stops if the internal relative humidity is lower than 80% because of evaporation or self-desiccation, and consequently, the strength gain stops (Mindess and Young 1981). Figure 5.8 shows the influence of moist curing on strength gain. At early age, the relative humidity does not influence the strength increase because a certain period is required before any effect is obtained. The strength at later age is higher for samples cured under higher relative humidity. The influence of the limited moisture curing is mainly a drying problem, which is related to the size and ambient relative humidity.

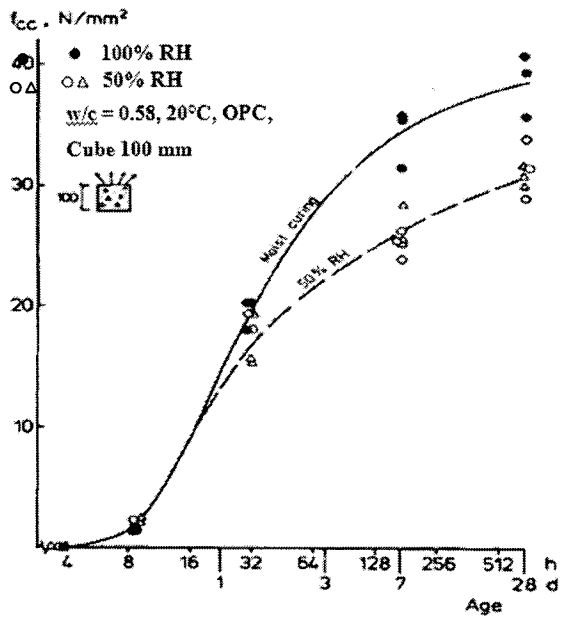

Figure 5.8: Effect of Moist Curing on Strength Gain (Adapted from Byfors 1980)

5.2.5 Air Content

Compressive strength changes with air content. Air voids, either entrapped air or entrained air, increases porosity. The increasing porosity, in turn, decreases concrete strength. The reduction depends on the w/c ratio and the cement content (Figure 5.9). Figure 5.9a shows that at given w/c, strength decrease as air content increases. Figure 5.9b shows that the strength loss is higher for concrete containing high amounts of cement. On the other hand, concrete with low amounts of cement has a small strength loss, even a small strength gain as the air content increases.

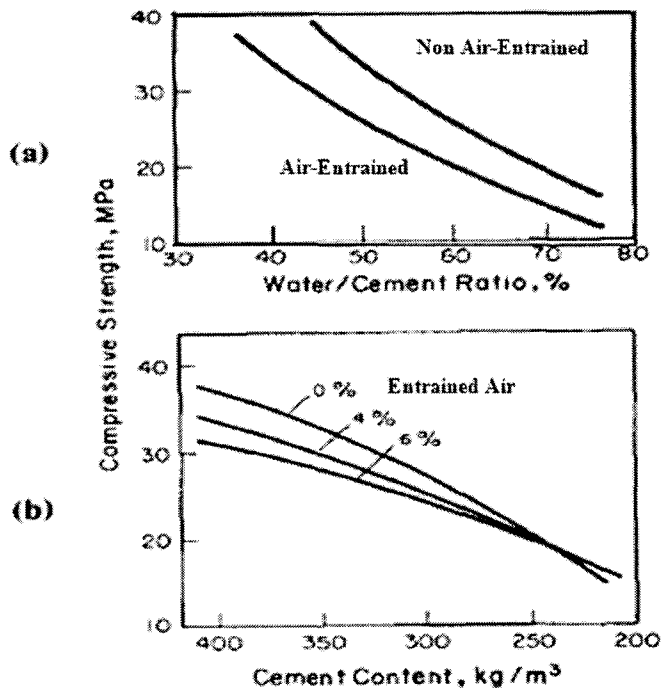

Figure 5.9: Influence of Air Content on Compressive Strength (Mindess and Young 1981)

5.2.6 Cement Content

Cement content affects the strength in two different ways. If a constant workability is maintained, the strength of concrete increases as the cement content increases due to the reduced water requirement (Mindess and Young 1981). However, if the w/c ratio is kept constant, concrete strength decreases as the cement content increases probably because the increased cement requires more water, which in turn, increases the total porosity. (Mindess and Young 1981, Popovics 1990). Due to its conflict effect on strength development and a limited database, the cement content is not incorporated in the developed models.

5.3 Data Source and Analysis

The scope of the database is important for model development. Large databases can produce a more reliable model. To account for the factors listed above, two sets of data were used for model development: laboratory test and literature. The laboratory test data

characterize the effect of SCMs. The literature data set illustrates the effect of different types of cement and w/c ratio.

5.3.1 Data from Laboratory Tests

To characterize the effect of SCMs, maturity and strength tests were performed for concrete made with four different types of fly ash and three different types of slag. The cement replacement level for each mix is listed in Table 3.3 and the concrete mix design is shown in Table 3.2. The test results are divided into three groups: (1) slag replacement, (2) fly ash replacement, and (3) slag-fly ash replacement.

Slag replacement

Figure 5.10 shows the maturity-strength relationship of concrete with different levels of slag replacement. The replacement of slag significantly reduces concrete strength at an early age. The strength reduction increases as the slag content increases. At the equivalent age of about10 days, all concrete reaches a similar compressive strength value. After that, the concrete with slag replacement starts to exceed the concrete without slag. The concrete with 60% slag replacement has the highest compressive strength at the equivalent age of about 40 days. The strength enhancement caused by the slag replacement is due to the Pozzolanic reaction, which is discussed in Section 2.2.2.6.

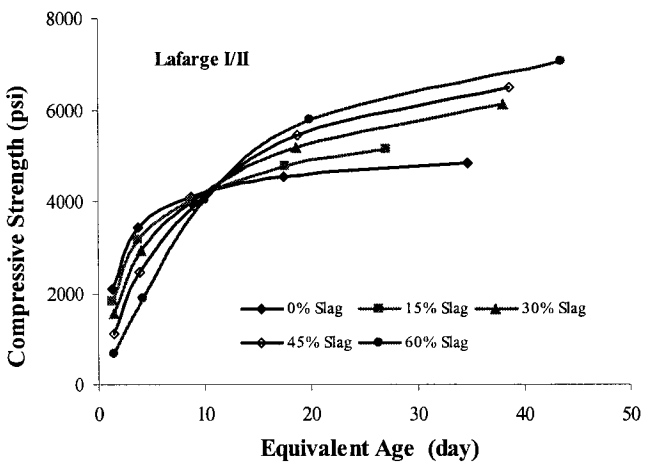

Figure 5.10: Effect of Slag Replacement on Strength Development

Figure 5.11 shows the strength development characteristics of concrete with different types of slag replacement. For the first few days, the compressive strength is similar for all different concrete mixtures. After about 3 days, the concrete containing Lehigh slag, which has a higher hydraulic index (HI), starts to gain strength much faster than concrete containing the other two types of slag. At later age, the strength difference among concrete containing these three types of slag is reduced. Concretes containing slag from Holcim and S.T., which have similar HI values, have similar compressive strength.

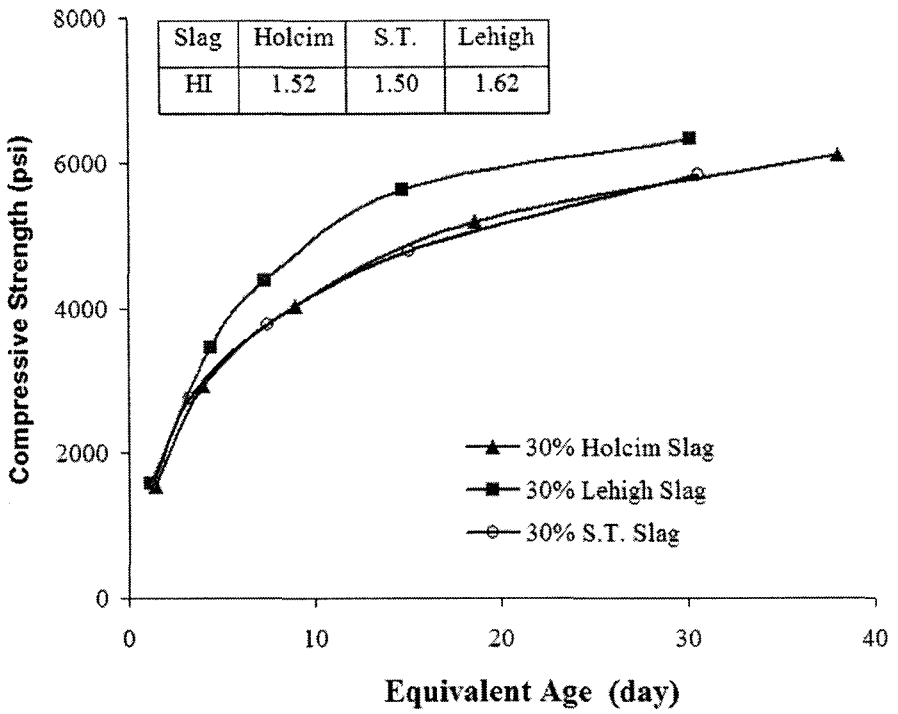

Figure 5.11: Effect of Different Slags on Strength Development

Fly ash replacement

Figures 5.12 and 5.13 show the influence of fly ash replacement on concrete strength development. The compressive strength decreases as the replacement of the fly ash increases at 1 day. After 4 days, the concrete with 30% fly ash replacement has the highest compressive strength. Compressive strength noticeably decreases as the fly ash content increases beyond 30%. The concrete with 60% fly ash replacement has the lowest compressive strength.

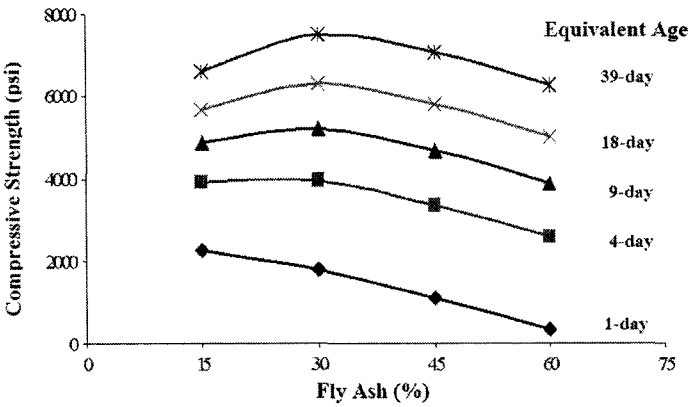

Figure 5.12: Effect of Fly Ash Replacement on Strength Development

Figure 5.13 indicates that concrete with different types of fly ash have different compressive strengths. The difference is mainly caused by their chemical composition, especially CaO content, which is listed in the figure. Since fly ash from Muscatine and Salix have similar CaO content, they have similar compressive strength. Concrete with fly ash from Coal Creek and Class F fly ash have similar compressive strengths despite the different chemical composition. This is due to the difference of the air content, which is only 3% for concrete with Class F fly ash and 6.4% for concrete containing fly ash from Coal Creek. The reduced air content increases the compressive strength. If both of them have the same air content, the concrete with Class F fly ash will have lower compressive strength.

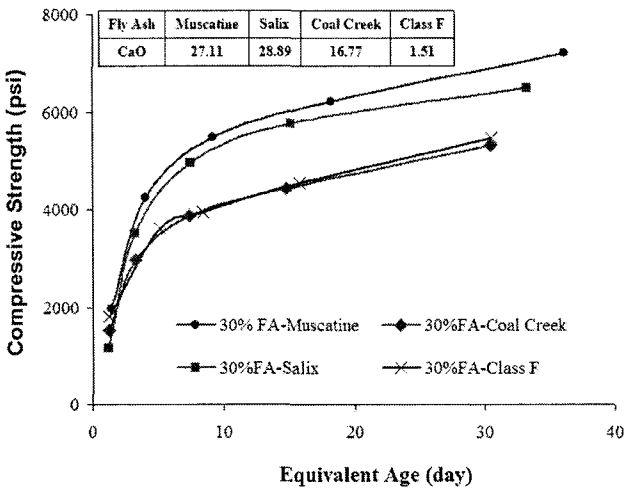

Figure 5.13: Effect of Different Fly Ash on Strength Development

Combined slag and fly ash replacement

Figure 5.14 shows the effect of the slag and fly ash combination on concrete strength where the slag-to-fly ratio is 3. Concrete containing slag and fly ash have lower compressive strength at early age and high strength at later age. The time that the strength exceeds the concrete without fly ash and slag is different for concrete with different replacement levels of fly ash and slag. This is different from concrete containing only slag.

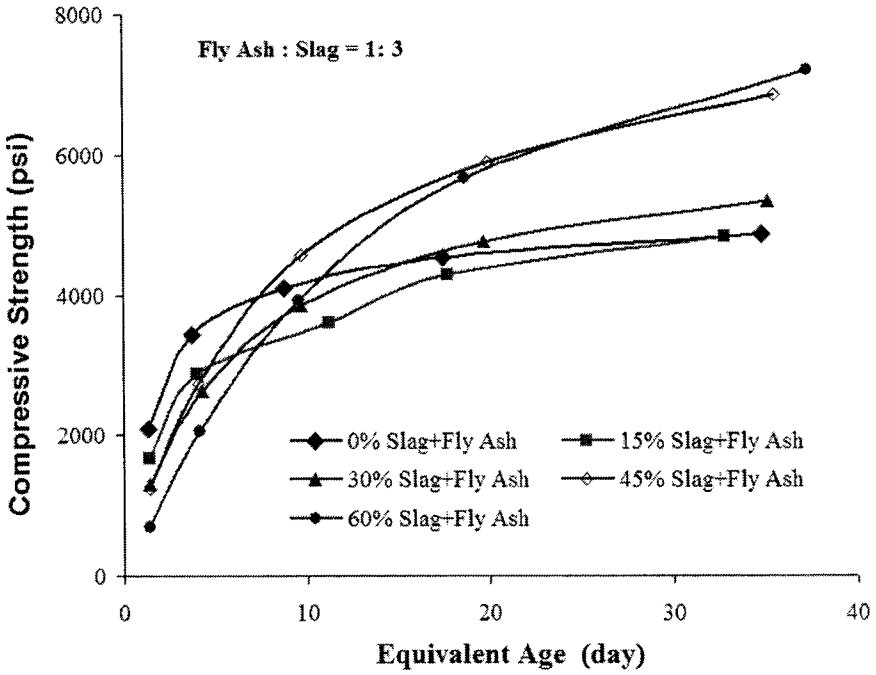

Figure 5.14: Effect of Fly Ash- Slag on Strength Development

5.3.2 Data from Literature

To develop the model, the compressive strength of 19 different cement mixtures, including all five types of cement, was adopted from Wood (1992). The cement are the same as those used for the heat of hydration model; their properties are listed in Table 4.1. All were used in concrete mixes of two different w/c ratios, 0.43 and 0.56. Air content ranges from 1.1% to 2.5%. The slump varies from 1.9 to 3 inches. The mixing proportions, air content, and slump of the concrete are listed in Appendix B.

The average compressive strength for concrete made with each type of cement with two different w/c ratios is presented in Figure 5.15. In general, concrete made with Type I and Type III cement have higher strengths at early age than concrete made with Types II, IV, and V cement. However, at time over 1 year, concrete made with Types II, IV, and V cement showed higher strengths than concrete made with Types I and III cement because of their chemical compositions. Normally, Types II, IV, and V cement contain more C_2S. Types I and III cement, on the other hand, contain more C_3S.

Since C_3S provides most of the early age strength and C_2S reacts much slower than C_3S, Types I and III cement have higher early age strength. Type III cement also has higher specific surface area, which can increase the reaction rate at early age.

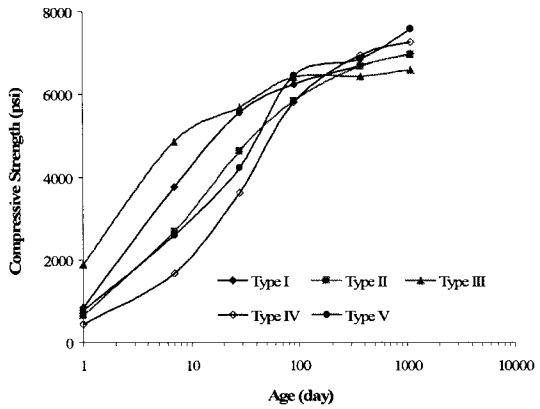

(a) w/c = 0.56

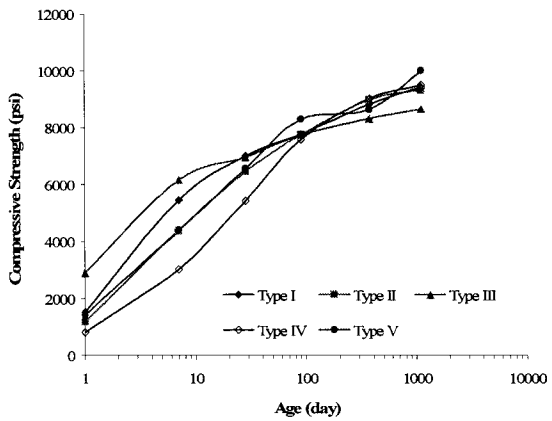

(b) w/c = 0.43

Figure 5.15: Strength Development for Different Types of Cement

5.3.3 Nonlinear Regression Analysis

As stated in Section 5.1, Equations 5.3 and 5.4 are able to predict compressive strength from maturity. Nonlinear regression was performed for each set of data to estimate the parameters in Equations 5.4 and 5.5. The JMP software was applied to perform the nonlinear regression. The criteria and stop limits are the same as used in the heat of hydration model, listed in Table 4.2.

According to the nonlinear regression results, which are presented in Figure B.1 of Appendix B, Equation 5.4 can predict strength better than Equation 5.3. The overall R^2 values are 0.994 and 0.981 for the prediction of Equations 5.4 and 5.3 respectively. The predicted values from Equation 5.4 are closer to the real values. Therefore, Equation 5.4 was selected as the maturity-strength relationship function:

$$S = S_u \cdot \exp(-\left(\frac{\tau}{t_{eq}}\right)^{\beta}) \qquad 5.4$$

The estimated S_u, τ, and β values through the nonlinear regression for each set of data are summarized in Tables 5.1 and 5.2 for the laboratory test and literature data respectively. Table 5.1 shows that the ultimate strength, Su, increases continuously as the slag replacement level increases. For concrete with fly ash, the S_u first increases and then decreases as the replacement level increases beyond 30%. However, for concrete with slag, the S_u increases continuously until 60% replacement, which is consistent with Maekawa et al. (1999). Unlike the replacement level trend, the S_u is almost the same for different types of fly ash and slag. The time parameter τ increases when SCM was added. The larger the τ, the slower the early age strength development. The slope parameter β decreases slightly and then increases as the SCM levels increase. Both τ and β depend on the type of SCMs.

Table 5.1: Estimated Parameters for Laboratory Test

Fly Ash (%)	Slag (%)	w/c	S_u (psi)	τ (hour)	β
0	0	0.42	6158	32.262	0.483
0	15	0.42	7344	59.919	0.446
0	30	0.42	8336	91.680	0.502
0	45	0.42	8672	121.894	0.592
0	60	0.42	9290	164.482	0.717
15	0	0.42	9081	56.981	0.403
30	0	0.41	10452	74.277	0.439
45	0	0.41	8629	79.868	0.599
60	0	0.41	7377	99.254	0.720
3.75	11.25	0.42	6578	56.833	0.426
7.5	22.5	0.42	7973	106.680	0.457
11.25	33.75	0.42	10792	161.275	0.492
15	45	0.42	11191	232.000	0.589
11.25	3.75	0.41	8311	42.698	0.512
22.5	7.5	0.41	9890	83.334	0.420
33.75	11.25	0.41	10490	137.498	0.488
45	15	0.40	10370	215.578	0.496
30	0	0.41	11352	221.413	0.318
30	0	0.41	9540	138.056	0.341
30	0	0.41	9372	82.297	0.516
0	30	0.42	8512	96.174	0.447
0	30	0.42	8599	74.967	0.538

Table 5.2 summarizes the estimated parameter values for the literature data set. Types II, IV, and V cement have higher S_u values than Types I and III cement for both w/c ratios. Type III cement has the lowest τ values, meaning that it hydrates fast at an early age. On average, Type IV cement has the highest τ values, which are 394 for a w/c ratio of 0.55 and 237 for a w/c ratio of 0.42. The β values are not influenced by w/c for all types of cement. Table 5.2 also shows that w/c ratio can affect S_u and τ. The S_u values decrease as the w/c ratio increases. The τ values, on the other hand, increase as the w/c ratio increases.

Table 5.2: Estimated Strength Parameters for Literature Data (Wood 1992)

Cement	w/c	S_u (psi)	τ (hour)	β	w/c	S_u (psi)	τ (hour)	β
11	0.56	6952	79.853	0.609	0.41	9075	70.084	0.609
12	0.55	7163	104.572	0.677	0.41	9448	75.014	0.681
13	0.57	6968	151.420	0.501	0.42	8950	98.837	0.509
14	0.55	6946	108.629	0.531	0.41	9112	89.313	0.533
15	0.59	6306	48.139	0.751	0.45	7974	39.955	0.757
16	0.56	6791	95.146	0.553	0.41	8824	63.677	0.535
17	0.61	6176	97.579	0.587	0.46	8506	81.529	0.575
18	0.58	6692	94.817	0.664	0.49	8501	76.389	0.629
Average		6749	97.519	0.609		8799	74.350	0.604
21	0.56	7966	263.110	0.489	0.40	9833	168.053	0.508
22	0.54	7140	158.599	0.578	0.41	9665	100.840	0.585
23	0.54	7345	138.479	0.456	0.42	9167	120.460	0.461
24	0.56	6492	144.700	0.497	0.42	8320	102.699	0.502
25	0.57	7185	210.285	0.491	0.42	9514	179.800	0.46
Average		7226	183.035	0.502		9300	134.370	0.503
31	0.6	6360	43.074	0.479	0.49	7836	40.170	0.484
33	0.55	6798	31.517	0.48	0.43	7853	23.981	0.446
Average		6579.1	37.300	0.480		7844	32.076	0.465
41	0.53	7928	482.917	0.472	0.40	10436	227.054	0.479
42	0.55	7963	426.764	0.432	0.42	10914	289.766	0.427
43	0.54	7550	273.460	0.498	0.42	9506	193.475	0.48
Average		7814	394.380	0.467		10285	236.765	0.462
51	0.54	8024	268.634	0.429	0.41	10239	138.489	0.426

5.4 Modeling of Concrete Strength Parameters

This section describes the development of models for the strength parameters, S_u, τ, and β. These models were developed in the same way as the models for heat of hydration parameters, described in Section 4.2.3.3.

After the initial analysis of literature data, it was found that ultimate strength is related to C_2S, w/c ratio, and air content; time parameter τ is related to w/c ratio, C_3S, C_3A, SO_3, and the Blaine value; and slope parameter β is related to C_3S+C_2S, C_3A, and the Blaine value. The analysis results are presented in Appendix B. The results in Table 5.1 reveal that the strength parameters, S_u, τ, and β, are related to fly ash and slag. The time and slope parameters, τ and β, are also affected by the type of the fly ash and slag. Thus, strength parameters can be expressed as follows.

Ultimate Strength S_u

$S_u = f$ (w/c, air, C_2S, FA, slag)

Time Parameter τ

$\tau = f$ (w/c, C_3S, C_3A, SO_3, Blaine, FA, FA-CaO, Slag, HI)

Slope Parameter β

$B = f$ (C_3S+C_2S, C_3A, Blaine, FA, FA-CaO, Slag, HI)

Where,

w/c = Water/cementitious material ratio

Air = Air content, %

C_2S, C_3S, C_3A, SO_3 = Cement compounds

FA = Weight ratio of fly ash to cementitious material

Slag = Weight ratio of slag to cementitious material

Blaine = Blaine fineness of cement, m^2/Kg

FA-CaO = Weight ratio of fly ash CaO to fly ash

HI = Hydraulic Index of slag

After identifying the important variables for each strength parameter, nonlinear regression analysis was performed to find the best-fit equation for each parameter. The results are listed in Equations 5.6 to 5.8.

$$S_u = \exp(-1.810 \cdot w/c + 10.143) \cdot (1 - 0.051 \cdot Air) \cdot \left(C_2S^{0.143} + 2.155 \cdot FA - 3.544 \cdot FA^2 + 0.711 \cdot Slag - 0.367 \cdot Slag^2\right) \quad 5.6$$

$$\tau = \exp[-4.462 \cdot (FA - CaO - 0.2711) - 2.147 \cdot (HI - 1.519)] \cdot [\exp(3.401 \cdot w/c - 2.709) \cdot C_3S^{-1.659} \cdot C_3A^{-0.378} \cdot SO_3^{-1.154} \cdot Blaine^{-0.229} + 120.306 \cdot FA + 190.939 \cdot Slag + 1221.717 \cdot FA \cdot Slag] \quad 5.7$$

$$\beta = \begin{bmatrix} \exp(3.039) \cdot (C_3S + C_2S)^{-0.653} \cdot C_3A^{0.303} \cdot Blaine^{-0.525}) \\ -0.463 \cdot FA + 1.377 \cdot FA^2 - 0.427 \cdot Slag + 1.392 \cdot Slag^2 \end{bmatrix} \cdot \exp[1.993 \cdot (FA - CaO - 0.2711) + 0.924 \cdot (HI - 1.519)] \quad 5.8$$

Where,

w/c = Water/cementitious material ratio

Air = Air content, %

C_2S, C_3S, C_3A, SO_3 = Cement compounds

FA = Weight ratio of fly ash to cementitious material

Slag = Weight ratio of slag to cementitious material

FA-CaO = Weight ratio of fly ash CaO to fly ash

HI = Hydraulic Index of slag

Blaine = Blaine fineness of cement, m^2/Kg

For Equations 5.7 and 5.8, the FA-CaO value is 0.2711 when there is no fly ash added. The HI value is 1.519 without slag added.

These newly developed parameter models are incorporated into the heat of hydration model and the FEMLAB program to predict concrete strength development from maturity. The application of this model is shown in Chapter 7.

The predicted values and experimentally determined values for each parameter are plotted in Figures 5.16 to 5.18. These figures indicate that the proposed Equations 5.6 to 5.8 accurately predict the strength parameters by considering the effect of the w/c ratio, air content, cement chemical composition, cement fineness, SCMs, chemical compositions of SCMs, and thermal activity of the cementitious material. The R^2 values for S_u, τ, and β are 0.955, 0.959, and 0.852 respectively, meaning that over 95% variation of the experimentally determined S_u, τ values can be explained by the proposed model, Equations 5.6 and 5.7. The R square of β is lower than the other two parameters, which may indicate that other variables not included in Equation 5.8 may also influence the parameter β.

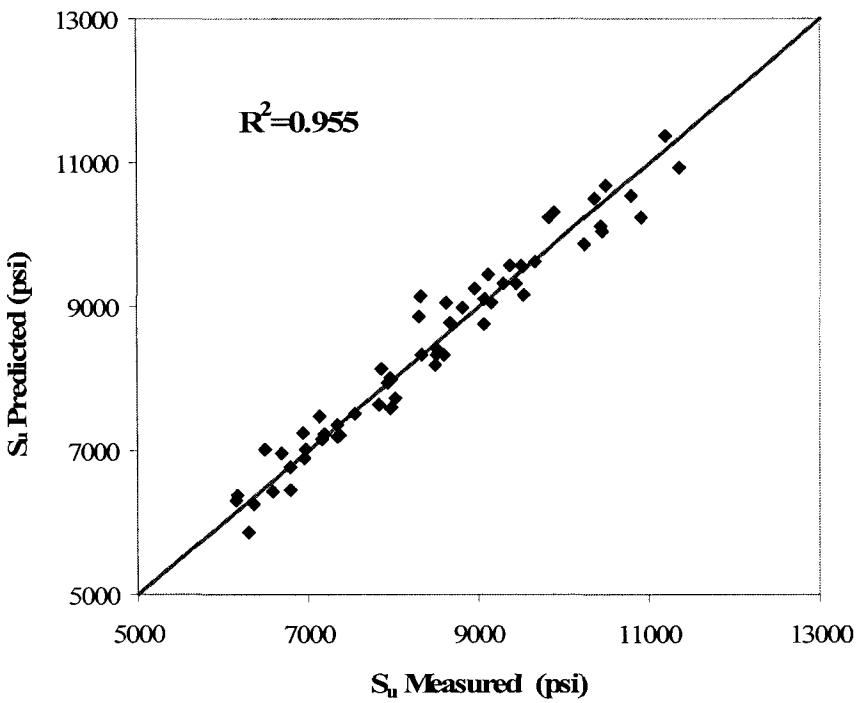

Figure 5.16: Predicted and Measured S_u

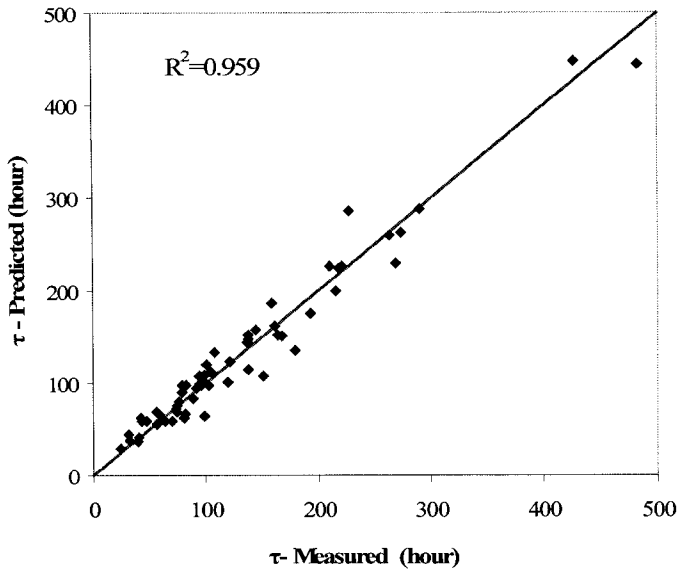

Figure 5.17: Predicted and Measured τ

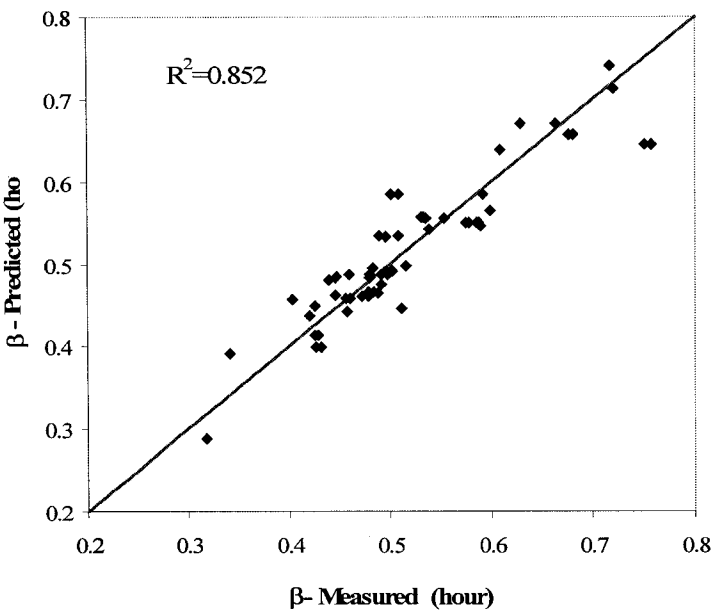

Figure 5.18: Predicted and Measured β

The scatter residual plots, which plot the residual versus the parameter, are shown in Figure 5.19. These figures show that the residuals are randomly distributed. No apparent patterns for residuals with strength parameters are observed. There are no apparent outliers in

the plot. The residues of the Su are within 1,000 psi and less than 10% of the test-estimated Su values.

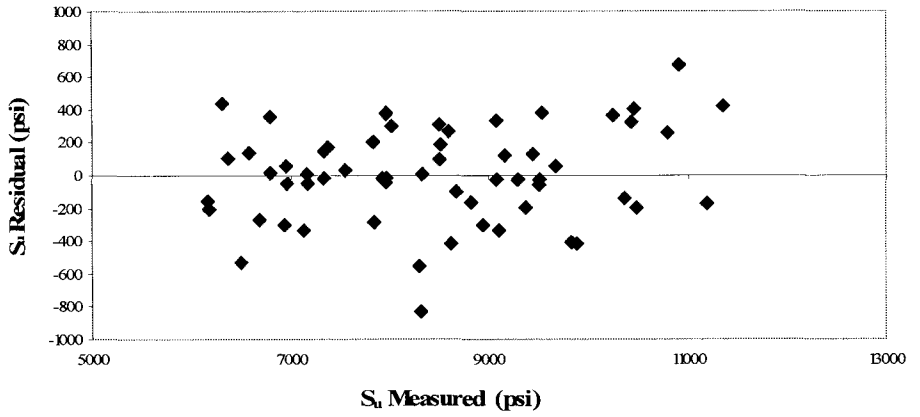

(a)

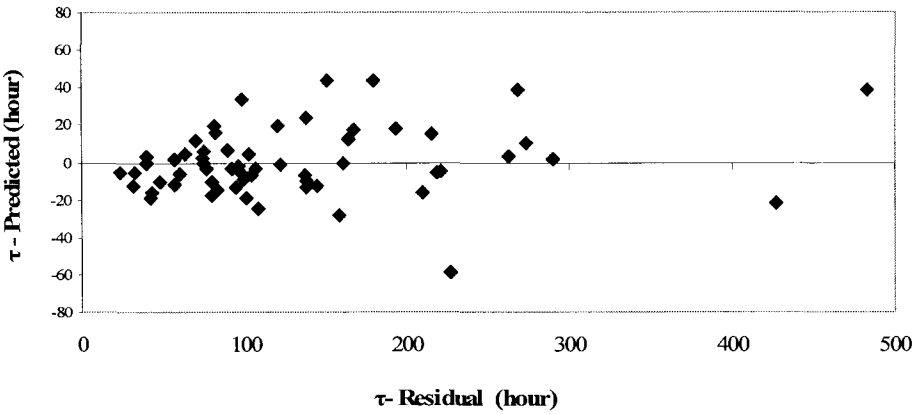

(b)

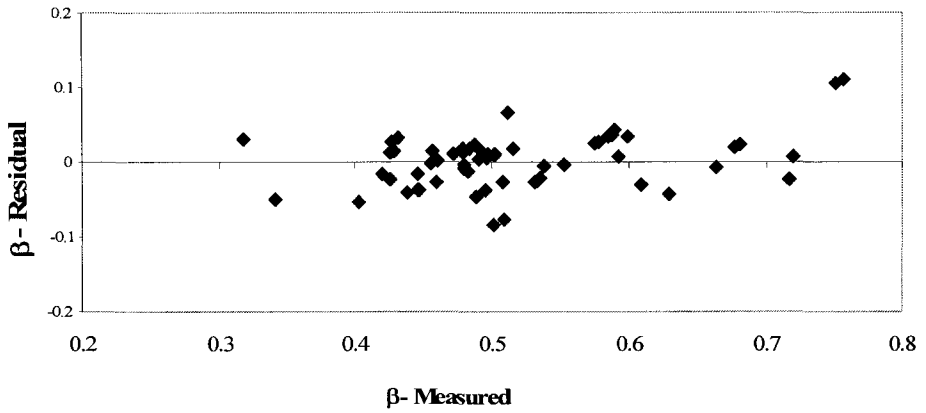

(c)

Figure 5.19: Residual vs Strength Parameters

5.5 Modified Maturity-Strength Model

The previous subsection contains the models for strength parameters. Combining these models with the maturity-strength relationship, Equation 5.6, the strength development with maturity for different cementitious materials can be predicted. The proposed maturity-strength model is expressed as follows:

$$S = S_u \cdot \exp\left(-\left(\frac{\tau}{t_{eq}}\right)^{\beta}\right) \qquad 5.9$$

Where,

$$S_u = \exp(-1.810 \cdot w/c + 10.143) \cdot (1 - 0.051 \cdot Air) \cdot \left(C_2S^{0.143} + 2.155 \cdot FA - 3.544 \cdot FA^2 + 0.711 \cdot Slag - 0.367 \cdot Slag^2\right) \qquad 5.9\text{ (a)}$$

$$\tau = \exp[-4.462 \cdot (FA - CaO - 0.2711) - 2.147 \cdot (HI - 1.519)] \cdot [\exp(3.401 \cdot w/c - 2.709) \cdot C_3S^{-1.659} \cdot C_3A^{-0.378} \cdot SO_3^{-1.154} \cdot Blaine^{-0.229} + 120.306 \cdot FA + 190.939 \cdot Slag + 1221.717 \cdot FA \cdot Slag] \qquad 5.9\text{ (b)}$$

$$\beta = \left[\exp(3.039) \cdot (C_3S + C_2S)^{-0.653} \cdot C_3A^{0.303} \cdot Blaine^{-0.525}) - 0.463 \cdot FA + 1.377 \cdot FA^2 - 0.427 \cdot Slag + 1.392 \cdot Slag^2\right] \cdot \exp[1.993 \cdot (FA - CaO - 0.2711) + 0.924 \cdot (HI - 1.519)] \qquad 5.9\text{ (c)}$$

The strength prediction from this modified maturity-strength model is presented in Figure 5.20 with an R^2 value of 0.975.

The following section shows the use of the modified maturity-strength model for prediction of concrete made with five different types of cement and cement with different SCM levels. Only several typical results are presented; the rest of the results are presented in Appendix B.

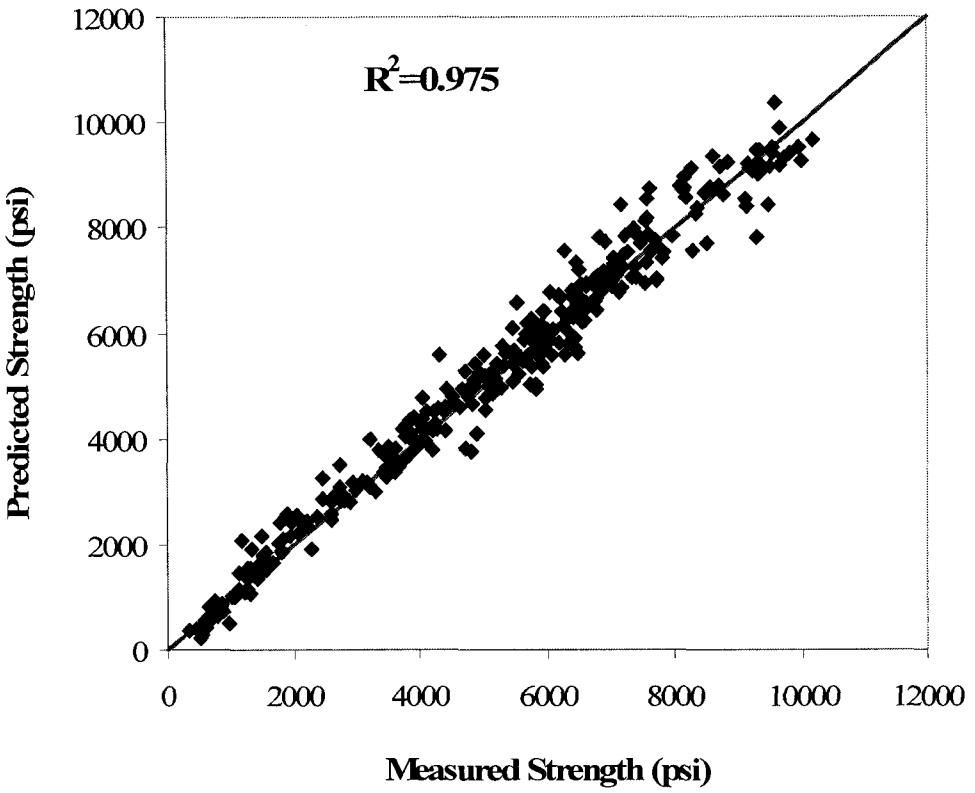

Figure 5.20: Measured vs Predicted Strength

Figures 5.21(a) and (b) show the comparison of the predicted and measured strength-tested maturity-strength results from Wood (1992) and model-fitted results for typical Types I, II, III, IV, and V cement concrete with different w/c ratios. Both figures show that the proposed model can predict strength development with maturity for various types of cement and different w/c ratios.

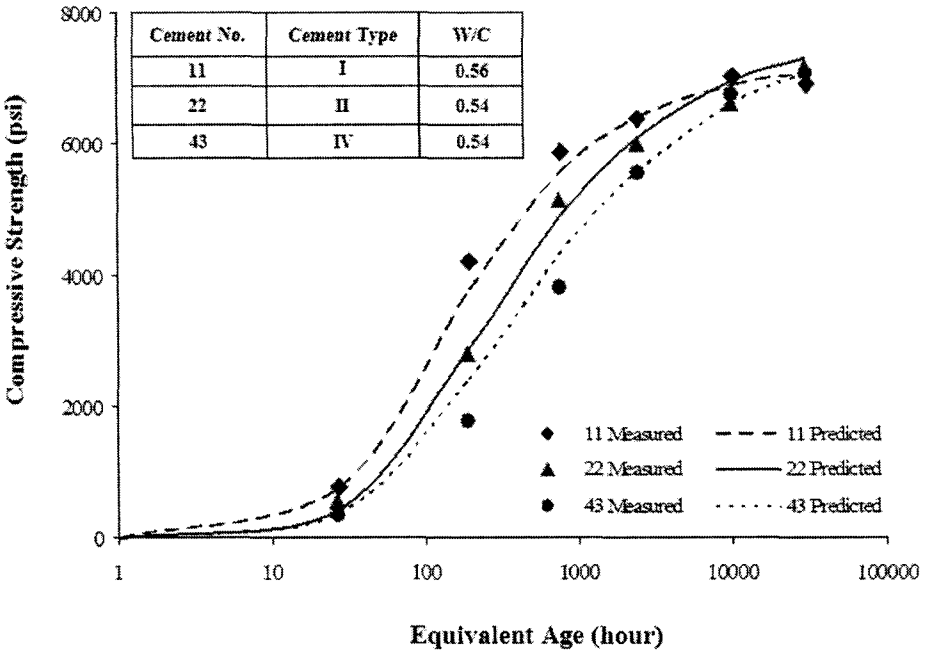

(a) Types I, II, and IV Cement

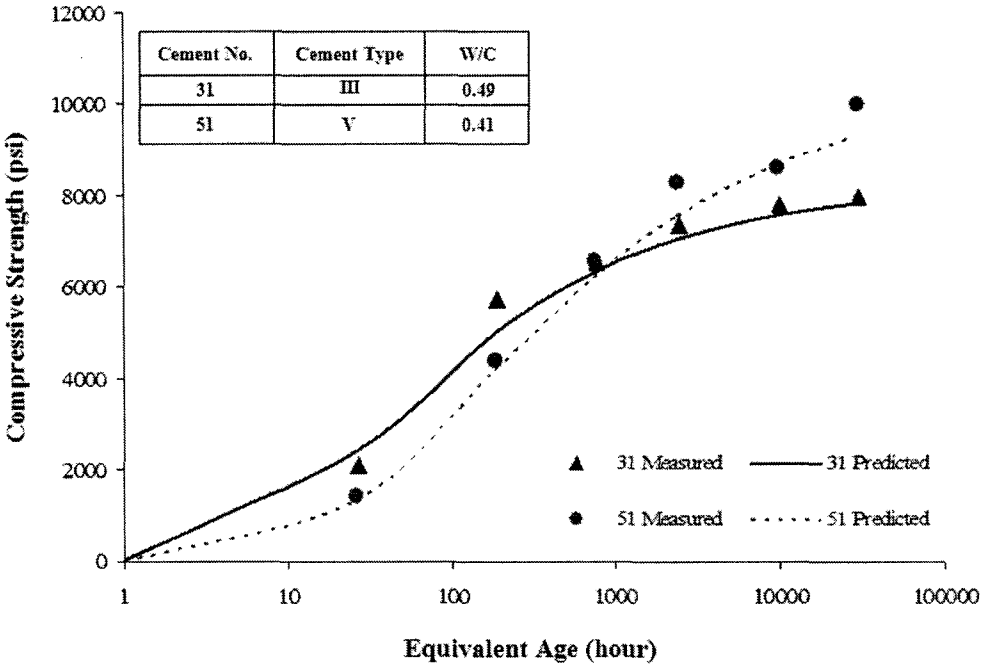

(b) Types III and V Cement

Figure 5.21: Measured vs Predicted Strength, Types III and V Cement

Figures 5.22 to 5.24 present the prediction results for blended cement concrete containing different amounts of fly ash and slag. The predicted results indicate that the proposed model is able to predict strength development for blended cement concrete containing different levels of fly ash, slag, and mixtures of fly ash and slag. The difference between the measured and predicted strength is fairly small.

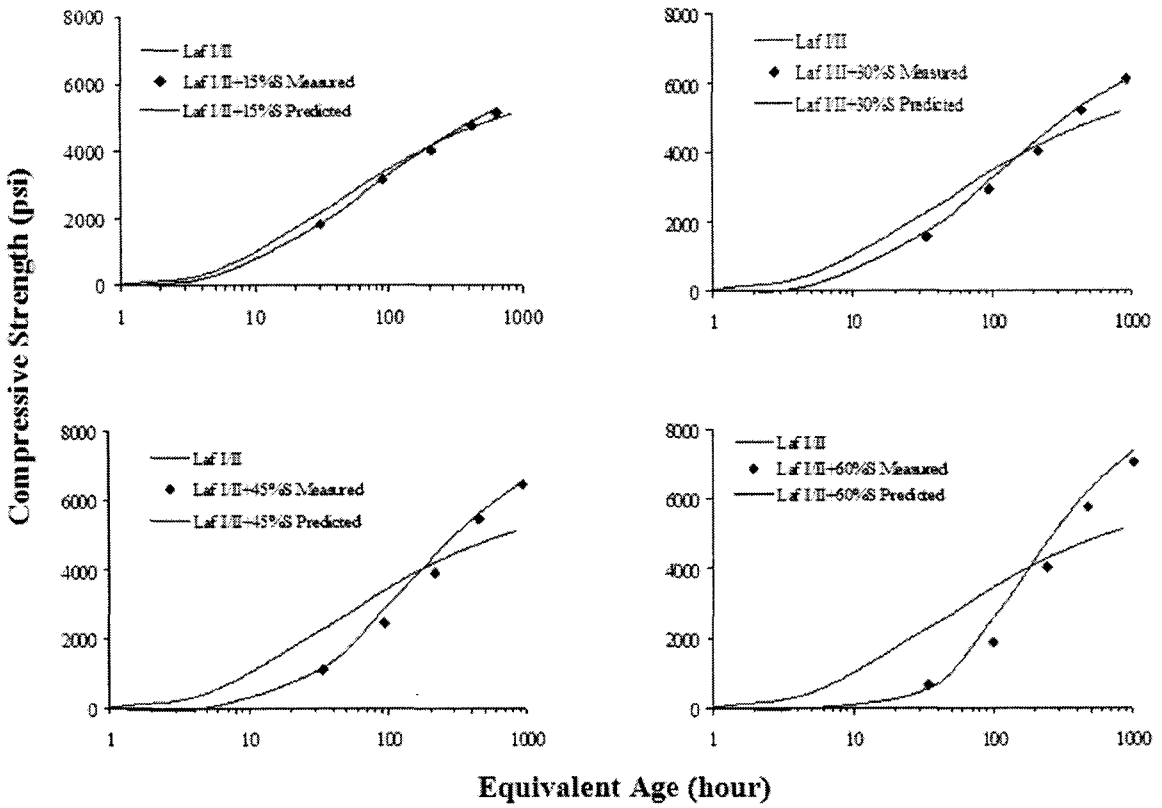

Figure 5.22: Measured vs Predicted Strength for Lafarge Types I/II Cement with Different Levels of Slag Replacement (w/b = 0.42)

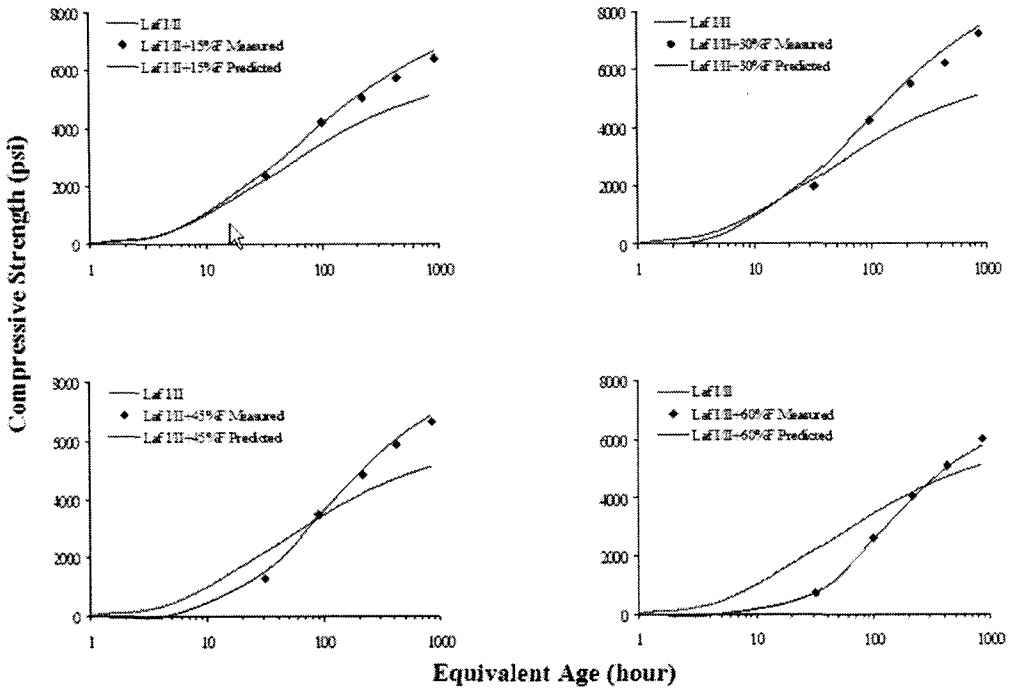

Figure 5.23: Measured vs Predicted Strength for Lafarge Types I/II Cement with Different Levels of Fly Ash Replacement (w/b = 0.42)

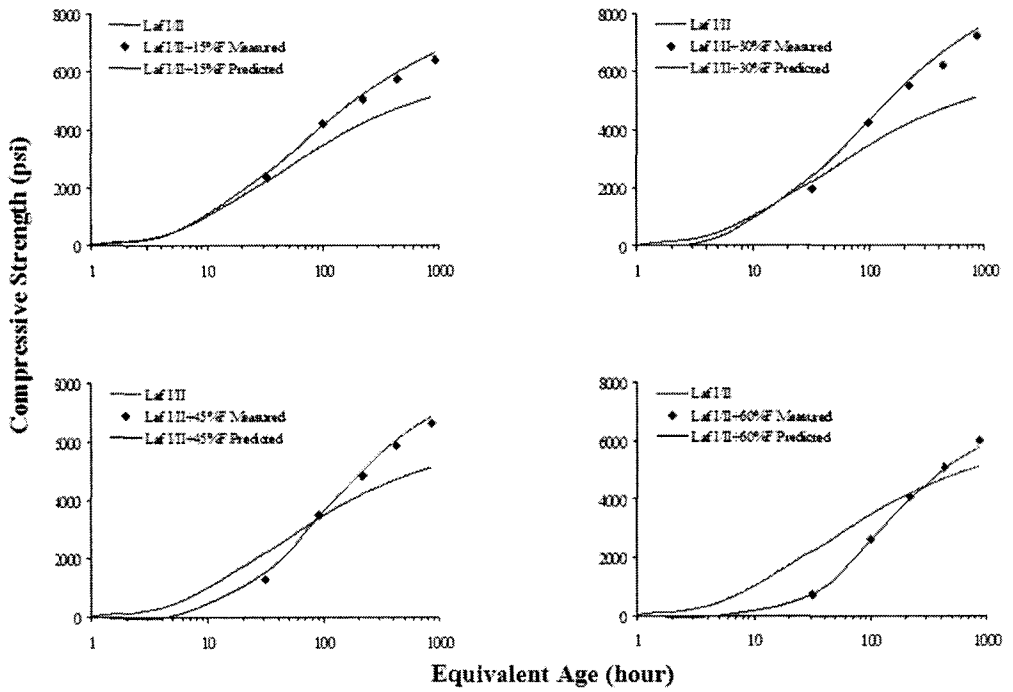

Figure 5.24: Measured vs Predicted Strength for Lafarge Types I/II Cement with Different Levels of Slag and Fly Ash Replacement (w/b = 0.42; slag : FA = 3:1)

5.6 Sensitivity Analysis

In addition to predicting concrete strength development, a reliable strength model can be used for sensitivity analysis of the factors that affect concrete strength. The results from such sensitivity analysis can provide engineers with insight into concrete mix design modification and field temperature management. The sensitivity analysis is performed by varying only one parameter at a time. During the sensitivity analysis, three values, including typical, high, and low values for normal concrete, are selected. The difference between the typical and low/high values is calculated. The results of the sensitivity analysis are tabulated in Table 5.4. The figures of the sensitivity analysis are presented in Appendix B.

The data show that the effect of each factor varies with time. On average, cement type has greater influence on strength at early age than on strength at later age. Type III cement has the highest strength at early age and lowest strength at later age. The properties of the cement are listed in Table 5.3.

Table 5.3: Chemical Composition and Properties of OPC

	I	II	III	IV	V
C_3S	50	45	60	25	40
C_2S	25	30	15	50	40
C_3A	12	7	10	5	4
C_4AF	8	12	8	12	10
$C\bar{S}H_2$	5	5	5	4	4
Blaine, m^2/Kg	350	350	450	300	350

The w/c ratio strongly influences strength. The lower the w/c ratio, the higher the strength. When the w/c ratio decreases from 0.45 to 0.3, the strength increases about 49% at early age and 33% at 1 year. The strength increase is caused by the reduced porosity and increased IT zone strength.

The influence of air content is constant regardless of age. Table 5.3 shows that the lower the air content, the higher the compressive strength. According to the model, Equation

5.9, the loss of concrete due to voids is about 5.1% for every 1% increase in air content. This is consistent with the value of 5.5% strength loss suggested by Mindess and Young (1981).

Cement with a high Blaine value gains higher strength at early age and lower strength at later age. When compared with other factors, the influence of the Blaine value is smaller.

The fly ash level and CaO content of fly ash significantly influences strength development. The influence of fly ash replacement level increases as time increases. The strength increases 15% at 7 days when fly ash increases from 0 to 30%. This value becomes 37% at 1 year. On the other hand, the influence of the CaO content in fly ash decreases as time increases. The strength values indicate that CaO is an effective means of differentiating the effect of different types of fly ash.

Similar to fly ash, the influence of slag replacement level increases as concrete age increases. Concrete containing slag has lower strength at early age and high strength at later age. The strength is reduced 20% at 7 days as 60% of the cement is replaced by slag. However, the strength for concrete containing 60% slag is 31% higher than the OPC concrete. Table 5.4 also shows that concrete containing slag with different HI has different strength development properties. Therefore, the HI of slag could be an effective means of differentiating the effect of different types of fly ash.

Table 5.4: Summary of the Sensitivity Analysis

Factors	Range	Compressive Strength, S (psi)								
		7 Days			28 Days			1 Year		
		S	ΔS*	ΔS/S (%)	S	ΔS	ΔS/S (%)	S	ΔS	ΔS/S (%)
Cement Type	I	3939	0	0	5202	0	0	6135	0	0
	II	3399	-541	-14	4770	-433	-11	6042	-93	-2
	III	3705	307	8	4709	-61	-2	5587	-456	-12
	IV	2157	-1549	-39	3935	-774	-20	6035	448	11
	V	2935	-1004	-25	4268	334	8	5834	-201	-5
w/c	0.45	3939	0	0	5202	0	0	6135	0	0
	0.30	5888	1949	49	7217	2015	39	8142	2008	33
	0.60	2512	-1427	-36	3674	-1528	-29	4603	-1532	-25
Air Content	6	3939	0	0	5202	0	0	6135	0	0
	4	4518	579	15	5967	765	15	7036	902	15
	9	3071	-868	-22	4055	-1147	-22	4782	-1352	-22
Blaine	350	3939	0	0	5202	0	0	6135	0	0
	289	4027	88	2	5342	140	3	6204	70	1
	580	3779	-160	-4	4934	-268	-5	5967	-168	-3
FA%	0	3939	0	0	5202	0	0	6135	0	0
	15	4541	602	15	6325	1122	22	7804	1669	27
	30	4547	607	15	6663	1461	28	8408	2273	37
CaO% of FA	10	3137	0	0	5005	0	0	7369	0	0
	1.5	2717	-420	-13	4336	-669	-13	6712	-657	-9
	28	4642	1505	48	6752	1747	35	8446	1077	16
Slag%	0	3939	0	0	5202	0	0	6135	0	0
	30	3624	-315	-8	5616	414	8	7292	1157	19
	60	3231	-708	-20	6436	1233	22	8419	2285	31
HI of Slag	1.5	3543	949	27	5534	838	15	7255	312	4
	1.7	4492			6372			7567		

* Strength difference

5.7 Summary and Recommendations

5.7.1 Summary

This chapter presents the process of modifying the existing maturity-strength model using test and literature data to fit strength parameters. The modified model is able to predict the strength with maturity for concrete containing different cementitious materials and curing under different conditions. Twenty-two sets of test data of different concrete mixtures, including different types of fly ash and slag, and 38 sets of literature data of 19 different types of cement and 2 different w/c ratios from Wood (1992) were used in the modeling.

The exponential expression of maturity-strength relationship proposed by Freiesleben Hansen, and Pedersen (1985), which has the same maturity-heat of hydration relationship, was selected. The modeling results show that the modified maturity-strength model is able to predict strength development accurately for concrete made with different cementitious materials. The R^2 for the overall prediction is 0.975, which indicates that 97.5% of the variations in strength can be explained by the model. To remain consistent with the heat of hydration model, a reference temperature of 21.1°C is used.

Sensitivity analysis was performed to analyze the effect of very single variable in the modified maturity-strength model. The results show that the influence of each factor varies with time. The Blaine value has a smaller influence on concrete strength compared with other factors. The w/c ratio, air content, fly ash, and slag content significantly influence concrete strength at both early and later age.

5.7.2 Limitations and Recommendations

During the model development, below assumptions were made.

- The effect of early age high temperature curing on ultimate compressive strength was not considered.
- The effect of the cement content was not able to be incorporated into the model due to the limited database.

- Effect of aggregate type on concrete strength was not considered
- The effect of chemical admixture was not considered.

In considering of above assumptions, the following recommendations are proposed to improve the accuracy of the maturity-strength model.

- Expand the database by considering the factors that were not considered during model development and modify the model based on the new database.
- If high accuracy is required, perform the maturity-strength test according to *ASTM C 1074* to obtain the real parameters in the model.
- Include the particle distribution of cementitious materials in the model.

CHAPTER 6
PREDICTION OF FIELD CONCRETE TEMPERATURE

This chapter describes the process of predicting field concrete temperature using FEMLAB, a finite element software. Field concrete is quite different from concrete under laboratory conditions because environmental conditions in the field, such as the temperature, wind speed, and solar radiation fluctuate diurnally. All of these changing values can affect cement hydration and the development of concrete properties. Therefore, it is important to consider environmental effects when predicting field concrete properties.

Field concrete temperature is determined by the heat of hydration of the cementitious materials and by the environmental conditions in the field. The heat of hydration of concrete can be predicted from the heat of hydration model developed in Chapter 4.

The finite element software FEMLAB (Finite Element Modeling Laboratory) is used to study the temperature distribution inside a concrete pavement. This method can also be applied to many other concrete structures with different boundary conditions. Using FEMLAB to model a pavement structure, the following parameters can be predicted:

- Temperature distribution in concrete at a certain time
- Temperature development or temperatue change with time at any position
- Other parameters, such as heat generation, change with time and location

The predicted concrete temperature from this model can be used to assess field concrete performance before construction. It can also help to control concrete placement temperature and construction conditions to prevent high thermal stress inside concrete.

This field concrete temperature model, combined with the concrete strength model, which is described in Chapter 5, can be used to predict the concrete strength development of each location in a pavement or the strength distribution inside concrete at a certain time. The prediction for the pavement concrete strength is discussed in detail in the next chapter.

6.1 General Considerations

During the process of field concrete temperature prediction, the following factors are considered: heat transfer inside concrete, rate of heat generation, thermal properties of concrete, boundary conditions, and initial pavement conditions.

6.1.1 Heat Transfer inside Concrete

Once concrete is placed in the field, its properties are significantly related to its thermal history. The temperature distribution in a cross section of concrete is the dynamic heat balance between the heat generated from the hydration of the cementitious materials and the heat loss to, or gain from, the surroundings.

For most concrete structures, the length of a structure element, such as pavement slabs, is much greater than the width and height. Therefore, it is reasonable to treat the temperature analysis as a two-dimensional problem by assuming that the temperature is uniformly distributed along the length. The temperature distributed inside the cross section can be described by the Fourier equation, Equation 6.1 (Holman 1990).

$$k\left(\frac{\partial^2 T}{\partial x^2}+\frac{\partial^2 T}{\partial y^2}\right)+q=\rho c_p\frac{\partial T}{\partial t} \qquad 6.1$$

Where,

k = Thermal conductivity, (w/m °C)

T = Temperature, (°C)

x,y = Coordinates at a particular point in the structure

q = Rate of internal heat generation, (w/m^3)

ρ = Concrete density, (Kg/m^3)

c_p = Specific heat of concrete, (J/Kg·°C)

t = Time

Equation 6.1 incorporating given boundary conditions is able to solve the dynamic temperature distribution inside the cross section of the concrete. Several heat transfer

mechanisms, including conduction, convention, solar absorption, and irradiation, will be considered in the boundary conditions for the heat transfer analysis These mechanisms will be discussed in detail in the following sections.

6.1.2 Rate of Heat Generation

The rate of heat evolution is the numerical differentiation with respect to time (t) of the total heat curve. The total heat curve is determined by Equation 4.12.

$$\dot{q} = \frac{dH}{dt} = \frac{d}{dt}\left(H_{ult} \cdot C_c \cdot \exp\left(-\left[\frac{\tau}{t_{eq}} \right]^{\beta} \right) \right) \qquad 6.2$$

Where,

$\dot{q}$ = Rate of heat generation, (w/m^3)

H = Concrete heat of hydration, (J/m^3)

H_{ult} = Ultimate heat of hydration of the cementitious materials, (J/Kg)

Cc = Content of the cementitious materials (Kg/m^3)

t_{eq} = Equivalent age, Equation 4.24

τ, β = Hydration parameters

Based on Equations 4.24 and 6.2, the rate of heat evolution can be expressed as follows:

$$\dot{q} = H(t_{eq}) \cdot \left(\frac{\tau}{t_{eq}} \right)^{\beta} \cdot \frac{\beta}{t_{eq}} \cdot \exp\left[-\frac{E}{R}\left(\frac{1}{273+T} - \frac{1}{273+T_{ref}} \right) \right] \qquad 6.3$$

In this study, the reference temperature, T_{ref}, is defined as 21.1°C. The hydration parameters, τ and β, are determined by the heat of hydration model developed in Chapter 4. The rate of heat generation is affected by the cementitious materials, mixing proportion, curing, and also initial temperature. The higher the initial temperature, the higher the rate of heat generation, which makes it necessary to control the concrete placement temperature during construction.

6.1.3 Thermal Properties of Concrete

Thermal properties to be used for field concrete temperature modeling include the specific heat of concrete and thermal conductivity.

6.1.3.1 Specific Heat of Concrete

The specific heat is the amount of heat per unit mass required to raise the temperature by one degree Celsius. The specific heat of concrete depends on the specific heat of the constituent materials. The mineralogical differences among aggregates have little influence on the specific heat of concrete due to the minor variation in the specific heat of rocks. On the other hand, the specific heat of the cement paste strongly depends on the water to cement (w/c) ratio, water content, and temperature (Mindess and Young 1981)

Concrete specific heat is not a constant during the process of hydration. Several researchers (De Schutter et al. 1995, Reinhardt et al. 1982, and Hansen et al. 1982) found that the specific heat of concrete decreases with time. The decline was found to be linear with the degree of hydration or the logarithm of time. However, there is no agreement concerning the magnitude of the decreases; it varies from 1% to 20%. The typical value of concrete specific heat is between 800 and 1200 J/Kg°C.

Van Breugel (1997) developed an expression for specific heat based on the fictitious specific heat of hydrated cement (Equation 6.4) because this equation takes into account the effects of mixing proportion, concrete temperature, and also degree of hydration. Van Breugel's model is used in this study to predict concrete temperature. The typical values of the specific heat for concrete constitutes are listed in Table 6.1.

$$c_p = \frac{1}{\rho} \cdot \left[G_C \cdot \alpha \cdot C_{cef} + G_c \cdot (1-\alpha) \cdot C_{ce} + G_a \cdot C_a + G_w \cdot C_w \right] \qquad 6.4$$

$$C_{cef} = 0.0084T + 0.339$$

Where,

G_c, G_a, G_w = Amount by weight of cement, aggregate, and water, (Kg/m^3)

C_{cef} = Fictitious specific heat of the hydrated part of cement, (KJ/Kg·°C)

C_a, C_{ce}, C_w = Specific heat of aggregate, cement and water, (KJ/Kg·°C)

T = Actual sample temperature (°C)

Table 6.1: Typical Specific Heat Values for Concrete Components

Material	**Specific Heat** (J/(Kg°C))	**References**
Cement	1140	Mindess and Young 1981
Granite	800	
Water	4179	Holman 1997
Limestone/Dolomite	860	Kong et al. 1983
Gravel	920	Klieger and Lamond 1994
Sand	800	
Quartz	750	

6.1.3.2 Thermal Conductivity

Thermal conductivity represents the ability of a material to transfer heat. It is defined as the ratio of the rate of heat flow to the temperature gradient. Thermal conductivity of the concrete governs the rate at which heat flows into, through, or out of a concrete structure (Scanlon et al. 1994). For normal weight concrete, the thermal conductivity is widely influenced by the mineralogical character of the aggregates, water content, temperature, and unit weight in dry condition (Scanlon et al. 1994, Kim et al. 2003). Table 6.2 shows the typical values of thermal conductivity for concrete containing different aggregate types. Within the normal climatic range, the temperature has little effect on the thermal conductivity of concrete. Above 100°C, the thermal conductivity decreases linearly with temperature (Mindess and Young 1981).

Table 6.2: Typical Thermal Conductivity Values of Concrete with Different Types of Aggregate (Mehta et al. 1993)

Aggregate Type	Thermal Conductivity	
	Btu in./hr ft^2°F	W/m°C
Quartzite	24	3.5
Dolomite	22	3.2
Limestone	18-23	2.6-3.3
Granite	18-19	2.6-2.7
Rhyolite	15	2.2
Basalt	13-15	1.9-2.2

Khan et al. (1998) conducted thermal conductivity tests on normal strength concrete in both the hardened and maturing states under different temperatures and found that the thermal conductivity decreased as the concrete hardened from 1.723 through 1.740 to 1.17 through 1.14 W/m°C. The hardened conductivity is 33% lower than the maturing conductivity, a trend confirmed by De Schutter et al. (1995) and Brown et al. (1970). They found a decline of 21% and 30% respectively. Ruiz et al. (2001) expressed the thermal conductivity as follows:

$$k = k_{\infty} \cdot (1.33 - 0.33 \cdot \alpha) \qquad 6.5$$

Where,

k = Current thermal conductivity, (W/m°C),

k_{∞} = Thermal conductivity of hardened concrete, (W/m°C)

α = Degree of hydration

In this study, Equation 6.5 will be used for the thermal conductivity calculation. The thermal conductivity of hardened concrete is from the recommended values in Table 6.2.

6.1.4 Boundary Conditions

Boundary heat transfer conditions, which are time or temperature dependent, are important for solving the differential Equation 6.1. As stated above, the four major boundary heat transfer mechanisms are conduction, convention, solar absorption, and irradiation. Figure 6.1 illustrates these four major heat transfer mechanisms. In the following sections,

each of them will be discussed in detail. Evaporation and condensation is another boundary condition that exists. It will not be considered in this modeling, because it is less significant for concrete under normal conditions (Wang 1994).

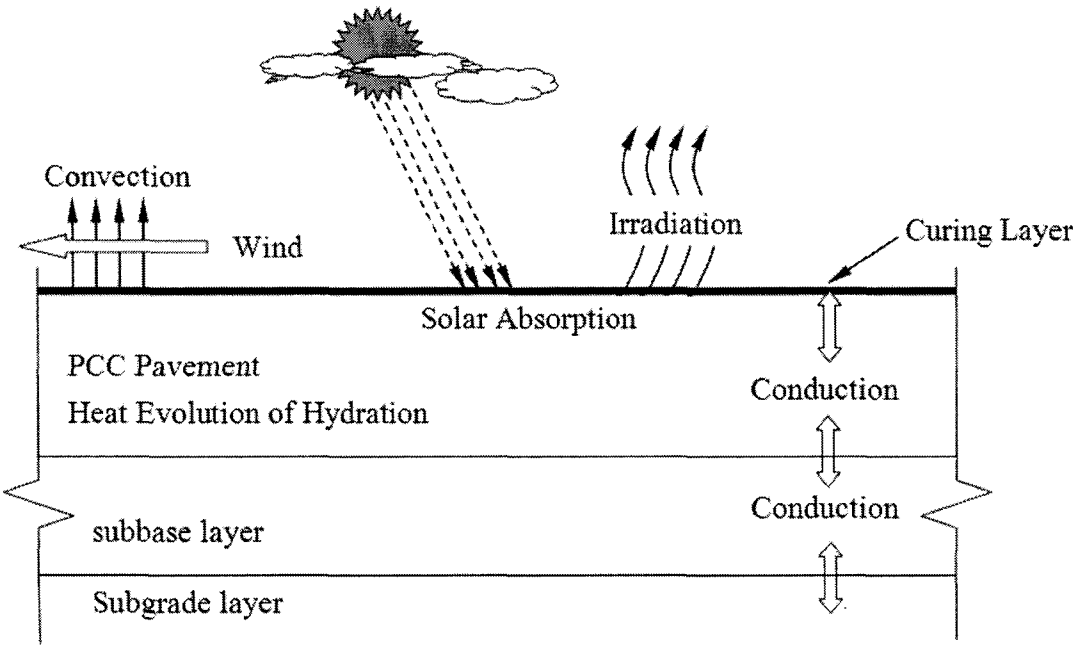

Figure 6.1: Heat Transfer Mechanism

6.1.4.1 Conduction

Thermal conduction is defined as "heat transport in a material by transfer of heat between portions of the material that are in direct contact with each other" (Andersen et al. 1992). As long as a temperature gradient exists, the transfer of heat will flow from the high-temperature region to the low-temperature region. Thermal conduction can be assessed by using Fourier's law (Holman 1990):

$$q = -k \cdot A \cdot \frac{dT}{dx} \qquad 6.6$$

Where,

q = Heat flow, (w)

k = Thermal conductivity, (w/m°C)

A = Area, (m^2)

dT/dx = Thermal gradient, (°C/m)

Heat conduction happens inside the concrete. Each point of a concrete element has a different rate of heat of hydration due to the effects of the environment. The pavement concrete slab lies directly on top of the subbase or subgrade. The heat exchange due to the temperature gradient between the concrete and the subbase layer happens in the form of conduction. The heat conduction between the pavement and the subbase layer affects cement hydration. In the summer, the subbase temperature could be much higher than the pavement. The heat transferred from the subbase to the pavement will increase the concrete temperature, which in turn, accelerates concrete cement hydration. On the other hand, in the winter, the subbase layer absorbs the heat from the pavement through conduction. The cement hydration becomes lower as the concrete temperature drops. Heat conduction also exists between the subbase and the subgrade. All of these heat conductions follow Fourier's law (Equation 6.6). The rate of conduction depends on the thermal properties. These properties of subbase and subgrade materials are listed in Table 6.3.

Table 6.3: Properties of Various Base Materials (Andersen et al. 1992)

Base Material	**Density**	**Thermal Conductivity** (W/m°C)	**Specific Heat** (J/Kg°C)
Gravel, dry	1703	0.52	838
Gravel, moist	1898	2.42	1047
Asphalt	2302	1.38	1047
Econcrete (?)	2339	3.32	1005
Subgrade	2066	1.59	1214

Besides heat conduction down to the base layer, there is also thermal conduction between the pavement and the curing layer. The curing insulation, used to protect against heat and water loss, includes insulation blankets, curing compounds, plastic sheets, and other products. The blankets are often used in cold conditions and situations that require very rapid

hydration. Applying insulation can trap the heat of hydration inside the concrete, which in turn, accelerates the cement hydration. The heat flow through the insulation layer can be estimated by the following equation (Holman 1990).

$$q = (T_s - T_a)/R_{th} \tag{6.7}$$

Where,

q = Heat flow, (w)

T_s = Surface temperature, (°C)

T_a = Air temperature, (°C)

R_{th} = Thermal resistance , (°C/w)

If more than one layer of the insulation is applied, an overall thermal resistance value can be calculated according to Equation 6.8 (Holman 1990). Table 6.4 shows the thermal properties of various insulation materials.

$$R_{th} = \frac{d_1}{k_1} + \frac{d_2}{k_2} + \cdots + \frac{d_n}{k_n} \tag{6.8}$$

Where,

R_{th} = Overall thermal resistance, (°C/w)

$d_1, d_2 \ldots d_n$ = Thickness of *n* successive layers, (m)

$k_1, k_2 \ldots k_n$ = Thermal conductivity of *n* successive layers, (w/m°C)

Table 6.4: Thermal Properties of Various Materials

Material	**Thermal Conductivity** (w/m°C)
Plastic sheet	0.043
Water	2.168
Blankets: Mineral fiber: ρ=0.4-2 lb/ft^3	0.039
Organic fiber: ρ=0.75-1.5 lb/ft^3	0.043
ρ=1.5-3 lb/ft^3	0.033
Blanket: Cotton wool mats: ρ=5 lb/ft^3	0.042
Blanket: Mineral wool mats: ρ=9.4 lb/ft^3	0.039
ρ=19.7 lb/ft^3	0.042
Polyurethane foam	0.035
Blanket: Glass fiber: ρ=1-2 lb/ft^3	0.055

6.1.4.2 Convection

Convection is heat transfer by mass motion of a fluid such as air or water when the heated fluid is caused to move away from the source of heat, carrying energy with it. In this study, convection heat transfer caused by air motion is considered. Newton's law of cooling is used to express the overall effect of convection (Holman 1990).

$$q = h \cdot A \cdot (T_s - T_a) \qquad 6.9$$

Where,

q = Heat flow (w)

h = Convection heat transfer coefficient ($w/m^2°C$)

A = Area (m^2)

T_s = Surface temperature (°C)

T_a = Air temperature (°C)

Convection can be either free or forced. Free convection, also called nature convection, is caused by air movement due to the density gradient. The forced convection studies the heat transfer between a moving fluid and a solid surface. In most cases, free convection may be neglected when there is a fluid flow, i.e., forced convection. For concrete pavement, wind velocity across the surface determines whether the convection is forced or free. During the daytime, wind movement over the concrete surface results in forced convection. When the wind speed reduces at night, the convection changes to free convection.

The rate of heat flow from a horizontal surface is mainly controlled by the magnitude of the temperature difference, the wind speed, and the surface texture of the member (McAdams 1954). Based on the experimental results, a model was developed for a smooth horizontal surface (ASHRAE 1993). Ruiz et al. (2001) further modified the model by taking the effect of a rough surface into account. The model is expressed by the following formula:

$$h = 3.727 \cdot C \cdot (0.9 \cdot (T_s + T_a) + 32)^{-0.181} \cdot (|Ts - Ta|)^{0.266} \cdot \sqrt{1 + 2.857 \cdot v_{wind}} \qquad 6.10$$

Where,

h = Convection heat transfer coefficient, (w/m^2°C)

C = Constant C = 1.79, for $T_s >= T_a$

C = 0.89, for $T_s < T_a$

T_s = Surface temperature, (°C)

T_a = Air temperature, (°C)

v_{wind} = Wind velocity, (m/s)

In some other temperature prediction models (Bentz 2000, McCullough et al. 1999), the following formulations have been used to calculate the heat transfer coefficient. In comparison with Equation 6.10, this approach does not include the effect of surface and air temperature. This approach is original from the test on a vertical plate. Therefore, this model is more suitable for vertical surfaces (Schindler 2002).

$$\begin{aligned} h &= 5.6 + 4.0 \cdot v_{wind} && \text{for } v_{wind} \le 5\ m/s \\ h &= 7.2 \cdot v_{wind}^{0.78} && \text{for } v_{wind} > 5\ m/s \end{aligned} \qquad 6.11$$

It is necessary to calculate the overall convection heat transfer coefficient (h_o), including the effects of the convection and insulation, because the heat transfer caused by surface convection can simultaneously occur in the presence of surface insulation over the pavement top surface. The overall convection heat transfer coefficient, h_0, is determined by Equation 6.12.

$$h_0 = \left(\frac{1}{h} + \frac{d_1}{k_1} + \frac{d_2}{k_2} + \cdots + \frac{d_n}{k_n} \right)^{-1} \qquad 6.12$$

6.1.4.3 Irradiation

Thermal irradiation is the electromagnetic radiation emitted by a body as a result of its temperature (Holman 1990). The total energy emitted is expressed by Stefan-Boltzmann's

law (Equation 6.13). The Stefan-Boltzmann constant has a value of 5.669×10^{-8} $w/m^2\cdot K^4$ (Siegel and Howell 2002).

$$q/A = \sigma \cdot (T_k)^4 = \sigma \cdot (T_c + 273)^4 \qquad 6.13$$

Where,

q/A = Heat flux per unit area, (w/m^2)

σ = Stefan-Boltzmann constant, ($w/m^2\cdot K^4$)

T_k = Temperature, (°K)

T_c = Temperature, (°C)

Equation 6.13 is for radiation into the vacuum of a blackbody. However, concrete is not a blackbody. The emissivity of a surface is applied to take into account the difference between the black and nonblackbody. The emissivity defines how well a real body radiates compared with a blackbody. The emissivity of concrete depends on the concrete's surface color and roughness. McCullough and Rasmussen (1999) recommended a value of 0.88. Siegel and Howell (2002) recommended a value of 0.94 for a rough concrete surface. Heat transfer between the concrete surface and sky due to radiation is expressed as follows:

$$q/A = \sigma \cdot \varepsilon \cdot \left(T_s^4 - T_{sky}^4\right) \qquad 6.14$$

Where,

ε = Emissivity

T_s = Surface temperature (°k)

T_{sky} = Effective sky temperature (°k)

Notice that the effective sky temperature, T_{sky}, is not equal to the ambient temperature. It accounts for the fact that the atmosphere is not at a uniform temperature and radiates only in certain wavelength bands. Berdahl and Martin (1984) predict the sky temperature with the dew point temperature, dry bulb temperature, and hour from midnight (Equation 6.15). The clear sky over North America appears to follow Equation 6.15 (Bowden

1998). However, the dew point temperature used to develop this model only covers a range from -20 °C to 30 °C, making this equation appropriate only for clear skies.

$$T_{sky} = T_a\left[0.711 + 0.0056 \cdot T_{dp} + 0.000073 \cdot T_{dp}^2 + 0.013 \cdot \cos(15t)\right]^{1/4} \quad 6.15$$

Where,

T_{dp} = Dew point temperature (K)

t = Hour from midnight (K)

T_a = Ambient temperature (K)

In this study, the following approach will be applied, which Bentz (2000) used in the temperature prediction model.

$$T_{sky} = \varepsilon_{sky}^{1/4} \cdot T_a \quad 6.16$$

Where the sky emissivity, ε_{sky}, is given by

$$\varepsilon_{sky} = 0.787 + 0.764 \times \ln(\frac{T_{dp}}{273}) \times F_{cloud} \quad 6.17$$

Where the cloud cover factor, F_{cloud}, is defined as

$$F_{could} = 1.0 + 0.024N - 0.0035N^2 + 0.00028N^3 \quad 6.18$$

Where,

N = Cloud cover (10^{-1})

Cloud cover, dew point temperature, and ambient temperature are available from meteorological stations. The ambient environmental conditions at any specific time are calculated by linear interpolation of the hourly values.

The effective sky temperature can be significantly cooler than the ambient air temperature. The effective sky temperature of a clear sky with a dew point temperature of 10°C and ambient temperature of 20°C at midnight is only 3°C, which is nearly freezing.

Therefore, irradiative cooling can cause frost even when the ambient temperature is above freezing.

6.1.4.4 Solar Absorption

Solar absorption is solar radiation absorbed by pavement surfaces during their exposure to incoming solar radiation. McCullough and Rasmussen (1999) proposed the following equation to account for the solar absorption of concrete pavement.

$$q_{sol} = \gamma_{abs} \cdot I_f \cdot q_{solar} \qquad 6.19$$

Where,

q_{sol} = Solar absorption of concrete, (W/m^2)

γ_{abs} = Solar absorptivity of the concrete

I_f = Intensity factor to account for angle of sun during a 24-hour day

q_{solar} = Instantaneous solar radiation, (W/m^2) as defined in Table 6.5

Solar radiation is a form of thermal radiation. The intensity of solar radiation strongly depends on atmospheric conditions, time of the year, and angle of incidence of the sun's ray on the surface of the earth (Holman 1990). The incidence angle is indicated by I_f, the intensity of solar radiation. During the nighttime, the solar radiation is negligible. During the daytime, I_f is assumed to be a sinusoidal distribution (Schindler 2002). The effect of atmospheric conditions on solar radiation is shown in Table 6.5. It is recommended getting the hourly instantaneous solar radiation according to historical data because solar radiation changes with location and time.

Table 6.5: Solar Radiation Values (McCullough and Rasmussen 1999)

Sky Conditions	**Solar Radiation,** (W/m^2)
Sunny	1000
Partly Cloudy	700
Cloudy	300

Solar absorptivity is the ratio between how much solar radiation is absorbed by a material to that absorbed by a standard black surface. The solar absorptivity of a material is

mostly dependent on its color. An ideal whitebody has a value of 0, and an ideal blackbody has a value of 1.0. The solar absorptivity of concrete is a function of the surface color. The typical values range from 0.5 to 0.6. The application of white curing compound reduces the solar absorptivity by 0.1 to 0.35.

6.1.5 Initial Pavement Conditions

6.1.5.1 Fresh Concrete Placement Temperature

Fresh concrete placement temperature is significant for concrete pavement. High initial temperatures can increase the rate of hydration, which in turn, decreases setting time and increases the possibility of thermal cracking. According to Mindess and Young (1981), the optimum concrete placement temperature should be in the range of 10 to 15°C or lower for mass concrete, and the placement temperature should not exceed 30 to 35°C. Even for cold weather concreting, fresh concrete temperatures above 21°C are not recommended (Mehta and Monteiro 1993). Fresh concrete temperatures can be regulated by controlling the temperature of the ingredients. The contribution of each constituent is determined by its temperature, specific heat, and weight fraction. Equation 6.20 can be used to calculate concrete temperature.

$$T_{cconcrete} = \frac{H \cdot (T_a W_a + T_c W_c) + T_a W_{wa} + T_w W_w}{H \cdot (W_a + W_c) + W_{wa} + W_w} \qquad 6.20$$

Where,

$T_{concrete}$ = Fresh concrete temperature (°F)

H = Approximate specific heat of cement and aggregate (0.22 Btu/lb·°F)

T_a = Temperature of aggregate (°F)

W_a = Dry aggregate weight (lbs)

T_c = Temperature of cement (°F)

W_c = Weight of cement (lbs)

W_{wa} = Aggregate moisture (lbs)

T_w = Temperature of mixing water (°F)

W_w = Weight of mixing water (lbs)

Since mixing water is the easiest to heat and cool and has the highest specific heat (about five times as much as cement or aggregate), heating or cooling the water is the most effective way to adjust fresh concrete temperatures, compared to adjusting the temperature of the aggregate or cement. Adding ice is more effective, because the melting ice absorbs heat. The ice must completely melt before mixing is completed. Equation 6.20 is then modified to account for the effect of the ice as follows:

$$T_{cconcrete} = \frac{H \cdot (T_a W_a + T_c W_c) + T_a W_{wa} + T_w W_w - F_i W_i}{H \cdot (W_a + W_c) + W_{wa} + W_w + W_i} \qquad 6.21$$

Where,

F_i = Latent heat of fusion (145 Btu/lb)

W_i = Weight of ice (lbs)

6.1.5.2 Initial Subbase and Subgrade Temperature

During early age, pavement temperature is affected by concrete placement temperature, rate of heat of hydration, environmental conditions, and also the initial temperatures of subbase and subgrade. Several assumptions are made for studying the effect of subbase and subgrade on pavement temperature: (1) The subbase temperature is uniformly distributed along the depth; (2) The temperature change is linearly from the deep ground to the bottom of the base layer; and (3) At a ground depth greater than 5 meters, the ground temperature has a constant value of 55°F.

6.2 FEMLAB Modeling for Field Concrete Temperature

The FEMLAB model for field concrete temperature is a multiphysic model, which includes the general form partial differential equations (PDEs) and transient heat transfer models. Since the heat of hydration model is based on equivalent age (Chapter 4), the PDE model is applied to calculate the equivalent age for each location in the pavement. The obtained equivalent age values are then used in the heat transfer model, which calculates the

rate of heat generation based on Equation 6.3 and the heat exchange between the pavement concrete and the environment to determine field concrete temperature. Figure 6.2 shows the flowchart of the process of field concrete temperature prediction with FEMLAB.

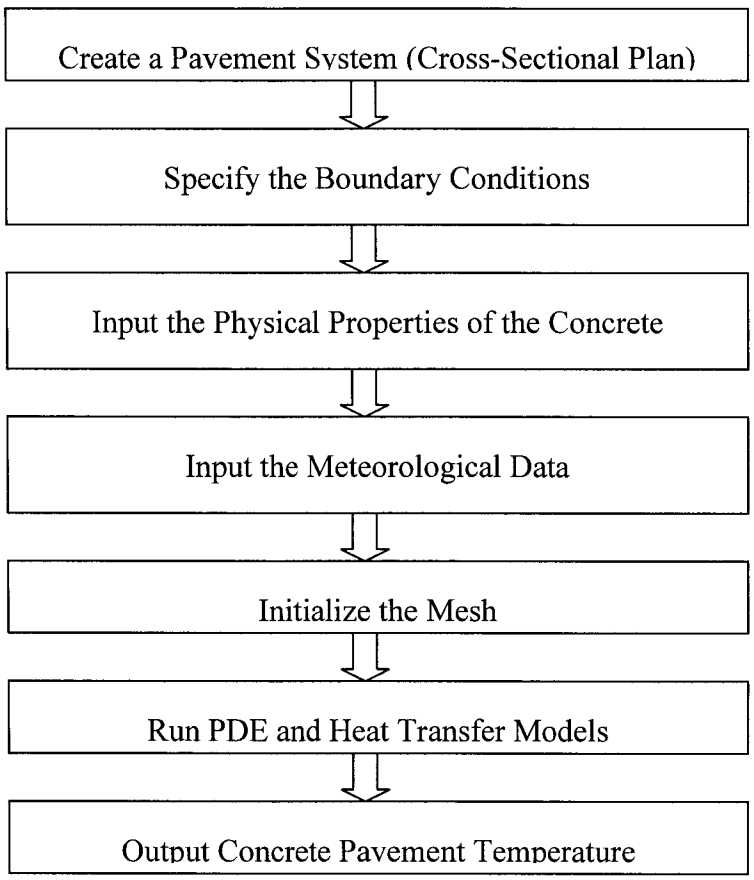

Figure 6.2: Flowchart of FEMLAB Modeling Process

Figure 6.3 shows the pavement cross-sectional plan. All dimension parameters can be changed according to the real pavement design. The pavement is 12 inches thick and covers a 6-inch subbase layer. The depth of the subgrade is selected as 16.4 feet (5 meters). The temperature at the bottom of the subgrade is assumed to be a constant 285°K.

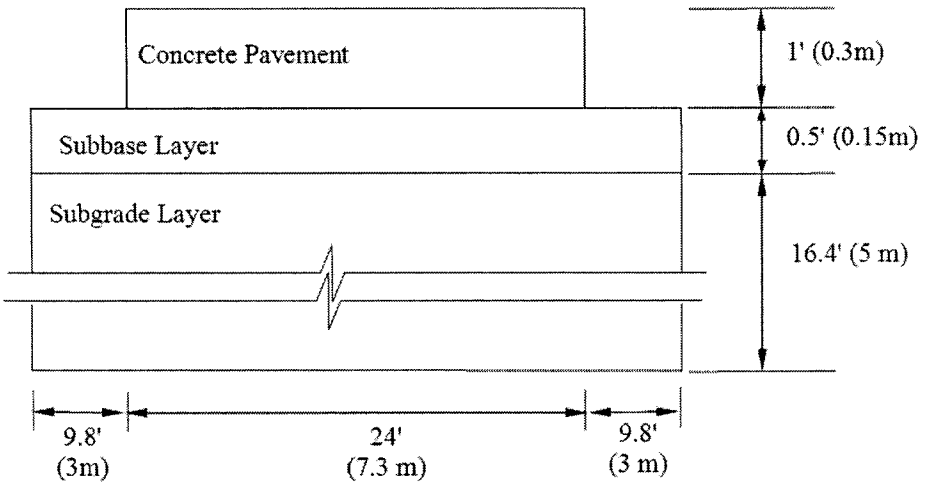

Figure 6.3: Cross Section of the Pavement

The boundary conditions of the pavement system are the same as that shown in Figure 6.3. They can be mathematically expressed as Equation 6.22. All coeffients for different boundary conditions are determined as described in Section 6.1.4. For each layer, the physical properties, which include density, heat capacity, thermal conductivity, and initial temperature, are required. The heat source for the concrete pavement is determined by Equation 6.3.

$$-n\cdot(-k\nabla T)=q_0+h\cdot(T_a-T)+\varepsilon\cdot\sigma\cdot({T_{sky}}^4-T^4) \qquad 6.22$$

Where,

n = Vector

k = Thermal conductivity (W/m°C)

T = Surface temperature (°C)

q_0 = Incoming heat source, i.e., solar absorption (W/m^2)

h = Convection heat transfer coefficient ($W/m^2°C$)

Ta = Air temperature (°C)

ε = Emissivity

σ = Stefan-Boltzmann constant, 5.67 x 10^{-8} $W\cdot m^{-2}\cdot K^{-4}$

T_{sky} = Effective sky temperature (°k)

In this study, three sets of meteorological data--which include the solar radiation, air temperature, dew point temperature, cloud cover, and wind speed--are adopted to represent weather conditions in the spring, summer, and fall. These data are from the Des Moines, Iowa Airport meteorological station and measured in 1990 (www.webmet.com 2005). The spring data is based on measurements collected between March and April. The summer data is from July recordings, and the fall data is from October recordings. Figures of these three data sets are presented in Appendix C. Summer has the highest solar radiation. At night, the solar radiation is zero. The solar radiation is also related to cloud conditions, the reason that some data are not continuous. In this study, spring has the lowest air temperature and dew point temperature; summer has the highest values. The fluctuation of the dew point temperature is much smaller than the air temperature.

During the process of meshing, finer meshes are used for concrete pavement slabs to get more accurate results. The meshes of the subbase and subgrade layers are coarser than the meshes for the slab section (Figure 6.4). The temperature outputs can be temperature development with time at any position or the distribution of the temperature inside the concrete at a certain time.

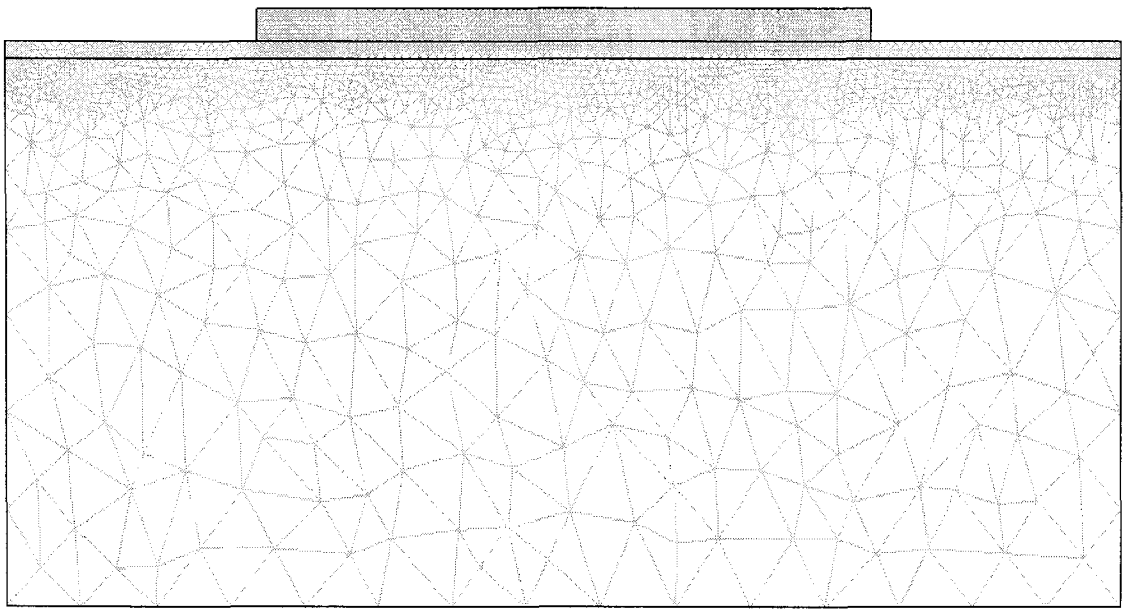

Figure 6.4: Mesh Model of the Pavement System

6.3 Results from FEMLAB Analysis

Numerous variables can influence concrete temperature. In this study, the following factors are studied: (1) Weather conditions; (2) Use of fly ash and slag; and (3) Construction and initial conditions. The ranges of the variables are listed in Tables 6.6 and 6.7. The effect of adding fly ash and slag was studied by performing temperature prediction under conditions listed in Table 6.6 for concrete containing 30% fly ash and slag respectively. In the study, the Iowa DOT C-3 mix (Table 3.2) was used.

Table 6.6: Variables for Temperature Analysis (°C)

	Spring			**Summer**			**Fall**		
Construction time	10:00 AM	2:00 PM	6:00 PM	10:00 AM	2:00 PM	6:00 PM	10:00 AM	2:00 PM	6:00 PM
Initial concrete temp	25	25	25	25	25	25	25	25	25
Subbase temp	10	10	10	25	30	25	20	25	20
Temp of the deep ground	12	12	12	12	12	12	12	12	12

Table 6.7: Ranges of Initial Condition Variables under Summer Conditions

Variables	**Range**				**Reference**
Slab thickness	0.2	0.3	0.4		0.3
Placement temperature	10	20	25		25
Subbase temperature	15	25	35	45	25

Field concrete pavement simulation results will be presented in the following sections. In each group, the typical results will be presented and discussed. Other figures will be presented in Appendix C.

6.3.1 Effect of Fly Ash and Slag

As discussed in Chapters 2 and 4, using fly ash and slag can reduce the heat generation of the supplementary cementitious materials (SCMs). In this section, the effect of SCMs on concrete temperature development is studied by replacing 30% cement, by weight,

with Class C fly ash or slag, when other parameters remain constant. Figure 6.5 shows the effect of fly ash and slag on field pavement concrete temperature development during three typical days in the summer. Adding fly ash or slag reduces the peak temperature about 2 to 3°C for the surface layer and about 4 to 5°C for both the middle and the bottom layers of pavement concrete. During the first several hours, the temperatures for the different concrete are similar; after that, the concrete without SCMs increases to a higher temperature. The biggest temperature difference is reached at about 9 to 11 hours after placement. After that, the difference in concrete temperatures decreases. The reduction for the bottom layer is slower than the reduction for the top and middle layer. The temperatures for pavements with fly ash and slag are similar. As Figure 6.6 shows, concrete with slag has a slightly higher temperature than concrete with fly ash at early age up to 12 hours, because the heat generated by concrete containing slag is higher than the heat generated by concrete containing fly ash. The figure also shows that concrete without SCMs generated more heat than concrete with SCMs, which is why concrete without SCMs has a higher temperature than concrete with SCMs.

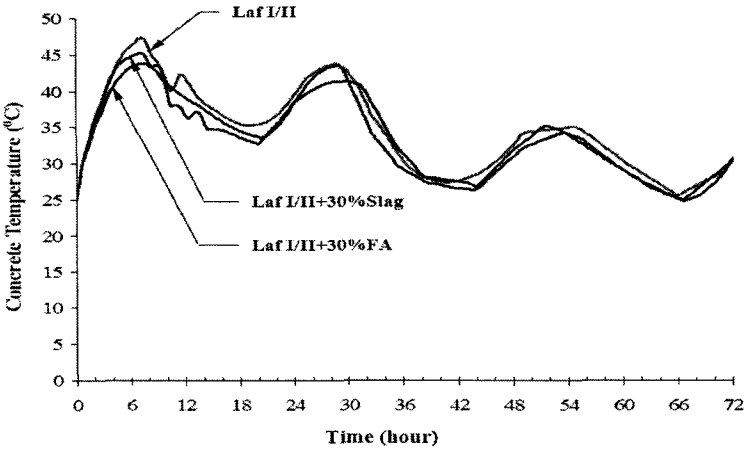

(a) Surface Layer

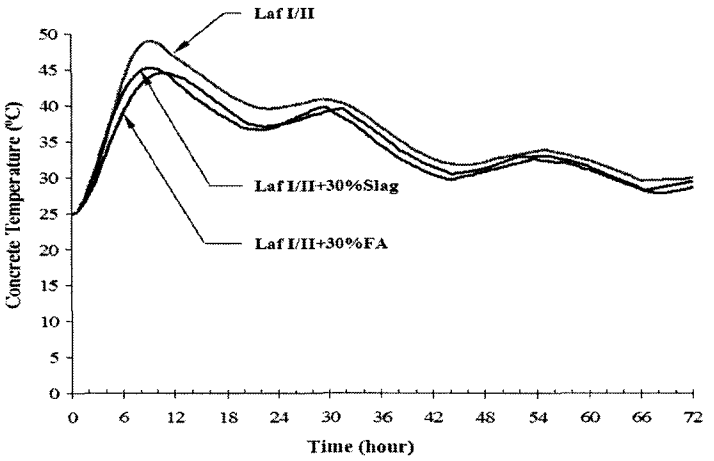

(b) Middle Layer

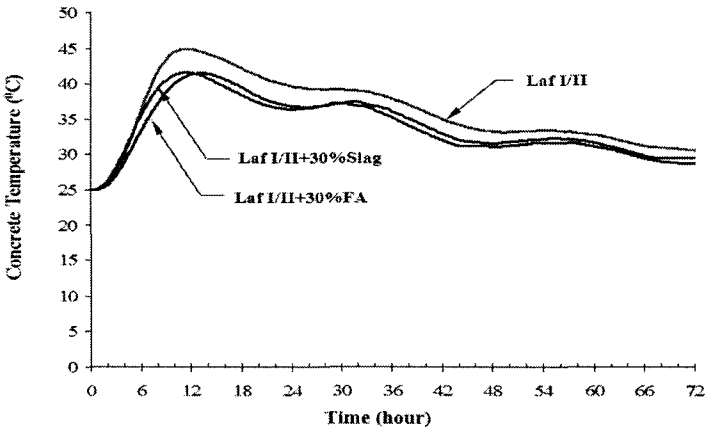

(c) Bottom Layer

Figure 6.5: Effect of SCMs on Field Concrete Temperature
(Constructed at 10:00 AM, Summer Conditions)

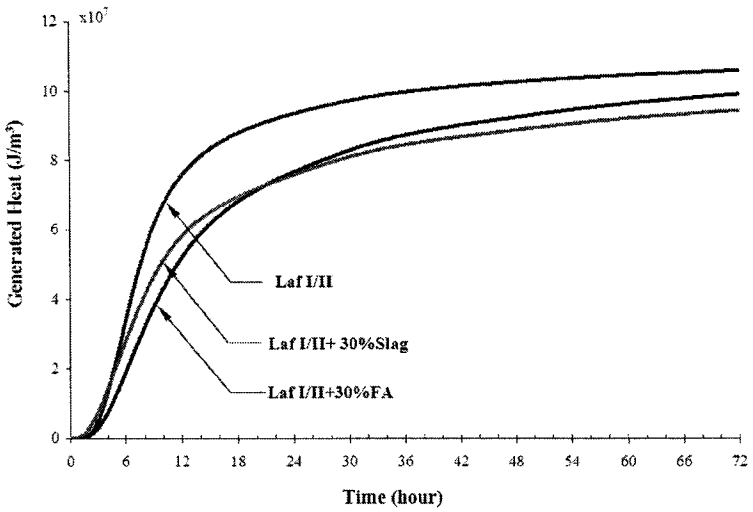

Figure 6.6: Heat Generation for Different Cementitious Materials
(Constructed at 10:00 AM, Summer, Middle layer)

6.3.2 Effect of Environment Conditions

Heat loss from concrete to the surrounding environment is related to weather conditions and concrete temperature. In this section, the effects of spring, summer, and fall weather conditions on field concrete temperature are studied. Winter conditions are not considered, because little concrete pouring is conducted in the winter.

Figure 6.7 illustrates the influence of weather conditions on concrete temperature development. Weather conditions significantly influence field concrete temperature. The temperature of concrete in the spring is much lower than its temperature in the summer. The maximum temperature is reduced from 49°C to 23°C. Low spring temperatures can cause a lower strength development rate. Therefore, in the spring, special protection may be required to increase the concrete temperature. Under certain seasonal conditions, the influence of a change in air temperature is reduced with the depth of the concrete slab due to the low thermal conductivity of concrete.

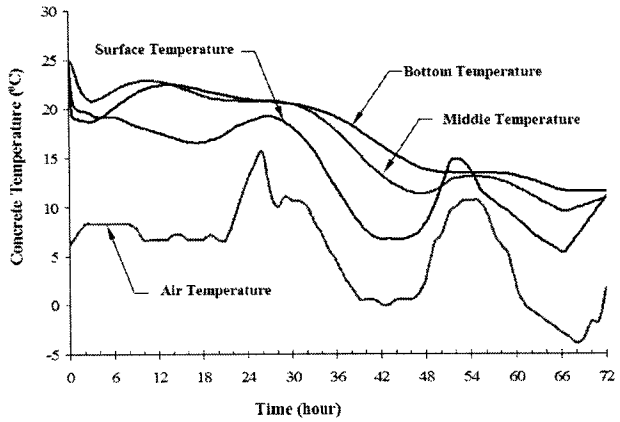

(a) Spring Conditions

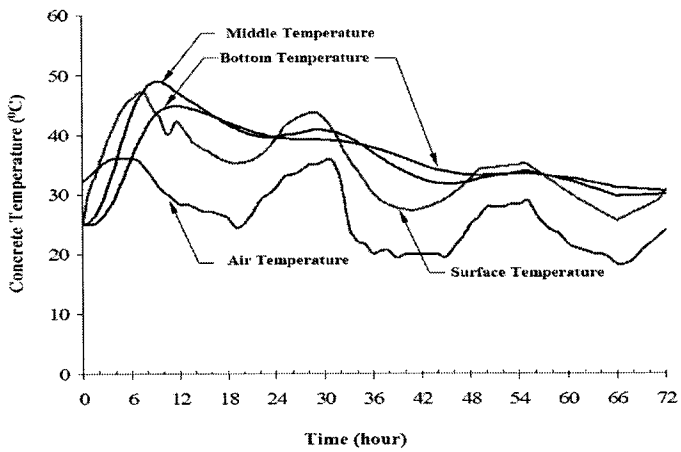

(b) Summer Conditions

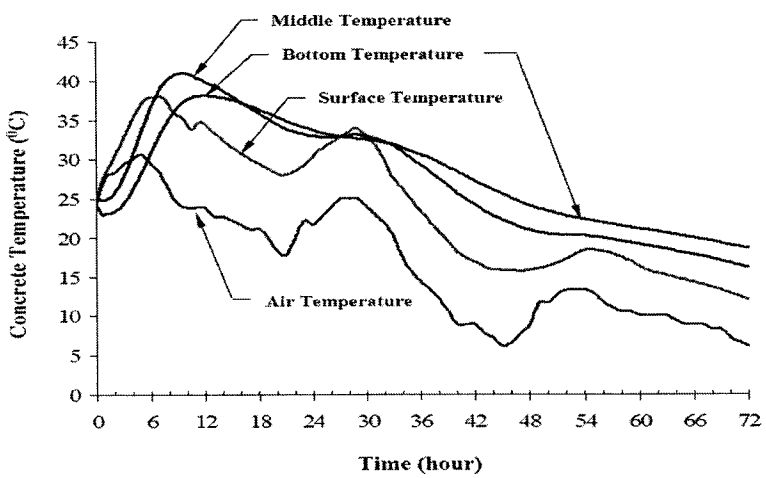

(c) Fall Conditions

Figure 6.7: Effect of Environmental Conditions on Pavement Temperature (10:00 AM, OPC)

For all three seasons, the trend of surface concrete temperature change is similar to that of ambient air temperature change. The greatest temperature drops always occur in the surface layer of concrete. The highest concrete temperature generally develops in the middle layer of pavement concrete about 10 hours after paving. During the nighttime, the bottom layer normally has the highest temperature, and the top layer has the lowest temperature.

In the spring [Figure 6.7(a)], concrete temperatures drop in the first few hours because the heat dissipates to the surrounding environment, which has a low air temperature. After that, the liberated hydration heat increases the concrete temperature. As time increases, the rate of heat generation starts to decrease. Concrete temperatures start to drop when the dissipated heat is higher than the generated heat of hydration and absorpted heat from solar radiation.

On the other hand, in the summer and fall, concrete temperatures increase just after placement, because the air temperature is higher than the concrete temperature. Heat is transferred from the surroundings to the pavement concrete. Compared to the middle layer, the bottom layer has a lower temperature at early age, because concrete conducts the heat to the base layer. The base temperatures are 10, 25, and 20°C for spring, summer, and fall. The initial concrete temperature is 25°C.

6.3.3 Effect of Construction and Initial Conditions

In this section, several factors related to construction and initial condition are discussed, including construction time, concrete placement temperature, initial subbase temperature, and pavement thickness. The results provided in the following section are for the summer, because it is a popular season for paving.

6.3.3.1 Effect of Paving Time

Concrete paving can start in the early morning and end in the late afternoon. Concrete placed at different times may have a different temperature history. Figure 6.8 shows the temperature development for concrete placed at different times.

Figure 6.8 shows that the temperature drop during the first 24 hours decreases as the paving time increases. For pavement paved at 6:00 PM, there is no temperature drop during the first 24 hours. Therefore, a later paving time reduces the thermal stress caused by temperature drop. Pavement placed in the morning has the highest temperature drop. For all three different paving times, the surface layer has the highest temperature drop.

For all three layers, concrete placed at 6 PM has the lowest temperature at early age. In the afternoon, both solar radiation and temperature start to drop. Therefore, less heat can be absorpted from the solar radiation and more heat will be dissipated to the environment due to the low temperature. All of these factors can cause a lower concrete temperature, which, in turn, reduces the rate of heat generation. For the bottom layer, the trend is similar to the middle layer.

For the first 10 hours [Figure 6.8(c)], the temperature of bottom layer concrete placed at 2:00 PM is slightly higher than the concrete cast in the morning. The higher temperature is caused by the higher subbase temperature, which is 30°C at noon and 25°C in the morning. Heat will be conducted from the base to the concrete, increasing the temperature and also the rate of heat generation at early age. The effect of subbase temperature will be discussed in the following section.

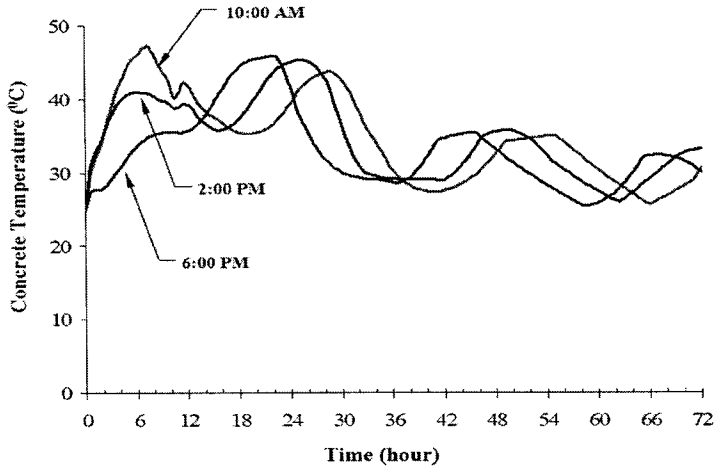

(a) Surface Layer

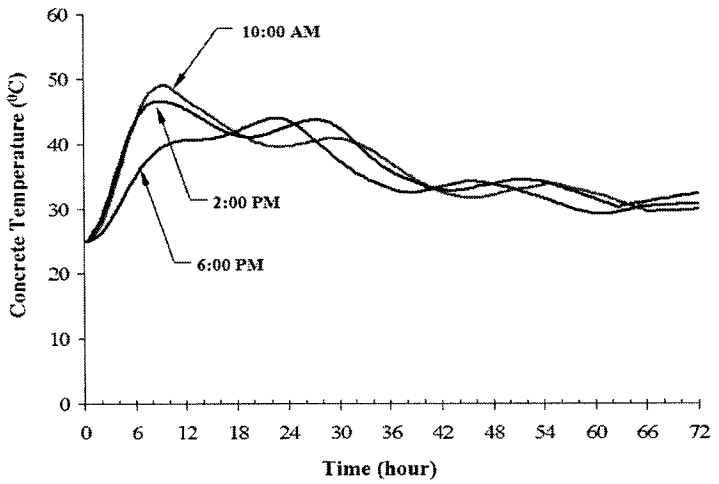

(b) Middle Layer

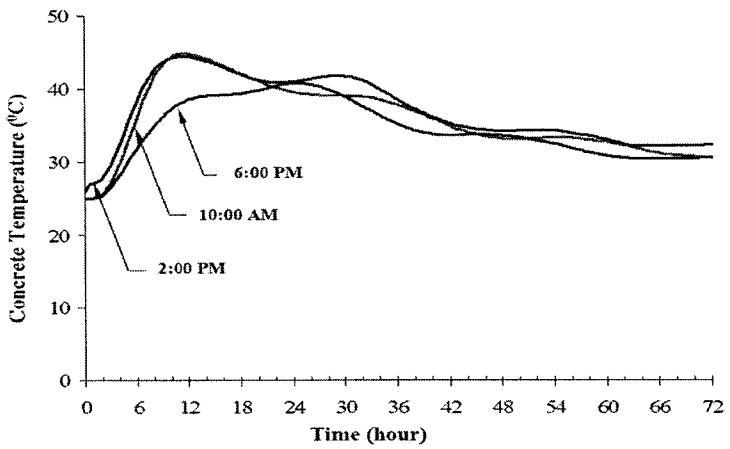

(c) Bottom Layer

Figure 6.8: Effect of Paving Time on Pavement Temperature (Summer Conditions)

6.3.3.2 Effect of Concrete Placement Temperature

As stated in Section 6.25, concrete placement temperature is critical for pavement. High placement temperature can decrease setting time and increase the possibility of thermal cracking. According to Mindess and Young (1981), the optimum concrete temperature should be in the range of 10 to 15°C or lower for mass concrete. Also, the temperature should not exceed 30 to 35°C. The effect of concrete placement temperature on pavement concrete temperature is shown in Figure 6.9. As concrete placement temperature increases, the peak temperature increases and the time it takes concrete to reach the highest temperature decreases. As concrete placement temperature increases from 10 to 30°C, concrete peak temperature increases to 5.2°C, 9.4°C and 7.5°C for the surface, middle, and bottom layer respectively. After about 24 hours, the concrete temperatures are similar regardless of concrete placement temperature. In this situation, the temperature variation is mainly caused by heat exchange between the concrete and environment. Like the peak temperature, the temperature drop also increases as the placement temperature increases. Therefore, a high placement temperature creates a higher risk of thermal cracking under hot weather conditions. Placement temperature should be controlled during pavement construction.

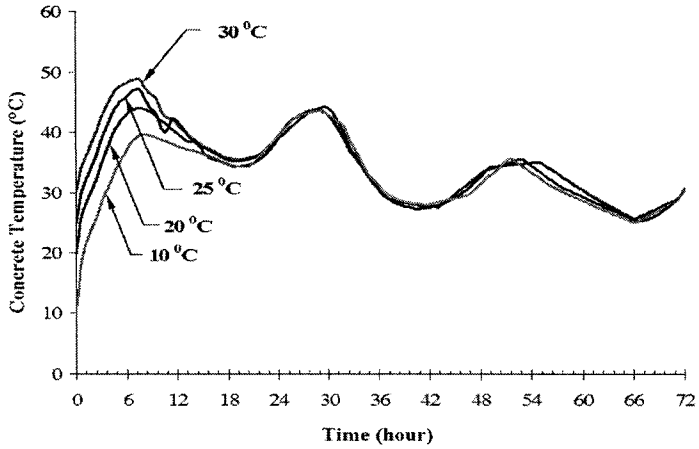

(a) Surface Layer

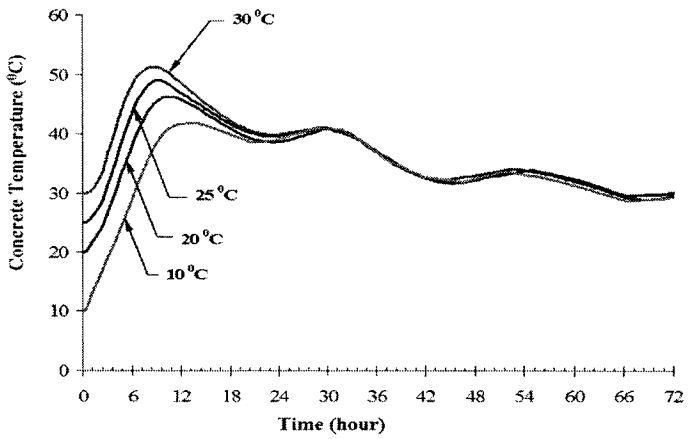

(b) Middle Layer

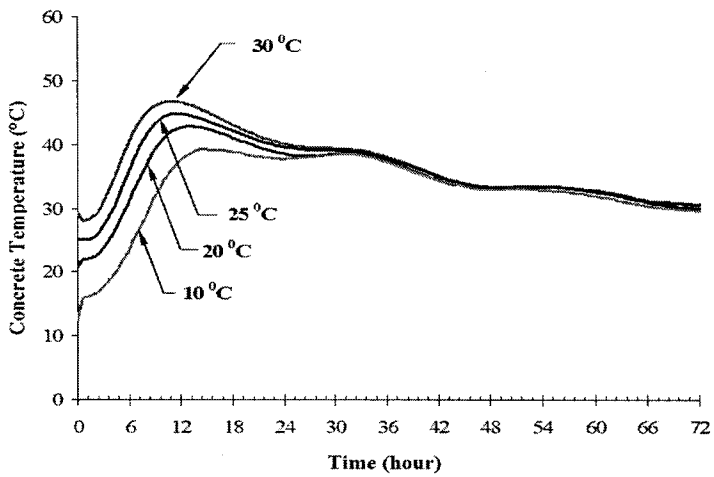

(c) Bottom Layer

Figure 6.9: Effect of Concrete Placement Temperature on Pavement Temperature (Summer Conditions, Paved at 10:00 AM, Subbase Temperature 25°C)

6.3.3.3 Effect of Subbase Temperature

Subbase temperature also influences concrete temperature development. It can determine the direction of the heat flow between concrete and the subbase during the first few hours. Figure 6.10 indicates that a higher subbase temperature can cause higher concrete temperatures for all three layers. The concrete placement temperature is 25°C for different subbase conditions. When the subbase temperature is higher than 25°C, the heat will be conducted from the subbase to the concrete, which will increase the concrete temperature and the rate of heat generation. Also, when the concrete temperature is higher than the subbase temperature, less heat will be lost from the concrete to the subbase with higher temperatures due to the smaller thermal gradient. Therefore, concrete temperatures will be higher when subbase temperatures are higher. As the subbase temperature increases from 15 to 45°C, the temperature increases by 6.1°C, 11.4°C, and 14°C for the surface, middle, and bottom layer respectively. The peak of concrete temperature is postponed by the lower subbase temperature. After concrete reaches the peak temperature, the influence of the subbase temperature decreases as time increases. The subbase temperature has a larger effect on the bottom layer than on the surface and middle layers.

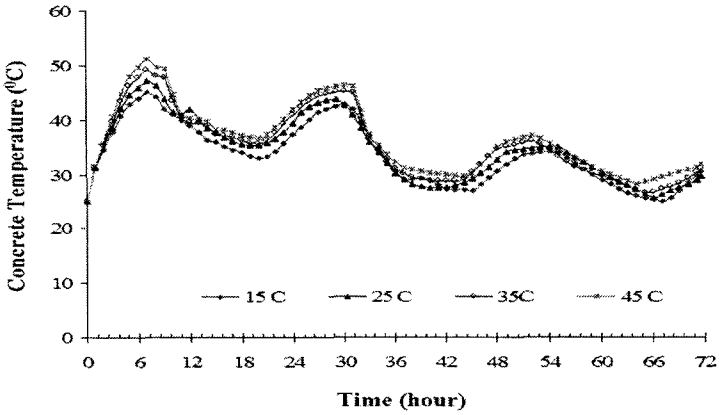

(a) Surface Layer

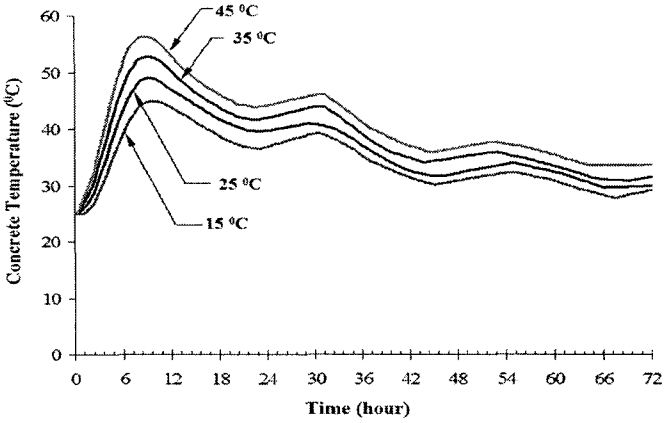

(b) Middle Layer

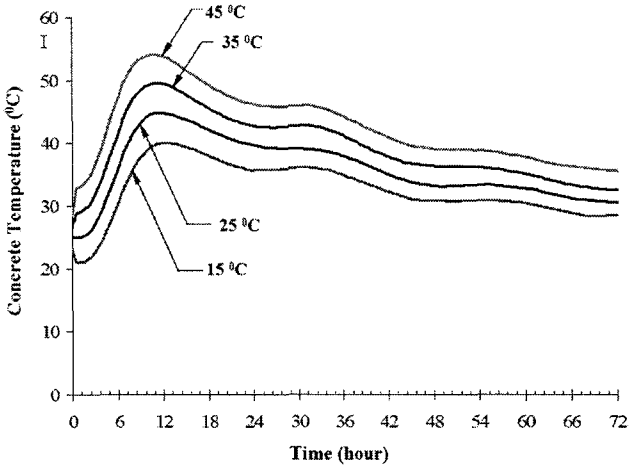

(c) Bottom Layer

Figure 6.10: Effect of Initial Subbase Temperature on Pavement Temperature (Summer Conditions, Paved at 10:00 AM)

6.3.3.4 Effect of Pavement Thickness

Pavement thickness varies with traffic, concrete material, subbase, and subgrade. Figure 6.11 shows that a thick pavement produces a higher temperature inside the concrete slab. In a thinner pavement, the heat can dissipate into the environment faster than the heat from a thick pavement. Both Figures 6.11(a) and (b) indicate that as slab thickness increases the temperature change in concrete due to the weather change decreases. Thick slab has a higher peak temperature and the peak temperature is postponed. As the time increases, all pavement concrete temperatures are nearly identical. Slab thickness has little effect on the surface layer.

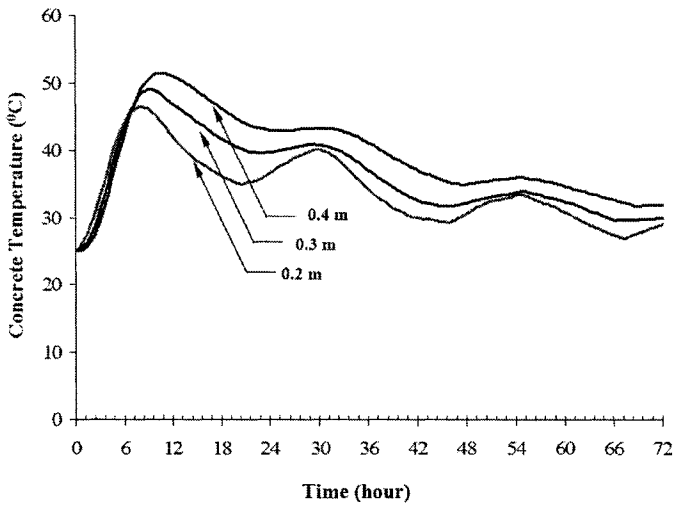

(a) Middle Layer

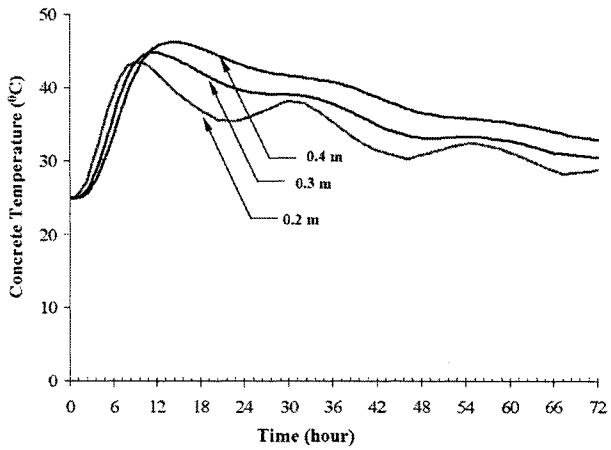

(b) Bottom Layer

Figure 6.11: Effect of Pavement Thickness on Pavement Temperature (Summer Conditions)

6.3.4 Temperature Distribution in Transverse Direction

In the previous discussion, all of the temperatures presented in the figures are from the midline of the concrete slab. However, concrete temperature is not uniform along the transverse direction, because heat exchange occurs between the pavement edge and the environment. This effect decreases as the distance from the edge increases. Figure 6.12 shows the temperature distribution along the transverse direction, indicating that the edge is significantly influenced by environmental conditions. As the distance becomes larger than 0.3 meter, the effect almost disappears. The temperatures become very similar. Therefore, in the field, the temperature should be measured at least 0.3 meter (1foot) from the edge to reduce its effect.

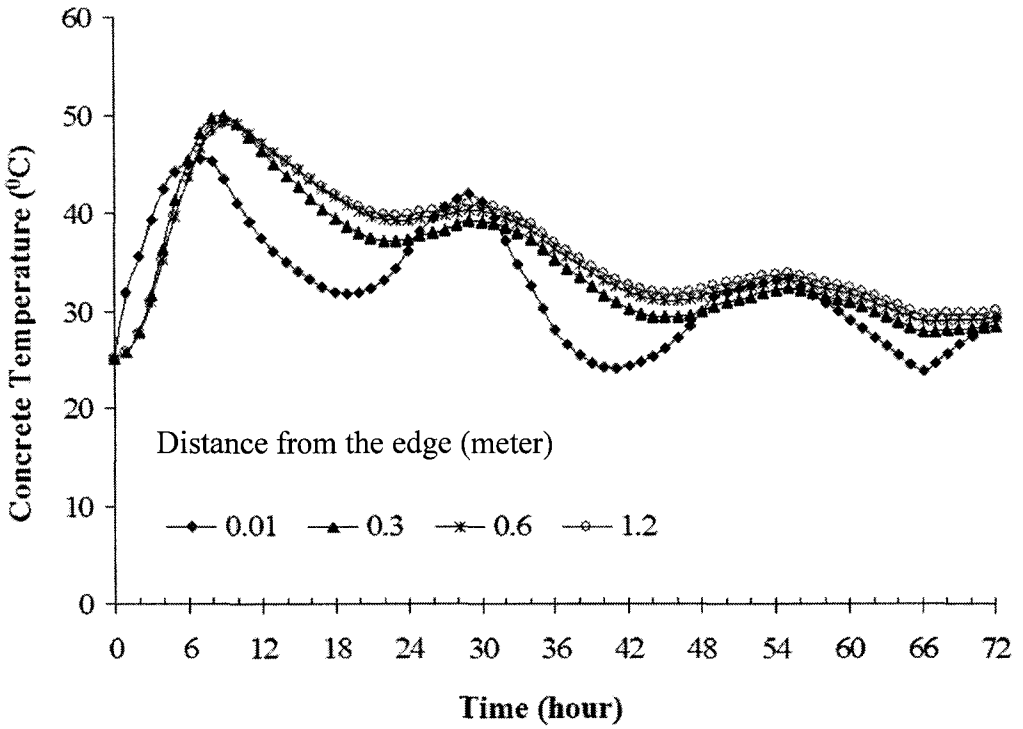

Figure 6.12: Temperature Distribution with Different Distances from the Edge (Summer Conditions, Middle Layer)

6.3.5 Temperature Distribution at a Certain Time

In the previous discussion, the temperature from top, middle, and bottom layers is discussed. The developed temperature model is also able to provide temperature distribution inside pavement slab at a certain time. Figure 6.13 shows the temperature distribution at one day. The pavement is constructed under summer condition.

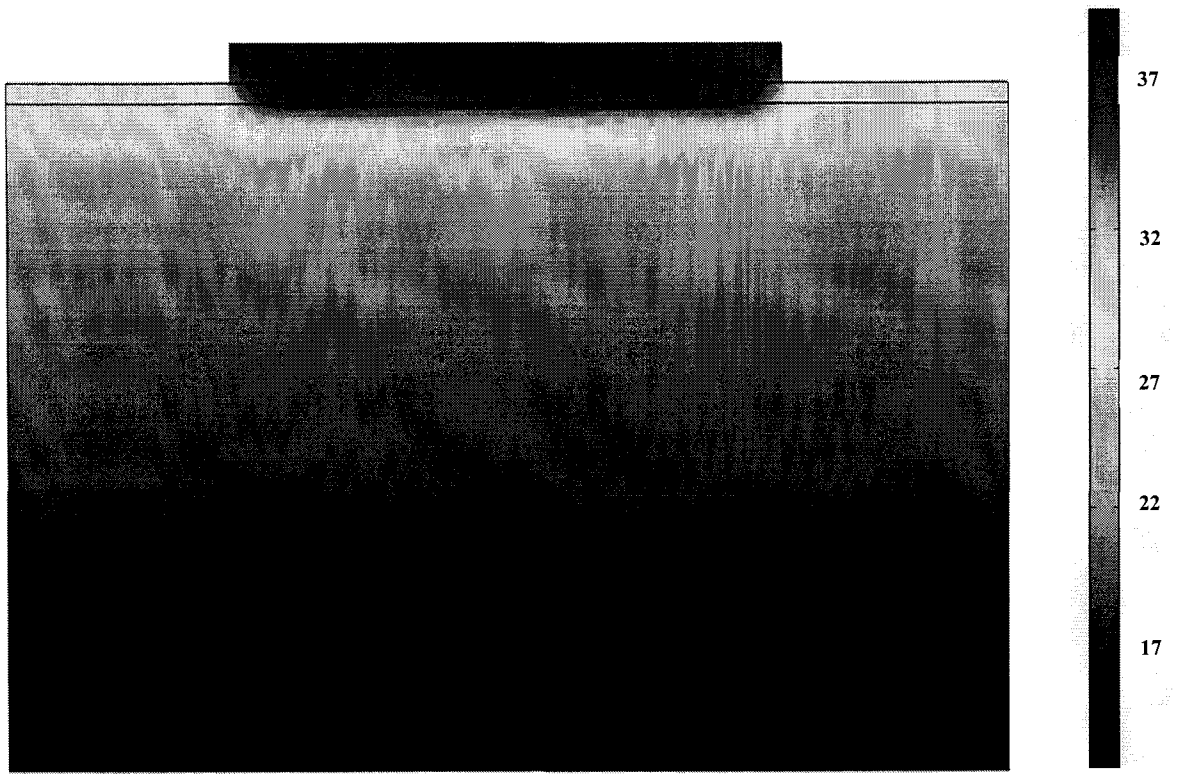

Figure 6.13: Temperature Distribution inside Concrete Slab at One Day

6.4 Summary

This chapter describes the process of predicting field concrete temperatures using FEMLAB, a finite element software. Field concrete temperature is determined by the heat of hydration of the cementitious materials and by the heat exchange between concrete and its surroundings. The heat of hydration of the cementitious materials is determined by the heat of hydration model developed in Chapter 4. The boundary conditions considered in this study include conduction, convection, irradiation, and solar absorption. The thermal properties of concrete, subbase, and subgrade, including specific heat and thermal conductivity, are important for temperature prediction.

In this study, FEMLAB is applied to calculate heat transfer and to predict field concrete temperature development with time. The FEMLAB model, a multiphysic model that includes the general PDE and transient heat transfer models, is able to predict the temperature distribution in concrete at a certain time and the temperature development over time at any position. It can also predict the change of other parameters with time and location.

Several factors can influence field concrete temperature. In this study, the following factors are studied: fly ash and slag, environmental conditions, paving time, concrete place temperature, subbase temperature, and pavement thickness. The ranges of these parameters are presented in Tables 6.6 and 6.7. The predicted temperature development can be used to assess field concrete performance before construction. It can also help to optimize the mix design and construction conditions.

During model development, neither precipitation nor freezing conditions were considered. Precipitation significantly affects heat transfer mechanisms. When pavement is frozen, the thermal properties are changed, which in turn, changes the process of heat transfer and concrete temperature development. Therefore, these factors should be incorporated into the model in the future.

CHAPTER 7
APPLICATION OF DEVELOPED MODELS

Chapters 4, 5, and 6 described the development of the heat of hydration of cementitious materials, concrete maturity-strength, and field concrete temperature models. This chapter provides two examples that show the application of these three models to prediction of the field concrete temperature and strength under different environmental conditions.

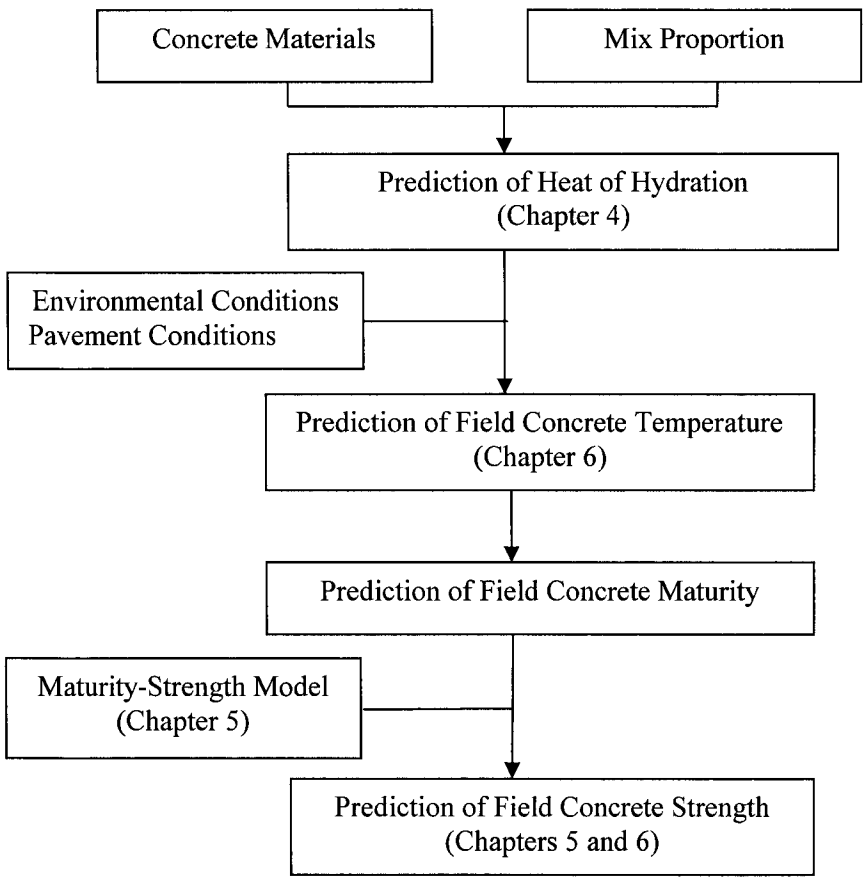

Figure 7.1: Procedures for Concrete Temperature and Strength Prediction

As shown in Figure 7.1, the field concrete temperature is determined by the heat of hydration of the cementitious materials under the field environment conditions described in Chapters 4 and 6. The concrete maturity, in terms of equivalent age, is then calculated based

on the predicted field concrete temperature. Finally, the compressive strength of field concrete is predicted, using the modified maturity-strength model described in Chapter 5.

The field temperature and strength prediction can be performed before concrete mix design, structure design, and construction. Measures can be taken to manage concrete temperature and ensure desirable concrete strength. These measures include changing the mix proportion of concrete, replacing cement with supplemental cementitious materials (SCMs), changing concrete placement temperature, and so on. For example, if the pavement temperature is too high, fly ash can be added or the concrete placement temperature can be reduced to lower field concrete temperature. The effects of these measures can be evaluated by running the models.

In this chapter, two types of weather conditions (hot and cold) and two types of cementitious materials (Type I/II cement and Type I/II cement with 20% slag and 20% fly ash) are studied. The weather conditions, shown in Appendix C, are the same as the spring and summer conditions used in Chapter 6. The other variables, which remained constant, are listed in Tables 7.1 and 7.2. (In the future, the influence of these variables will be further studied.) The Iowa C-3 mix was used and the water/cement ratio was kept constant at 0.42. The air content was assumed to be 6%.

Table 7.1: Material Properties

Parameter	**Heat of Hydration**		**Concrete Strength**	
	OPC	**OPC+SCMs***	**OPC**	**OPC+SCMs**
Hult (KJ/Kg)	354.4	414.596	-	-
Su (psi)	-	-	6158	9959
β	0.890	0.601	0.483	148.41
τ (hour)	16.269	38.923	32.262	0.425

*OPC+20% Fly Ash+20% Slag

Table 7.2: Pavement Conditions

Weather	**Thickness (m)**		**Initial Temperature (°C)**		**Paving Time**
	Slab	Subbase	Slab	Subbase	
Cold	0.3	0.15	25	10	10:00 AM
Hot	0.3	0.15	25	25	10:00 AM

7.1 Results of Example 1--Hot Weather Conditions

The predicted results from the three models--heat of hydration, temperature, and strength--are presented in this section. Figure 7.2 shows the generated heat and the rate of heat of hydration over time as predicted by the heat of hydration model. For both ordinary Portland cement (OPC) concrete and concrete containing fly ash and slag, the surface layer has the highest peak value for heat generation. The peak is postponed as the depth increases. The generated heat for all layers becomes similar at the end of 3 days. The higher rate of heat generation is mainly caused by the higher temperature. Under hot weather conditions, the air temperature is normally higher than the concrete placement temperature. The heat flows to the concrete and causes higher temperatures in the surface layer, which in turn, cause a higher rate of heat of hydration.

Concrete with fly ash and slag generates less heat and has a lower rate of heat generation. The average total heat at 3 days is reduced from 10.4×10^7 to 9.1×10^7 J/m^3 for the different layers. The peak values are reduced to 5.3, 5.2, and 4.1 W/cm^3 for the surface, middle, and bottom layer respectively. The reduced values are almost the same as the peak values for concrete with fly ash and slag. The reduced rate and generated heat causes the lower temperatures for this concrete mixture (Figure 7.3).

Figure 7.3 shows field temperature and strength development under hot weather conditions. The strength development of field concrete is delayed by adding the fly ash and slag. The strength reduction is due to both the addition of fly ash and slag and the low concrete temperature. Low temperature results in low maturity, which causes reduced concrete strength. At the end of 3 days, however, the strength of concrete with and without fly ash and slag is nearly identical for all three layers. The strength difference is less than 150 psi at the end of the third day.

For both concrete with and without fly ash and slag, the highest concrete temperature occurs around 7.5 to 13 hours after paving. The surface layer reaches the highest temperature earlier than the middle and the bottom layers because of the higher rate of heat generation at an early age (Figure 7.2). Adding SCMs reduces the maximum temperature and concrete

temperature for the first day. After about 1day, the temperatures for concrete with and without fly ash and slag are nearly identical. The temperatures become similar for two reasons. First, at that time, the rates of heat generation are close and low for both concrete with and without fly ash and slag (Figure 7.2). Second, both types of concrete are placed and cured under the same weather conditions. Therefore, the heat exchange between the concrete and its surroundings will be similar for both types.

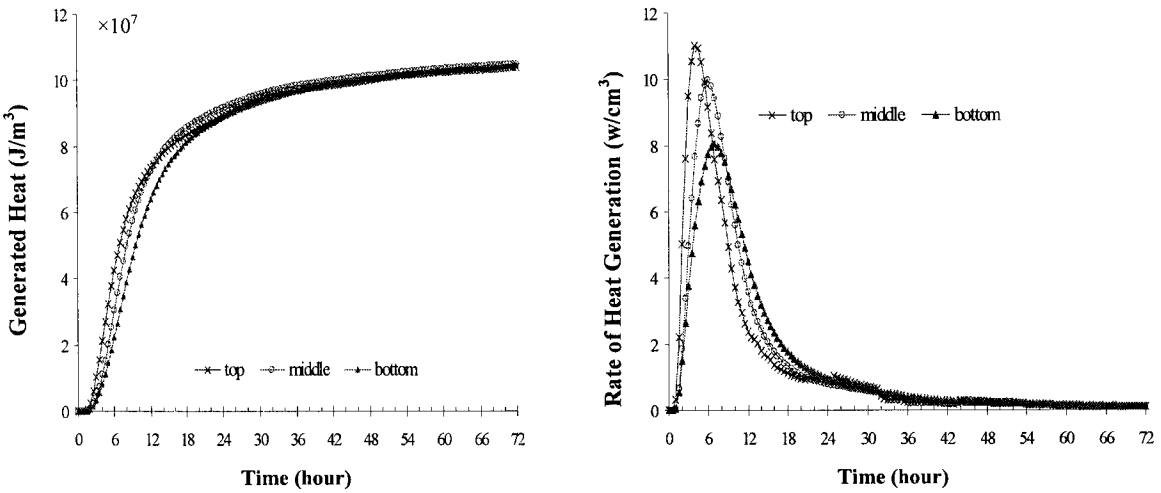

(a) OPC Concrete

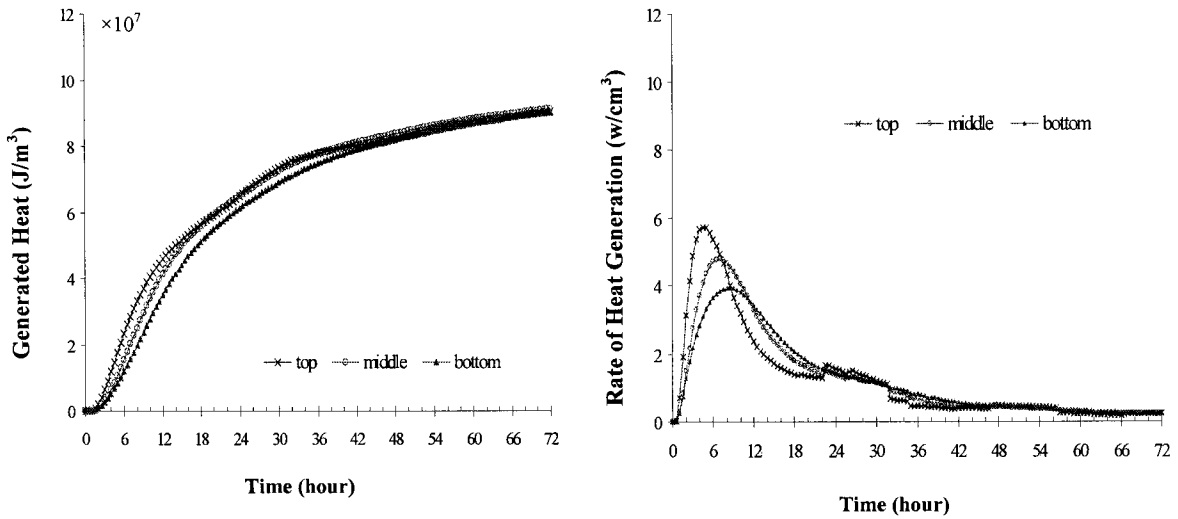

(b) OPC +20% Fly Ash +20% Slag

Figure 7.2: Heat of Hydration of Field Concrete under Hot Weather Conditions

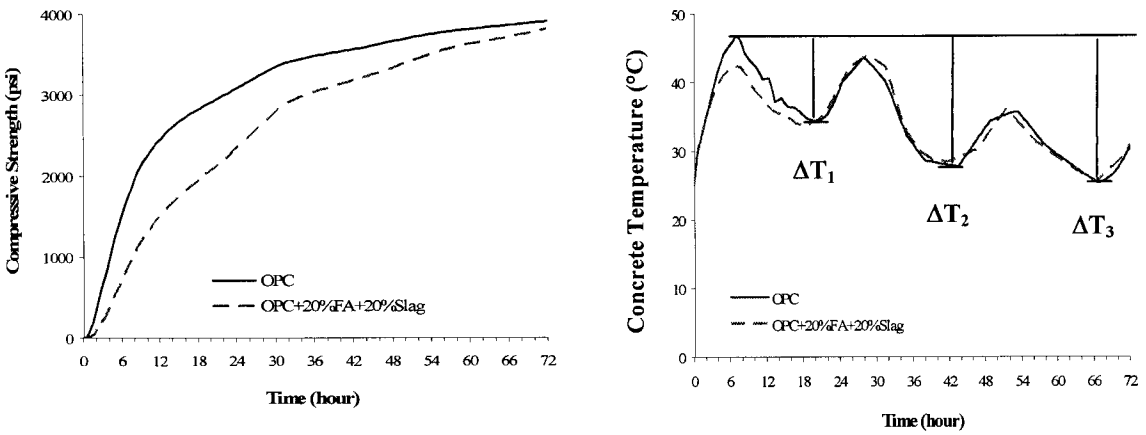

(a) Surface Layer

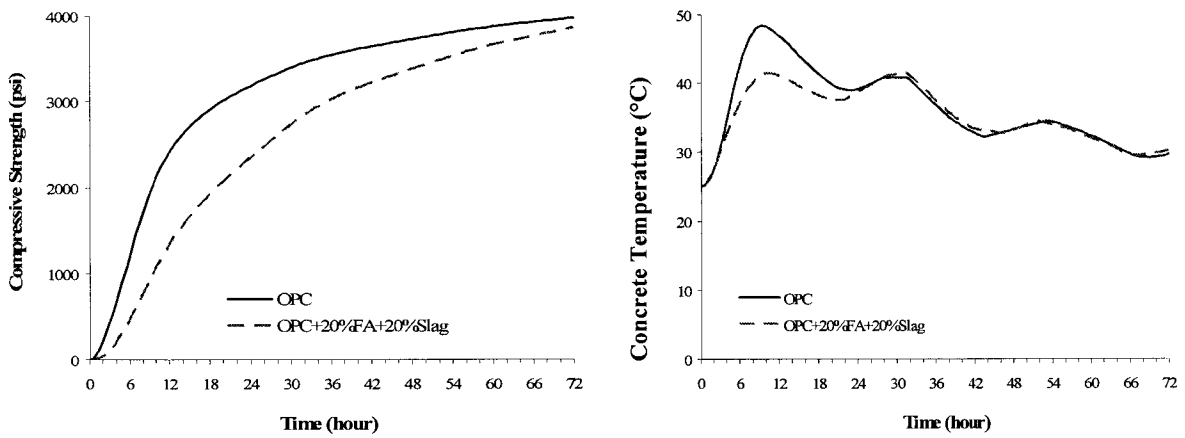

(b) Middle Layer

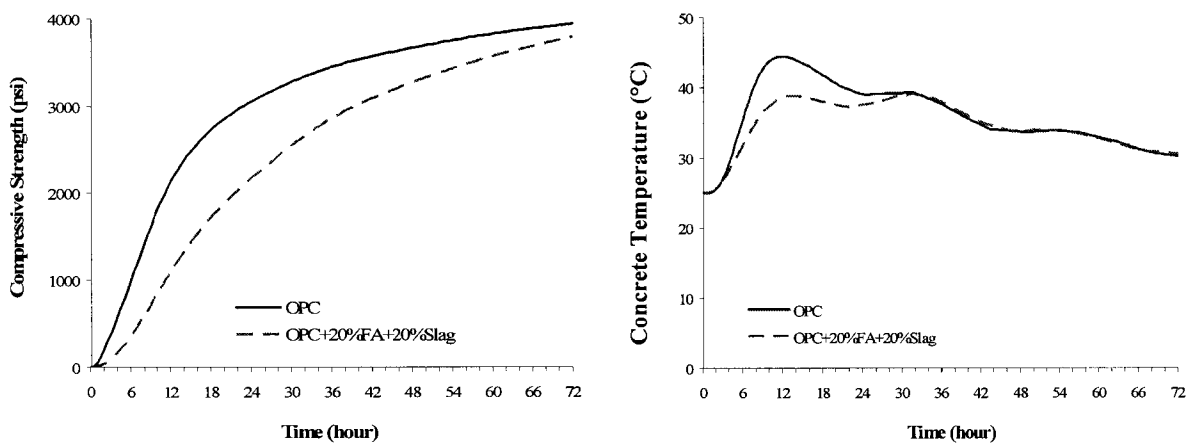

(C) Bottom Layer

Figure 7.3: Field Concrete Temperature and Strength under Hot Weather Conditions

Concrete temperature drop is important for field concrete. Temperature drop induces thermal tensile strength inside concrete, which can possibly cause cracking. The maximum temperature and temperature drop at 1, 2, and 3 days are listed in Table 7.3. The surface layer has the largest temperature drop. Therefore, the surface layer is most prone to thermal cracking. The bottom layer has the lowest temperature drop.

Table 7.3 shows that the maximum temperature and temperature drop are reduced by adding fly ash and slag to all three layers. The middle layer has the highest reduction, an average reduction of 6.7°C. The reduction of the temperature drop reduces the thermal stress inside the concrete.

Table 7.3: Maximum Temperature Drop for Hot Weather Conditions

		OPC Concrete			**Concrete with SCMs**		
		Top	Middle	Bottom	Top	Middle	Bottom
Max. Temp. (°C)		46.7	48.4	44.5	43.9	41.5	39.1
Temp. Drop, ΔT (°C)	ΔT_1	12.4	9.4	5.4	10.1	4.0	1.9
	ΔT_2	18.9	16.3	10.8	15.4	8.8	5.4
	ΔT_3	21.2	19.2	14.3	18.3	12.0	8.6

7.2 Results of Example 2--Cold Weather Conditions

The same analysis of concrete pavement was also conducted under cold weather conditions. Figure 7.4 shows the generated heat and the rate of heat of hydration with time. Unlike the hot weather conditions, the surface layer generates less heat and has the lowest rate of heat generation. The middle and bottom layers have similar values. The maximum rate of heat generation is reduced to about half of the value under hot weather conditions for all three layers and concrete with and without fly ash and slag.

Like heat development, temperature and strength development under cold weather conditions are also less than that under hot weather conditions. Pavement concrete temperature under cold weather conditions continuously drops after the paving (Figure 7.5).

The temperature of the middle and bottom layers of OPC concrete increases slightly after about 4 hours. The temperature of the top layer starts to increase after 20 hours. In concrete with fly ash and slag, the temperature of all three layers begins to increase after about 20 hours. Adding SCMs to concrete can reduce the maximum temperature and temperature drop under hot weather conditions, but this effect is not apparent under cold weather conditions. The maximum temperature and temperature drop are reduced less than 2°C for all three layers. On the other hand, using fly ash and slag significantly reduced concrete strength during the first 3 days. The 3-day strength, for concrete with on average of three layers, is 30% lower than the 3-day strength of concrete without fly ash and slag (Figure 7.5).

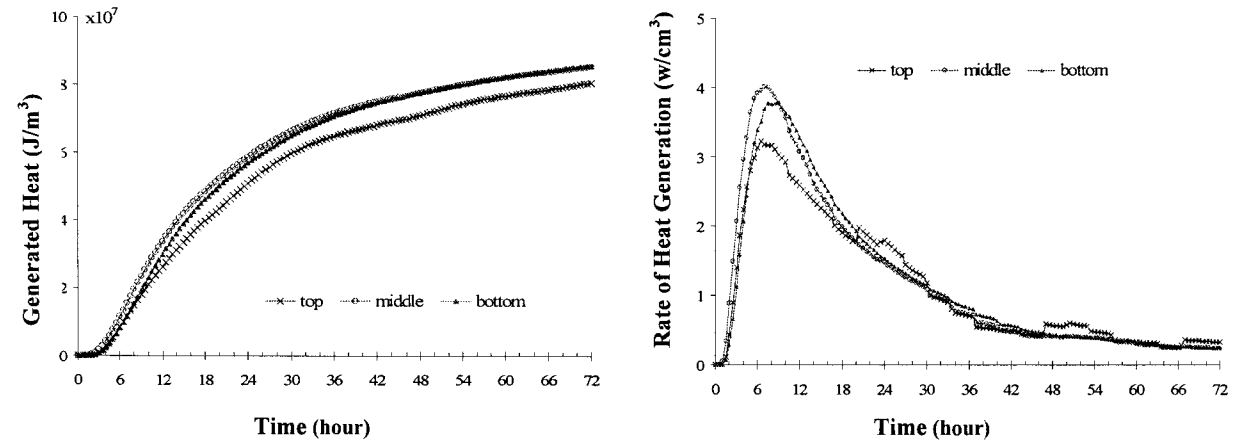

(a) OPC Concrete

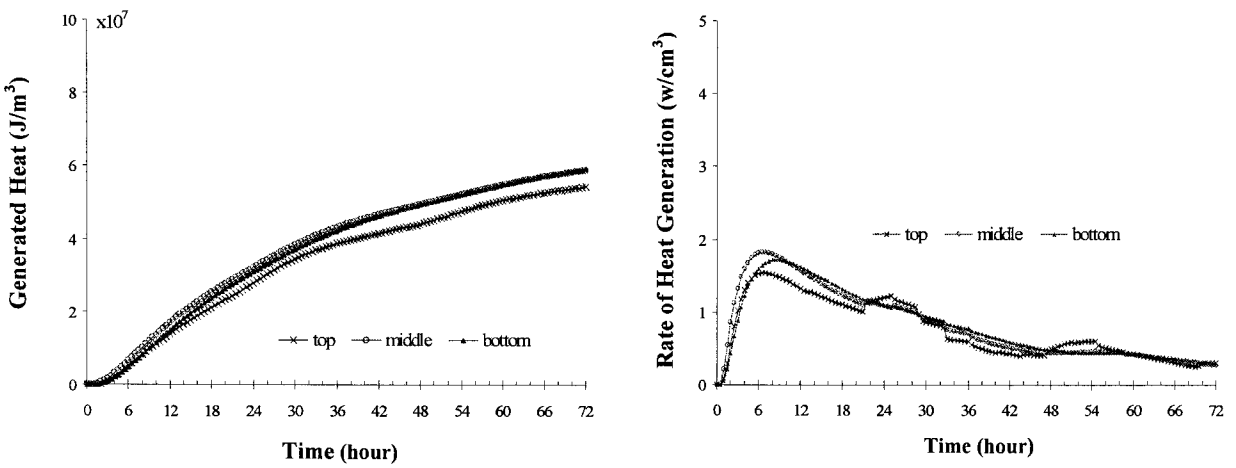

(b) Concrete with Fly Ash and Slag

Figure 7.4: Heat of Hydration of Field Concrete under Cold Weather Conditions

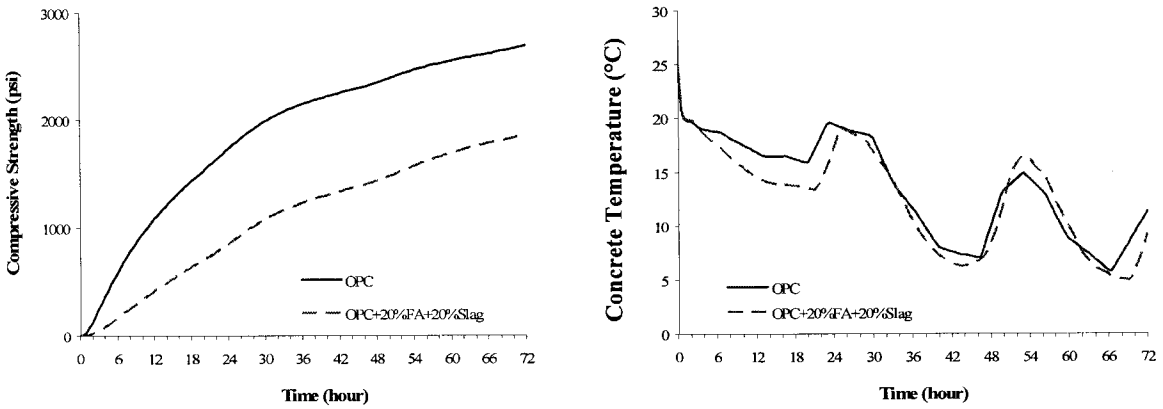

(a) Surface Layer

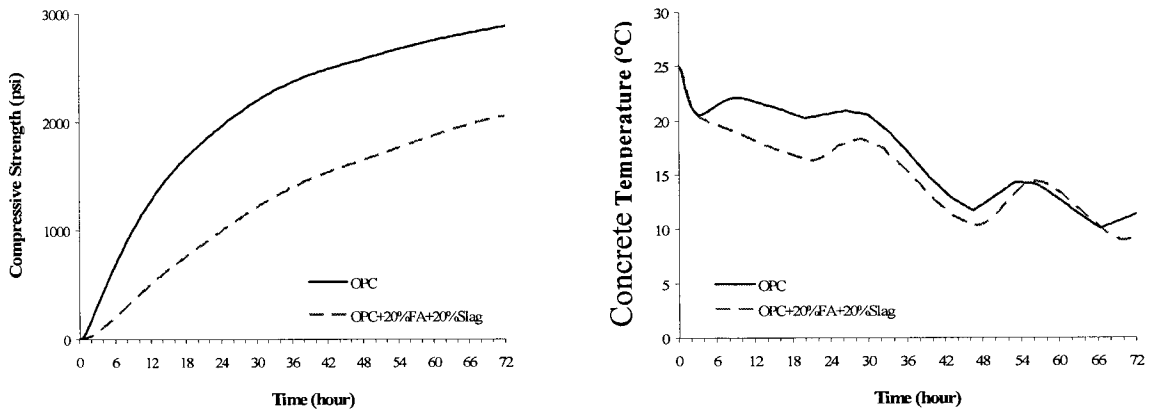

(b) Middle Layer

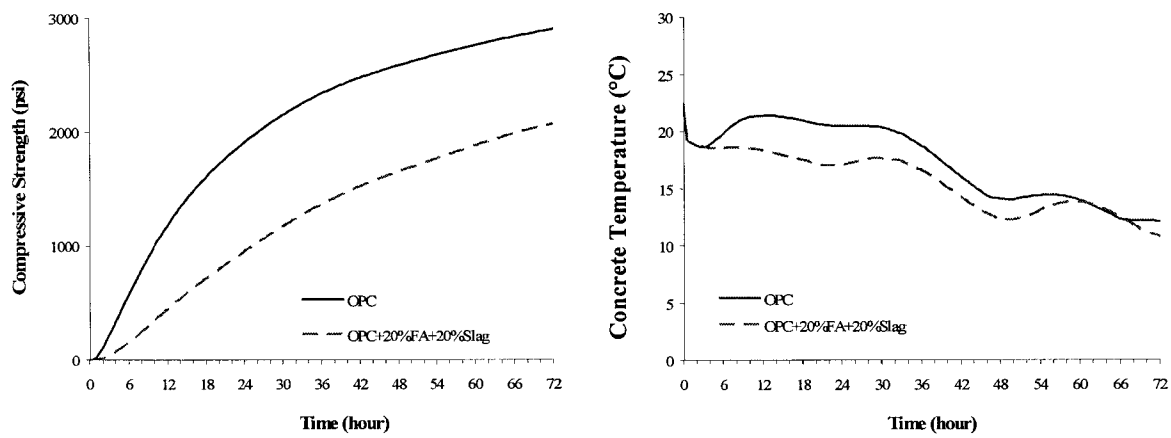

(c) Bottom Layer

Figure 7.5: Field Concrete Temperature and Strength under Cold Weather Conditions

7.3 Application of the Modeling Results

To ensure good performance, concrete mixes may be designed differently for different weather conditions. In the summer, SCMs may be used to reduce the temperature (Figure 7.3). In the winter, the use of SCMs reduces concrete early age strength (Figure 7.5), and therefore, the amount of SCMs in concrete may be reduced.

The simulation developed in the present study can be used for concrete mix design, field concrete performance assessment before construction, and joint cutting time determination.

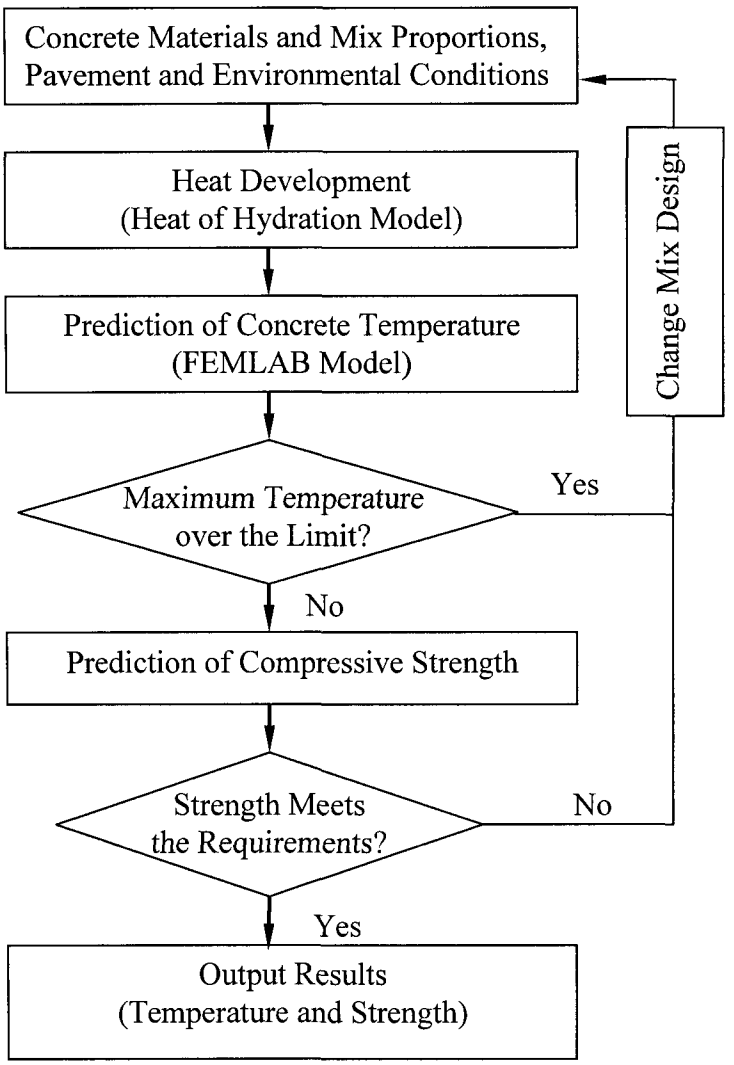

Figure 7.6: Flowchart of Use of Developed Models for Concrete Mix Design and Performance Control

The flowchart in Figure 7.6 illustrates the simulation process for concrete mix design based on control of concrete temperature and strength. This simulation for modeling analysis can be performed before the mix design or during the process of construction. During the analysis, concrete materials and mix proportions together with the initial conditions are input into the computer program, FEMLAB. The temperature is then predicted by the developed models. If the highest temperature is over the limit, the concrete mix design has to be modified to a reduced temperature. The process is repeated until the temperature meets the requirement. Next, the compressive strength is predicted. If the strength is lower than the proposed value, the mix design has to be modified again. The same process can be used to adjust concrete placement temperature and construction under different weather conditions.

The developed model can also predict joint cutting time. New pavement must have to develop enough strength to resist joint raveling when the slab is cut by saw equipment. The developed model can predict field concrete strength development over time, that is, it can predict when the pavement will be strong enough to withstand saw equipment. Similarly, the predicted strength can also be used to estimate concrete pavement opening time.

Another potential use of the developed model is to predict the risk of thermal and drying cracking at an early age. The model for estimating thermal stress is necessary for this application. The predicted temperature can be used in the thermal stress model to estimate the thermal stress. The tensile strength can be estimated from the degree of hydration, which can be predicted from the heat of hydration results. Further research is needed to develop other models that explain the quantitative relationship between thermal and drying shrinkage and the tensile strength of concrete.

7.4 Summary

This chapter provides two examples that use the developed heat of hydration, maturity-strength, and field concrete temperature models to predict the pavement concrete temperature and strength under two different conditions. The quantitative results show that concrete with and without fly ash and slag have different temperature and strength characteristics under different weather conditions. Using fly ash and slag reduces the

maximum temperature drop under hot weather conditions but not under cold weather conditions.

The modeling results can be used to modify concrete mix design under different weather conditions, to assess field concrete performance before construction, to estimate the time for pavement joint sawing and opening time, and to control concrete placement temperature and construction conditions based on temperature and strength.

The developed models can also be used to predict how various design variables will affect concrete temperature and strength development under different weather and construction conditions.

CHAPTER 8
SUMMARY AND RECOMMENDATIONS

8.1 Summary

The objective of the present study is to develop a practical method to predict field pavement concrete temperature and strength. The following three models were developed to fulfill this objective: (1) heat of hydration, (2) field concrete temperature, and (3) modified maturity-strength. The heat of hydration and modified maturity-strength models were developed from existing models, but their model parameters were modified by available laboratory and literature test data. Nonlinear regression analyses were used to establish the relationships among model parameters and fatctors that affect heat of hydration and concrete strength development. Field concrete temperatures were predicted with partial differential equations (PDEs) and with transient heat transfer modes in FEMLAB, a commercially available computer software.

The modified heat of hydration model was developed with heat of hydration test results of 43 different mixes from the present experimental work and literature, including 21 different types of cement, four different types of fly ash, and three different types of slag. The tests were performed with a semi-adiabatic calorimeter (IQdrum). The effects of cement chemical composition, cement fineness, amount and chemical composition of fly ash and slag, and water/cement (w/c) ratio were considered in the model. The research results show that the modified heat of hydration model is able to approximately predict the heat generated from the hydration of cementitious materials and to characterize the hydration properties of concrete with different cementitious materials and mix design.

The field concrete temperature model is able to predict the field concrete temperature for different concrete pavements under various weather, structural, and construction conditions. Concrete pavement boundary conditions considered in the temperature model include conduction, convection, solar absorption, and irradiation. Concrete mix proportions, concrete physical properties, pavement configuration, construction conditions, and

environment conditions were also considered. This field concrete temperature model is able to provide the following results: the temperature distribution in pavement concrete at a given time and any position; the temperature development or temperature change with time at any position; and the heat generated in the pavement with time and location.

The modified concrete maturity-strength model was developed from the strength and maturity test results of 60 different mixes from the present experimental work and literature, including 20 different types of cement, four different types of fly ash, and three different types of slag. This model considered the effects of cement chemical composition, cement fineness, amount and chemical composition of fly ash and slag, w/c ratio, air content, and curing temperature. The modeling results show that the modified maturity-strength model is able to approximately predict the strength development of concrete made with different cementitious materials.

These three models are combined together to predict the temperature and strength development of field pavement concrete based on the chemistry of the cementitious materials and mix proportions. With the combined model, researchers and engineers can evaluate and quantify the effects of most factors that affect field concrete temperature and strength development. The models can also be used to select concrete mix design and pavement placement temperature under different weather conditions as well as to estimate joint cutting and pavement opening time. In addition, the developed models can be used to estimate thermal and drying shrinkage cracking.

8.2 Major Research Findings

The models developed in the present research can be used to predict concrete temperature and strength distributions in a pavement slab under given material, environment, and structural conditions. This analysis method can also be used to quantify the effects of (1) materials and mix design, (2) environmental conditions, and (3) pavement structural conditions on field concrete temperature and strength development. The major findings drawn from the present testing and modeling can be summarized as follows:

1. Effects of Materials and Mix Design
   - Cement type, supplemental cementitious materials (SCMs), and mix design influence concrete heat of hydration, temperature, and strength development. Generally, replacing Portland cement with fly ash and slag for Portland cement reduces the generated heat and concrete strength at early age and lowers maximum pavement temperature.
   - The effect of fly ash and slag depends on both the percentage of replacement and the chemical composition. Fly ash with a higher calcium oxide (CaO) content or slag with a higher hydraulic index, defined in Equation 4.17, provides concrete with more heat and higher strength.
   - For up to 60% of slag replacement, the compressive strength of concrete decreases at early age but increases at later age. The change in strength due to slag replacement increases as the slag replacement level increases.
   - Based on the materials used in present study, at 1 day, concrete compressive strength decreases as fly ash replacement increases. At later age, concrete strength first increases and then decreases as fly ash replacement increases. Concrete containing 30% Class C fly ash has the highest strength.
   - Sensitivity analysis of the heat of hydration model shows SO_3 significantly affects the hydration process. High content of SO_3 reduces the hydration at early age and increase it at later age. Therefore, it is important to use the proper amount of gypsum, hemihydrate, or anhydrate during the clinker grind process to achieve the desired sulfate content in the final cement product. Sensitivity analysis of the modified maturity-strength model shows that w/c ratio, fly ash/slag content, cement type, and air content have significant influence on concrete strength.

2. Effects of Environmental and Construction Conditions
   - Concrete placed under hot weather conditions develops much higher maximum temperatures than does concrete placed under cold conditions. The highest temperature drop normally occurs at the surface layer of the pavement. The trend of surface concrete temperature change is similar to ambient air temperature change.

- Due to environmental change with time, concrete placed at different times has a different temperature history, and results in different strength development. Therefore, field concrete control management can be achieved by scheduling concrete placing time.
- Concrete with higher placement and initial subbase temperatures normally has higher maximum temperatures. However, the influence of placement temperature is significantly reduced after 1 day. The initial subbase temperature strongly influences the bottom layer temperature.

3. Effects of Pavement Structural Conditions
   - Concrete temperature is not uniform along the transverse and vertical directions due to the heat exchange between the surface edge and surroundings. The thicker a pavement slab, the higher temperatures in the middle layer of the concrete, and the less temperature variation with weather. The edge effect on temperature almost disappears when concrete is 0.3 meter/1 foot away from the edge.

8.3 Limitations and Recommendations

The following assumptions are made in the present models:

1. Only effects of the reactivity index of slag and the CaO content of fly ash on heat of hydration and maturity-strength properties of concrete are considered in the developed models
2. The total heat generated from hydration of slag is constant (461 KJ/Kg). The total heat generated from hydration of fly ash is related to the CaO content.
3. The ultimate degree of hydration for cementitious materials containing different types of fly ash is the same.
4. The effects of fly ash and slag on heat of hydration and strength of the concrete made with different types of cements are the same.
5. Proper curing is provided to the field concrete

Because of the above assumptions, the application of the developed models may have certain limitations. Therefore the following recommendations are proposed for the further research.

1. Expect for SCMs (fly ash and slag), other admixtures or additives as well as aggregate properties have not been considered in the present model development. The effect of concrete admixtures (such as water reducing agent, accelerator, and retarder) and aggregate properties (such as gradation) should be considered in the future heat of hydration and strength models
2. Further study is necessary to verify the assumption used in the present research (such as assumption on the ultimate degree of hydration of concrete) and to extend the model with laboratory and field test results beyond the limitations of the present study.
3. The proposed models were developed based on available literature data and some short-term test data, and they shall be further verified by long-term test results of field concrete.

REFERENCES

Adams, L.D., 1976, The Measurement of very early hydration reactions of Portland cement clinker by a thermoelectric conduction calorimeter, *Cement and Concrete Research*, Vol. 6, 293-308.

Andersen, P.J., M.E. Andersen, and D. Whiting, 1992, A guide to evaluating thermal effects in concrete pavements, SHRP-C-321, Strategic Highway Research Program, National Research Council, Washington, D.C.

ASHRAE, 1993, *ASHRAE Handbook*, American Society of Heating, Refrigerating and Air-Conditioning Engineers, Incorporated, Atlanta.

ASTM C39, 2002, Standard Test method for compressive strength of cylindrical concrete specimens, *Annual Book of ASTM Standards*, Vol. 4.02.

ASTM C 138, 2002, Standard test method for density (unit weight), yield and air content (gravimetric) of concrete, *Annual Book of ASTM Standards*, Vol. 4.02.

ASTM C 143, 2002, Standard test method for slump of hydraulic cement concrete, *Annual Book of ASTM Standards*, Vol. 4.02.

ASTM C 150, 2002, Standard specification for Portland cement, *Annual Book of ASTM Standards*, Vol. 4.02.

ASTM C 186, 2002, Standard test method for heat of hydration of hydraulic cement, *Annual Book of ASTM Standards*, Vol. 4.01.

ASTM C 192, 2002, Standard practice for making and curing concrete test specimens in the laboratory, *Annual Book of ASTM Standards*, Vol. 4.02.

ASTM C 219, 2002, Standard terminology relating to hydraulic cement, *Annual Book of ASTM Standards*, Vol. 4.01.

ASTM C 231, 2002, Standard test method for air content of freshly mixed concrete by the pressure methods, *Annual Book of ASTM Standards*, Vol. 4.02.

ASTM C 618, 2002, Standard specification for coal fly ash and raw or calcined natural Pozzolan for use as mineral admixture in Portland cement concrete, *Annual Book of ASTM Standards*, Vol. 4.02.

ASTM C 1074, 2002, Standard practice for estimating concrete strength by the maturity method, *Annual Book of ASTM Standards*, Vol. 4.02.

Ballim, 2004, A numerical model and associated calorimeter for predicting temperature profiles in mass concrete, *Cement Concrete and Composites*, Vol.26, 695-703.

Basma, Adnan A., S. A. Barakat, and Salim Al-Oraimi, Prediction of cement degree of hydration using artificial neural networks , *ACI Materials Journal*, v 96, n 2, March/April, 1999, p 167-172

Ben-Bassat, M., 1995, Water reducing/retarding admixtures, *Application of Admixtures in Concrete, State-of-the-art report,* RILEM TC 84-AAC.

Bentz, D.P., V. Waller, and F. de Larrard, 1998, Prediction of adiabatic temperature rise in conventional and high-performance concretes using a 3-D microstructure model, *Cement and Concrete Research*, Vol. 28, No. 2, 285-297.

Bentz, D.P., 2000, *A Computer Model to Predict the Surface Temperature and Time-of-Wetness of Concrete Pavements and Bridge Decks*, NISTIR 6551, U.S. Department of Commerce.

Bernhardt, C.J., 1956, Hardening of concrete at different temperatures, especially below the freezing point, in *Proc. RILEM Symp. of Winter Concreting Session BII*, Copenhagen, Danish Institute for Building Research.

Bland, C.H., and J.H. Sharp, 1991, Conduction calorimetric study of gasified slag-Portland cement blends, *Cement and Concrete Research*, Vol. 21, No.2-3, 359-367.

Bogue, R.H., 1929, Calculation of the compounds in Portland cement, *Ind. Eng. Chem. Anal. Ed.* 1, 192-7.

Bogue, R.H., 1947, *The Chemistry of Portland Cement*, Reinhold Publishing Corporation, New York.

Bowden, G., 1998, *Diurnal Heat Transfer through Concrete*, NLC ME NOTE, No. 14-98 Rev 0.

Breugel K. van, 1997, *Simulation of Hydration and Formation of Structure in Hardening Cement-Based Materials*, 2nd Edition.

Brown, T.D., and M. Y. Javaid, 1970, The thermal conductivity of fresh concrete, *Materials and Structures*, Vol. 3, 411-416

Brown P.W., J. Pommersheim, and G. Frohnsdorff, 1985, A kinetic model for the hydration of tricalcium silicate, *Cement and Concrete Research*, Vol. 15, No. 1, 35-41.

Byfors, J. 1980, *Plain Concrete at Early Ages*, CBI report FO 3:8, Swedish Cement and Concrete Research Institute, Stockholm, Sweden.

Carino, N.J., 1981, *Temperature Effects on Strength-Maturity Relations of Mortar*, NBSIR 81-2244, U.S. National Bureau of Standards.

Carino N. J., 1984, The maturity method: Theory and application, *Cement, Concrete, and Aggregates*, Vol. 6, No. 2, 61-73.

Carino N. J., and R. C. Tank, 1991, Rate constant functions for strength development of concrete, *ACI Materials Journal*, Vol. 88, No. 1, 74-83.

Carino N. J., and R. C. Tank, 1992, Maturity function for concrete made with various cements and admixtures, ACI Materials Journals, Vol. 89, No. 2, 188-196.

Carino N.J., 2004, The maturity method, In *Handbook on Nondestructive Testing of Concrete*, CRC Press, Boca Raton, FL, 2nd edition.

Copeland L. E., D. L. Kantro, and G. Verbeck, 1962, Chemistry of hydration of Portland cement, Proceeding, 4th International Symposium on the Chemistry of Cement, NBS Monograph 43, Washington, D.C., 429-465.

Crow, R.D. and E.R. Dunstan, 1981, Properties of fly ash concrete, *Effects of Fly Ash Incorporation in Cement and Concrete, Proceedings, Symposium N, Materials Research Society*, 214-224.

Dabic, P., R. Krstulovic, and D. Rusic, 2000, A new approach in mathematical modelling of cement hydration development, *Cement and Concrete Research*, Vol. 30, No. 7, 017-1021.

D' Aloia L., and G. Chanvillard, 2002, Determining the "apparent" activation energy of concrete E_a-numerical simulations of the heat of hydration of cement, *Cement and Concrete Research*, Vol. 32, No. 8, 1277-1289.

De Schutter, G. and L. Taerwe, 1995, General hydration model fro Portland cement and blast furnace slag cement, Cement and Concrete Research, Vol. 25, No. 3, 593-604.

Douglas, E., and G. Pouskouleli, 1991, Prediction of compressive strength of mortars made with Portland cement - blast-furnace slag - fly ash blends, *Cement and Concrete Research*, Vol. 21, No. 4, 523-534.

Escalante-Garcia, J. I., and J. H. Sharp, 2000, The Effect of temperature on the early hydration of Portland cement and blended cements, *Advances in Cement Research*, Vol. 12, No. 3, 121-130.

Freiesleben Hansen, P., and E.J. Pedersen, 1985, *Curing of Concrete Structures, Draft DEBGuide to Durable Concrete Structures*, Appendix 1, Comité Euro-International du Béton, Lausanne, Switzerland.

Gauthier, E. and M. Regourd, 1982, The hardening of cement in function of temperature, *Proc. RILEM Int. Conf. On Concrete at Early Ages*, Ecole nationale Des Ponts et Chausees, Paris, Vol. I, 145-150.

Geiker, M. and T. Knudsen, 1982, Chemical shrinkage of Portland cement pastes, *Cement and Concrete Research*, Vol. 12, No. 5, 603-610.

Geiker, M., 1983, Studies of Portland cement hydration by measurements of chemical shrinkage and systematic evaluation of hydration curves by means of the dispersion model, Ph.D. Dissertation, Technical University of Denmark.

Guo Chengju, 1989, Maturity of concrete: Method for predicting early-stage strength, *ACI Materials Journal*, V. 86, No. 4, 341-353.

Hankins, K., Y.C. Suh, and B.F. McCullough, 1991, *Field Evaluation of coarse Aggregate Types:Criteria for Test Sections*, Research Report 422/1244-1, Center for Transportation Research, The University of Texas at Austin.

Hansen, P.F., Hansen, J., K.V. Hougaard, and E.J. Pedersen, 1982, Thermal properties of hardening cement paste, *Proceeding of RILEM International Conference on Concrete at Early Ages*, Paris, 23-26.

Hansen, T. C., 1986, Physical structure of hardened cement paste, A classical approach, *Materials and Structures*, Vol. 19, No. 114, 423-436.

Hogan, F.J. and J.W. Meusel, 1981, Evaluation for durability and strength development of a ground granulated blast furnace slag, *Cement Concrete, and Aggregates*, CCAGDP, Vol. 3, No. 1, 40-52.

Holman, J.P., 1990, *Heat Transfer*, 7th edition, New York: McGraw Hill.

Jonasson, J.E., 1988, *Hett – A Computer Program for the Calculation of Strength, Equivalent Hydration Period and Temperature*, Swedish Cement and Concrete Research Institute, Stockholm.

Joshi, R.C. and R. P. Lohtia, 1997, *Fly Ash in Concrete*, Gordon and Breach Science Publishers.

Kada-Benameur, H., E. Wirquin, and B. Duthoit, 2000, Determination of apparent activation energy of concrete by isothermal calorimetry, *Cement and Concrete Research*, Vol. 30, No. 2, 301-305.

Khan, A.A., W.D. Cook, and D. Mitchell, 1998, Thermal properties and transient analysis of structural members during hydration, *ACI Materials Journal*, Vol. 95, No. 3, 293-302.

Kim, K. H., S.E. Jeon, J.K. Kim, and S. Yang, 2003, An experimental study on thermal conductivity of concrete, *Cement and Concrete Research*, Vol. 33, No.3, 363-371.

Kishi, T., and K. Maekawa, 1994, Thermal and mechanical modeling of young concrete based on hydration process of mutli-component cement minerals, In *Thermal Cracking in concrete at Early Ages*, Proceeding of RILEM, Edited by Springenschmid, R., 11-18.

Kjellsen, K. O., R. J. Detwiler, and Odd E. Gjorv, 1991, Development of microstructures in plain cement pastes hydrated at different temperatures, *Cement and Concrete Research*, Vol. 21, No. 1, 179-189.

Kjellsen K. O., and R. J. Detwiler, 1993, Later-age strength prediction by a modified maturity model, *ACI Materials Journal*, 220-227.

Klieger, P., and A.W. Isberner, 1967, Laboratory studies of blended cements- Portland blast-furnace slag cements, *Journal of the PCA Research and Development Laboratories*, Vol. 9, No. 3, 2-22.

Klieger, P, and J.F. Lamond, 1994, *Significance of tests and properties of concrete and concrete-making materials*, American Society for Testing and Materials, Philadelphia.

Knudsen, T., 1982, Modeling hydration of Portland cement - The effect of particle size distribution, *Conference Proceedings, Characterization and Performance Prediction of Cement and Concrete*, Edited by Young, J.F., United Engineering Trustees, Inc., New Hampshire, 125-150.

Kong, F.K., R. H. Evans, E. Cohen, F. Roll, 1983, Handbook of Structural Concrete, New York: McGraw Hill.

Langan, B.W., K. Weng, and M.A. Ward, 2002, Effect of silica fume and fly ash on heat of hydration of Portland cement, *Cement and Concrete Research*, Vol. 32, No. 7, 1045-1051.

Lea, F.M., 1970, *The Chemistry of Cement and Concrete*, Third edition London, Edward Arnold Publication Ltd.

Lerch, W., F. W. Ashton, and R. H. Bogue, 1929, The sulfoaluminates of calcium, *journal of Research of National Bureau Standards,* Vol. 2, 715-731.

Lerch, W., R.H. Bogue, 1934, Heat of hydration of Portland cement pastes, *journal of Research of National Bureau Standards*, Vol.12, 645-664.

Lerch, W., 1946, the Influence of gypsum on the hydration and properties of Portland cement pastes, *Proceedings of American Society for Testing Materials*, Vol. 46, 1252-1297.

Lerch, W., and C.L. Ford, 1948, Long-term study of cement performance in concrete: Chapter 3.chemical and physical tests of the cements, *ACI Journal*, Vol. 19, No. 8, 745-795.

McAdams, W.H., 1954, *Heat Transmission*, McGraw Hill Series in Chemical Engineering, McGraw Book Company, New York.

Maekawa, K, R. Chaube, and T. Kishi, 1999, *Modelling of Concrete Performance*, E & FN Spon,

Mantel, D.G., 1994, Investigation into the hydraulic activity of five granulated blast furnace slags with eight different Portland cements, *ACI Material Journal*, Vol. 91, No. 5, 471-477.

Massazza, F. and U. Costa, 1980, Effect of superplasticizers on the C_3A hydration, *Proceedings of Seventh International Symposium on Chemistry of Cement*, Paris, Vol. 4, 529-534.

Ma, W., D. Sample, R. Martin, and P.W. Brown, 1994, Calorimetric study of cement blends containing fly ash, silica fume, and slag at elevated temperatures, *Cement, Concrete, and Aggregates*, CCAGPD, Vol. 16, No.2, 93-99.

McAdams, W.H., 1954, *Heat Transmission*, McGraw Hill Series in Chemical Engineering, McGraw Book Company, New York.

McCullough, B.F., D. Zollinger, and T. Dossey, 1998, *Evaluation of the Performance of Texas pavements Made with Different Coarse Aggregates*, Research Report 3925-1F, Center for Transportation Research, The University of Texas at Austin.

McCullough, B.F., and R.O. Rasmussen, 1999, *Fast track paving: Concrete Temperature Control and Traffic Opening Criteria for Bonded Concrete Overlays*, Task G, Final Report, FHWA, U.S. Department of Transportation.

Mc Intosh J.D., 1956, Effect of low temperature curing on the compressive strength of concrete, *Proceedings of the RILEM Symposium on Winter Concreting*, Danish Institue for Building Research, Session B-II, Copenhagen, 3-17.

Mehta, P. K., and Paulo J. M. Monteiro, 1993, *Concrete-Structure, Properties, and Materials*, Prentice-Hall, Englewood Cliffs, N.J.

Mills, R.H., 1966, Factors influencing cessation of hydration in water-cured cement pastes, Special Report No. 90, *Proceedings of the Symposium on the Structure of Portland Cement Paste and Concrete,* Highway Research Board, Washington, D.C., 406-424

Mindess, S. and J.F. Young, 1981, *Concrete*, Englewood Cliffs, N. J.: Prentice-Hall, Inc

Morabito, P., 1998, Methods to determine the heat of hydration of concrete, *In: Prevention of the Thermal Cracking in Concrete at Early Ages*, edited by R. Springenschmid, E&FN Spon, 1-25

Nagashima, M., 1992, *Hydration, Setting and Hardening, Cement and Concrete*, N 544, 36-44

Nagataki, S., 1995, *Hardening Accelerators, Application of Admixtures in Concrete, State-of-the-art report*, RILEM TC 84-AAC.

Nakamura, H., S. Hamada, T. Tanimoto, and A. Miyamoto, 1999, Estimation of thermal cracking resistance for mass concrete structures with uncertain material properties, *ACI Structural Journal*, Vol. 96, No. 4, 509-518.

Neville, A.M., 1972, *Properties of Concrete*, Pitman Publishing.

Newkirk, T.F., 1952, The alkali phases in Portland cement clinker. *In: International Symposium on the Chemistry of Cement*, London, 151-171.

Nocuñ-Wczelik, W., 2001, Heat evolution in hydrated cementitious systems admixtured with fly ash, *Journal of Thermal Analysis and Calorimetry*, Vol. 65, 613-619.

Oh, B.H., and S.W. Cha, 2003, Nonlinear analysis of temperature and moisture distributions in early-age concrete structures based on degree of hydration, *ACI Materials Journal*, Vol. 100, No. 5, 361-370.

Pane, I., and W. Hansen, 2002, Concrete hydration and mechanical properties under nonisothermal conditions, *ACI Materials Journal*, Vol.99, No. 6, 534-542.

Parrot, L. J., and D. C. Killoh, 1984, Prediction of cement hydration, *British Ceramic Proceedings*, No. 35, 41-53.

Parrot, L.J., W.A. Gutteridge, and D. Killoh, 1990, Monitoring Portland cement hydration: comparison of methods, *Cement and Concrete Research*, Vol. 20, 919-926.

Plowman, J.M., Maturity and the strength of concrete, *Magazine of Concrete Research*, Vol.8, No. 22, 13-22.

Popovics, S., 1990, Analysis of the concrete strength versus water-cement ratio relationship, *ACI Materials Journal*, Vol 87, No. 5, 517-529.

Powers, T.C., 1947, A discussion of cement hydration in relation to the curing of concrete, *Proceedings of the Highway Research Board*, V. 27, 178-183.

Radjy, F.F., and D.W. Vunic, 1994, Heat signature testing of concrete, *Proceedings of Structural Materials Technology, an NDT Conference*, Atlantic City, 8-15.

Rastrup E., 1954, Heat of hydration in concrete, *Magazine of Concrete Research*, Vol. 6, No. 17, 79-92.

Regourd, M., 1980, Structure and behavior of slag Portland cement hydrates, *Proc. 7th Int. Congress on the Chemistry of Cement,* Paris, Vol. I, 2-10.

Regourd, M., B. Mortureux, E. Gauthier, H. Hornain, and J. Volant, 1980, Characterization and thermal activation of slag cements, *7th Int. Cong. On the Chemistry of Cement*, paris, Vol. III, 105-111.

Reinhardt, H. W., J. Blaauwendraad, J. Jongedijk, 1982, Temperature development in concrete structures taking account of state dependent properties, *Proceeding of RILEM International Conference on Concrete at Early Ages*, Paris, 211-218.

RILEM 42-CEA, 1981, Properties of set concrete at early ages: State of the art report, *Materials and Structures*, Vol.14, No. 84, 399-450.

RILEM Technical Committee 119-TCE, 1998, Adiabatic and semi-adiabatic calorimetry to determine the temperature increase in concrete due to hydration heat of cement, *RILEM Report 15, Prevention of Thermal Cracking in Concrete at Early Ages*, Edited by R. Springenschmid, E & FN Spon, London, 315-330.

Roy, D.M. and G. M. Idorn, 1982, Hydration, structure, and properties of blast furnace slag cements, *ACI Journal*, Vol. 79, No.6, 444-457.

Roy, D. M, K. Luke, and S. Diamond, 1985, Characterization of fly ash and its reactions in concrete, Materials *Research Society Symposia Proceedings*, Vol. 43, 3-20.

Ruiz, J. M., A. K. Schindler, R. O. Rasmussen, P. J. Kim, and G. K. Chang, 2001, Concrete temperature modeling and strength prediction using maturity concepts in the FHWA HIPERPAV software, *7th International Conference on Concrete Pavements*, Orlando, Florida.

Saul, A.G.A., 1951, Principles Underlying the steam curing of concrete at atmospheric pressure, *Magazine of Concrete Research*, Vol. 2, No. 6, 127-140.

Sadgrove B. M., 1970, The early development of strength in concrete, *CIRIA technical note* Vol.12, 43.

Schindler, A.K., 2002, *Concrete Hydration, Temperature Development, and Setting at Early-Ages*, PhD dissertation, The University of Texas at Austin.

Schindler, A.K., 2003, Influence of supplementary cementing materials on the heat o hydration of concrete, *Advance in Cement and Concrete*, 17-26.

Schindler A.K., and K.J. Folliard, 2003, Influence of supplementary cementing materials on the heat of hydration of concrete. *Proceedings of the Ninth conference on Advances in Cement and Concrete*, Colorado, 10-14.

Siegel R., and J.R. Howell, 2002, *Thermal Radiation Heat Transfer*, 4th Edition, Taylor & Francis.

Suzuki, Y., S. Harada, K. Maekawa, and Y. Tsuji, 1989, Evaluation of adiabatic temperature rise of concert measured with the new testing apparatus, *Concrete Library of JSCE*, No. 13, 71-83.

Tanaka, S., K. Inoue, Y. Shimoyama, and R. Tomita, 1995, Methods of estimating heat of hydration and temperature rise in blast furnace slag blended cement,*ACI Materials Journal*, Vol. 92, No. 4, 429-436.

Taylor, H.F.W., 1997, *Cement Chemistry*, Thomas Telford Publishing, London.

Thompson, M.R., B.J. Dempsey, H. Hill, and J. Vogel, 1998, Characterizing temperature effects for pavement analysis and design, *Transportation Research Record 1121*, 14- 22.

Thorvaldson, T., W.G. Brown, and C.R. Peaker, 1930, Studies on the Thermochemistry of the compounds occurring in the system $CaO.Al_2O_3.SiO_2$. III. The heat of hydration of calcium oxide, *Journal of the American Chemical Society*, Vol. 52, 910-915.

Tishi, T., and K. Maekawa, 1995, Thermal and mechanical modelling of young concrete based on hydration process of multi-component cement minerals, *Thermal Cracking in Concrete at Early Age*, RILEM.

Uchikawa, H. 1986, Effect of blending components on hydration and structure formation, 8th International Congress on the Chemistry of Cement, Rio De Janeiro, 249-280.

Verbeck, G.J., and C.W. Foster, 1950, Long-time study of cement performance in concrete: Chapter 6- The heats of hydration of the cements, *Proceedings- American Society for Testing and Materials*, Vol. 50, 1235-1262.

Verbeck, G.J., and R.A. Helmuth, 1968, Structures and Physical Properties of Cement Paste, Chemistry of Cement, *the Fifth International Symposium,* Tokyo, Part II, 1-32.

Wang, Ch., and W.h. dilger, 1994, Prediction of Temperature distribution In hardening concrete, thermal cracking in concrete at early age, *Proceedings of the International RILEM Symposium*, Edited by Springenschmid, R., E&FN SPON, 21-28.

Wang, K. and Z. Ge, 2003, *Evaluating Properties of Blended Cements for Concrete Pavements*, project report, The Center for Portland Cement Concrete Pavement and The Center for Transportation Research and Education.

Wang, P. Z. R. Trettin, V. Rudert, and T. Spaniol, 2004, Influence of Al_2O_3 content on hydraulic reactivity of granulated blast-furnace slag, and the interaction between Al_2O_3 and CaO, *Advances in Cement Research*, Vol. 16, No. 1, 1-7.

Wirquin E., M. Broda, and B. Duthoit, 2002, Determination of the apparent activation energy of one concrete by calorimetric and mechanical means influence of a superplasticizer, *Cement and Concrete Research*, Vol 32, No. 8, 1207-1213.

Wood, S. L., 1992, *Evaluation of the Long-Term Properties of Concrete*, Portland Cement Association.

Woods, H., 1932, Heat evolved by cement in relation to strength, *Engineering News Record*, 435-437.

www.webmet.com, 2005

Xiong, X., and K. van Breugel, 2001, Isothermal calorimetry study of blended cements and its application in numerical simulations, *HERON*, Vol. 46, No. 3, 151-159.

APPENDIX A. HEAT OF HYDRATION MODEL

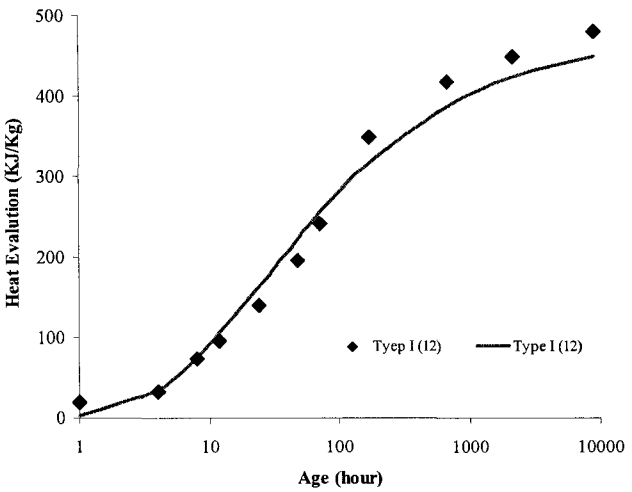

Figure A.1: Measured Vs Predicted Heat

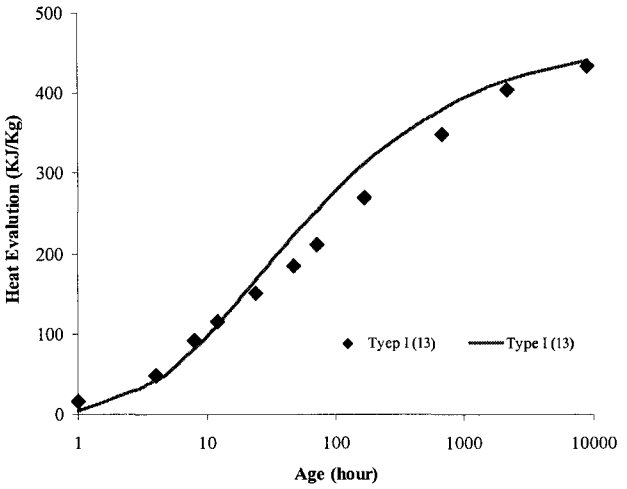

Figure A.2: Measured Vs Predicted Heat

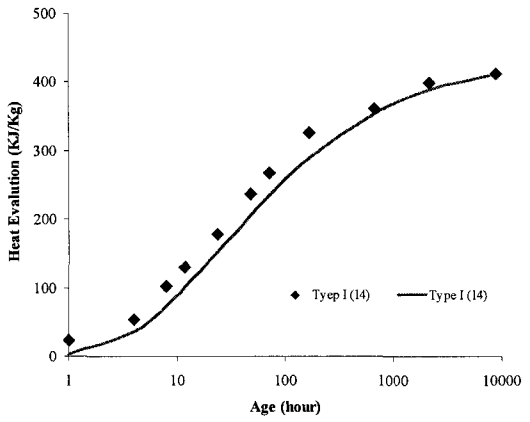

Figure A.3: Measured Vs Predicted Heat

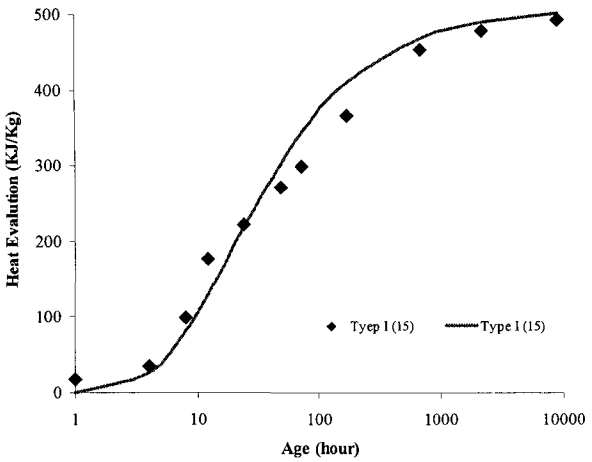

Figure A.4: Measured Vs Predicted Heat

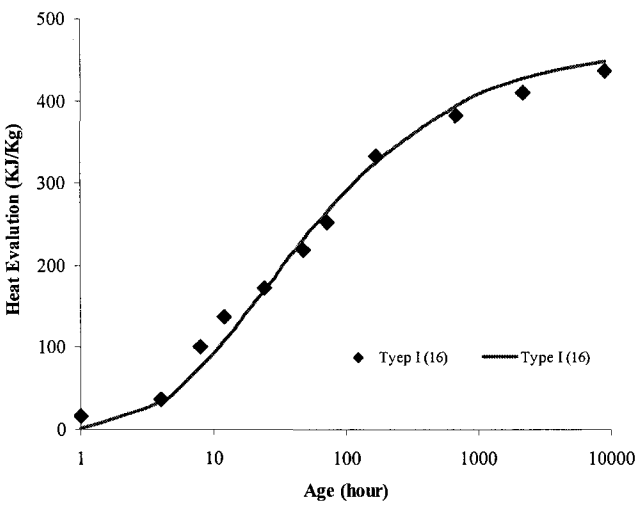

Figure A.5: Measured Vs Predicted Heat

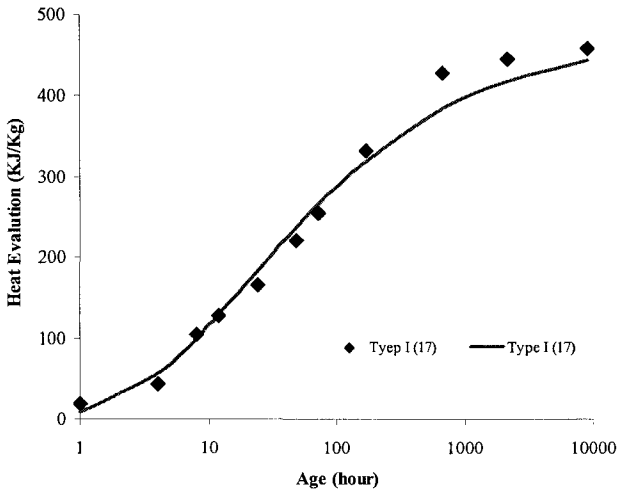

Figure A.6: Measured Vs Predicted Heat

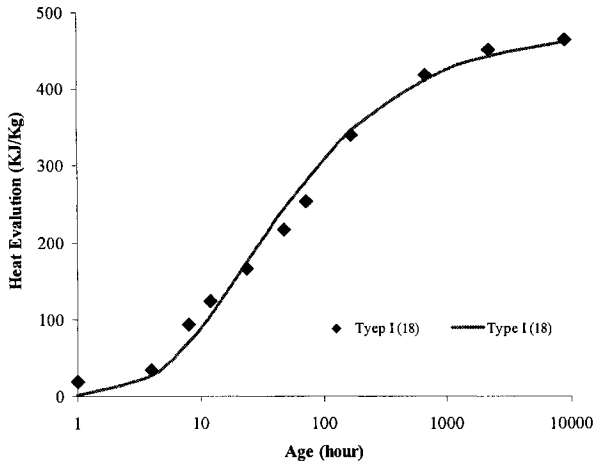

Figure A.7: Measured Vs Predicted Heat

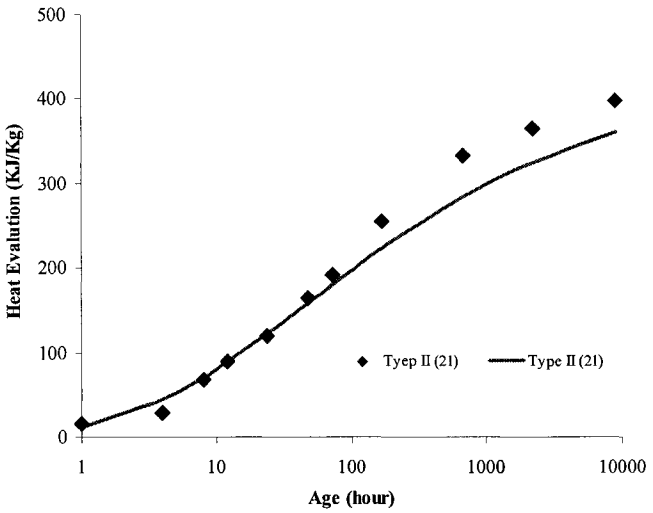

Figure A.8: Measured Vs Predicted Heat

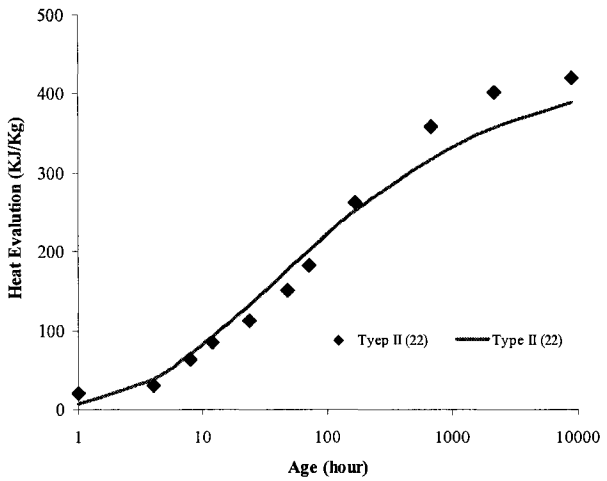

Figure A.9: Measured Vs Predicted Heat

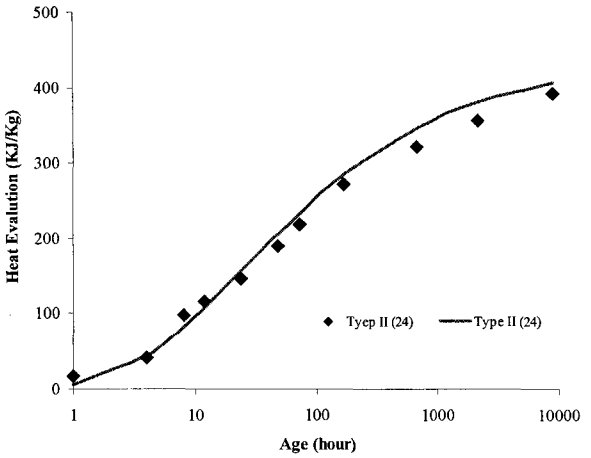

Figure A.10: Measured Vs Predicted Heat

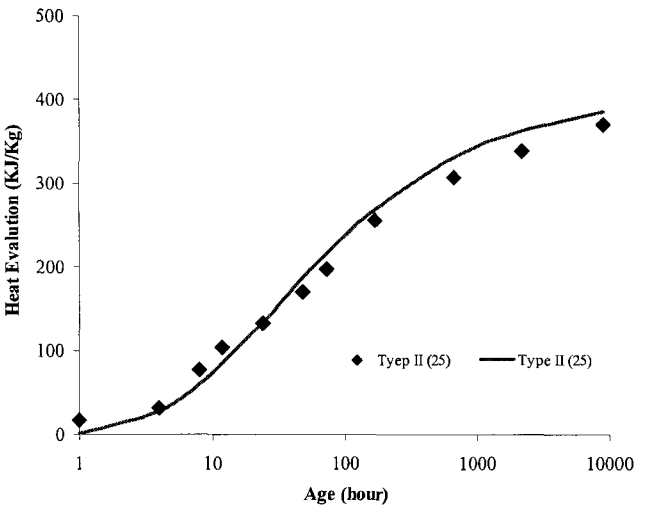

Figure A.11: Measured Vs Predicted Heat

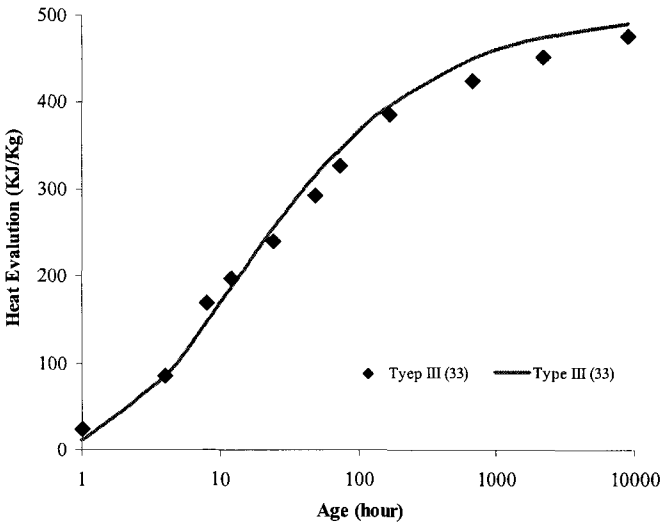

Figure A.12: Measured Vs Predicted Heat

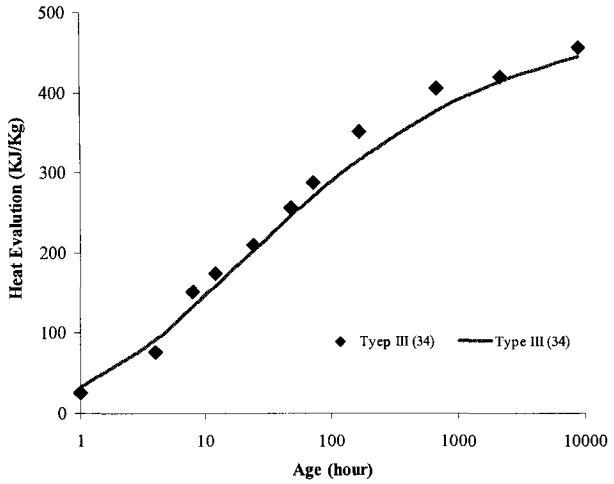

Figure A.13: Measured Vs Predicted Heat

Figure A.14: Measured Vs Predicted Heat

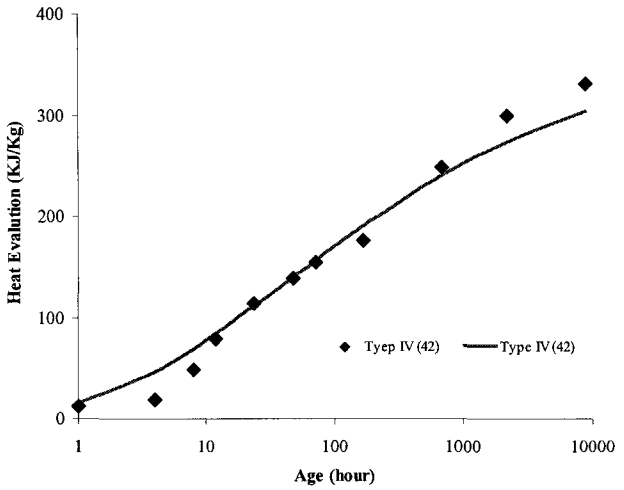

Figure A.15: Measured Vs Predicted Heat

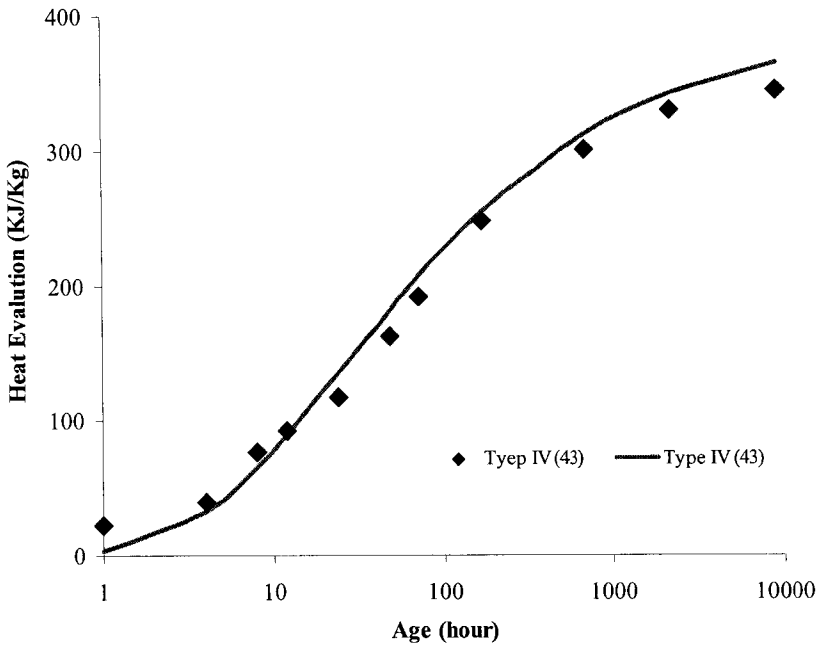

Figure A.16: Measured Vs Predicted Heat

APPENDIX B. MATURITY-STRENGTH MODEL

Table B.1: Mixing Proportion and Concrete Properties (Adopted from Wood, 1992)

Cement	W/C	Cement Content (lb/yd^3)	Fine Aggregate (lb/yd^3)	coarse Aggregate (lb/yd^3)	Slump inch	air content %
11	0.56	423	1368	2054	2.5	1.4
12	0.55	423	1368	2054	2.9	1.7
13	0.57	426	1362	2045	2.4	1.2
14	0.55	426	1364	2048	2.4	1.8
15	0.59	425	1354	2034	2.4	1.3
16	0.56	424	1366	2051	2.1	1.6
17	0.61	423	1348	2024	2.2	1.3
18	0.58	427	1358	2040	2.6	1.2
21	0.56	427	1368	2054	2.5	1.3
22	0.54	424	1371	2059	2.7	1.7
23	0.54	426	1372	2060	2.3	1.5
24	0.56	426	1358	2039	2.8	1.8
25	0.57	428	1359	2040	2.4	1.7
31	0.6	427	1349	2026	3	1.2
33	0.55	423	1365	2049	2	1.6
41	0.53	426	1368	2054	2.4	2
42	0.55	427	1371	2059	2.1	1.4
43	0.54	425	1356	2036	2.4	2.5
51	0.54	423	1377	2068	2.4	1.5
11	0.41	565	1226	2090	1.9	1.3
12	0.41	564	1226	2089	2.3	1.5
13	0.42	565	1219	2077	2.5	1.1
14	0.41	564	1223	2085	2.4	1.6
15	0.45	565	1204	2052	2.4	1.2
16	0.41	565	1226	2090	1.9	1.4
17	0.46	566	1198	2043	2.3	1.2
18	0.49	566	1210	2063	2.8	1.2
21	0.4	565	1219	2078	2.6	1.1
22	0.41	565	1231	2098	2.5	1.4
23	0.42	565	1224	2086	2.5	1.3
24	0.42	566	1217	2074	2.7	1.6
25	0.42	566	1220	2079	2.2	1.6
31	0.49	565	1185	2019	2.9	1.2
33	0.43	563	1210	2063	2.3	1.3
41	0.4	566	1225	2088	2.3	1.9
42	0.42	567	1222	2083	2.5	1.2
43	0.42	564	1214	2069	2.7	2.1
51	0.41	565	1232	2101	2.1	1.3

Selection of parameters

Response: LN(Su)

Model	Number	RSquare	RMSE
LNC2S ,LNFree Cao ,WC,LN(1-0.05air content)	4	0.9350	0.0719
LNC2S ,LNAlkaline ,WC,LN(1-0.05air content)	4	0.9327	0.0747
LNC2S ,LN SO3 ,WC,LN(1-0.05air content)	4	0.9321	0.0752
LNC2S ,LNC3A ,WC,LN(1-0.05air content)	4	0.9310	0.0753
LNC2S ,LN Blaine ,WC,LN(1-0.05air content)	4	0.9305	0.0764
LNC3A ,LNFree Cao ,WC,LN(1-0.05air content)	4	0.9007	0.0804
LNC3A ,LN Blaine ,WC,LN(1-0.05air content)	4	0.8624	0.0823
LNC3A ,LN SO3 ,WC,LN(1-0.05air content)	4	0.8592	0.1444
LNC3A ,LNAlkaline ,WC,LN(1-0.05air content)	4	0.8578	0.1445
LN SO3 ,LNFree Cao ,WC,LN(1-0.05air content)	4	0.8548	0.1445
LNAlkaline ,LNFree Cao ,WC,LN(1-0.05air content)	4	0.8510	0.1446
LN Blaine ,LNFree Cao ,WC,LN(1-0.05air content)	4	0.8509	0.1450
LNC2S ,LN SO3 ,LN Blaine ,WC	4	0.8461	0.1454
LNC2S ,LNAlkaline ,LN SO3 ,WC	4	0.8432	0.1458
LNC2S ,LNAlkaline ,LNFree Cao ,WC	4	0.8415	0.1458
LNC2S ,LN SO3 ,LNFree Cao ,WC	4	0.8394	0.1460
LNC2S ,LNC3A ,LN SO3 ,WC	4	0.8370	0.1462
LNC2S ,LNC3A ,LNAlkaline ,WC	4	0.8316	0.1489
LNC2S ,LNAlkaline ,LN Blaine ,WC	4	0.8311	0.1489
LNC2S ,LNC3A ,LNFree Cao ,WC	4	0.8182	0.1490
LNC2S ,LN Blaine ,LNFree Cao ,WC	4	0.8179	0.1499
LNAlkaline ,LN SO3 ,WC,LN(1-0.05air content)	4	0.8141	0.1502
LN SO3 ,LN Blaine ,LNFree Cao ,WC	4	0.8141	0.1506
LNC2S ,LNC3A ,LN Blaine ,WC	4	0.8140	0.1508
LNAlkaline ,LN Blaine ,WC,LN(1-0.05air content)	4	0.8119	0.1514
LN SO3 ,LN Blaine ,WC,LN(1-0.05air content)	4	0.8104	0.1521
LNC3A ,LN SO3 ,LNFree Cao ,WC	4	0.8028	0.1537
LNAlkaline ,LN SO3 ,LNFree Cao ,WC	4	0.7884	0.1583
LNC3A ,LNAlkaline ,LNFree Cao ,WC	4	0.7872	0.0440
LNC3A ,LN SO3 ,LN Blaine ,WC	4	0.7793	0.0448
LNC3A ,LNAlkaline ,LN SO3 ,WC	4	0.7734	0.0450
LNC3A ,LN Blaine ,LNFree Cao ,WC	4	0.7636	0.0453
LNAlkaline ,LN SO3 ,LN Blaine ,WC	4	0.7595	0.0455
LNAlkaline ,LN Blaine ,LNFree Cao ,WC	4	0.7455	0.0544
LNC3A ,LNAlkaline ,LN Blaine ,WC	4	0.7296	0.0641
LNC2S ,LNC3A ,LNFree Cao ,LN(1-0.05air content)	4	0.3198	0.0648
LNC2S ,LNC3A ,LN Blaine ,LN(1-0.05air content)	4	0.3150	0.0651
LNC2S ,LNC3A ,LNAlkaline ,LN(1-0.05air content)	4	0.3113	0.0658
LNC2S ,LNC3A ,LN SO3 ,LN(1-0.05air content)	4	0.3111	0.0666
LNC2S ,LN SO3 ,LN Blaine ,LN(1-0.05air content)	4	0.3076	0.0667
LNC2S ,LN Blaine ,LNFree Cao ,LN(1-0.05air content)	4	0.3056	0.0677
LNC2S ,LNAlkaline ,LN Blaine ,LN(1-0.05air content)	4	0.3053	0.0684
LNC2S ,LNAlkaline ,LNFree Cao ,LN(1-0.05air content)	4	0.3039	0.0688
LNC2S ,LN SO3 ,LNFree Cao ,LN(1-0.05air content)	4	0.3037	0.0692
LNC2S ,LNAlkaline ,LN SO3 ,LN(1-0.05air content)	4	0.3005	0.0697
LNC3A ,LN Blaine ,LNFree Cao ,LN(1-0.05air content)	4	0.2778	0.0709
LNC3A ,LN SO3 ,LNFree Cao ,LN(1-0.05air content)	4	0.2771	0.0710
LNC3A ,LNAlkaline ,LNFree Cao ,LN(1-0.05air content)	4	0.2767	0.0736
LNC2S ,LNC3A ,LN SO3 ,LNFree Cao	4	0.2655	0.0737
LNC2S ,LN SO3 ,LN Blaine ,LNFree Cao	4	0.2618	0.0745
LNC2S ,LNAlkaline ,LN SO3 ,LNFree Cao	4	0.2602	0.0745
LNC2S ,LNC3A ,LN SO3 ,LN Blaine	4	0.2600	0.0745
LNC2S ,LNC3A ,LNAlkaline ,LN SO3	4	0.2599	0.0749
LNC2S ,LNAlkaline ,LN SO3 ,LN Blaine	4	0.2570	0.0752
LNC2S ,LNC3A ,LNAlkaline ,LNFree Cao	4	0.2534	0.0767
LNC2S ,LNC3A ,LN Blaine ,LNFree Cao	4	0.2503	0.0794
LNC2S ,LNC3A ,LNAlkaline ,LN Blaine	4	0.2481	0.0797
LNC2S ,LNAlkaline ,LN Blaine ,LNFree Cao	4	0.2474	0.0811
LNC3A ,LNAlkaline ,LN Blaine ,LN(1-0.05air content)	4	0.2466	0.0822
LNC3A ,LN SO3 ,LN Blaine ,LN(1-0.05air content)	4	0.2407	0.0840
LNC3A ,LNAlkaline ,LN SO3 ,LN(1-0.05air content)	4	0.2337	0.0847
LNC3A ,LN SO3 ,LN Blaine ,LNFree Cao	4	0.2305	0.0871
LNC3A ,LNAlkaline ,LN SO3 ,LNFree Cao	4	0.2237	0.0898

LNC3A ,LNAlkaline ,LN Blaine ,LNFree Cao	4	0.1963	0.1424
LNC3A ,LNAlkaline ,LN SO3 ,LN Blaine	4	0.1878	0.1429
LNAlkaline ,LN SO3 ,LNFree Cao ,LN(1-0.05air content)	4	0.1842	0.1433
LNAlkaline ,LN Blaine ,LNFree Cao ,LN(1-0.05air content)	4	0.1727	0.1433
LN SO3 ,LN Blaine ,LNFree Cao ,LN(1-0.05air content)	4	0.1709	0.1437
LNAlkaline ,LN SO3 ,LN Blaine ,LNFree Cao	4	0.1657	0.1439
LNAlkaline ,LN SO3 ,LN Blaine ,LN(1-0.05air content)	4	0.1569	0.1439
LNC2S ,WC,LN(1-0.05air content)	**3**	**0.9304**	**0.1441**
LNC3A ,WC,LN(1-0.05air content)	3	0.8578	0.1441
LNFree Cao ,WC,LN(1-0.05air content)	3	0.8508	0.1444
LNC2S ,LN SO3 ,WC	3	0.8354	0.1467
LNC2S ,LNAlkaline ,WC	3	0.8310	0.1468
LNC2S ,LNFree Cao ,WC	3	0.8177	0.1469
LNC2S ,LNC3A ,WC	3	0.8137	0.1480
LNC2S ,LN Blaine ,WC	3	0.8123	0.1484
LN SO3 ,WC,LN(1-0.05air content)	3	0.8086	0.1485
LN Blaine ,WC,LN(1-0.05air content)	3	0.8076	0.1485
LNAlkaline ,WC,LN(1-0.05air content)	3	0.7954	0.1486
LN SO3 ,LNFree Cao ,WC	3	0.7871	0.1488
LNC3A ,LN SO3 ,WC	3	0.7731	0.1492
LNC3A ,LNFree Cao ,WC	3	0.7636	0.1495
LN SO3 ,LN Blaine ,WC	3	0.7578	0.1497
LNAlkaline ,LN SO3 ,WC	3	0.7544	0.1498
LNAlkaline ,LNFree Cao ,WC	3	0.7455	0.1499
LN Blaine ,LNFree Cao ,WC	3	0.7347	0.1505
LNC3A ,LN Blaine ,WC	3	0.7236	0.1512
LNC3A ,LNAlkaline ,WC	3	0.7211	0.1515
LNAlkaline ,LN Blaine ,WC	3	0.6923	0.1521
LNC2S ,LNC3A ,LN(1-0.05air content)	3	0.3110	0.1548
LNC2S ,LN Blaine ,LN(1-0.05air content)	3	0.3038	0.1556
LNC2S ,LNFree Cao ,LN(1-0.05air content)	3	0.3037	0.1560
LNC2S ,LNAlkaline ,LN(1-0.05air content)	3	0.3004	0.1571
LNC2S ,LN SO3 ,LN(1-0.05air content)	3	0.2996	0.1572
LNC3A ,LNFree Cao ,LN(1-0.05air content)	3	0.2767	0.1577
LNC2S ,LN SO3 ,LNFree Cao	3	0.2602	0.1585
LNC2S ,LNC3A ,LN SO3	3	0.2599	0.0449
LNC2S ,LN SO3 ,LN Blaine	3	0.2569	0.0642
LNC2S ,LNAlkaline ,LN SO3	3	0.2568	0.0657
LNC2S ,LNC3A ,LNFree Cao	3	0.2482	0.0690
LNC2S ,LNC3A ,LN Blaine	3	0.2466	0.0700
LNC2S ,LNAlkaline`,LNFree Cao	3	0.2457	0.0727
LNC2S ,LN Blaine ,LNFree Cao	3	0.2456	0.0735
LNC2S ,LNAlkaline ,LN Blaine	3	0.2446	0.0737
LNC2S ,LNC3A ,LNAlkaline	3	0.2433	0.0745
LNC3A ,LN Blaine ,LN(1-0.05air content)	3	0.2395	0.0747
LNC3A ,LN SO3 ,LN(1-0.05air content)	3	0.2257	0.0770
LNC3A ,LNAlkaline ,LN(1-0.05air content)	3	0.2240	0.0785
LNC3A ,LN SO3 ,LNFree Cao	3	0.2237	0.0811
LNC3A ,LNAlkaline ,LNFree Cao	3	0.1951	0.0827
LNC3A ,LN Blaine ,LNFree Cao	3	0.1927	0.0838
LNC3A ,LNAlkaline ,LN SO3	3	0.1877	0.0843
LNC3A ,LN SO3 ,LN Blaine	3	0.1828	0.0859
LN SO3 ,LNFree Cao ,LN(1-0.05air content)	3	0.1709	0.0877
LNAlkaline ,LN SO3 ,LNFree Cao	3	0.1619	0.0895
LN Blaine ,LNFree Cao ,LN(1-0.05air content)	3	0.1607	0.0899
LN SO3 ,LN Blaine ,LNFree Cao	3	0.1573	0.0944
LNAlkaline ,LNFree Cao ,LN(1-0.05air content)	3	0.1571	0.1413
LNC3A ,LNAlkaline ,LN Blaine	3	0.1542	0.1420
LNAlkaline ,LN Blaine ,LN(1-0.05air content)	3	0.1488	0.1420
LNAlkaline ,LN SO3 ,LN(1-0.05air content)	3	0.1487	0.1423
LNAlkaline ,LN SO3 ,LN Blaine	3	0.1304	0.1424
LN SO3 ,LN Blaine ,LN(1-0.05air content)	3	0.1216	0.1447
LNAlkaline ,LN Blaine ,LNFree Cao	3	0.1065	0.1464
LNC2S ,WC	2	0.8120	0.1464
WC,LN(1-0.05air content)	2	0.7917	0.1467
LN SO3 ,WC	2	0.7533	0.1467
LNFree Cao ,WC	2	0.7340	0.1476
LNC3A ,WC	2	0.7131	0.1477

LN Blaine ,WC	2	0.6918	0.1478
LNAlkaline ,WC	2	0.6715	0.1478
LNC2S ,LN(1-0.05air content)	2	0.2996	0.1479
LNC2S ,LN SO3	2	0.2567	0.1480
LNC2S ,LN Blaine	2	0.2437	0.1484
LNC2S ,LNFree Cao	2	0.2426	0.1498
LNC2S ,LNC3A	2	0.2408	0.1499
LNC2S ,LNAlkaline	2	0.2395	0.1499
LNC3A ,LN(1-0.05air content)	2	0.2191	0.1527
LNC3A ,LNFree Cao	2	0.1898	0.1529
LNC3A ,LN SO3	2	0.1826	0.1534
LNC3A ,LN Blaine	2	0.1540	0.1538
LN SO3 ,LNFree Cao	2	0.1533	0.1550
LNFree Cao ,LN(1-0.05air content)	2	0.1499	0.1558
LNAlkaline ,LN SO3	2	0.1300	0.1559
LNC3A ,LNAlkaline	2	0.1259	0.1562
LN Blaine ,LN(1-0.05air content)	2	0.1167	0.1563
LN SO3 ,LN(1-0.05air content)	2	0.1111	0.1565
LN Blaine ,LNFree Cao	2	0.1051	0.1570
LN SO3 ,LN Blaine	2	0.1029	0.1570
LNAlkaline ,LNFree Cao	2	0.0925	0.1587
LNAlkaline ,LN(1-0.05air content)	2	0.0902	0.1595
LNAlkaline ,LN Blaine	2	0.0734	0.1609
WC	1	0.6706	0.0728
LNC2S	1	0.2378	0.0766
LNC3A	1	0.1259	0.0833
LN SO3	1	0.1009	0.0865
LNFree Cao	1	0.0923	0.0899
LN Blaine	1	0.0613	0.0932
LN(1-0.05air content)	1	0.0602	0.0962
LNAlkaline	1	0.0102	0.1404

Response: LN(tau)

Model	Number	RSquare	RMSE
LNC3S ,LNC3A ,LNFree Cao ,LNAlkaline ,LN SO3 ,LN Blaine ,WC	7	0.9300	0.2266
LNC3S ,LNC3A ,LNAlkaline ,LN SO3 ,LN Blaine ,WC	6	0.9292	0.2244
LNC3S ,LNC3A ,LNFree Cao ,LNAlkaline ,LN SO3 ,WC	6	0.9273	0.2274
LNC3S ,LNC3A ,LNFree Cao ,LN SO3 ,LN Blaine ,WC	6	0.9266	0.2284
LNC3S ,LNFree Cao ,LNAlkaline ,LN SO3 ,LN Blaine ,WC	6	0.9005	0.2660
LNC3S ,LNC3A ,LNFree Cao ,LNAlkaline ,LN Blaine ,WC	6	0.8984	0.2688
LNC3S ,LNC3A ,LNFree Cao ,LNAlkaline ,LN SO3 ,LN Blaine	6	0.8673	0.3072
LNC3A ,LNFree Cao ,LNAlkaline ,LN SO3 ,LN Blaine ,WC	6	0.7086	0.4552
LNC3S ,LNC3A ,LN SO3 ,LN Blaine ,WC	5	0.9264	0.2253
LNC3S ,LNC3A ,LNAlkaline ,LN SO3 ,WC	5	0.9240	0.2289
LNC3S ,LNC3A ,LNFree Cao ,LN SO3 ,WC	5	0.9235	0.2296
LNC3S ,LNFree Cao ,LN SO3 ,LN Blaine ,WC	5	0.8999	0.2627
LNC3S ,LNAlkaline ,LN SO3 ,LN Blaine ,WC	5	0.8996	0.2631
LNC3S ,LNC3A ,LNAlkaline ,LN Blaine ,WC	5	0.8970	0.2665
LNC3S ,LNFree Cao ,LNAlkaline ,LN SO3 ,WC	5	0.8952	0.2688
LNC3S ,LNC3A ,LNFree Cao ,LN Blaine ,WC	5	0.8868	0.2793
LNC3S ,LNC3A ,LNFree Cao ,LNAlkaline ,LN SO3	5	0.8668	0.3031
LNC3S ,LNC3A ,LNAlkaline ,LN SO3 ,LN Blaine	5	0.8655	0.3045
LNC3S ,LNC3A ,LNFree Cao ,LNAlkaline ,WC	5	0.8618	0.3088
LNC3S ,LNC3A ,LNFree Cao ,LN SO3 ,LN Blaine	5	0.8597	0.3111
LNC3S ,LNFree Cao ,LNAlkaline ,LN Blaine ,WC	5	0.8500	0.3216
LNC3S ,LNFree Cao ,LNAlkaline ,LN SO3 ,LN Blaine	5	0.8451	0.3268
LNC3S ,LNC3A ,LNFree Cao ,LNAlkaline ,LN Blaine	5	0.8307	0.3416
LNC3A ,LNFree Cao ,LNAlkaline ,LN SO3 ,WC	5	0.7086	0.4483
LNC3A ,LNFree Cao ,LN SO3 ,LN Blaine ,WC	5	0.7086	0.4483
LNC3A ,LNFree Cao ,LNAlkaline ,LN Blaine ,WC	5	0.6925	0.4605
LNC3A ,LNFree Cao ,LNAlkaline ,LN SO3 ,LN Blaine	5	0.6472	0.4932
LNC3A ,LNAlkaline ,LN SO3 ,LN Blaine ,WC	5	0.6247	0.5087
LNFree Cao ,LNAlkaline ,LN SO3 ,LN Blaine ,WC	5	0.3935	0.6467
LNC3S ,LNC3A ,LN SO3 ,WC	**4**	**0.9217**	**0.2289**
LNC3S ,LN SO3 ,LN Blaine ,WC	4	0.8987	0.2604
LNC3S ,LNAlkaline ,LN SO3 ,WC	4	0.8952	0.2648
LNC3S ,LNFree Cao ,LN SO3 ,WC	4	0.8946	0.2657

Model	Number	RSquare	RMSE
LNC3S ,LNC3A ,LN Blaine ,WC	4	0.8867	0.2753
LNC3S ,LNC3A ,LNAlkaline ,LN SO3	4	0.8636	0.3022
LNC3S ,LNC3A ,LN SO3 ,LN Blaine	4	0.8593	0.3069
LNC3S ,LNC3A ,LNFree Cao ,LN SO3	4	0.8590	0.3072
LNC3S ,LNAlkaline ,LN Blaine ,WC	4	0.8485	0.3184
LNC3S ,LNAlkaline ,LN SO3 ,LN Blaine	4	0.8450	0.3221
LNC3S ,LNFree Cao ,LN Blaine ,WC	4	0.8445	0.3226
LNC3S ,LNFree Cao ,LNAlkaline ,LN SO3	4	0.8433	0.3238
LNC3S ,LNFree Cao ,LN SO3 ,LN Blaine	4	0.8420	0.3252
LNC3S ,LNC3A ,LNFree Cao ,WC	4	0.8356	0.3317
LNC3S ,LNC3A ,LNAlkaline ,WC	4	0.8326	0.3348
LNC3S ,LNC3A ,LNAlkaline ,LN Blaine	4	0.8282	0.3391
LNC3S ,LNC3A ,LNFree Cao ,LN Blaine	4	0.8104	0.3562
LNC3S ,LNC3A ,LNFree Cao ,LNAlkaline	4	0.8041	0.3621
LNC3S ,LNFree Cao ,LNAlkaline ,LN Blaine	4	0.7913	0.3738
LNC3S ,LNFree Cao ,LNAlkaline ,WC	4	0.7742	0.3887
LNC3A ,LNFree Cao ,LN SO3 ,WC	4	0.7085	0.4417
LNC3A ,LNFree Cao ,LN Blaine ,WC	4	0.6906	0.4550
LNC3A ,LNFree Cao ,LNAlkaline ,WC	4	0.6823	0.4611
LNC3A ,LNFree Cao ,LNAlkaline ,LN SO3	4	0.6466	0.4863
LNC3A ,LNFree Cao ,LN SO3 ,LN Blaine	4	0.6460	0.4868
LNC3A ,LNFree Cao ,LNAlkaline ,LN Blaine	4	0.6276	0.4993
LNC3A ,LN SO3 ,LN Blaine ,WC	4	0.6146	0.5079
LNC3A ,LNAlkaline ,LN Blaine ,WC	4	0.6094	0.5113
LNC3A ,LNAlkaline ,LN SO3 ,WC	4	0.6042	0.5147
LNC3A ,LNAlkaline ,LN SO3 ,LN Blaine	4	0.5553	0.5456
LNFree Cao ,LNAlkaline ,LN SO3 ,WC	4	0.3917	0.6381
LNFree Cao ,LNAlkaline ,LN SO3 ,LN Blaine	4	0.3609	0.6541
LNFree Cao ,LN SO3 ,LN Blaine ,WC	4	0.3556	0.6567
LNAlkaline ,LN SO3 ,LN Blaine ,WC	4	0.3304	0.6695
LNFree Cao ,LNAlkaline ,LN Blaine ,WC	4	0.3299	0.6697
LNC3S ,LN SO3 ,WC	3	0.8945	0.2619
LNC3S ,LNC3A ,LN SO3	3	0.8578	0.3041
LNC3S ,LNAlkaline ,LN SO3	3	0.8433	0.3192
LNC3S ,LN SO3 ,LN Blaine	3	0.8416	0.3210
LNC3S ,LN Blaine ,WC	3	0.8414	0.3211
LNC3S ,LNFree Cao ,LN SO3	3	0.8402	0.3224
LNC3S ,LNC3A ,WC	3	0.8131	0.3486
LNC3S ,LNC3A ,LN Blaine	3	0.8102	0.3513
LNC3S ,LNAlkaline ,LN Blaine	3	0.7909	0.3687
LNC3S ,LNFree Cao ,LN Blaine	3	0.7790	0.3791
LNC3S ,LNC3A ,LNAlkaline	3	0.7758	0.3818
LNC3S ,LNC3A ,LNFree Cao	3	0.7687	0.3878
LNC3S ,LNAlkaline ,WC	3	0.7612	0.3940
LNC3S ,LNFree Cao ,WC	3	0.7552	0.3990
LNC3S ,LNFree Cao ,LNAlkaline	3	0.7326	0.4170
LNC3A ,LNFree Cao ,WC	3	0.6765	0.4586
LNC3A ,LNFree Cao ,LN SO3	3	0.6454	0.4801
LNC3A ,LNFree Cao ,LNAlkaline	3	0.6223	0.4956
LNC3A ,LNFree Cao ,LN Blaine	3	0.6215	0.4961
LNC3A ,LN Blaine ,WC	3	0.6049	0.5069
LNC3A ,LN SO3 ,WC	3	0.5907	0.5159
LNC3A ,LN SO3 ,LN Blaine	3	0.5498	0.5411
LNC3A ,LNAlkaline ,LN SO3	3	0.5420	0.5457
LNC3A ,LNAlkaline ,LN Blaine	3	0.5363	0.5491
LNC3A ,LNAlkaline ,WC	3	0.5205	0.5584
LNFree Cao ,LNAlkaline ,LN SO3	3	0.3605	0.6448
LNFree Cao ,LN SO3 ,WC	3	0.3545	0.6479
LNFree Cao ,LN SO3 ,LN Blaine	3	0.3330	0.6586
LNFree Cao ,LN Blaine ,WC	3	0.3093	0.6701
LNAlkaline ,LN SO3 ,WC	3	0.3029	0.6733
LNFree Cao ,LNAlkaline ,LN Blaine	3	0.2946	0.6772
LNAlkaline ,LN SO3 ,LN Blaine	3	0.2917	0.6787
LNAlkaline ,LN Blaine ,WC	3	0.2700	0.6890
LNFree Cao ,LNAlkaline ,WC	3	0.2631	0.6922
LN SO3 ,LN Blaine ,WC	3	0.2398	0.7031
LNC3S ,LN SO3	2	0.8402	0.3179

Model	Number	RSquare	RMSE
LNC3S ,LN Blaine	2	0.7773	0.3752
LNC3S ,LNC3A	2	0.7481	0.3990
LNC3S ,WC	2	0.7456	0.4010
LNC3S ,LNAlkaline	2	0.7189	0.4215
LNC3S ,LNFree Cao	2	0.7059	0.4312
LNC3A ,LNFree Cao	2	0.6117	0.4954
LNC3A ,LN Blaine	2	0.5351	0.5421
LNC3A ,LN SO3	2	0.5342	0.5426
LNC3A ,WC	2	0.5196	0.5511
LNC3A ,LNAlkaline	2	0.4620	0.5832
LNFree Cao ,LN SO3	2	0.3327	0.6495
LNFree Cao ,LN Blaine	2	0.2821	0.6737
LNAlkaline ,LN SO3	2	0.2709	0.6789
LNFree Cao ,WC	2	0.2559	0.6858
LNFree Cao ,LNAlkaline	2	0.2400	0.6931
LNAlkaline ,LN Blaine	2	0.2287	0.6983
LN SO3 ,LN Blaine	2	0.2166	0.7037
LN Blaine ,WC	2	0.2080	0.7076
LN SO3 ,WC	2	0.1979	0.7121
LNAlkaline ,WC	2	0.0617	0.7701
LNC3S	1	0.6964	0.4321
LNC3A	1	0.4620	0.5752
LNFree Cao	1	0.2361	0.6855
LN SO3	1	0.1822	0.7092
LN Blaine	1	0.1810	0.7098
LNAlkaline	1	0.0411	0.7680
WC	1	0.0120	0.7795

Response: LN(beta)

Model	Number	RSquare	RMSE
LN(C2S+C3S),LNC3A ,LN Blaine ,LN SO3 ,LNAlkaline	5	0.8285	0.0683
LN(C2S+C3S),LNC3A ,LN Blaine ,LN SO3	4	0.8275	0.0675
LN(C2S+C3S),LNC3A ,LN Blaine ,LNAlkaline	4	0.8272	0.0675
LNC3A ,LN Blaine ,LN SO3 ,LNAlkaline	4	0.8198	0.0689
LN(C2S+C3S),LNC3A ,LN SO3 ,LNAlkaline	4	0.6664	0.0938
LN(C2S+C3S),LN Blaine ,LN SO3 ,LNAlkaline	4	0.4651	0.1188
LN(C2S+C3S),LNC3A ,LN Blaine	**3**	**0.8257**	**0.0668**
LNC3A ,LN Blaine ,LN SO3	3	0.8191	0.0681
LNC3A ,LN Blaine ,LNAlkaline	3	0.8055	0.0706
LN(C2S+C3S),LNC3A ,LN SO3	3	0.6621	0.0930
LNC3A ,LN SO3 ,LNAlkaline	3	0.6168	0.0991
LN(C2S+C3S),LNC3A ,LNAlkaline	3	0.5639	0.1057
LN(C2S+C3S),LN Blaine ,LNAlkaline	3	0.4579	0.1178
LN(C2S+C3S),LN SO3 ,LNAlkaline	3	0.3841	0.1256
LN(C2S+C3S),LN Blaine ,LN SO3	3	0.2682	0.1369
LN Blaine ,LN SO3 ,LNAlkaline	3	0.2115	0.1421
LNC3A ,LN Blaine	2	0.8012	0.0704
LNC3A ,LN SO3	2	0.6106	0.0985
LN(C2S+C3S),LNC3A	2	0.5636	0.1043
LNC3A ,LNAlkaline	2	0.5622	0.1044
LN(C2S+C3S),LN Blaine	2	0.2650	0.1353
LN(C2S+C3S),LNAlkaline	2	0.2512	0.1366
LN(C2S+C3S),LN SO3	2	0.1971	0.1414
LN Blaine ,LN SO3	2	0.1401	0.1463
LN Blaine ,LNAlkaline	2	0.1278	0.1474
LN SO3 ,LNAlkaline	2	0.0453	0.1542
LNC3A	1	0.5622	0.1030
LN(C2S+C3S)	1	0.0985	0.1478
LN Blaine	1	0.0871	0.1487
LNAlkaline	1	0.0451	0.1521
LN SO3	1	0.0009	0.1556

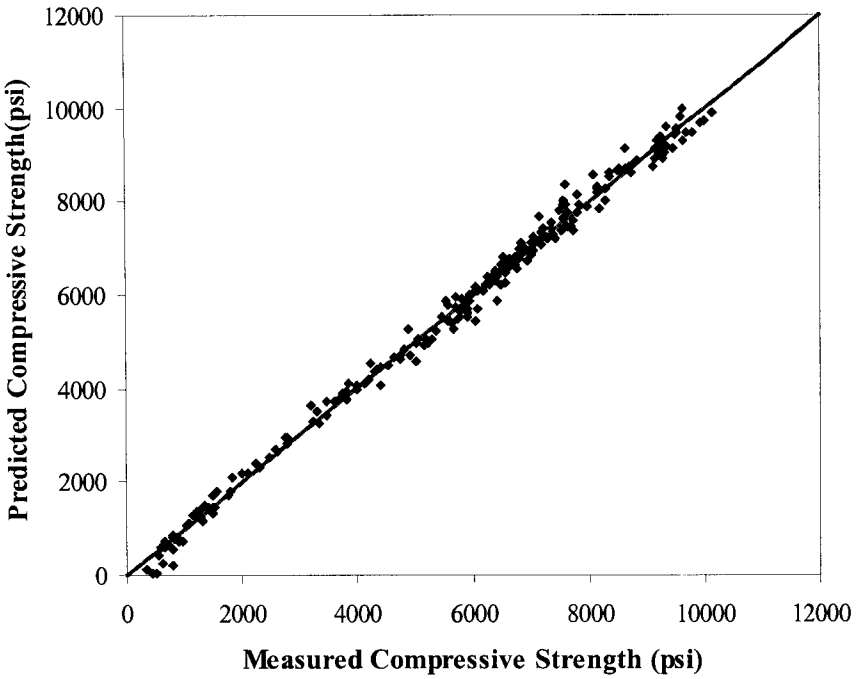

(a)

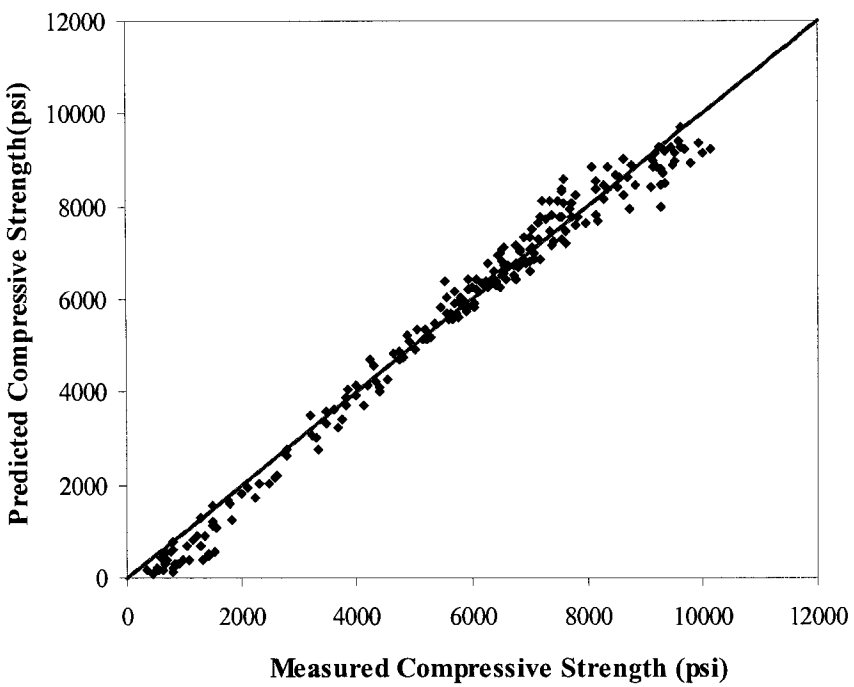

(b)

Figure B.1: Measured Vs Predicted Strength
(a): Equation 5.4; (b) Equation 5.3

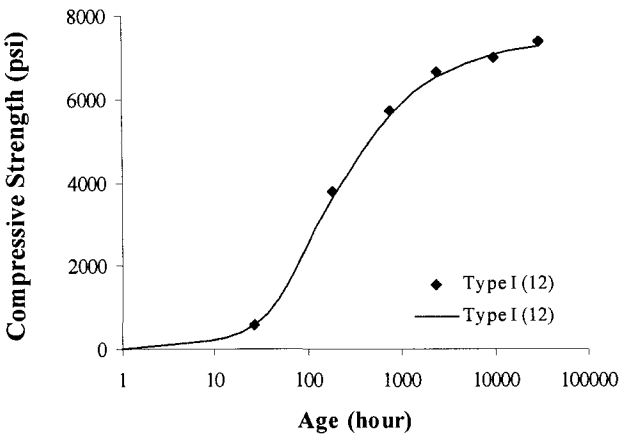

Figure B.2: Measured Vs Predicted Strength

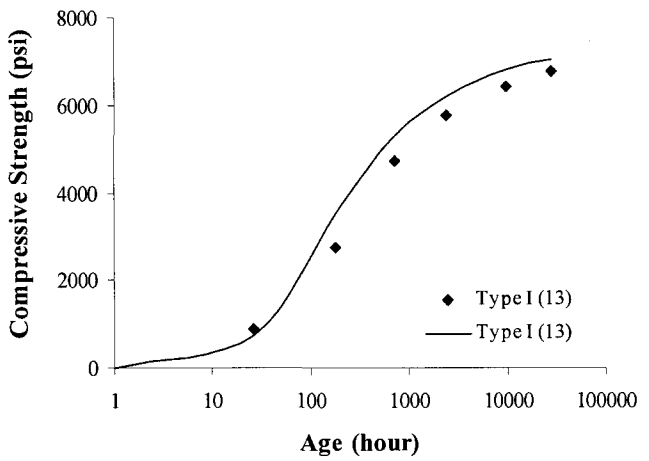

Figure B.3: Measured Vs Predicted Strength

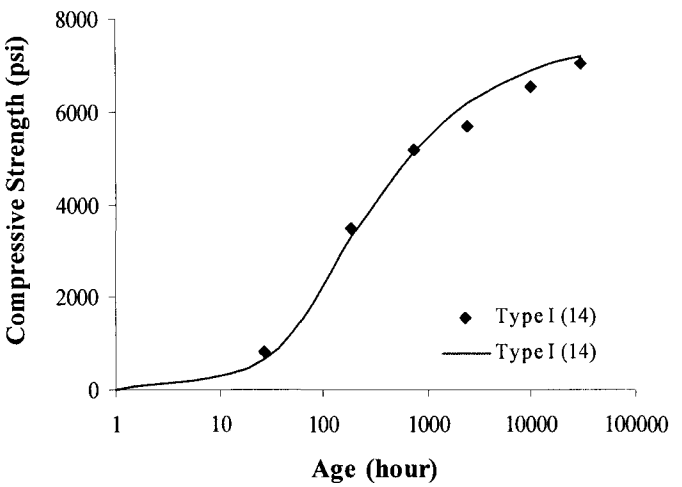

Figure B.4: Measured Vs Predicted Strength

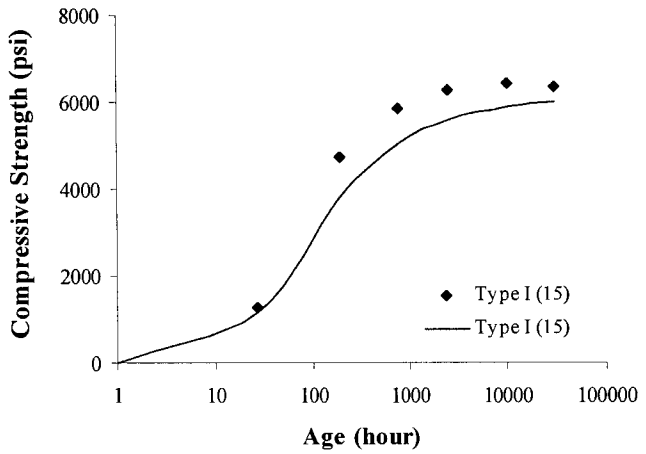

Figure B.5: Measured Vs Predicted Strength

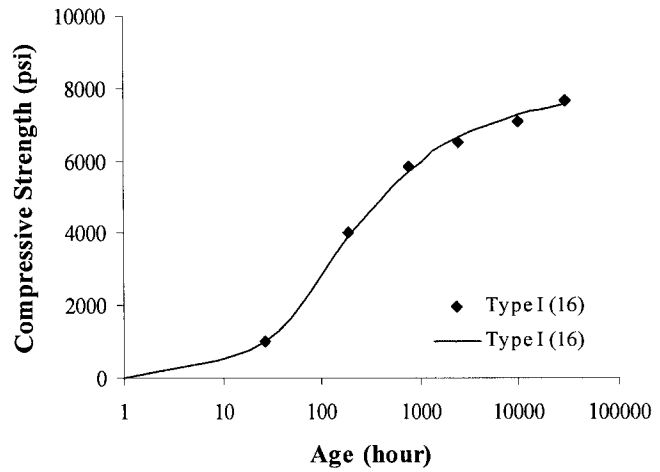

Figure B.6: Measured Vs Predicted Strength

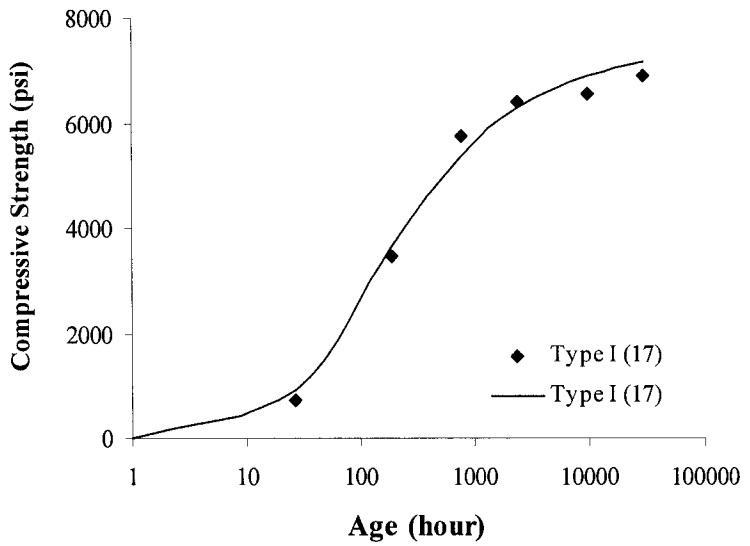

Figure B.7: Measured Vs Predicted Strength

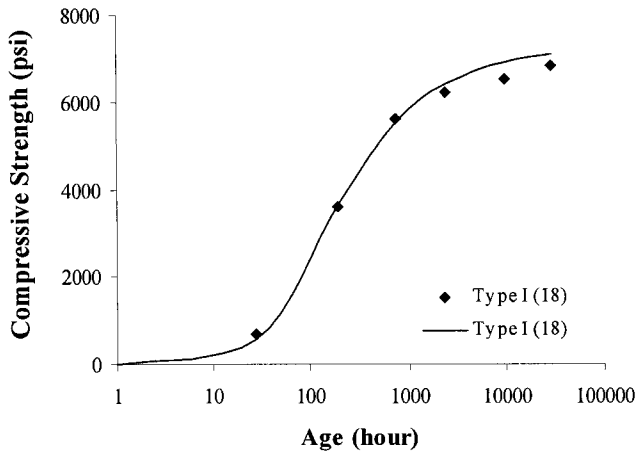

Figure B.8: Measured Vs Predicted Strength

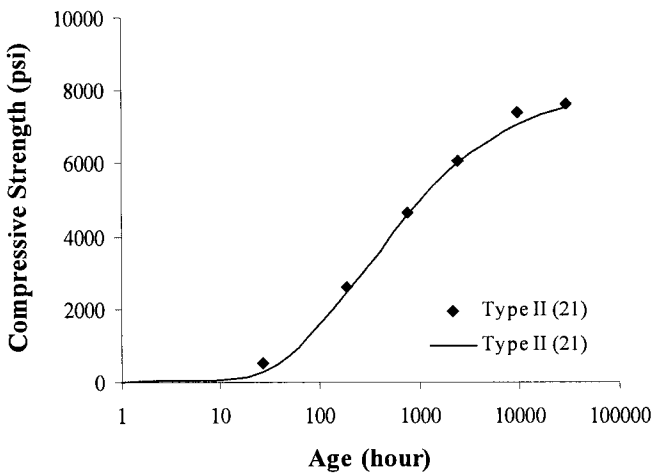

Figure B.9: Measured Vs Predicted Strength

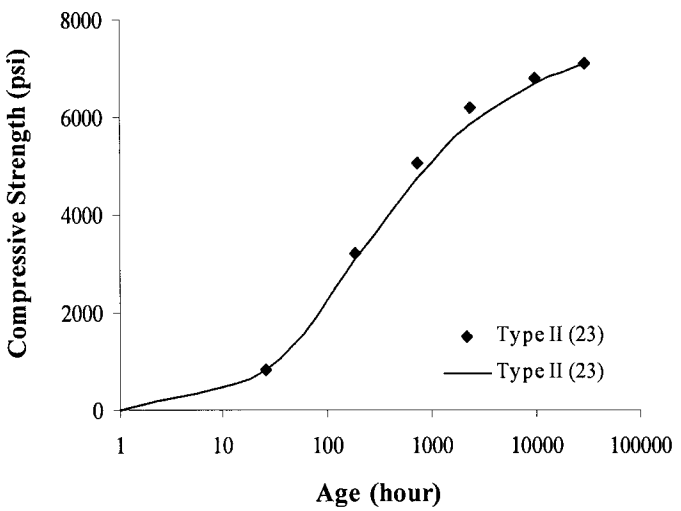

Figure B.10: Measured Vs Predicted Strength

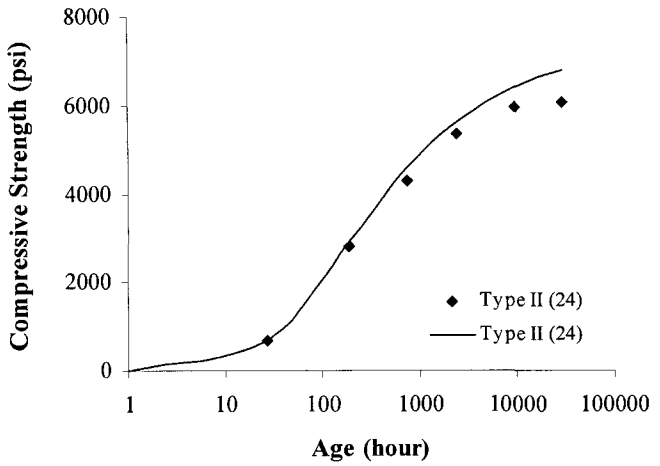

Figure B.11: Measured Vs Predicted Strength

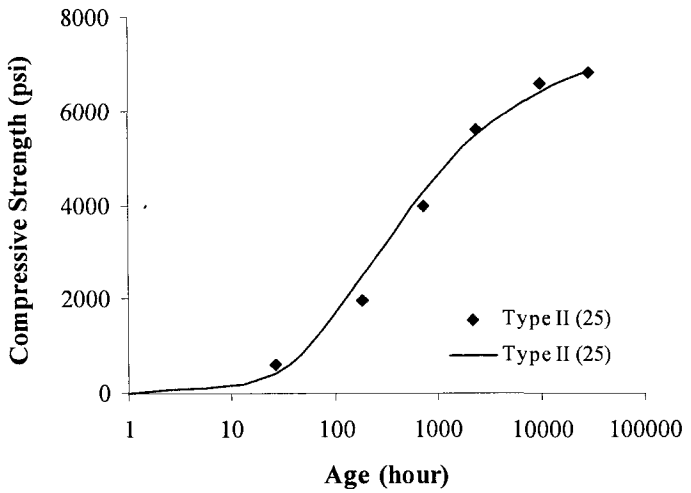

Figure B.12: Measured Vs Predicted Strength

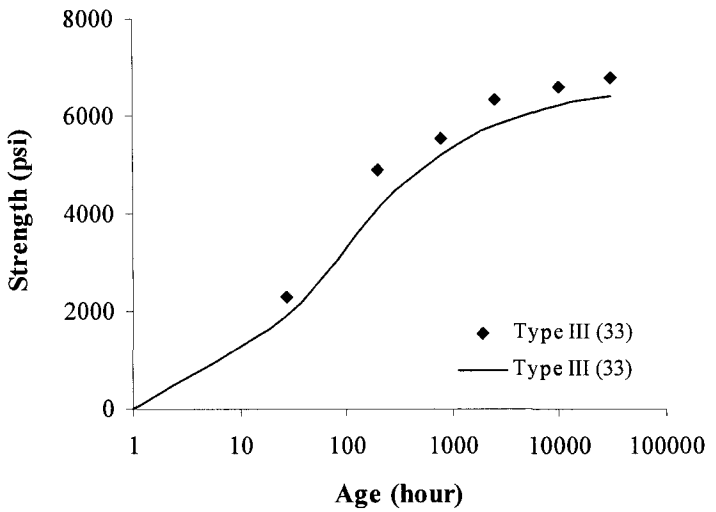

Figure B.13: Measured Vs Predicted Strength

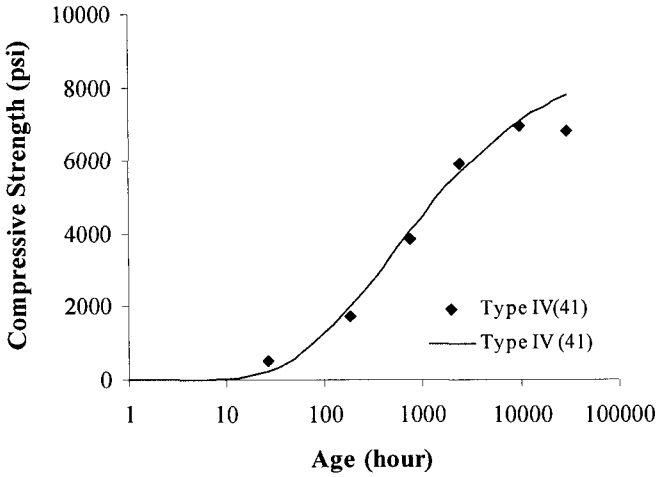

Figure B.14: Measured Vs Predicted Strength

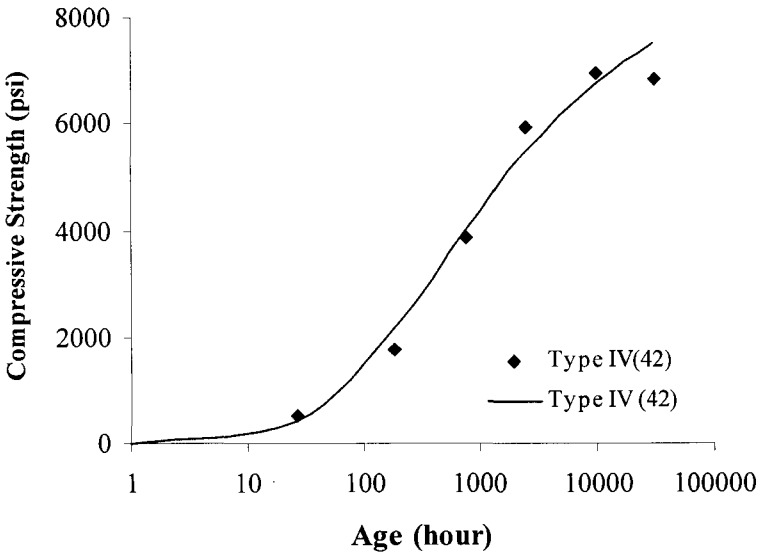

Figure B.15: Measured Vs Predicted Strength

APPENDIX C. TEMPERATURE PREDICTION

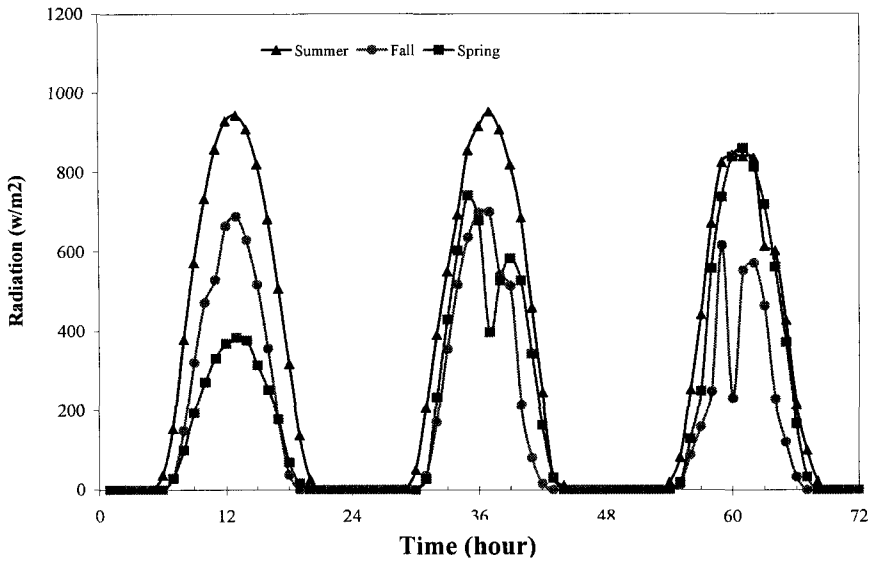

Figure C.1: Solar Radiation Input for FEMLAB

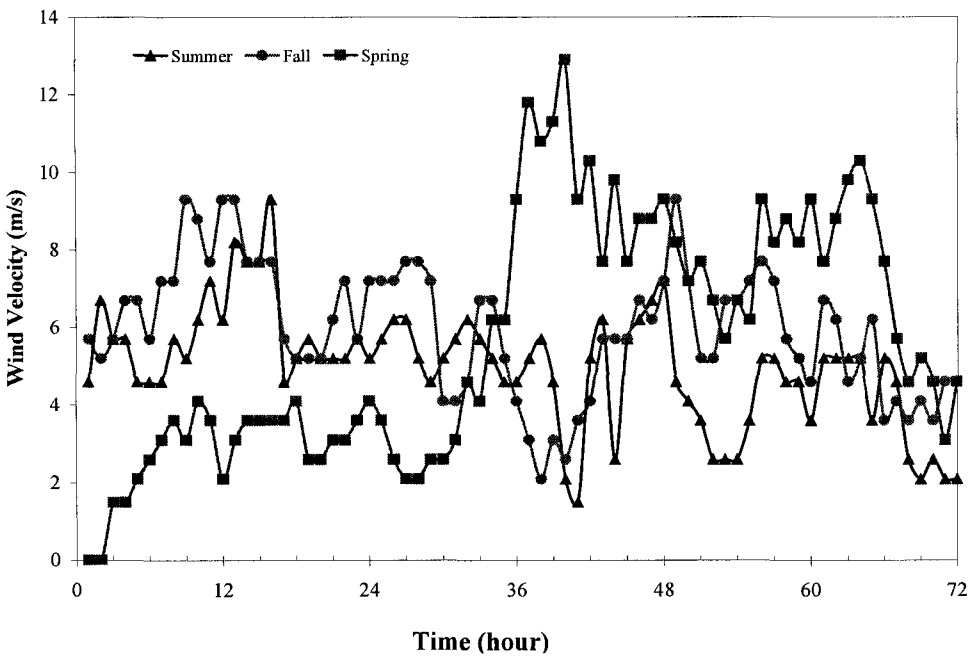

Figure C.2: Wind Speed Input for FEMLAB

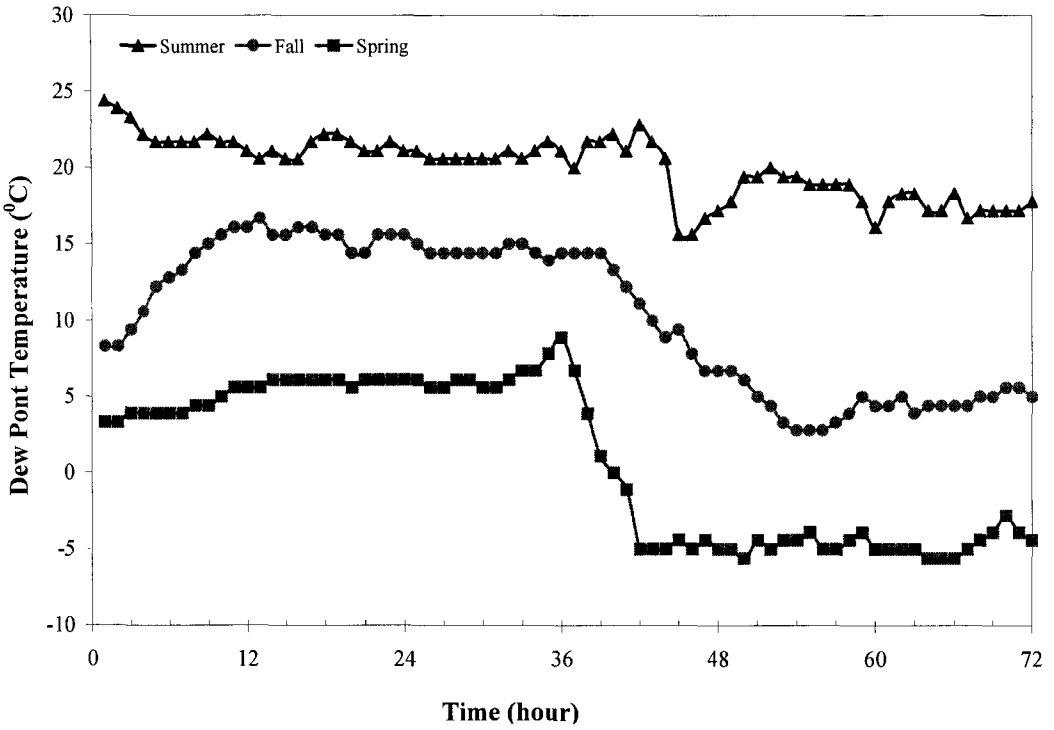

Figure C.3: Dew Point Temperature Input for FEMLAB

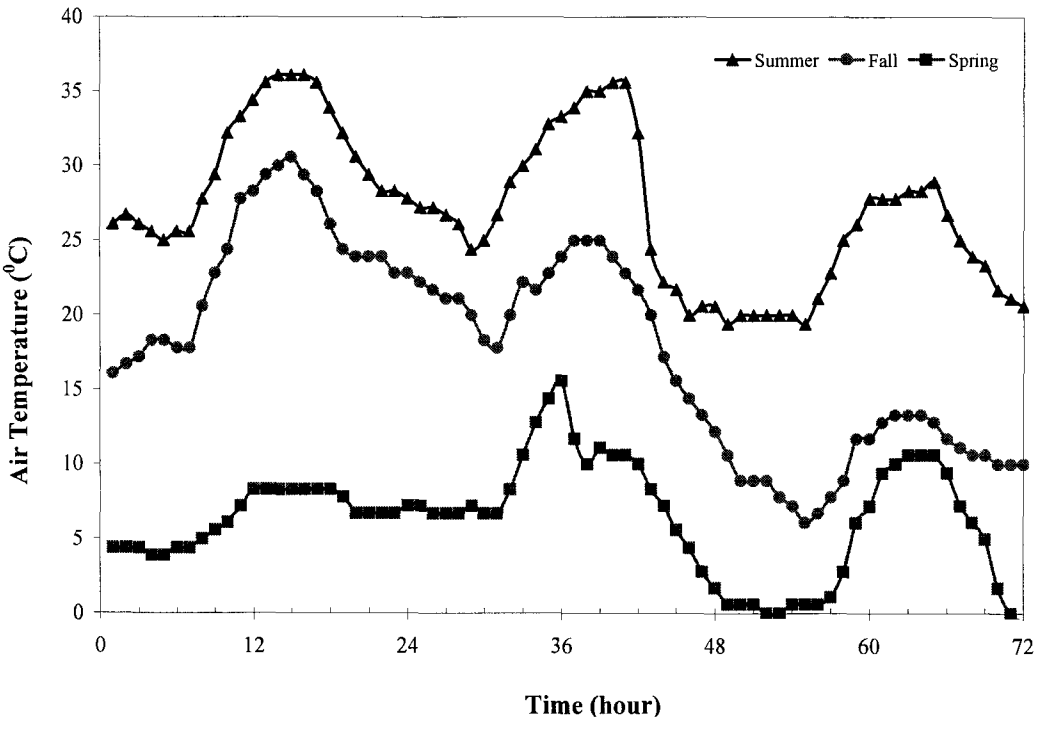

Figure C.4: Air Temperature Input for FEMLAB

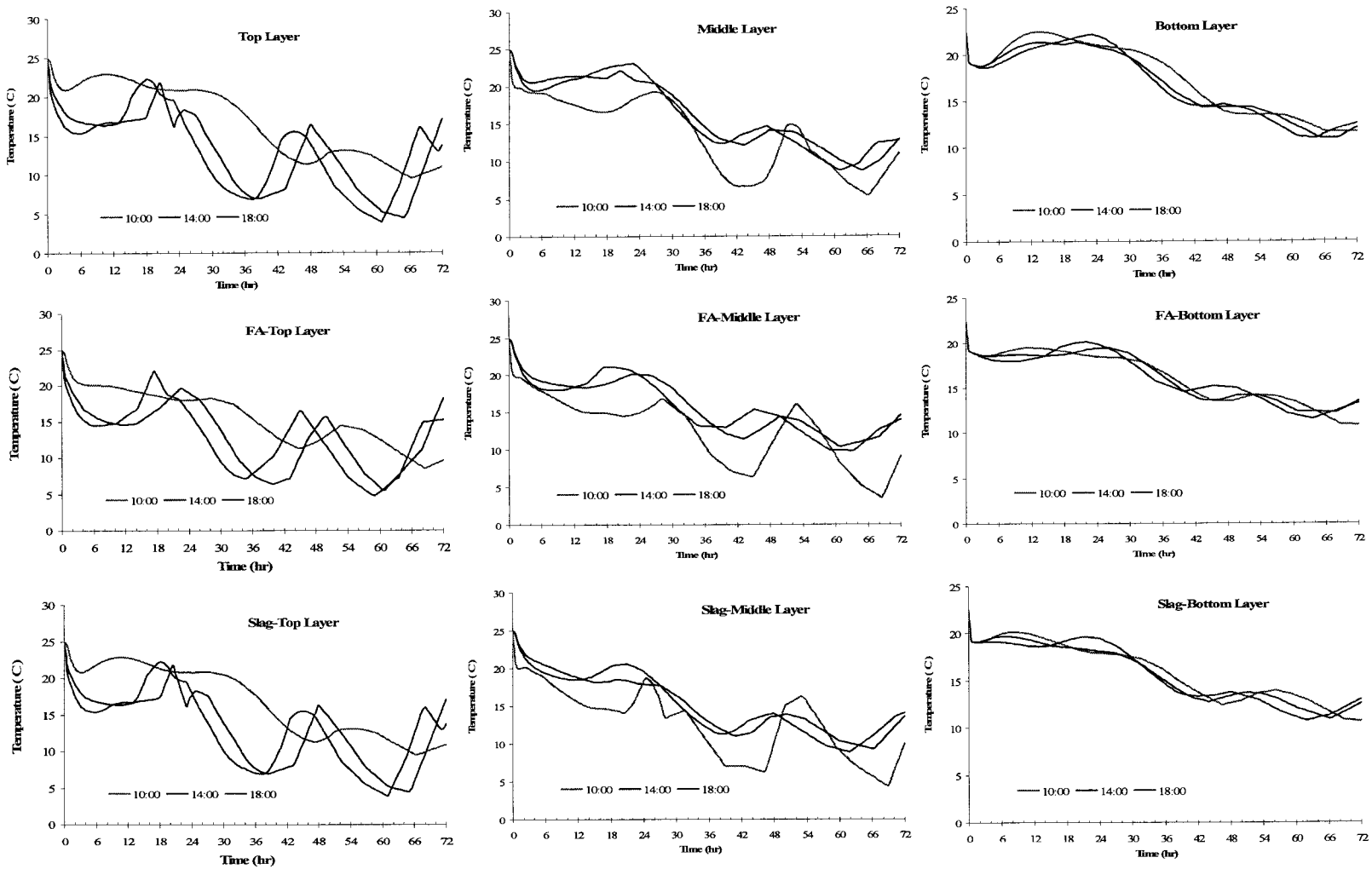

Figure C.5: Effect of SCM and Construction Time on Concrete Temperature (Spring Condition)

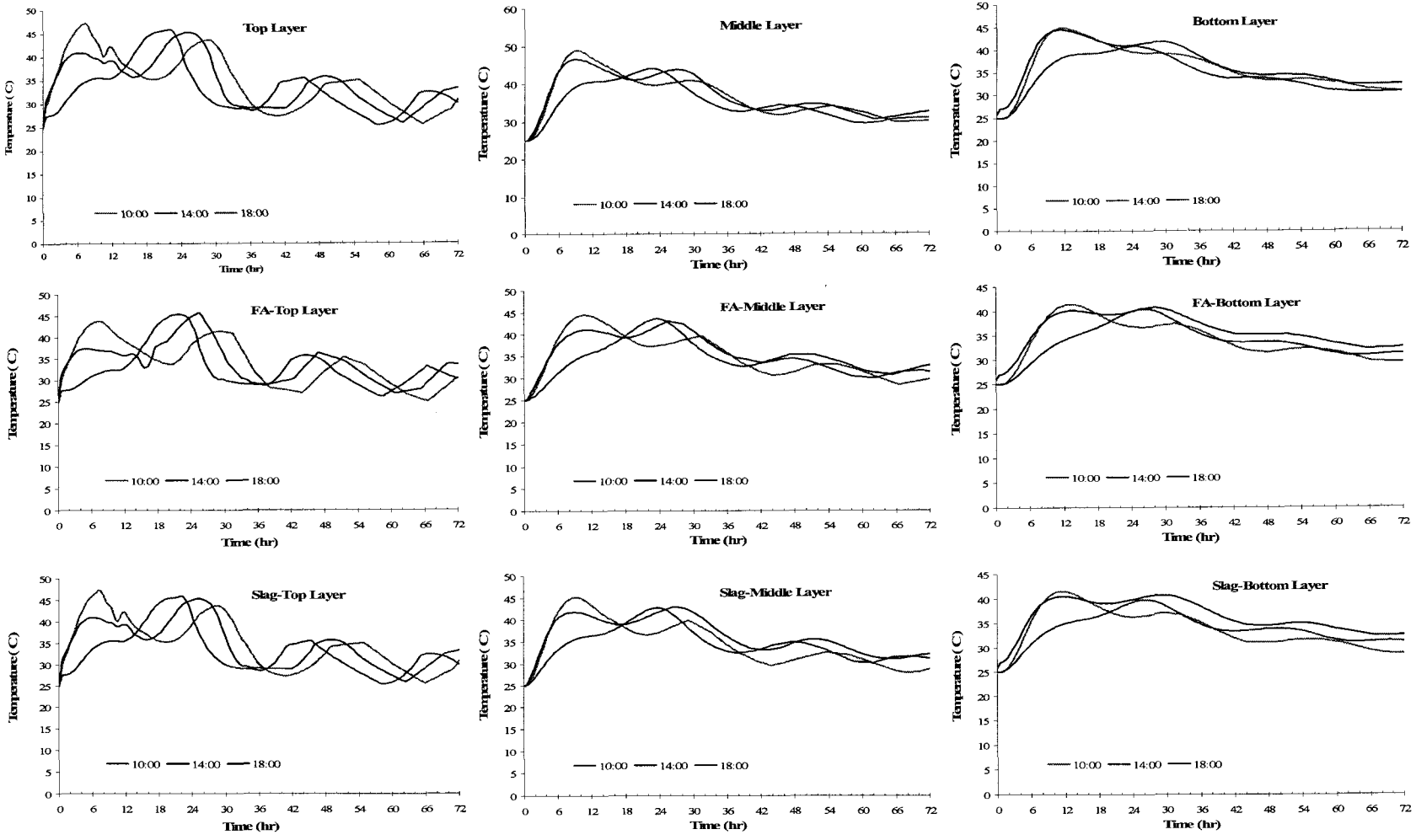

Figure C.6: Effect of SCM and Construction Time on Concrete Temperature (Summer Condition)

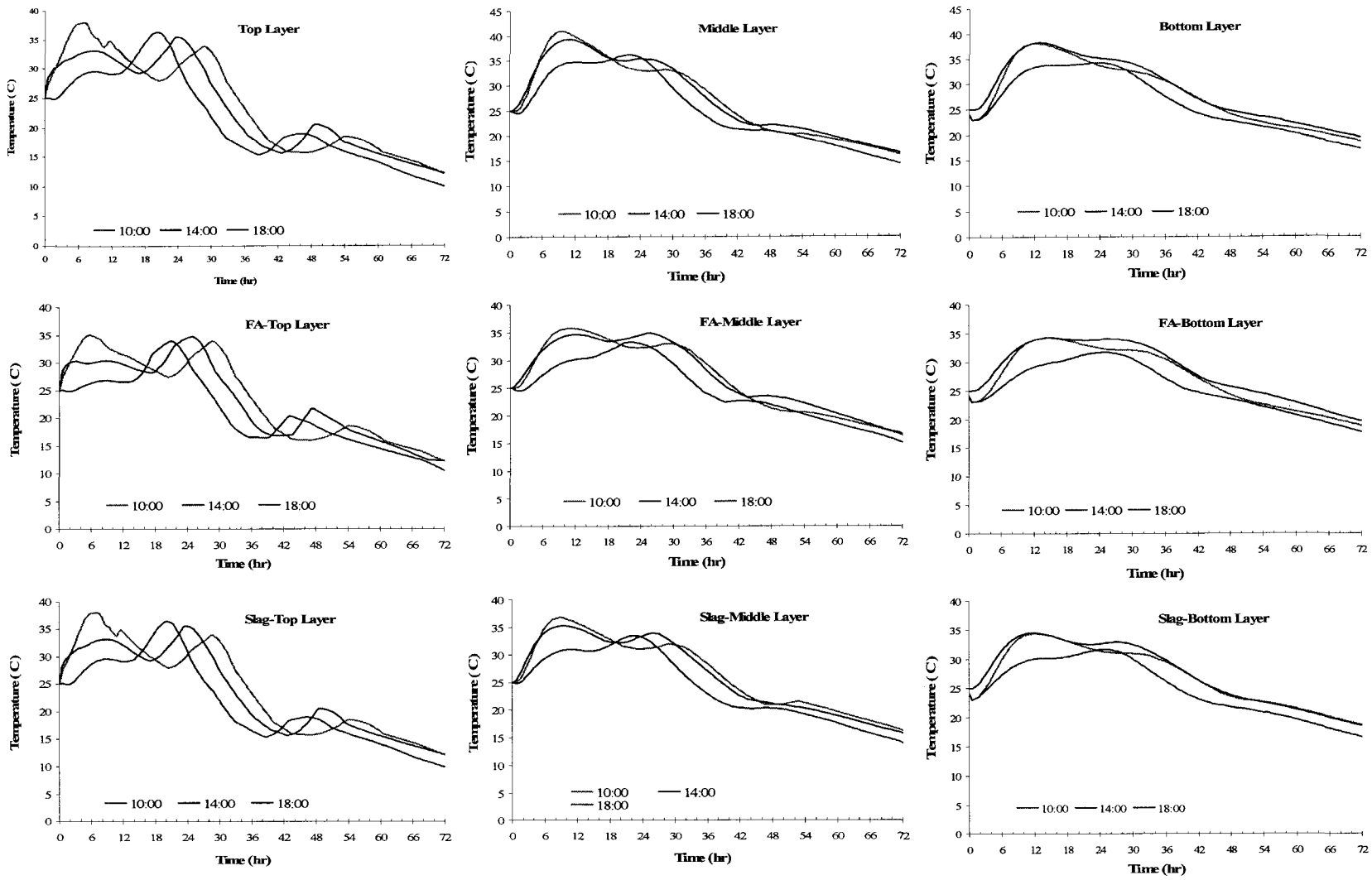

Figure C.7: Effect of SCM and Construction Time on Concrete Temperature (Fall Condition)

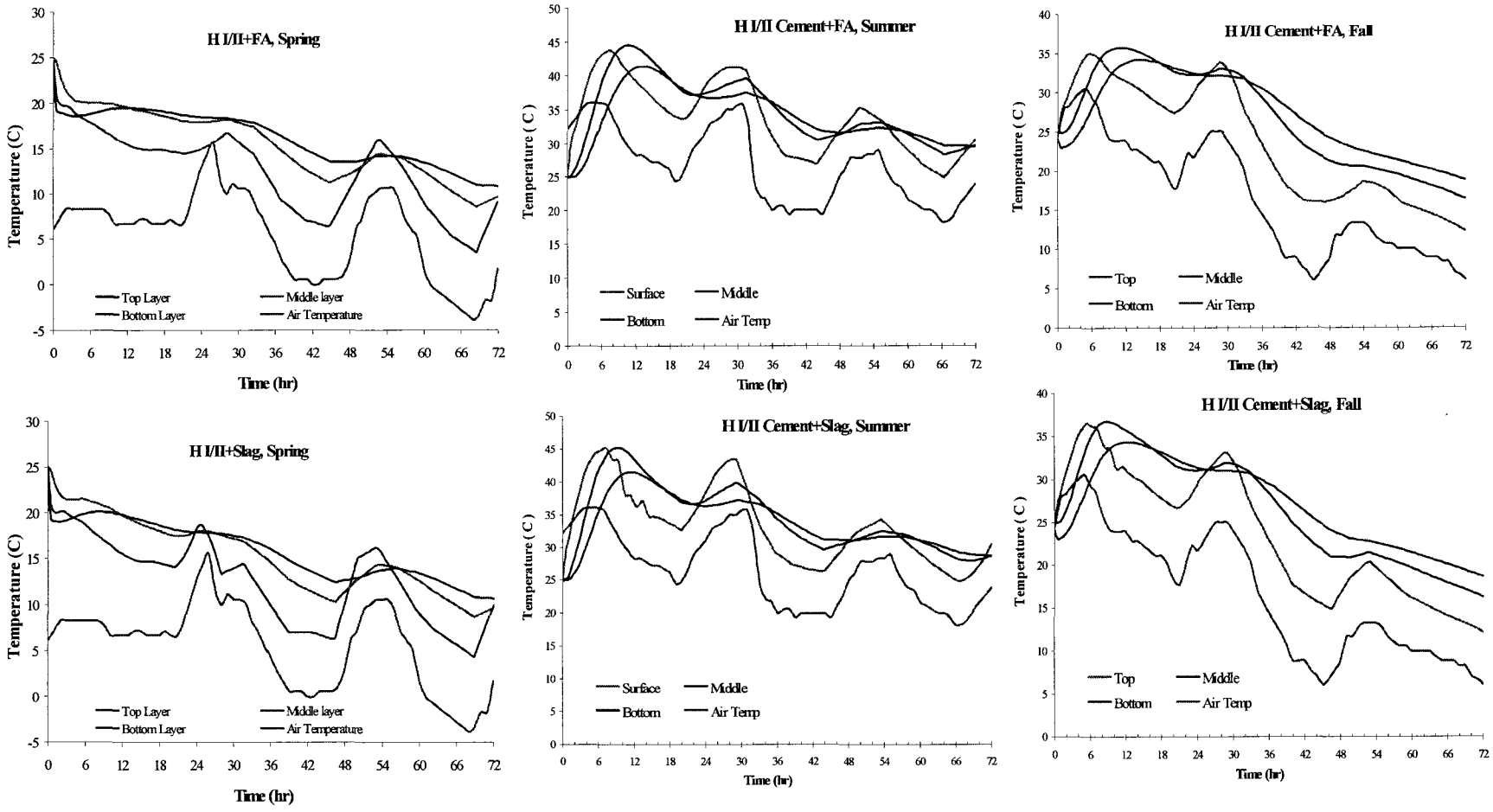

Figure C.8: Effect of SCM and Environment on Concrete Temperature (Constructed at 10 AM)

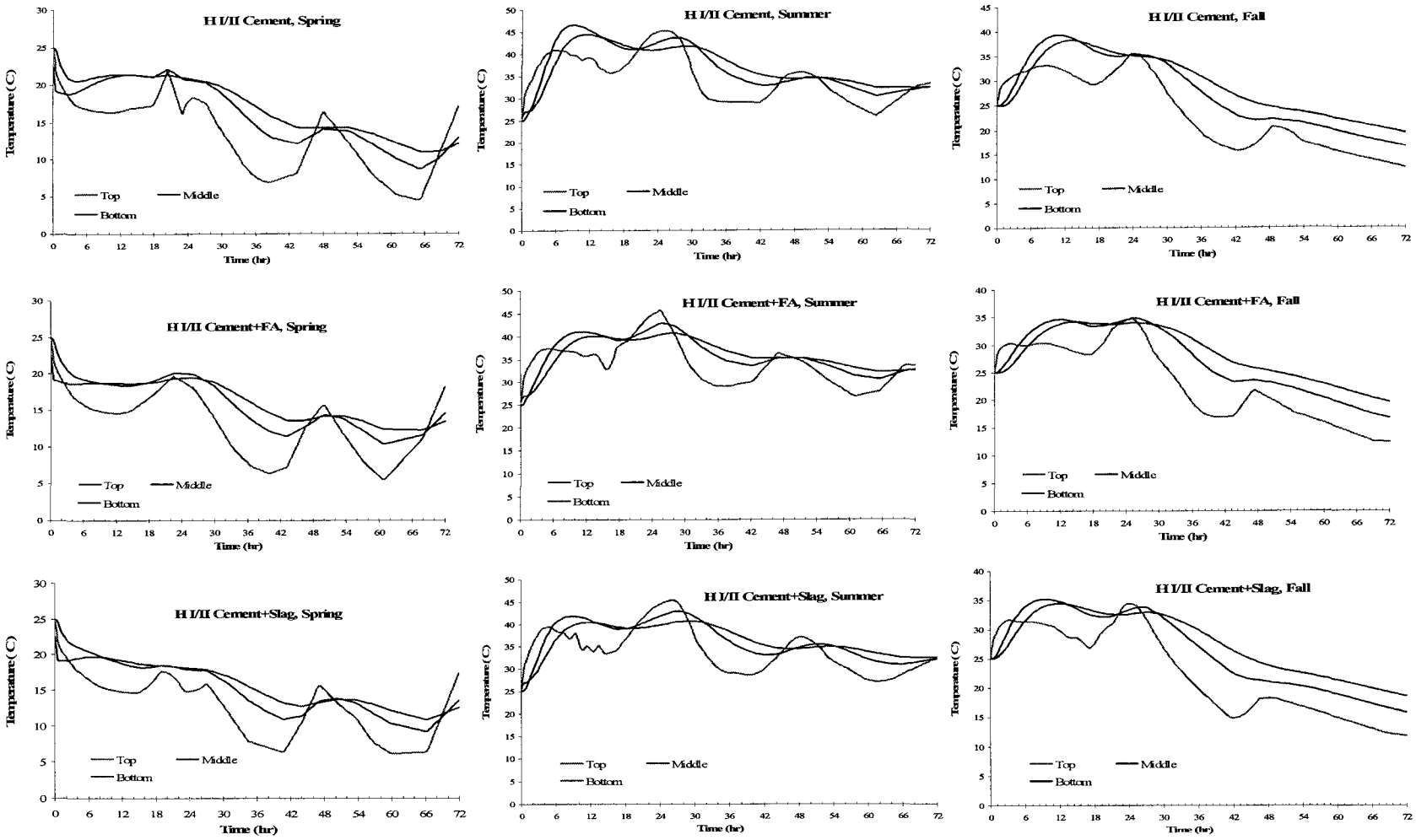

Figure C.9: Effect of SCM and Environment on Concrete Temperature (Constructed at 2 PM)

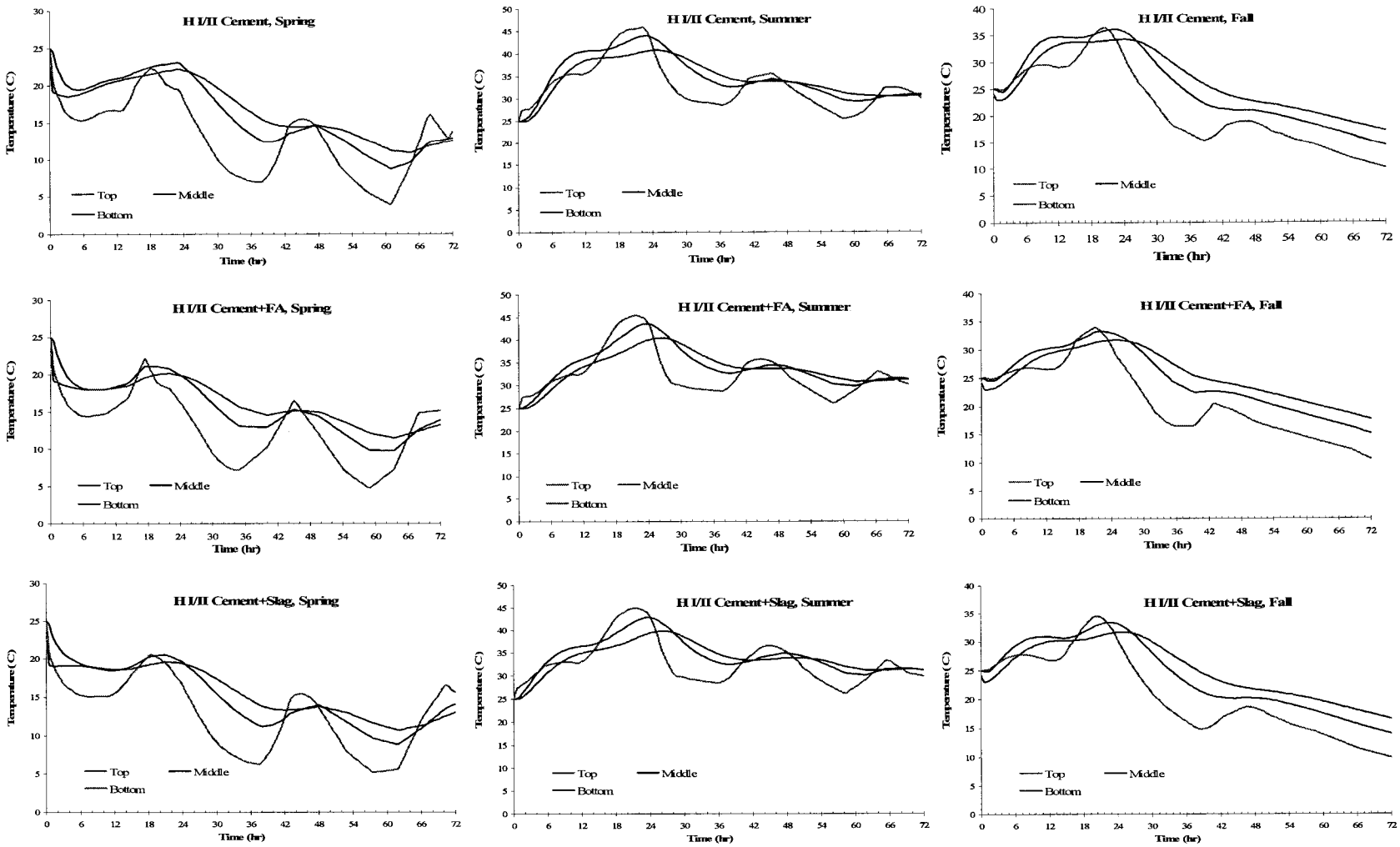

Figure C.10: Effect of SCM and Environment on Concrete Temperature (Constructed at 6 PM)

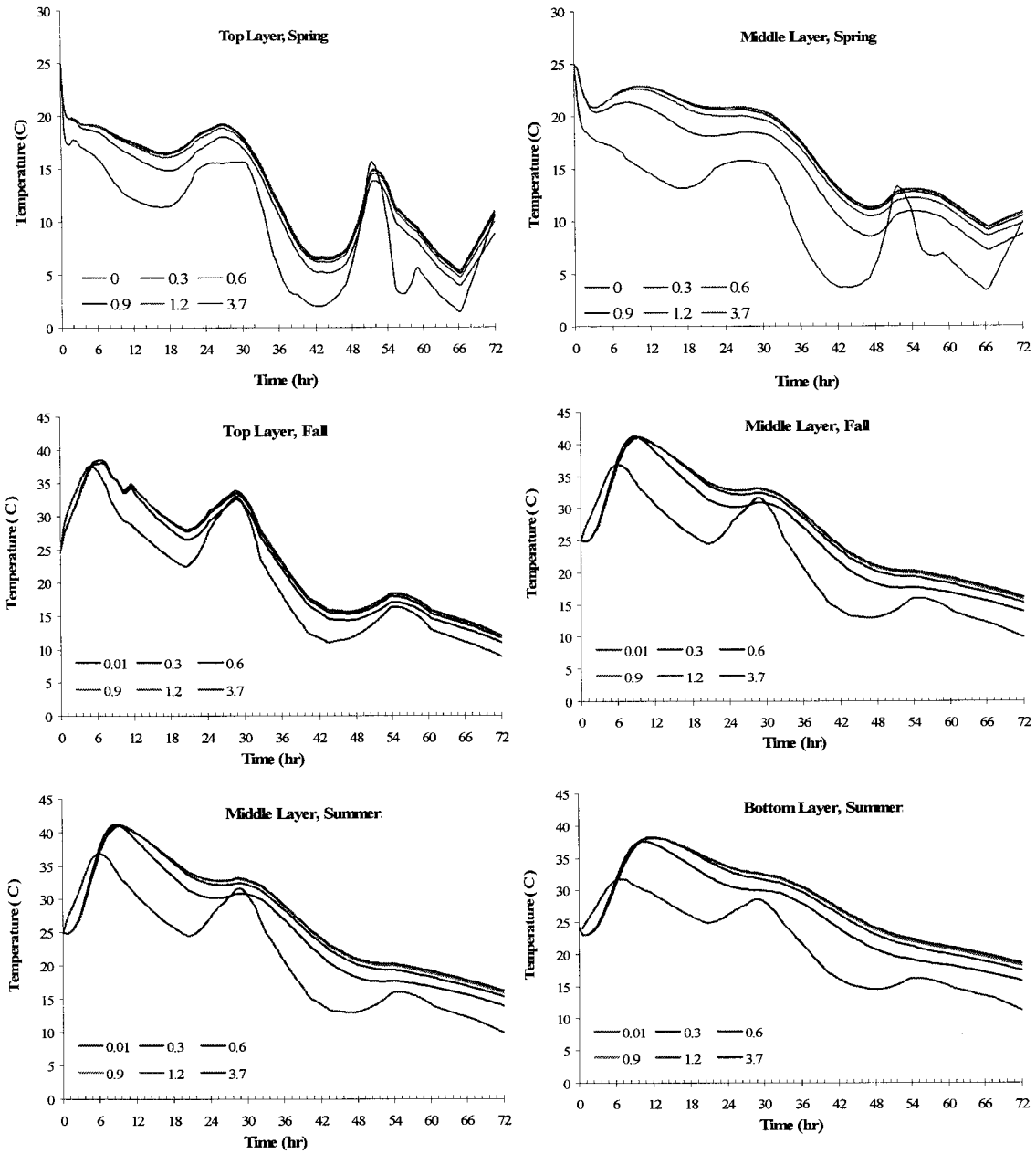

Figure C.11: Transverse Temperature Distribution (Constructed at 10 AM)